EVALUATION OF REACTION KINETICS AND MATERIAL PROPERTIES OF CEMENTITIOUS CERAMIC MATERIALS USING ULTRASONIC VELOCITY AND ATTENUATION MEASUREMENTS

A thesis submitted for the degree of Doctor of Philosophy

by

Robert Round

Department of Physics, Brunel University

June 1996

This thesis is dedicated my to wife, Gill, and my children, Janine and Adam, who suffered me, and succoured me, throughout this work.

ABSTRACT

Ultrasonic velocity and attenuation measurements have been used to characterise a range of phosphate bonded, alumina filled, magnesia ceramics and other ceramic materials. Measurements were made over a range of frequency from 50kHz - 10MHz, using a variety of commercial probes and equipment, and a variety of techniques.

An ultrasonic double-probe method was used to monitor the setting process of the cementitious ceramics using commercial 2.25MHz and 2MHz transducers, for compressional and shear wave modes, respectively, in samples with alumina content in the range of 0 - 60 wt %. The elastic properties of the material were determined from ultrasonic velocity measurements and were found to be dependent upon the filler volume fraction. The measured elastic moduli were found to increase as porosity decreased, and this effect might possibly be used to estimate porosity .

The composition dependence of the elastic moduli is compared with the Hashin and Shtrikman theoretical bounds for the elastic moduli of two-phase materials. All data lie between these bounds, suggesting that the alumina particles were well dispersed and well bonded to the matrix. However, the fact that the data are slightly above the lower bound suggested that the particles are not spherical, and this, together with other evidence obtained from an analysis of reaction rates, indicates the predominence of plate-like grain structures.

ACKNOWLEDGEMENTS

I would like to thank my supervisors Prof. B. Bridge and Prof. D. C. Imrie for their advice and support throughout this work. My gratitude is also due to my fellow researchers, Mr K. S. Tan and Miss T. Katerina for their collaboration in parts of this thesis, and to Dr. S. R. Oaten and Dr S. B. Joshi. Encouragement and support were also gratefully received from Professor C. A. Hogarth, Mr. K. Schlachter, Mr. L. Lightowler and other members of staff of the Physics Department of Brunel University. .

I am indebted to the Science and Engineering Research council, Polaris House, Swindon, and Thorn EMI, Central Research Labroratories, Hayes, for financial support, and to BA Chemicals Ltd. for the provision of the basic materials required for this study.

CONTENTS

1. INTRODUCTION.

Inherent brittleness and a tendency towards catastrophic failure are the major factors preventing the use of ceramics in many structural applications. As a result the toughness of the composite is often increased by reinforcement with filler and fibre phases. Measurements on the toughness and strength achieved on incorporating alumina and glass fibres, and particulate alumina, in a magnesium aluminium phosphate matrix were the initial topics of the present study. The basic material had been formulated and characterised by workers at Thorn-EMI and co-workers using various techniques. Their results will be discussed briefly in the appropriate context.

The main aims of this research were to evaluate current methods of nondestructive evaluation (NDE) for this ceramic material and to counter the problems of catastrophic failure by the development of suitable NDE techniques to detect and reject substandard artifacts.

There are a number of well researched and reported cementitious systems, ie materials which harden from a paste by chemical activity. Many of these materials involve the phosphate bonding of a range of

oxides, and have been extensively reviewed, see for example Kingery (1950) and Cassidy (1977). A number of compositions were investigated at Thorn-EMI, see chapter 4. Following initial evaluation and feasibility studies a range of materials based on the reaction between magnesia and aluminium orthophosphate were selected for further trials and evaluation, including non destructive evaluation.

The materials under consideration, the product of the exothermic reaction of magnesium oxide with aluminium orthophosphate acidic solution, filled with variable proportions of alumina, and with lesser amounts of carbon or glass fibre as reinforcing phases. This material, whilst combining excellent thermal and electrical insulation properties with stiffness, fracture toughness and forgiving fracture is almost as easy to mould as a polymer, and needs no sintering. In the composites discussed here, typical dimensions of the alumina and magnesia powder particles were 0.5-10μm and 3-40μm, respectively, whilst the milled fibres were typically, 150μm x10μm diameter.

The material was characterised by Finch and Sharp, Finch (1989), and discovered to be largely composed of crystalline newberyite,

$MgHPO_4.3H_2O$ and an amorphous phase taken to be hydrated $AlPO_4$. A new hydrate was observed in some compositions depending upon the source of the acidic component. This was referred to as hayesite and is assumed to be a lower hydrate of $MgHPO_4$ probably $MgHPO_4.H_2O$ or $MgHPO_4.2H_2O$. These matters are discussed in chapter 4, where the preparation of samples is considered and in chapter 5, where the structure and composition of the material is described.

For many years similar ceramic materials have been used for refractory lining bricks and gunned furnace repairs. Such materials have also found applications in dental surgery, particularly for repairs to teeth and cementing prosthetic devices to teeth or bones. By virtue of its unusual combination of thermal and mechanical properties the material has also been suggested for stealth technology applications, e.g. the minimisation of infrared signatures from aeroengine casings. It also has a large potential impact on the mass marketing of domestic appliances if used, for instance, as lightweight oven casings with integral hobs and pipework. Simple one piece units can thus replace the complex fabrications currently required to achieve the desired physical requirements.

The fillers and reactants need to be dispersed in the acid solution in order to produce samples with good mechanical properties. Therefore, the mixing method must be able to wet the powders with the acid solution and, since the composite changes from a slurry to a set composite, any mixing equipment must be able to handle materials of varying viscosity. Both continuous and batch mixers were assessed by workers at Thorn-EMI. The outcome of this work is briefly discussed in relation to the initial preparation of test samples in chapter 4.

The development of chemical bonds to unite the matrix and to cause it to adhere to the other phases is dependent upon the temperature, which itself is dependent upon the rates of exothermic chemical reactions and the physical configuration of the reacting mass. Thus it is clear that the development of the microstructure is by no means simple and the production of identical components cannot be assumed in all circumstances. This problem is compounded by the possibility of an inhomogenious mix, and by the short mixing times imposed by the increasing viscosity of the setting mass. Indeed the larger the mass the greater the restriction on mixing time.

From the foregoing it is reasonable to expect variations in the

microstructure of the matrix due to local variations in the chemical composition, the proportions of component materials, and the rate of reaction. The distribution of reinforcing fibres, filler and porosity will also be subject to variation. In addition to these material variations, faults of a mechanical origin, including cracks, distortions, inclusions and voids (as distinct from pores) are likely to be present. The prototype material did indeed have serious void defects several millimetres in diameter.

The primary aim of the current research programme was to investigate the feasibility of nondestructively evaluating the structure of this and other ceramic materials by ultrasonic and other nondestructive methods commonly used for quality control and process control applications.

The ceramic was characterised by a number of complementary ultrasonic techniques in the frequency range 24kHz-5MHz for velocity measurements and 100Hz-10MHz for broadband attenuation measurements. Optical microscopy, radiography and electrical methods were also employed, thus providing complementary data and verification of various observations and assumptions.

The evaluation technology and theoretical background had first to be developed and understood to enable an accurate interpretation of the above test data from ceramic composites, and they are discussed in chapters 2 and 3. Chapter 2 covers the history and development of cementitious systems, and the properties of brittle ceramics and cements, and goes on to discuss their measurement by conventional mechanical and nondestructive means. The more relevant theoretical background to ultrasonic evaluation is discussed in chapter 3.

As a result of the strong absorption and scattering in this material at high frequencies, good ultrasound propagation is obtained only at low frequency. Unfortunately, measurement problems occur at low frequencies, where the wavelength is greater than the sample dimensions.

It would have been a simple matter to produce larger samples, blocks or cylinders with dimensions of the order of 0.2-0.5m, more suited to analysis by the methods and equipment used. However one of the objectives of the research project was to develop a method of NDE which would remain viable in a production environment. It was therefore considered preferable to tailor the ultrasonic technique to

the artefact to be evaluated, rather than tailoring the artefact to the available evaluation methods. Thus it was considered necessary to gain an understanding of the nature of wave propagation in the circumstances outlined. The lowest frequency at which the ultrasonic propagation and properties are dependent on the material structure alone, i.e. independent of sample size, was established to be 2MHz with conveniently sized test pieces of dimensions 1.5 x 1.5 x 6 cm. At this frequency the ultrasonic wavelength in the material was approximately 2mm. The variety of equipment used and the techniques employed in the evaluation of the materials are described in chapter 6.

Dynamic elastic moduli measurements have been found to agree well with elastic constants calculated theoretically by treating the matrix and filler as end members of a two phase material whose properties obey the lower Hashin and Shtrikman bound, see chapter 3.6. In addition, the bulk modulus of the matrix computed theoretically from crystallographic data, making an allowance for porosity, agreed closely with the experimentally determined modulus. Thus, ultrasound velocity measurements, (from which moduli can be calculated) combined with a simple theory, can be used for nondestructive monitoring and quality control of the ceramic

composition.

The theoretically determined bulk modulus of the ideal, pore free matrix is 10.4GPa. This matrix modulus is far less than the moduli of the constituent oxides in the starting mixture because of the large expansion in the size of closed rings of the cation-oxygen network bonds that takes place during the reaction, rather than structural weakening (breaking of rings of network bonds) by hydration.

The frequency dependence of ultrasonic attenuation has been used to identify scattering regimes and thus determine the dimensions of the major scattering particles. Grain sizes determined ultrasonically for the three compositions showed excellent agreement with values determined by optical microscopy.

Following some success with the evaluation and inspection of fully cured artifacts the more difficult problem of monitoring the chemical bonding process and the prediction of final properties from initial data was investigated.

For this study an ultrasonic double-probe method was used to monitor

the setting process of phosphate bonded, alumina-filled, magnesia ceramics using commercial (mainly Krautkramer and Sonatest) 2.25MHz and 2MHz transducers, for compressional and shear wave modes respectively, in samples with alumina content in the range of 0 - 60 wt %. Various elastic properties of the material i.e. bulk, shear, and Young's moduli and Poisson's ratio were determined from the ultrasonic velocity measurements, using equations 11-13, chapter 3.6. These properties were found to be dependent upon the filler volume fraction, as expected. The reaction rate was also investigated using the same ultrasonic data and found to increase with increasing filler volume fraction overall.

The composition dependence of the elastic moduli is compared with the Hashin and Shtrikman theoretical bounds for the elastic moduli of two-phase materials. All data lie between these bounds, suggesting that the alumina particles were well dispersed and well bonded to the matrix. However, the fact that the data lie well above the lower bound suggests that the particles are not spherical, and this together with other evidence obtained from an analysis of reaction rates, indicates the predominance of plate-like grain structures.

The measured elastic moduli were found to increase greatly as

porosity decreased. This behaviour can be used to measure or estimate porosity.

The experimental procedures and the data thus obtained are discussed in chapters 7 and 8. Chapter 7 deals primarily with the aquisition and the interpretation of data for samples assumed to be effectively fully cured. Chapter 8 is concerned with the rate of development of the strength of the material as the chemical reactions progress. Here the use of ultrasound velocity data to monitor the changes in elastic moduli, and the inference of chemical reaction kinetics are discussed.

2. CEMENTS, CERAMICS AND CONVENTIONAL EVALUATION TECHNOLOGY.

2.1 CEMENTS AND CHEMICALLY BONDED CERAMICS.

Cements may be defined as substances, capable of uniting fragments or masses of solid matter together to form a single structure, usually by the action of hardening from a liquid or paste to a solid. Such a system relying upon some such material to form a solid mass or coating, to adhesively bond two or more components, or to bind aggregates or fillers into monolithic solids, have been classified by G.C. Bye, as cementitious systems, Bye (1983). Aggregates are particles of various sizes, generally from 1 to several tens of millimetres, and of a range of materials, often fragments of minerals, used singly or as a mixture of different materials. The cheapest, and therefore the most widely used, practical systems incorporate a mineral aggregate, often assorted gravel or pebbles, bound by an inorganic cement, usually ordinary portland cement.

An inorganic cementitious material functions by forming a fluid or fictile paste when mixed with water, or aqueous solution of reactants,

in appropriate amounts, and subsequently develops rigidity, or sets, due to chemical reaction. There may be a further development of compressive strength, referred to as hardening, due to the progress of further chemical reactions. The simplest cements involve hydration reactions whereby an anhydrous material or a low hydrate (a crystal form with few waters of crystalisation), the result of calcination of a naturally occuring higher hydrate (a crystal form with more waters of crystalisation), or mixture of materials, is further hydrated. The subsequent crystal growth must interlock with itself and any aggregate if strength is to be developed and the material therefore warrant the term cement. A cement which undergoes strength development in the presence of excess water, or even underwater, is said to be a hydraulic cement.

The predominance of gypsum plaster (calcium sulphate hemihydrate) and portland cement (mainly tri-calcium silicate, di-calcium silicate, and tri-calcium aluminate) are such that they are generally referred to as plaster and cement respectively. This convention is not adhered to in this thesis.

Portland cements are the basis for most cements and concretes used for construction. A concrete is basically, a composite material

produced by binding a coarse and fine aggregate (usually sand and gravel or a crushed rock such as limestone and granite) with a cement to form a dense and coherent mass. Concrete can be cast into any shape or size desired, and became particularly popular at the turn of this century with the movement toward streamlined shapes in design and architecture. For large scale architectural use concrete is generally reinforced using steel girders and with the discovery of a method of pre-stressing concrete and so improving the strength of the concrete in 1927, taller buildings became possible. The material is now so widely used and so durable that the very word "concrete" has come to have a secondary meaning: substantial, intransient, definite, certain, etc.

2.1.1 Historical perspective.

The first manufactured cements were probably produced where outcrops of limestone or gypsum rock were quarried and the rocks stacked in fires or bank kilns, and burnt, or calcined using wood or charcoal. The earliest attempts to make cements and concretes would, in all probability, have resulted in weak, friable materials with limited durability. Such materials would be unlikely to remain extant

in any recognisable form. The oldest concrete structures still in existence, hut floors dating from about 5600BC, were excavated at Lepenski Vir, Yugoslavia, Stanley (1989).

Gypsum cements were used as mortar (for bedding, jointing or setting bricks or masonry), notably in the Egyptian pyramids at Giza and the tombs at Sakkara in Egypt. Egyptian mortars were thinly layered between the great blocks of stone which made up the massive ancient structures and were used as a lubricant to enable the heavy blocks to be accurately placed, rather than as an adhesive medium.

The Romans developed the techniques of calcining lime in the form of chalk, limestone or coral to about 900°C, thereby converting it into quicklime. For building purposes the quicklime was then slaked with water to produce hydrated lime. Roman concrete was a combination of slaked lime, volcanic ash, sand, grit or pebbles as aggregates, and strangely, 2 eggs per bucketful of mix, probably as a plasticiser.

The Romans found that by incorporating the pozzolanic material known as tufa (volcanic ash) resulted in a superior product, a stronger mortar. This pozzolanic ash was first found in the village of Pozzuoli, near Vesuvius in Italy. In Britain they used a grog of crushed bricks or

tiles which produced a similar effect, in the absence of a local natural pozzolana. The action of silica and alumina in the ash and grog combined with the lime to produce pozzolanic cement. Whilst calcined lime mortars would not harden under water, the pozzolanic concrete could be used in waterlogged ground or in sea defences. It could also be used to construct water impermeable linings for baths, tanks, aqueducts etc. As a testament to the strength and the resistivity of Roman mortars several structures remain in existence, for example, the cement bonded masonry of the Colosseum in Rome, the Pont du Gard aqueduct, near Nimes, and in the ruins of Pompeii where the soft stone structures of the buildings are eroding faster than the mortars.

The methods and technologies developed during the Roman Empire were lost by the Middle Ages. There was a definite decline in the quality and quantity of cements used in mediaeval constructions. Usually they were non-hydraulic (non-pozzlanic) cements. It was not until the 16th. and 17th. centuries that Dutch pozzolanas (known as Dutch trass) and lime mixtures were used, usually consisting of one part trass to two parts slaked lime. The engineer John Smeaton (1726-1792), visited Holland in 1754 and investigated a cement containing equal parts of lime and trass. He then experimented with various limes and

found that the blue lias at Aberthaw, South Wales could be used satisfactorily. This contained clay, and he concluded that by deliberately mixing and burning together limestone and clay one might produce a superior or at least consistent mortar. Equal proportions of these materials were found to produce the best mortar. By recognising the role of clay in cements, Smeaton was the first to demonstrate an understanding the chemical properties of hydraulic limes.

At the end of the 18th. century James Parker of Northfleet in Kent, found that he could make hydraulic cements by calcining nodules of argillaceous limestone found washed out of the London Clay Cliffs along the Thames estuary. It was referred to as "Roman cement" and this name was used until the middle of the 19th century. Thomas Telford (1757-1834) used Roman cement in the construction of the Chirk Viaduct on the Ellesmere Canal (1795-1801), and Isambard Kingdom Brunel (1769-1849) incorporated this material in his tunnel under the Thames, linking Wapping to Rotherhithe.

James Frost patented the first bulk wet cement process in 1811, and Joseph Aspdin, a Leeds builder took out the patent for "Portland Cement" in 1824. The name Portland cement was given originally due

to the resemblance of the colour and quality of the set cement to Portland stone, a limestone quarried on Portland Bill, Dorset. However the prototype of modern cement was made in 1845 by Isaac Johnson at Swanscombe, Kent. The process involved the mixing of finely dispersed clay and chalk and higher temperature calcination in a bottle kiln. Johnson's product was strongly cementious and relatively consistent.

At the end of the 19th century the first rotary kilns were introduced, leading to a better controlled, continuous process and more consistent products. Comminution technologies also advanced allowing the possibility of the grinding of the harder, higher fired clinkers.

In recent years the continuous rotary kiln production method has changed from a wet to a dry process, resulting in improved energy efficiency. In this process the raw materials are finely ground, during which process the hot gases recycled from the kiln remove the moisture from the materials. Once the dry ingredients are mixed they pass down the inclined rotary kiln in a controlled schedule designed to produce a phase assemblage tailored to the conditions of intended use.

The Romans were probably the first to appreciate the advantages of

cement in the construction of arches, vaults and domes. The Roman engineers thus avoided the laborious hand carved stone structures by means of which earlier civilisations constructed these features. Instead this cheap readily available material could be used in conjunction with brick built ribs or frameworks. Principally these cements were used in surface finishes, concrete cores, mortars and in underwater constructions. However the earliest concrete structures were often podia or platforms on which their temples were constructed.

Another major use was in the cement surface finishes known as stucco which is a vague term applied to both internal and external renderings of lime, gypsum and cement mixtures. Some of the Roman stucco are highly ornate delicately modelled relief designs.

In 1818 the civil engineer Ralph Dodd placed wrought iron bars in concrete to improve its performance in construction, and in 1825 Thomas Telford when building the Menai Bridge placed iron bars in the concrete abutments, i.e. the structure against which the limb of an arch rests for support. Fox and Barratt aquired a patent in 1844 for their fireproof floors of cast iron beams buried in lime concrete, this technique was used in Balmoral Castle. Further developments were

made in both insitu and precast concretes, the difference being that the insitu concretes are mixed on the building sites and poured into form work or shuttering before solidifying while precast concrete components are prepared elsewhere and conveyed to the site for erection, the sections being bolted and/or cemented together. Other materials and configurations of reinforcements have been investigated, eg, wire mesh, glass and carbon fibres.

At the beginning of the 20th. century, more and more reinforced concrete was being used in commercial and municipal buildings, however it was nearly always covered with some other material. The principal features of this architecture were steel and reinforced concrete framework and floors, and non-load bearing concrete slabs used in the construction of partitioning and walls. This also revolutionised the internal lighting of buildings as large non-load bearing windows could now be constructed allowing more natural light into the rooms.

2.1.2 Types of cements and concretes.

The chemical reactions which produce ceramic cements fall into three

categories, the first of which involves reaction with water i.e. hydration or hydrolysis, as in the case of Portland cement and gypsum plaster. Hydraulic cements depend upon water rather than air for strength development and as the water is added an immediate chemical reaction occurs. These hydraulic cements stiffen at first and later develop strength. The stoichiometric quantity of water required to hydrate cement is insufficient to promote the required rheological properties. Additional water is required for this purpose and this evaporates leaving voids, which reduces the density, strength and durability of the products, see for example Lea (1970), Taylor (1966, 1981) and Glasser (1990)

A second type of cementitious system involves a chemical reaction, or reactions, between two or more constituent compounds, where water may or may not be a by-product e.g. the two compounds alumina and phosphoric acid react to give aluminium phosphate cement and water.

Magnesium oxychloride or Sorel cement is the product of a reaction between calcined magnesia and a strong solution of magnesium chloride. The product formed is magnesium oxychloride, which is strong and hard but hygroscopic and is mainly used as a flooring with a nonreactive filler and a colouring pigment.

The third type of cementitious bonding involves condensation or polymerisation reactions where the cement molecules join by condensation into polymer molecules, frequently releasing water.

2.1.3 Development of novel strong cementitious materials.

The strength of portland cement concretes has been improved in recent years and their range of application has been extended. Birchall, Howard and Kendall, Birchall (1983a), discussed these developments and went on to consider economic and environmental issues. Beyond the price per unit mass is an energy cost, where the amount of energy and, in particular, fossil fuel consumed in the winning, ie the mining or quarrying, of raw materials and subsequent processing is considered.

According to Birchall et al this is high for metals and very much lower for cements. Sintered ceramics would have an energy cost slightly less than, but of the same order as, that of metals. Rock and aggregate have the lowest cost, but polymers are quite expensive because their raw materials are fossil-fuel derivatives.

The major problem with hydraulic cement is its very low tensile strength, largely due to pores left by evaporation of surplus water. This is required to give rheological properties commensurate with conventional forming techniques. These problems are overcome in the construction industry by the use of massive, steel reinforced structures designed to be loaded in compression. For smaller scale domestic applications, of necessity more aesthetically designed, this approach is unacceptable and with smaller quantities of material and higher value products a greater cost per kilogram can be tolerated.

New developments in the production of strong cementitious materials have resulted from (i) modifying cement compositions (and the associated hydration, consolidation, and densification processes) and (ii) manipulating the microstructures. The different routes to generating such materials, include curing at slightly elevated temperature and pressure, high-shear mixing with polymer additions, and the making of fibre and particulate reinforced composites. There are also many new reaction cement formulations which have moved away from traditional portland cements and instead rely upon a diverse range of chemical reactions.

Together, these developments have produced about tenfold

enhancements in their properties which approach those of many traditional ceramics or modem composites. Strength, toughness, durability, impermeability, and abrasion resistance of these new materials have all been greatly improved, as have certain electrical and acoustical properties. These materials were given the classification of chemically bonded ceramics (CBC) by Della M. Roy, Roy (1987), since the bonding that takes place is due to a chemical reaction which proceeds at an acceptable rate at ambient or slightly elevated temperature, as opposed to fusion or sintering at some greatly elevated temperature in excess of 1000 °C. The bonding in such CBCs is a mixture of ionic, covalent, and van der Waals bonding, with the ionic and covalent dominating; in traditional cement hydration products, van der Waals and hydrogen bonding dominate.

Portland and other similar cements—and the concretes made by combining them with different kinds of aggregates—are used in greater quantities than any other man-made materials. Such cements lack toughness, are weak in tension but offer modest strength and stiffness in compression. Yet even with the extremely primitive cement technology that prevailed in ancient times, some Greek and Roman structures have lasted for 2000 to 3000 years as mentioned.

Normal hydraulic cement (commonly called ordinary portland cement, or OPC) is supplied as a finely ground powder the particles of which comprise four major components or phases. These are tricalcium silicate ($3CaO.SiO_2$), dicalcium silicate ($2CaO.SiO_2$), tricalcium aluminate ($3CaO.Al_2O_3$), and calcium aluminoferrite solid solution ($Ca_2Fe_x\ Al_{2-x}\ O_5$). Small amounts of gypsum ($CaS0_4\ .2H_2O$) and other minor components, such as alkali sulphates, are also present. When mixed with water the cement undergoes an exothermic hydration-hydrolysis reaction. Immediately after the paste is formed, there is a period of time— possibly several hours—in which to place and, if necessary, finish shaping the desired object in a simple fashion at room temperature, before the setting reaction precludes further handling. This is an essential feature of cementitious compositions, and the amount of working time will, together with the workability or consistency of the paste, govern the nature of the placing and forming techniques which may be employed. Conversely for a given application a cement with a suitable setting rate, workability and working time must be selected, suitably modified, or formulated.

The reaction rate and consequent rate of heat evolution are a function of the total chemical composition, the crystal chemistry of the cement

minerals, the fineness of the powder, and the temperature of setting. Setting and hardening are the result of a complex sequence of processes. Hardened cement paste has a finely intergrown microstructure, a very high surface area, and submicrometer-sized noncrystalline fibres or particles of calcium silicate hydrate (CSH). These grow between and link together larger crystallites and residual anhydrous cement grain cores, leaving a microporous material with minimal interconnected capillaries. The solidification of cement paste is a constant-volume process. When higher density cement particles are mixed with lower density water, they react to form a solid hydration product consisting of solids of intermediate density and interspersed residual porosity.

The strength of hardened cement paste increases as the ratio of water to cement is reduced. Because the residual porosity distribution, and the excess molecular water cause most of the limitations on the properties of conventional hardened cement pastes, many attempts have been made to reduce the amount water. There is a practical limit if the mixture is to remain workable. Some decades ago it was discovered that increased workability at constant water-cement ratio could be achieved with admixtures that contain small amounts of chemicals such as lignosulphonates and related dispersants. However,

the setting is retarded when such admixtures are used. New chemical admixtures made with superplasticisers provide much better control of the setting of cement pastes and improve the properties of the concrete, Roy (1980).

The utility of porous hydraulic cement products has been limited by their low tensile strength (≈3 MPa), and their low work of fracture (≈20 J/m^3), despite a compressive strength of ≈30MPa. In addition to the presence of spherical pores and voids, cement pastes with a normal w/c ratio (0.40) may undergo shrinkage during drying, which induces microcracking when material is exposed to low-humidity environments. This is a source of "Griffith flaws" which initiate fracture under load, see section 2.2.

Since 1970 cement matrix composites have been developed

Four major advances have taken place:

(i) the formation of special densified or warm-pressed cement pastes which have properties approximating those of fired ceramics;

(ii) modification of the chemical composition of the cement;

(iii) the formation of macrodefect-free cements prepared by special processing; and

(iv) the manufacture of a variety of cement-based composites.

2.1.4 Macrodefect-free cements.

The engineering of a new class of high-strength materials called macrodefect-free (MDF) cements was pursued originally by Birchall and co-workers at Imperial Chemical Industries and Oxford University, Birchall (1981, 1982a, 1912b), Kendall (1983), Birchall (1983a, 1983b). MDF refers to the absence of relatively large voids or defects which are usually present in conventionally mixed cement pastes because of entrapped air and inadequate dispersion. Such voids and defects limit the strength that can be achieved by acting as stress concentrators. In the MDF process 4 to 7% of one of several water-soluble polymers (such as hydroxypropylmethyl cellulose, polyacrylamide, or hydrolysed polyvinylacetate) is added as a rheological aid to permit cement to be mixed with very small amounts of water. Subsequent high-shear mixing produces a plastic, cohesive mixture which can be shaped by extrusion or other forming technique and which sets in times ranging from minutes to hours. The highest strength materials have been prepared with calcium aluminate cements, which harden rapidly, although portland cements have been

used less successfully. Besides being a processing aid, the polymer appears to be a significant structural component. Control of the particle size distribution (for optimum particle packing) was also considered important for generating strength. A final processing stage, in which entrapped air is removed by applying modest pressure (≈5 MPa), resulted in a paste that is free of all large defects. The mechanical properties of MDF cements are remarkable when compared with those of normal cements. The strength at any given flaw size was higher than for normal cement pastes because the MDF cements had a higher elastic modulus (≈40 GPa) and higher fracture surface energy (≈200 J/m2). Very low porosity materials have been achieved (<1%) (23) at considerably lower pressures than with warm-pressing techniques, Roy (1973), as well as flexural strength of≈150 MPa , a compressive strength of≈300 MPa, and a Young's modulus of ≈50 GPa.

A second major family of cement-based composites has emerged which incorporate fine particles of oxide materials. Enhanced strength and durability can be obtained by deliberately blending hydraulic cements with various types of particulates, for instance ground granulated blast furnace slag, fly ash, or silica fume. When combining such particulates in a cementitious composite, it is necessary to consider: (i) the particulate characteristics (such as size, shape, and density)

which affect rheology and optimal particle packing and

(ii) the chemical reactivity of the particles, which affects the rheology and the strength of the particle-matrix bonding.

When two monodisperse powders of the same material, one with course and the other with fine grains, are mixed, the fine particles will pack within the interstices between the course grains. The density of the paste or compact will be greater than that of a similar paste or compact containing either powder alone, since the void space is reduced. The addition of a third monodisperse powder, with superfine grains small enough to pack within the interstices of the fine grains, would cause a further densification.

In real polydisperse systems, soluble chemical species from the fine particulates and the surfaces of the larger cement grains can react with ease and speed. A colloidal particulate such as silica fume, (fine or colloidal silica) initially reacts with the alkaline cement solution, but much unreacted residue remains as slow reactions produce ultrafine calcium silicate hydrate reaction products. This decreases the mean pore size.

Because of this type of reaction, the microstructures and pore

structures developed from composites of cement with fine glassy slag or silica fume, or both, are much finer and possess lower ionic diffusivities than normal cements, and are much more chemically resistant and durable. The combined physical and chemical effects cause enhanced resistance to chloride-enhanced corrosion and increased durability of steel-containing cementitious composites such as in highways and bridges. Proper particle packing also achieves very high strengths and stiffnesses .

Fine silica fume (also called condensed silica fume or microsilica) can be substituted for portland cement in amounts ranging up to 25% . Concretes containing 5 to 15% silica fume have high compressive strengths (up to and above 100 MPa), flexural strengths (up to 12 MPa), and Young's moduli (up to 34 GPa). They also have very low permeabilities to water. The microstructure of the critical interfacial zone between cement paste and the aggregates in concrete is more dense and uniform than when conventional pastes are used, Hjorth (1983), Hirsch (1983), and the bond between paste and other embedded materials such as aggregates and fibres appears to be improved.

Good properties have been achieved with silica fume substituted

pastes with up to 20 to 25% silica fume at a water to solids (w/s) ratio of 0.12 to 0.22 using mechanical compaction. Compressive strengths of up to 270 MPa with Young's moduli up to 80 GPa have been achieved in such compositions. A dense but fairly fluid paste is formed by the combination and chemical dispersion of particles that have dissimilar size ranges. No major air voids, and only a few very small capillary pores, remain in carefully processed products. Shrinkage upon drying of the cement hydration product is limited, and the residual cement grain cores act as a strong internal filler or "microaggregate".

Dense silica fume-based cementitious composites are used to resist severe mechanical erosion in impeller screws for moving coal and fly ash and in flooring for industrial buildings, Hjorth (1983). Another version is commercially available as a tooling and moulding material in applications where vacuum tightness or mirror finishes are required. The latter material retains a compressive strength of ≈ 300 MPa up to about 500°C and ≈200 MPa at about 700°C.

One approach to toughening brittle ceramic and cementitious materials is to incorporate strong fibres into the microstructure. The lack of ductility and the low tensile strength of cementitious

materials have long been remedied on a large scale by the use of steel reinforcing bars or mesh. In a typical civil engineering application, steel rods may contribute less than 1% by volume.

On a much finer scale, composites of cement incorporating asbestos fibre have been used since about 1900 but are now unpopular because of asbestos hazards, despite their outstanding tensile properties and durability. Other types of fibres investigated include steel, glass and polypropylene.

The reinforcement of cement paste by glass fibres initially was limited by the poor resistance to corrosion of glass fibres in the highly alkaline environment in the pores, where the pH $\approx$ 12. Alkali-resistant glass fibres were developed by Majumdar, Majumdar (1983) and co-workers at the Building Research Establishment, Watford. These have a high ZrO_2 content and can resist the degrading effects of the cement paste environment for some years. The long-term (10 to 100 years) stability of the fibres is uncertain, this, once assured, will lead to the widespread use of such materials.

Incorporation of fine fibres into brittle materials increases their

tensile strength severalfold and their toughness by several orders of magnitude. Ultimate tensile strengths of about 15 MPa are common, while modulus of rupture (MOR) values of 35 to 40 MPa are possible. The work of fracture, or toughness, increases more substantially. This assumes that after the first matrix crack has appeared there are sufficient fibres and adequate bonding to support the load.

2.1.5 Reaction cements based upon phosphoric compounds.

In 1950 Kingery wrote the first comprehensive study of phosphate bonding in refractories,which was subsequently quoted in other reviews of these materials, for example that published by Cassidy, Kingery (1950), Cassidy (1977).

In the intervening years progress has been made in three major areas:

(i) The fundamental chemistry of the bonding processes;

(ii) The development of more sophisticated phosphate bonds;

(iii) The application of phosphate-bonded materials.

2.1.5.1 The chemistry of phosphate Bonds.

Kingery considered three methods of achieving phosphate bonding :

(i) the reactions between siliceous materials and phosphoric acid;

(ii) the reactions between oxides and phosphoric acid;

(iii) the direct addition or formation of acid phosphates.

Cassidy considered a wider variety of bonding systems available in both liquid and solid form, including ammonium phosphate, chromium-aluminium phosphate, alkali polyphosphates, magnesium acid phosphates, aluminium chlorophosphate hydrate, and mixtures of aluminium phosphate hydrate and urea phosphate. Phosphoric acid and solutions of monoaluminium phosphate (MAP) are widely used and well studied bonding agents.

New bonding agents have been developed to overcome problems associated with the use of liquid bonds particularly with certain aggregates. The alkali polyphosphates are particularly useful in bonding basic aggregates; phosphoric acid or solutions of MAP tend to react very rapidly. Aluminium chlorophosphate hydrate (ACPH) is a dry powder designed for use in castable refractories and counters bond

migration and bloating due to reaction with metallic iron, and improves storage properties. Its setting reactions do not require the formation of intermediate metaphosphate phases.

Mixtures of aluminium phosphate and urea phosphate have been specifically developed to give a dry powder bonding agent, countering the problem of hygroscopicity encountered with the use of solid monoaluminium phosphate.

2.1.5.2 Phosphoric acid.

Phosphoric acid reacts with metal oxides and hydroxides at temperatures ranging from 20 to 200° C to form hard, solid shapes,which can be built into structures without the need for firing. They are also often employed as castable refractories (ie. compositions which set without firing), to make monolithic refractory structures or effect repairs to existing structures. In practice the most favoured are the amphoteric oxides, because they react at a controlable rate. Cassidy states that hardening systems based on H_3P0_4 and TiO_2, CaO, FeO, Fe_20_3, NiO, ZnO, ZrO_2, MgO, Al_20_3, and CrO_3 have all been investigated. The H_3P0_4-Al_20_3 system, and the

mechanisms and phase transformations occurring therein, have been investigated and the phases formed by reacting H_3P0_4 with either alumina, Al_20_3, or the hydrated form Gibbsite, $Al(OH)_3$, have been found to be similar. It is generally understood that the process involves the formation of acid phosphates of the type $Al(H_2P0_4)_3$ initially. However, on subsequent heating and in the presence of excess Al_20_3 the final bonding phase is almost certainly $AlP0_4$.

Direct calorimetric analysis (DCA) studies, O'Hara(1972), on tabular alumina-phosphoric acid cementitious systems have shown that the bonding reactions start at about 127 °C. Most of the reactions occur over the temperature range 127-427 °C and involve the formation of aluminium phosphates and possibly formation and melting of pyrophosphoric acid. At about 510 °C a change in slope occurs which remains up to 732 °C. Continuous changes in slope occur over the temperature range 732-1327 °C, arising from the formation of aluminium phosphate bonding phases and phase transitions therein. It is suggested that this devitrification of the bond accounts for the fact that specimens fired to 1093 °C have a lower strength than those fired to either 371°C or 815° C. These authors also confirmed that the addition of CrO_3 increases the thermal stability of the phosphate bond.

It has long been established, initially by Sheets and co-workers, Sheets (1958), that compositions based on particular grogs (ground prefired ceramic materials) such as zirconia, beryllia, mullite, and silicon carbide exhibit material properties which, not surprisingly, differ from those of materials based on pure alumina or other grogs.

Therefore it is not possible to make any general statement about the properties of phosphate bonded materials without specification of both the type of bond used and the composition and grading of the grog or aggregate, particularly so if one is to compare the relative properties of different binder systems.

These authors also found that it was not possible to get a cold set using mixtures of phosphoric acid with either alumina grog, fine reactive alumina, or hydrated alumina, but that such compositions had to be dried. However, the addition of ammonium fluoride enabled a cold-setting mixture to be produced.

Although phosphoric acid is a good bonding agent for high-alumina refractories, ramming mixtures may experience premature hardening and loss of workability associated with the formation of insoluble

$AlPO_4$ hydrate. Sequestering agents, which promote the formation of complexes with soluble ions and thus reduce the chemical activity of the system, can be added to stabilise the mix: 5-Sulphosalicylic acid, acetylacetone, dextrin, oxalic acid and citric acid can all be used.

2.1.5.3 Aluminium acid phosphates.

Cassidy asserts that the most important characteristic of a liquid binding agent is the acidity, which is denoted by x, the molar P_2O_5:Al_2O_3 ratio, and that mixtures with $x < 3$ are metastable, Cassidy (1977). Mixtures in which $x \approx 2.3$ throw down a deposit and harden on prolonged storage, and mixtures with $x < 2.3$ are even more unstable.

Typical commercial products have $x \approx 3$, and are about 50% w/w solutions of $Al(H_2P0_4)_3$.

It must be remembered, however, that real systems contain an excess of some reactive phase, TiO_2, ZrO_2, MgO, SiO_2 and SiC. Under these conditions solutions of aluminium phosphate bond in two ways: by acidic metaphosphate binding and by chemical (or reaction) bonding

with the aggregate. Chemical bonding takes place when the acid phosphates react with weakly basic or amphoteric oxides. This results in the formation of crystalline orthophosphates as the bond. Cold-setting cements and concretes are usually formulated as two-pack systems, and can be prepared by adding a reactive oxide, such as MgO, to the system. The reaction between MgO and aluminium acid phosphate has been studied. Various systems were investigated in which the molar P: (Al + Mg) ratio was varied using a reagent grade MgO, monoaluminium phosphate, and aluminium hydroxide. As the amount of MgO increased so the rate of setting increased. The reaction was endothermic and the heat of reaction increased with the magnesia content. $MgHP0_4.3H_2O$ is formed as a crystalline salt: some gel-like $(AlH_3(P0_4)_2.3H_2O$ is also found. The details of these reactions are discussed in chapter 4.

Attempts to form a cold-setting system in which the P: (Al + Mg) ratio was greater than 1, have failed due to the formation of water soluble $MgH_2(P0_4)_2O$. On subsequent heat treatment the various phase changes which occur also depend on the molar P: (Al + Mg) ratio.

Various concretes based on this system have been patented and are

now commercially available in both single-pack and two-pack systems. This type of material is the basis of the fibre and particulate ceramic composite materials which are the subject of this thesis.

2.1.6 Properties of phosphate-bonded ceramics.

Phosphate-bonded refractory bricks, mortars, ramming mixes, plastics, and cold setting castables utilising almost all the known refractory oxides and silicon carbide are now widely used. In general

(i) they do not show 'weak' regions on heating.

(ii) they have good refractoriness,

(iii) they possess high abrasion resistance at elevated temperatures,

(iv) they have good slag resistance and melt repellency.

These desirable properties can only be achieved by the correct choice of phosphate bond and aggregate. They can be further enhanced, particularly with regard to mechanical strength and fracture toughness by the correct choice of reinforcement or particulate filler, with regard to both type and proportions.

'Cement free' phosphate-bonded castables are available as either one-pack systems based on solid phosphate bonds such as ACPH, or

two-pack systems containing liquid bonds (such as monoaluminium phosphate). They set in the cold by the reaction of the acid bond with MgO. The properties of these materials vary depending on the type and amount of bond used and the type and grading of the aggregate. Cassidy compared hot strengths of ACPH-bonded SiC, Al_2O_3 and bauxite castables, with those of calcium aluminate products and with thermally processed materials, Cassidy (1977). Tabular alumina-based materials showed a fall-off in hot strength at temperatures above 800 °C, the rate of strength decrease being more marked with the presence of MgO.

These materials are used widely in chemical plant, and have proved to be very effective in ferrous metallurgical applications such as in electric arc-furnace roofs. Phosphate-bonded high-aluminas make effective patching materials for coal gasification reactors.

With ACPH-bonded silicon carbide the modulus increases up to 1100 °C and then decreases probably due to the formation of silicophosphates. The addition of silicon carbide to high alumina, phosphate-bonded

products results in an increase in their hot strengths.

2.2 THE MECHANICAL TESTING OF BRITTLE CERAMICS.

At room temperature, both crystalline and noncrystalline ceramics are inclined to fracture before any plastic deformation can occur in response to an applied tensile load. The brittle fracture process consists of the formation and propagation of cracks through the cross section of material in a direction perpendicular to the applied load. Crack growth in crystalline ceramics is usually through the grains (i.e., transgranular) and along specific crystallographic (or cleavage) planes, planes of high atomic density.

The measured fracture strengths of ceramic materials are substantially lower than predicted by theory from interatomic bonding forces. This may be explained by very small and omnipresent flaws in the material which serve as stress focussing points, at which the magnitude of an applied tensile stress is effectively amplified. The degree of stress amplification depends on crack length and tip radius of curvature, being greatest for long and pointed flaws ie cracks and delaminations, Davidge (1989), Callister (1994). These stress

focussing flaws may be minute surface or interior cracks (microcracks), internal pores, and grain corners, which are virtually impossible to eliminate or control. Even moisture and contaminants in the atmosphere can introduce surface cracks in freshly drawn glass fibres, which deleteriously affect the strength. A stress concentration at a flaw tip can cause a crack to form, which may propagate until the eventual failure of the piece.

The measure of a ceramic material's ability to resist fracture when a crack is present is specified in terms of fracture toughness. The stress intensity for plane strain, K_I, is defined according to the expression, Callister (1994):

$$K_I = Y\sigma\sqrt{(\pi a)} \qquad (1)$$

where Y is a dimensionless parameter which is a function of both specimen and crack geometries, σ is the applied stress, and a is the length of a surface crack or half of the length of an internal crack.

Crack propagation will not occur as long as the right-hand side of the

above equation is less than the plane strain fracture toughness of the material. Effectively for a given system with fixed flaws this implies that there is a critial value of stress,σ_f , at which failure occurs. Conversely, when components or test pieces are subjected to particular service or test stress conditions, there is a a critical flaw size at which crack growth would proceed rapidly to failure.

The critical stress intensity or plane strain fracture toughness, K_{Ic}, is defined according to the expression, Callister (1994):

$$K_{Ic} = Y\sigma_f\sqrt{(\pi a)} \qquad (2)$$

Plane strain fracture toughness values for ceramic materials are smaller than for metals; typically they are below 10 $MPam^{-3}$. Under some circumstances, fracture of ceramic materials will occur by the slow propagation of cracks, when stresses are static in nature, and the stress intensity is less than K_{Ic}. This phenomenon is called static fatigue, or delayed fracture; use of the term "fatigue" is somewhat misleading since fracture may occur in the absence of cyclic stresses. This type of fracture is especially sensitive to environmental conditions, specifically when moisture is present in the atmosphere. A stress-corrosion process probably occurs at the crack

tips where the combination of an applied tensile stress and material dissolution leads to a sharpening and lengthening of the cracks until, ultimately, one crack grows to a size capable of rapid propagation. Furthermore, the duration of stress application preceding fracture diminishes with increasing stress. Consequently, when specifying the static fatigue strength, the time of stress application should also be stipulated. Silicate glasses are especially susceptible to this type of fracture; it has also been observed in portland cement, and other ceramic materials including porcelain, high-alumina ceramics, barium titanate, and silicon nitride.

There is usually considerable variation and scatter in the fracture strength for many specimens of a specific brittle ceramic material. This phenomenon may be explained by the dependence of fracture strength on the probability of the existence of a flaw that is capable of initiating a crack. This probability varies from specimen to specimen of the same material and depends on fabrication technique and any subsequent treatment. Specimen size or volume also influences fracture strength; the larger the specimen, the greater this flaw existence probability, and the lower the fracture strength. For compressive stresses, there is comparatively little amplification associated with any existent flaws. For this reason, brittle ceramics

display much higher strengths in compression than in tension, and they are generally utilised when load conditions are compressive. Also, the fracture strength of a brittle ceramic may be enhanced dramatically by imposing residual compressive stresses at its surface.

2.2.1 Flexural testing.

The stress-strain behaviour of brittle ceramics is not usually ascertained by a tensile test as is often the case with metals for several reasons, Quinn (1991), Callister (1994). Firstly it can be difficult to prepare and test specimens having the required geometry. Secondly there is a significant difference in results obtained from tests conducted in compressive and in tensile modes. Ceramics are typically weak in tensile loading and it is considered prudent to avoid loading ceramic structures in tension and to endeavour to ensure compressive loading as far as possible. Tensile testing would not approximate service conditions to any degree and would thus lead to an inaccurate and inappropriate value.

Therefore, a more suitable transverse bending test is most frequently employed, in which a rod specimen having either a circular or

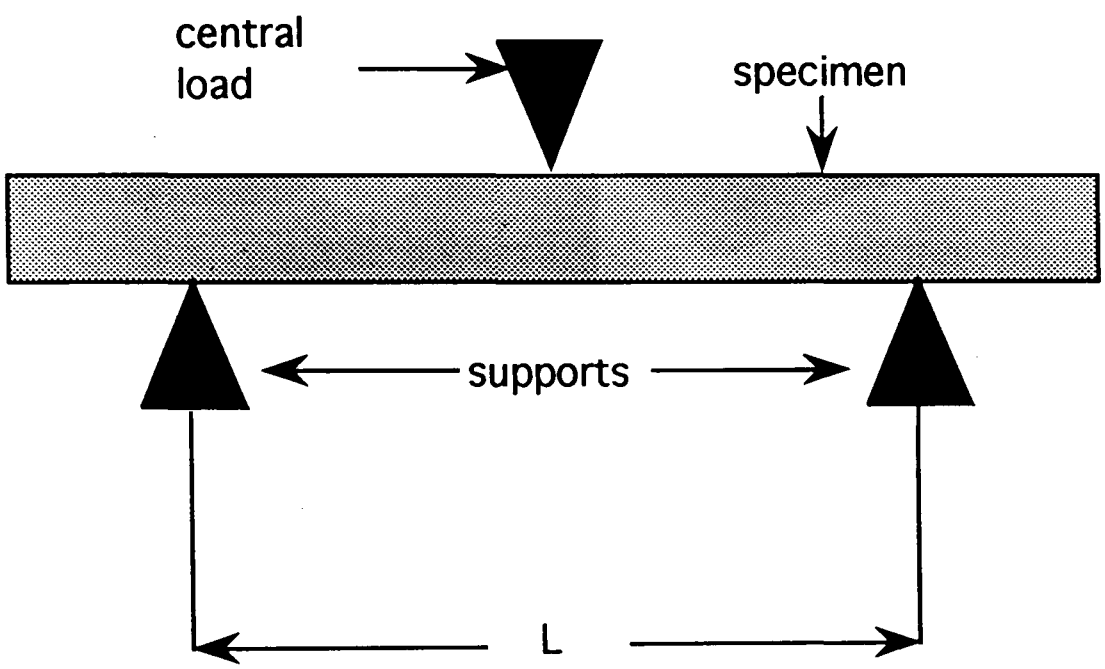

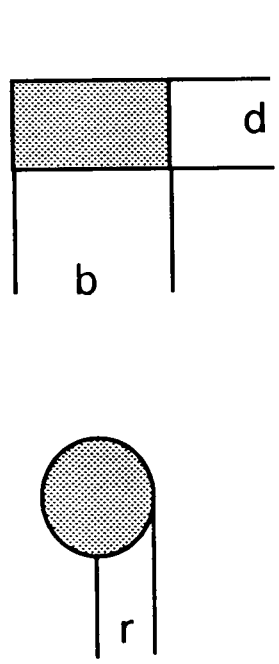

Figure 2.1 A three point loading scheme for a flexural test indicating specimen dimensions.

rectangular cross section is loaded until fracture takes place, using a three- or four-point loading technique; the more common three-point loading scheme is shown in Figure 2.1. Many commercial test rigs are available where the load my be applied hydraulically or mechanically with a gauge giving a suitable readout of the load at fracture, or more simply by a mass of water delivered via a microswitch controlled valve, and shut off and weighed following fracture. At the central point of loading, the surface of the specimen proximal to the load point is placed in a state of compression, whereas the distal surface is placed in tension. The stress is calculated from the specimen thickness, the bending moment, and the moment of inertia of the cross section; these parameters are given in Figure 2.1 for rectangular and circular cross sections.

The maximum stress, or stress at fracture using this bend test, is known as the modulus of rupture, or the bend strength, an important mechanical parameter for brittle ceramics. For a rectangular cross section, the modulus of rupture (MOR) is given by the well known expression, Askeland (1996):

$$MOR = {}^{3PL}/_{2bd^2} \qquad (3)$$

where P is the load at fracture, L is the distance between support points, and the other parameters are as indicated in Figure 2.1. When the cross section is circular, then:

$$MOR = {}^{PL}/_{\pi r^3} = {}^{8PL}/_{\pi d^3} \qquad (4)$$

where r is radius of the specimen and d is its diameter. The latter form is more commonly quoted as the diameter of the specimen is easier to obtain.

Since, during bending, a specimen is subjected to both compressive and tensile stresses, the magnitude of its modulus of rupture is greater than the tensile fracture strength.

Furthermore, MOR will depend on specimen size; as with increasing specimen volume (under stress) there is an increase in the probability of encountering significant flaws and, consequently, a decrease in the modulus of rupture values obtained. It is usually specified that the aspect ratio of the portion of the specimen under test should be approximately 7:1.

2.2.2 The testing of cement and concrete structures.

The testing of cement and concrete structures is somewhat different to the testing of fired ceramics. They are designed for compressive loading, and are extremely weak in tension. The castable nature of such materials enables easy installation of reinforcement for areas subject to tensile stresses, but also introduces the complication of age related mechanical properties and greater variability. Thus in cementitious materials strength data is quoted for a range of ages and for specified, standardised curing conditions, Neville (1987). The mechanical testing of cementitious materials is accomplished by several means the most widely applied being compressive or crushing strength determinations. Such determinations are made using 150 x 300 mm cylinders in the US and 150 mm cubes in the UK, although standards permit the use of other smaller specimens depending on the maximum size of aggregate.

A range of reusable moulds can be made from steel, cast iron, brass and various plastics, whilst expendable single use moulds can be made from sheet metal, plastic, waterproof paper products or other materials which satisfy the physical requirements of watertightness,

absorptivity and rigidity. A mould release agent, eg. a thin layer of mineral oil, is usually applied to the inside surfaces of most types of moulds in order to prevent bonding between the concrete and the mould. Concrete is then placed in the mould in layers. Compaction of the concrete may be achieved in two or three layers, each layer being compacted by means of a steel punner, or ramming bar, or by internal or external vibration according to an appropriate national standard. The top surface of the cast specimen, finished by a trowel, is not plane and smooth enough for testing, and so requires further preparation. There are two methods of obtaining a plane and smooth surface: grinding or capping. Grinding is satisfactory but expensive and time consuming. For capping, three materials can be used: a stiff Portland cement paste on freshly-cast concrete, and either a mixture of sulphur and a granular material (e.g. milled fired clay) or a high-strength gypsum plaster on hardened concrete. The cap should be thin, preferably 1.5 to 3 mm thick, and have a strength similar to that of the concrete being tested. Probably the best capping material is the sulphur-clay mixture which is suitable for concrete strengths up to 100 MPa, but the use of a fume cupboard is necessary.

In addition to being plane, the end surfaces of the test specimen should be normal to its axis, and this guarantees also that the end planes are

parallel to one another. No significant variation in the measured value of strength occurs as a result of a small deviation from the normal, or a small lack of parallelism between the end surfaces of a specimen does not affect its strength, provided the testing machine is equipped with a seating which can align freely. Opposing cast faces of a cube present fewer problems in this respect.

The curing conditions, eg the temperature and humidity, for the standard test cylinders are specified in the appropriate standard so that moisture loss is prevented. Subsequently, the de-moulded specimens should be stored under the same temperature and humidity conditions or in saturated lime water until the prescribed age at testing. Because they are subjected to standard conditions, these specimens give the potential strength of concrete. In addition, service specimens subjected to the same conditions as the structure may be used to determine, as near as possible, the actual quality of the concrete in the structure. This data can be used to decide when formwork may be struck, when further construction may continue, or when the structure may be put into service.

The compressive strength of each specimen is determined at a constant loading rate again as specified in the appropriate standard. The maximum recorded load divided by the area of cross section of the

specimen gives the compressive strength, which is reported to an accuracy of 0.05 MPa.

In the UK, the test cube is cast in steel or cast-iron moulds of prescribed dimensions and planeness with narrow tolerances, with the mould and its base clamped together. BS 1881: Part 108: 1983 prescribes filling the mould in layers of approximately 50 mm. Compaction of each layer is achieved by not less than 35 strokes (for 150mm cubes), or 25 strokes (for lOOmm cubes), of a 25mm square steel punner; alternatively, vibration may be used. Further treatment of the test cubes is prescribed by BS 1881: Part 111: 1983. After the top surface has been finished by a trowel, the cube should be stored at a temperature of 20±5 °C when the cubes are to be tested at, or more than, 7 days or 20±2 °C when the test age is less than 7 days. The preferred relative humidity is not less than 90 per cent, but storage under damp material covered with an impervious cover is adequate. The cube is de-moulded just before testing at 24 hours. For greater ages at test, demoulding takes place between 16 to 28 hours after adding water to the mix, and the specimens are stored in a curing tank at 20±2 °C until the prescribed age. The most frequently used age at test is 28 days, but additional tests can be made at 1, 2, 3, 7 and 14 days, 13 and 26 weeks and 1 year, 3 and 7 days being quite frequently

used.

BS 1881: Part 116: 1983 specifies that the cube is placed with the cast faces in contact with the platens of the testing machine, such that the position of the cube under test is at right angles to the position as cast. The load is applied at a constant rate of stress within the range of 0.2 to 0.4 MPa/s , and the crushing strength is reported to the nearest 0.5 MPa (50 psi).

Pure uniaxial compression would be the ideal mode of testing, but the compression test imposes a more complex system of stresses, mainly because of lateral forces developed between the end surfaces of the concrete specimen and the adjacent steel platens of the testing machine. These forces are induced by the restraint of the concrete, which attempts to expand laterally (Poisson effect), by the several-times stiffer steel, which has a much smaller lateral expansion. Consequently, in addition to the imposed uniaxial compression, there is a lateral shearing stress, the effect of which is to increase the apparent compressive strength of concrete.
The effect of shear is always present, although it decreases towards the centre of the cube, so that the sides of the cube have near-vertical cracks, or completely disintegrate so as to leave a relatively

undamaged central core. This happens when testing in a rigid testing machine, but a less rigid machine can store more energy so that an explosive failure is possible where one face, touching the platen, cracks and disintegrates so as to leave a pyramid or a cone. Other types of failure are regarded as unsatisfactory and indicate a probable fault in the testing procedure or a defective specimen.

When the ratio of height to width of the specimen increases, the influence of shear becomes smaller so that the central part of the specimen may fail by lateral splitting. This is the situation in a standard cylinder test where the height/diameter ratio is 2. Sometimes cylinders of different height/diameter ratios are encountered, for example, with test cores cut from in situ concrete: the diameter depends on the core-cutting tool while the height of the core depends on the thickness of the slab or member. If the core is too long it can be trimmed to a height/diameter ratio of 2 but with too short a core it is necessary to estimate the strength which would have been obtained using a height/diameter ratio of 2 by applying correction factors.

Since the influence of platen restraint on the mode of failure is greater in a cube than in a standard cylinder, the cube strength is

approximately 1.25 times the cylinder strength, but the actual relation between the strengths of the two types of specimen depends on the level of strength and on the moisture condition of concrete at the time of testing. Compared with the cube test, the advantages of the cylinder are less end restraint and a more uniform distribution of stress over the cross section; for these reasons, the cylinder strength is probably closer to the true uniaxial compressive strength of concrete than the cube strength. The great advantage of the cube over the cylinder is that the capping procedure is unnecessary.

2.2.3. Mechanical evaluation of actual structures with minimal damage.

A group of tests aimed at the assessment of in situ concrete strength has become established, with principal methods covered by BS 1881,part 207. They all cause localised surface damage, necessitating repairs, but considerably less damage than that caused by the removal of core samples, Bungey (1993). The basic features of the more widely used of these tests are discussed below together with the factors which influence the choice of test in given circumstances and their correlation with mechanical test parameters. The range of

application includes quality control of fresh concrete and the assessment of older structures Bungey (1993).

2.2.3.1 Penetration resistance.

Penetration resistance, also known as the Windsor probe test, is a determination of the depth of penetration by a metal rod driven into the concrete by a given amount of energy, generated by a standard charge of powder. The penetration depth is inversely proportional to the compressive strength of concrete but the actual relationship depends on the hardness of the aggregate. Charts of strength versus penetration (or length of exposed probe) are available for aggregates with hardness of between 3 and 7 on Moh's scale. In practice, the penetration resistance should be correlated with the compressive strength of standard test specimens or cores of the actual concrete used.

This test basically measures hardness and cannot yield absolute values of strength, but the hardness is measured over a certain depth of concrete and not just at the surface, unlike most hardness tests. In large structures the penetration resistance test approaches

nondestructive status as the damage is localised and repairable, and it is possible to retest in the vicinity.

2.2.3.2 Pull-out test.

The pull-out test measures the force required to pull out a cast-in steel rod with an embedded enlarged end . The rod assembly is pulled out with a lump of concrete in the approximate shape of a frustum of a cone. The pull-out strength is calculated as the ratio of the force to the idealised area of the frustum, the strength being close to that of the shearing strength of concrete. The pull-out force or strength correlates well with the compressive strength of cores or standard cylinders for a wide range of curing conditions and ages. The disadvantages of this method lie in the greater amount of damage and the requirement to place costly single use rods in the structure.

2.2.3.3 Rebound hammer.

This test is also known as the Schmidt hammer, impact hammer or sclerometer test, and is a nondestructive method of testing concrete.

The test is based on the principle that the rebound of an elastic mass depends on the hardness of the surface against which the mass impinges. The rebound hammer has a spring-loaded mass which has a fixed amount of energy imparted to it by extending the spring to a fixed position by pressing a plunger against a smooth surface of concrete. Upon release, the mass rebounds from the plunger which remains in contact with the concrete surface, and the distance travelled by the mass, expressed as a percentage of the initial extension of the spring, is called the rebound number. This is indicated by a rider moving along a graduated scale. The rebound number is an arbitrary measure since it depends on the energy stored in the given spring and on the size of the mass.

The test is sensitive to the presence of aggregate and of voids immediately underneath the plunger so that it is necessary to take 10 to 12 readings over the area to be tested. The device must be held such that the plunger is normal to the concrete surface, but the position of the hammer relative to the vertical affects the rebound number because of the influence of gravity on the moving mass. Thus, for a given concrete, the rebound number of a floor is smaller than that of a ceiling, whilst inclined and vertical surfaces show intermediate values.

There is no unique relation between hardness and strength of concrete but experimental relationships can be determined for a given concrete; the relationship is dependent upon factors affecting the concrete surface, such as degree of saturation and carbonation. The Schmidt hammer test is therefore useful as a measure of uniformity and relative quality of concrete in a structure or in the manufacture of a number of similar precast members but not as an acceptance test.

2.2.3.4 Lok test.

A number of 25mm diameter metal discs are cast into the structure some 25mm below the surface. This is fitted with a connecting bolt and pulled using a hydraulic jack having a 55mm inside diameter reaction ring bearing on the concrete surface. Whilst there is some discussion of the detailed analysis of the fracture mechanics involved, what is certain is that the results are more closely related to compressive strength values, and are subject to fewer variables than with other tests. The Capo test is a variation for application to existing structures, whereby a hole is drilled and under reamed to take a compressed steel split pin, which is expanded into the groove , and pulled out as before.

2.2.4 Proof-testing.

Following statistical analysis of the data generated from the destructive mechanical testing of a suitable representative sample from the prepared batch of components one is presented with a probability of survival for a given period under given service conditions. The pessimistic view of this is that a small percentage of components will fail, within the same period under the same service conditions. With ceramic materials failure is probably catastrophic, ie the component fails suddenly, the crack, once initiated, propagating rapidly across the piece. Where such failure is intolerable, expensive or inconvenient such statistical probabilities are inadequate.

Proof-testing is a technique whereby individual samples from a batch, which are not up to specification, can be identified and removed before entering service, Davidge (1989). In its simplest form a proof test would subject components to particular conditions relating to performance requirements. The statistical analysis would be verified as some pieces would would fail, the remainder could then be expected to perform satisfactorily in service with 100% survival for the given period under the given service conditions. This would be acceptable for ceramics only if there were no time dependence of strength,this is

not the case and the fraction of specimens failing at σ_p, the proof stress, depends on the time chosen for the proof test and the rate of load, Davidge (1989). Furthermore the stresses applied during the proof test markedly weaken the weaker of the survivors of the test.

During a realistic proof test only a small fraction of the specimens would be rejected given an appropriate selection of proof-test conditions. Despite of the weakening effect of the proof test on the weaker survivors, the strength distribution of these survivors is generally greatly improved when compared with that of the original population. It would be possible under ideal conditions to give a guarantee for the performance of all the survivors, but conditions are rarely ideal.

Ideally proof-testing should be conducted under conditions where sub-critical crack growth is absent. The effects of the environment could be eliminated by testing in vacuum or at very low temperatures but this would still leave the less significant intrinsic crack growth. When crack growth occurs during the proof test, growth at the proof stress is accounted for automatically by the appropriate analysis. Unfortunately any crack growth on unloading from the proof stress can

not be accounted for and, although this effect may be small, it effectively nullifies the guarantee of performance, which can now only be expressed in statistical terms.

The situation is further complicated by the fact that most experimental and theoretical data for the strength of ceramics relate to a simple condition of uniaxial tensile stress. Many engineering ceramic components, despite the best efforts of the designer to confine loading to compressive loads only, are not subjected to this simple stress state and a multiaxial-stress state is much more common.

2.3 NONDESTRUCTIVE TESTING AND EVALUATION.

2.3.1 The Nature of nondestructive testing.

It is clear that the greatest disadvantage to these mechanical tests is the sheer number of specimens required for destructive testing and statistical analysis. This is particularly disadvantageous in the case of cementitious materials due to the higher degree of variation due to the chemical bonding process requiring a greater sample population, and the extra variable of age. The number of samples required for

statistical analysis, generally considered to be a minimum of 50 must then be multiplied by the number of ages for which data is required, to determine the number of samples required.

NDE however enables the repeated testing of each component over a period of time. Each value can be compared directly with the previous and subsequent values obtained by examination of the same item in the same location under the same specified conditions. Mean values for each age and location can be calculated with a view to quality monitoring of production and accept/ reject criteria can be applied on an individual basis thus removing substandard articles from service. For any material a laboratory study of the reaction kinetics of chemical bonding process with a view to optimising the curing process, identifying minimum or optimum ages for demoulding and finishing operations thereby optimising the manufacturing operation. The same study would also enable a simple evaluation at an early stage of curing with a view to the estimation of the projected strength of the article prior to any further effort and expense. There also exists the possibility of 100% testing and with it the ability to assure satisfactory service of all products.

The aim of NDT is to detect defects, which can be defined as flaws in

the material that create a substantial risk of failure. Whether or not a small flaw is a significant defect is determined primarily by its nature and size.

Reynolds points out that generally in comparison with metals, ceramic materials are significantly lighter and stiffer but they characteristically show low values of fracture toughness, Reynolds (1989). Their thermal and electrical conductivities are very low and many have poor acoustic propagation characteristics. Thus the physical parameters which have governed the evolution of NDT procedures for metallic artefacts are no longer appropriate, and their problems must be addressed from first principles. Different techniques are required for the examination of unsintered or unfired mouldings which may be in a friable condition and likely to disintegrate in contact with water. A further range of techniques would be required for the evaluation of large cementitious structures, with the added complications of inhomogeneities and chemical variations.

Individual significant defects in engineering ceramics may range in size from 10 to 100 μm, or defect populations may require statistical assessment. In addition, the morphology, chemical nature and

position of the defect may be decisive factors. In particular, a surface defect is generally much more significant than one of the same size situated internally, and a defect in a region stressed in tension is more likely to cause failure than if the stress is in compression or shear.

The defects generally found in ceramics are cracks, delaminations, inclusions of foreign material, voids and variations in porosity or density. Surface scratches, pits or gouges arising during machining may also be important.

Edwards advises that porosity is inevitable, because complete densification of the ceramic even with best practice sintering is impossible, Edwards (1989). Acceptable levels of porosity can range from almost 40% in alumina refractory blocks to 0.01% in fine alumina ceramics. For insulating refractories porosity is advantageous and can be induced by various means, in which case this would not be a defect condition unless the pores consolidated to produce large voids. In fine engineering ceramics, failures can be initiated from pores no more than 10 μm across.

During sintering, the loss of volatile constituents is the usual cause of

porosity. Inclusions may originate from the surroundings and the atmosphere, eg dust, insects or fragments thereof, or wear debris from the machinery used to crush, sieve and filter the ceramic powders. Combustible materials may burn off in oxidising atmospheres leaving significant voids in the structure. Delaminations and cracks caused by internal stresses may arise during shaping and firing. Stresses are also set up when a ceramic is used in conjunction with other materials, including other dissimilar ceramics, or when welding a ceramic to a metal, because gross differences in thermal expansion may occur between the ceramic and the other materials. Surface cracks arising during machining present a particularly difficult problem and place a severe limitation on the machining of ceramic components.

Critical flaw size is determined by material properties and the service conditions of ceramic components. Ceramic materials are extremely brittle and they are therefore weak when subjected to thermal shock and suffer brittle fracture on impact. This is a consequence of the strong bonds between atoms in ceramics which, whilst they impart their toughness and wear resistance, also make dislocation movement difficult and local high stress concentrations cannot therefore be dissipated. In contrast, the dislocations within metals require much

less energy to move so metals are ductile to some degree. Great care is therefore needed in designing ceramic components to avoid notches and other stress concentrations, and if possible to ensure that the ceramic is under compressive loading. Even small flaws cannot be tolerated in regions subjected to tension because fracture, once initiated, will propagate catastrophically.

To improve their toughness ceramics may be produced with second, metastable phases which lead to transformation-toughening mechanisms. Here the second phase is in a lower volume, higher density, form which is only stable at room temperature whilst it is compressed within the major phase. Should a crack impinge upon this phase, a phase transition or transformation ensues, resulting in a volume increase, thereby impeding the propagation of the crack. There is also an interest in the incorporation of ceramics into composite materials, for example by reinforcement of ceramic matrices with carbon, glass, ceramic, metal or other fibres.

2.3.2 Selection of nondestructive testing methods.

The applicability of nondestructive tests to ceramic components can

be assessed on the basis of four criteria:

i. the nature and size of the defect.

ii. the properties of the ceramic material.

iii. the type of ceramic component or structure.

iv. the conditions and restrictions imposed by the situation.

The strength of a ceramic is heavily dependent upon the size and location of the small flaws created during the material processing and manufacturing stages. The maximum permissible flaw size is difficult to determine, because of the variability of destructive mechanical test results. Statistical methods are therefore necessary to establish fracture strengths under various test conditions and a probabilistic view of failure and its consequences, and assessment of critical flaw size, must be taken.

The service conditions which drive design engineers to specify engineering ceramics generally include high temperatures and high levels of abrasion. The choice of such materials is based upon their refractory properties, ability to retain mechanical strength at high temperature, and low density. Thus the inclusion of ceramic materials in reciprocating engines would be expected to lead to greater fuel efficiency because of the possibility of higher operating

temperatures and lower mass.

The material properties and extreme operating conditions therefore dictate that critical flaw sizes are small in such applications. For many applications the maximum flaw dimension may be only 25μm. This sort of resolution requirement increases the sophistication required of the technique and drives up the expense of testing. The decision of whether nondestructive testing on 100% of components is justified, must be based upon the acceptability of the consequences of the failure of a component or structure. This would be based upon a failure probability predicted by a statistical analysis of destructive test data from a small sample of components or test pieces.

The material properties will determine the penetration of X-rays and ultrasound and the levels of noise which may obscure defect images or signals. Fortunately most special purpose engineering ceramics present few problems in this respect. Other ceramic materials may exhibit poor sound propagation properties, thus limiting ultrasonic evaluation to low frequency operation, possibly only tens of kiloHertz. Small components of complex shape are difficult to inspect with any NDT method, because the presence of geometric features may obscure defects. This problem is intensified as the frequency of the ultrasonic equipment is reduced, thus increasing its wavelength,

eventually to the same order of magnitude as the specimen to be inspected, or beyond. The difficulty is usually overcome by confining tests to specific critical areas of the component for which the geometric images or signals can be carefully monitored. This, as was explained earlier, was of particular concern in the current study, creating dificulties in the interpretation of data. The main solution to the difficulties created by these effects was to limit the frequencies recomended for practical systems to minimum values of 2MHz. This is also approaching a maximum frequency limit imposed by poor propagation of ultrasound in the material.

Edwards suggests that the conditions set out for selecting a new test method should include the following, Edwards (1989):

1. The test should be relevant.

A test capable of detecting one type of defect may not necessarily detect another. Planar defects are a particular problem because their orientation may determine whether or not they are detected. A crack has to lie in a plane parallel to the X-ray beam, for example, to create an image on the radiograph. Small pieces may be turned to eliminate this problem, this may not be so easily accomplished with large components.

2. The test should be precise.

It must be able to give quantitative data on which to base simple accept/reject criteria, otherwise it is of no use in quality control.

3. The test should be reproducible.

It may be the only way of communicating information about the severity of a defect and this may require comparisons with other tests.

4. The test should be accurate and reliable.

Otherwise, design margins have to become large, resulting in greater redundancy, less efficiency and greater cost.

5. The test should not be complex.

It must be practicable in the manufacturing environment, where it will be in the hands of less-skilled operators. Detailed analysis should be avoided or delegated to a computer, preferably in a self contained unit capable of digital readout of parameters and data logging and transfer.

6. The test should be cost-effective.

There is little point in the expense of several thousands of pounds to inspect all components in order to save several hundreds of pounds in

repair costs and downtime due to a few failures. However where a component is vital, in its true sense, cost effectiveness should cease to be an issue.

2.4 ELECTRICAL AND ELECTROMAGNETIC RADIATION METHODS.

2.4.1 Electrical methods.

Ceramic materials used for structural purposes are not normally required to exhibit any particular electrical properties, save perhaps to offer electrical resistance in some cases, and therefore values for such properties as conductance or dielectric constant are deemed to be irrelevant. However various electrical parameters may be measured, and have been shown to be indicative of the mechanical or microstructural attributes of materials. Properties such as a.c. impedance, dielectric constant, dielectric loss and d.c. resistivity can be used to evaluate materials, particularly composite materials, where the volume fraction, size, shape and electrical properties of the disperse phase govern the magnitude of the above parameters, Gerhardt (1994).

It is well known that dissimilar phases will have dissimilar responses

to an applied electromagnetic field and indeed this is the basis of many N.D.E. technologies, for example eddy current analysis, although these are generally applied to conductive materials. Eddy current methods would be suitable for measuring the thickness of ceramic coatings on metals using the 'lift-off' effect, where a test signal is created as the coil is lifted from the surface, where a resolution of the order of 0.001 mm is possible.

When such phases are intimately joined, and in three dimensions, as in composite materials additional interactions may occur dependent upon the nature of the phases and of the interface. Orientation of fibres can be expected to lead to anisotropic properties especially when the fibre content is high. In particular where the fibre is a much better conductor than the insulating matrix one may expect to find significant conduction only in a direction parallel to the long axes of the fibres. Similarly hot pressed samples may be expected to exhibit anisotropy with respect to the axis of pressing. It is important therefore in the application of these methods, to such components, that the orientation of the samples should be maintained consistent.

As the volume fraction of the disperse phase is increased the d.c resistance and the a.c. impedance of the composite may rise or fall

depending upon whether the disperse phase is a poorer or better conductor, than the matrix, respectively. The dielectric constant of the material will also tend to rise and fall over a range of compositions. Here however a further complication of frequency arises where a more linear response can be expected at higher frequencies. This is due to the tendency of lower frequency measurements to be more susceptible to localised space charge and interfacial effects than higher frequencies, which as a consequence will give more representative data for the bulk composite material.

Impedance analysis using sophisticated equipment allows the small conductivity of specimens to be determined. Capacitative measurements can be made using the ceramic as the dielectric in a simple two plate capacitor, where one plate could be a metal substrate or coating, the other plate being, effectively, the probe. Moisture levels could be problematical if not controlled, however taking a converse view, for a given material with known properties, variations in capacitance or impedance could be indicative of moisture content, and given that moisture tends to reside in pores some information on the distribution of porosity may also be gleaned.

Capacitance measurements were carried out on these materials, using a Hewlett-Packard impedance analyser, as an adjunct to the work reported in this thesis, Maturana (1988). The paste was placed in a mould cell with plates built into opposite walls. One plate was smaller than the other to ensure consistent conditions. Measurements of capacitance, and hence dielectric constant, and dielectric loss, were made during the curing process over several days, showing considerable variation in the value of the dielectric constant.

The method was used to monitor the setting process of phosphate bonded ceramic, by measuring the dielectric constant and the Dielectric Loss. The measured values of the dielectric constant values at low frequency values are dominated by the high levels of free water in the early stages. This predomination is lost as frequency increases, and the other components of the ceramic material come into play. It was possible to monitor chemical reactions and reaction kinetics during the process, and to measure the amount of alumina contained in the material by monitoring the first maximum present. The optimum frequency for this system was found to be approximately 1kHz.

The dielectric loss measurements proved suitable for monitoring the

curing reaction for the alumina filled phosphate bonded materials, but inadequate for determination of the alumina contents.

2.4.2 Optical methods.

Detection of subsurface defects in machined silicon nitride ceramics by Optical Scattering

Optical scattering has previously been used to study surface features of metals often intended for optical applications. The technique is now showing promise for application in advanced ceramics for analysis of surface features and where the material properties allow light transmission, for subsurface features and defects, Ellingson (1993).

Fundamental geometric optics indicates that on a perfect reflector the angle of incidence is equal to the angle of reflection and the reflectance is 1. However where the material is transparent or partially so the reflectance is less than 1 and a transmitted component exists. The reflected component will undergo scattering from various surface features & defects including surface roughness,

scratches, cracks and particulate and liquid residues. The transmitted component will also encounter subsurface material defects and grain boundaries and a proportion of the light will be scattered towards the detection device.

By the use of a laser light source and polarised detector systems and careful choice of relative positioning to avoid configurations resulting in high signal to noise (s/n) ratios, and optimise the surface or subsurface scattered light component, as appropriate to the mode of application, optical scattering data can be gathered. Ellingson et al have demonstrated some success in surface and subsurface analysis of defects in machined silicon nitride by this means. Refinement of their techniques should lead to the ability to detect intrinsic defects and defects originated by the machining operation in these and other materials.

2.4.3 Radio and microwave methods.

Radio wave methods can used for determining physico-mechanical properties and revealing structure defects in raw materials, pastes, cements and refractories. A variety of radio wave parameters may be

informative, such as phase, amplitude, or polarisation plane. The greatest effect has been obtained by using the phase velocity of a refracted wave as the measured parameter from which evaluation and control of the physico-mechanical properties of refractories such as apparent density, density gradient, porosity, and mechanical strength is possible, Rapoport (1994).

The phase transition radio wave method is based on the functional correlation between dielectric permeability, density, and structure, which is characterised by a change in free energy. The method is used for controlling properties of oxide and tar-bonded refractories, as well as the activity of initial powders. A correlation between the measured phase incursion of the refracted wave and the apparent density of the material in the exposure zone has been demonstrated and can be used for construction of calibration graphs. In edge zones under conditions where radio wave diffraction has a certain effect an experimentally determined correction is required in the calibration graph. The close correlation between the radio wave phase incursion and apparent density makes it possible to control the porosity of materials, in particular open porosity. The ultimate compressive strength of refractories may be evaluated from the phase velocity of radio waves. If the technological process is not stable, a second

parameter, i.e., the weight of articles, is used for more accurate determination of the mechanical strength.

The creep of refractories at high temperatures depends on certain changes in their structure. which may be revealed by measuring the phase incursion of a refracted radio wave. For estimating the extent of sintering of refractory articles on roasting, the dielectric permeability measured by the phase method is approximated to a pore-free structure. The radio wave phase method also makes it possible to reveal microfailures occurring in articles at early stages of thermocycling well before the appearance of visible large cracks. This effect can be used for quicker and more reliable testing of the thermal stability of refractories.

The radio wave method for moisture estimation is based on the dependence of the attenuation of super-high-frequency (SHF) electromagnetic radiation, with wavelengths of th order of 3cm, on the weight fraction of moisture in the material. The masking factors, such as inhomogeneity of the sample, variable grain composition, etc, affect the statistical nature of the correlation.

It is possible to use the above technique in an imaging system by the

incorporation of a scanning system, and gathering radio wave data and associated spatial data, which can subsequently by analysed using computer systems to generate an image. This has proved useful in the microstructural control of fused badellyite-corrundum refractories for glass furnace linings, Vainberg (1993).

2.4.4 Thermal methods.

2.4.4.1 Thermoelectrical and thermomechanical analysis

Properties such as thermal conductivity, specific heat, and thermal diffusivity can be evaluated for database use or production monitoring by measuring certain electrical responses of the test material. Materials required to meet specific thermal-property requirements frequently are evaluated by performing basic "pass/fail" electrical measurements that correspond to these properties. Thermoelectrical analysis can reveal significant information about the composition or microstructural condition of materials, or it can simply distinguish one material from another.

New equipment and new techniques have been developed to meet a diverse array of needs. For example, researchers at Oak Ridge

National Laboratory's high-temperature materials laboratory routinely evaluate high-temperature graphite and carbon/carbon composites by measuring thermal diffusivity and specific heat, using an automated system based on laser-flash technology to measure specimen temperatures ranging from -170 to 2,000°C, Bittence (1989). A pulsed laser beam irradiates one side of a specimen whilst temperature rise is measured on the other side. The system, automatically plots thermal diffusivity as a function of temperature. Both thermal conductivity and diffusivity can be taken as a measure of insulation characteristics,

Traditionally, thermomechanical analysis techniques have been used to evaluate properties such as thermal linear-expansion coefficient, flexural and elastic moduli, and the glass-transition temperature of materials, can be used either directly or indirectly through computer-assisted calculations of characteristics that are valuable at the production level for process or quality control. These characteristics can be included in materials specifications to meet specific design requirements, and can be used in designing new materials.

The basic T.M.A. system measures uniaxial displacement of a uniformly

heated specimen as a function of time and temperature, and hence the coefficient of expansion, by means of a probe which measures temperature while a displacement load is applied. The point at which a sample undergoes a phase change can also be identified, when the change involves an abrupt change in the coefficient of expansion. Typically, this test can show the glass transition temperature and softening point in polymers.

Further sophistication of the basic system is obtained by including torsional or bending load cells, tensile-strain measuring devices, and a variety of other sensors. Manufacturers offer modules that can be assembled to customise a system to meet particular needs, and appropriate computer software.

The ability to apply a variable or dynamic load to the specimen can reveal many useful mechanical characteristics, including the cure stage of a polymer resin. Frequencies can be selected by computer for cyclic loading, and elastic and flexural moduli, along with thermal characteristics, can be measured, to provide information on dynamic relaxation, thermodynamic equilibrium, and activation energy. Dynamic mechanical relaxation dynamic relaxation can be related to a material's toughness, allowing producers to materials to meet specific

toughness requirements. This parameter also is important in the design of pressure-sensitive adhesives for ceramic/metal/polymer bonding.

Operating on a slightly different principle, stress-pattern analysis by thermal emission (S.P.A.T.E.), introduced a few years ago, is capable of noncontact measurement of surface stress. This technique is particularly useful in evaluating materials in actual loading applications and in monitoring structural damage due to impact or fatigue loading. The method is based on a phenomenon common to many ceramics, metals and polymers, where a reversible temperature change is generated with the application of mechanical stress, Bittence (1989).

The temperature change of a cyclically loaded part is measured by infrared detection, which produces a stress map revealing relative surface-stress conditions. Stresses are calculated by means of a computer relating temperatures to various properties of the material including surface emissivity, thermal expansion, and specific heat. For materials evaluation, this technique is especially suitable to detect subsurface defects which modify surface stresses. Typical defects which can be detected include voids or cracks in ceramics and

in metal castings, debonding and broken fibres in reinforced composites, delaminations in laminates and disbonds in honeycomb composite structures. S.P.A.T.E. is also expected to prove useful in the assessment of impact or fatigue damage in materials, and the automotive and aerospace industries have expressed an interest.

2.4.4.2 Infrared Thermography

For ceramic materials and particularly for composite materials an assumption may be made that volumetric material defects, inhomogeneities, particle agglomerations and anisotropy due to fibre lay-up direction can be detected by monitoring the infrared wavelength spectra emitted by localised hot and cold regions. The data can be displayed in the form of isothermal contour lines on a map or plan of the surface of a material. Colours can be ascribed to temperature regions on the isothermally mapped surface, by appropriate computer software, greatly facilitating the interpretation of the information and identifying suspect regions in the artifact.

Infrared thermography may be used as a passive technique, where externally applied heat is allowed to thermally conduct through a

material of interest. The alternative is an active method where a non-thermal energy source is used and this energy is transformed into thermal energy within the material. Both of these techniques will produce the surface temperature gradients which are representative of the aforementioned internal material defects and anomalies. The active monitoring technique can be used in conjunction with a non-contact, real-time sensor unit. With the use of this sensor, temperature gradient values can be calculated with a sensitivity of ≈0.2°C. Data processing with the real time infrared thermography system can include frame averaging, either over the total surface area of the material of interest, or in the area where the most damage is expected (i.e. a stress concentration cross-sectional area).

Post-testing data processing can be performed on video-taped data in order to calculate point and linear temperatures and emissivity values of specific specimen locations where material damage was observed, Boving (1989), Gianaris (1991).

Sumitoyo industries have patented a method of evaluation of specific heat of samples at ambient temperatures and the comparison of this value with a standard. This comparison is subsequently analysed with reference to standard data to infer values of various mechanical

properties including creep strength. Yamikawa (1993). A method of applying thermography to poor thermal conductors such as concrete brick or fibrous composites using an array of infrared heaters and the subsequent observation of the cooling process by means of a thermal imaging camera has been patented, Milne (1991).

Infrared thermography has found application in various materials including the study of electrical contacts in use, insulators and refractories, Deperrois (1988), and the monitoring of fatigue in thick composite materials under compressive load, Gianaris (1991).

Thermography was carried out on samples of phosphate bonded ceramic in conjunction with British Airways, using an infrared heat source behind the sample. Concentrations of porosity large flaws and cracks could be imaged, Anjorin (1988).

2.4.5 Radiography.

Edwards advises that the radiological test procedures used on ceramics are different from those used on metals for three reasons:

1. Because they are made up of elements of low atomic number the X-ray absorption coefficient of ceramics is lower than that of metals. The image contrast improves when using low energy X-rays, typically less than 50 kV.

2. The image contrast of inclusions is low, because they too are made of elements with a low atomic number.

3. The critical flaw size in ceramics may be of the order of 25 μm and this is beyond the resolution capabilities of conventional radiography.

Micro-radiography is then necessary and there are two methods:

Contact radiography:

This method uses a conventional single wall-single image technique with the object in contact with the radiographic film, but with a long film-to-tube focus distance. This reduces the geometric unsharpness or penumbra to a limit, where definition of the image on the film is governed only by the energy of the X-rays and the graininess of the film. By using the radiographic films designed for lithography and spectrography, which have an ultra-fine grain size and an emulsion on one surface only, the images can be optically magnified 200 times for

viewing and yet retain good image quality. However, there is some loss in image quality because of the large amounts of scattered radiation reaching the film.

Projection radiography:

This method places the object close to the X-ray tube and projects the image over a distance of typically 2m on to the radiographic film. To reduce the geometric unsharpness to acceptable levels, the focal spot size in the X-ray tube is as small as 10-100 μm in diameter. With a magnification of 40 X, a lateral resolution in the image of 20 μm is achievable.

The projection technique using a micro-focus X-ray tube is preferable to a contact technique using a conventional X-ray tube because there is less scattered radiation reaching the film and this improves image quality. The method is suited for use with an image intensifier to capture a video image instead of using radiographic film. Digital image processing of the video image can improve the inherently poor defect contrast in ceramics. There is also the possibility of real-time imaging and scanning of the component. Unless real-time imaging is used, the method is suitable for off-line inspection only.

Radiography is sensitive to volumetric flaws in ceramics if the kV is low and the image can be magnified. Cracks may be detected with ease when appropriately orientated, ie substantially along the axis of projection of the X-ray beam, but otherwise only with difficulty. The geometry of the component may make interpretation of the radiographic image difficult, if defect images are superimposed on images from geometric features, but this is true of any material. The visualisation of the bulk porosity, and the detection of inhomogeneious distribution of porosity and constituents, particularly fillers and aggregates whose densities differ substantially from that of the matrix is readily achieved. Contact radiography techniques were used to help characterise the material and to verify findings for publication during the course of this research, Round (1988a).

X-rays are widely used to inspect metal structures and can also be used successfully on ceramics. Although X-ray methods are easy to apply to items such as firebricks, most NDT on such components is done by ultrasound, which is cheaper and simpler, and in real time. With larger structures such as refractory lined pipes and precast concrete blocks, X-rays are more commonly used, but since it is still usually necessary to bring the specimen to the X-ray machine, rather than vice-versa, very large structures tend to be inspected using

gamma-ray techniques. Gamma-ray back scattering can be used to measure the density of refractories, with the significant advantage that access to only one surface is required. It is possible to produce a plot of density against distance from the surface, which is extremely useful in locating cracks and poorly bonded areas.

2.4.6 Computed tomography.

The development of many new materials and processes is generating a need for improved nondestructive inspection technology. Conventional methodologies, (ultrasonics, radiography and visual), may be inappropriate or inadequate for many advanced materials. New inspection methods such as computed tomography (C.T.) are needed to characterise properties and defects of advanced materials and processes. C.T. provides quantitative volumetric measures of density, constituents and dimensions, and offers considerable potential to reveal three-dimensional information, potentially useful for design, manufacturing, inspection and analysis.

In conventional radiography, a source of radiation, X-rays or gamma–rays, is used to project a shadowgraph image of a three

dimensional object onto a two dimensional film. A real-time alternative is to display the two dimensional image on a cathode ray tube. In either case information in the image is superimposed, and a skilled interpreter is often required to examine the image, if useful data is to be acquired, Georgeson (1991), Phillips (1993).

In computed tomography, a partially collimated, thin "fan shaped slice" of radiation is passed through the object, and the transmitted intensity measured by a detector array which is suitably curved and orientated. The object is rotated and translated relative to the source, in order to obtain views from all aspects, about the object. The data is sent to a computer and the computer reconstructs the object interior, as if it were sliced open. The image data points are small volumetric measurements directly related to the X-ray linear attenuation coefficient of the material present in the volume elements defined by the slice thickness and the cross-sectional resolution capability of the C.T. system. The interior of the object is visualised in its true dimensional orientation. From sequential, multiple slices taken over the whole part, a complete three dimensional image can be built up and suitably displayed, normally in a two dimensional format. The advantages of C.T. lie in the ready interpretation of complicated geometries and quantitative nature of the data for dimensional and

density information. It can be used for density or constituent variations with excellent sensitivity. Dimensional measurements are a common application of C.T. and can be quite accurate in the typical range of 0.050 to 0.25 mm.

C.T. offers considerable potential for nondestructive evaluation, but it requires more sophisticated and precise equipment than other NDE methods, thus the overall cost of C.T. data acquisition will generally be high. However, C.T. can be cost effectively applied to many advanced material applications.

New materials or products usually involve an iterative cycle of manufacture and testing to bring the manufacturing process under control. Understanding the interior configuration of a new product or the effect of a new process on materials and dimensions is key to the development of the product. Because C.T. allows for quantitative measurements of material density and dimensions, it is ideal for providing important information on many advanced material processes.

Accurate dimensional analysis with cross-sectional image information can reduce development cycle times considerably, thereby affording considerable cost savings. This is particularly true for new

composite developments where C.T. provides critical information on the location of resin variations, consolidation, porosity, voids, delaminations and, in some cases, wrinkles.

Many polyamide matrix resin composites contain cracks and separations which, in some cases, would be very difficult to evaluate with other N.D.E. methods, but C.T. is easily able to image these defects.

Engineers can thus apply the information obtained by these methods to modify manufacturing processes for optimisation of production. Cost savings are difficult to quantify accurately for C.T. as an enabling technology, but they are real and significant. In one example, C.T. conservatively represented better than a 25% reduction in the development cycle costs for a new graphite epoxy/kevlar wrap design, Georgeson (1991).

As flight technology heads toward higher speeds, there is an increasing interest in oxygen protection of carbon composites, such as silicon carbide coated carbon-carbon composites used for high temperature aeroplane surfaces. Methods for inspecting the coatings and the composite underneath need to be developed, and C.T. has the potential to meet this need. There exist a number of review articles

indicating the widespread application of C.T. techniques to a variety of materials including turbine blades and intercontinental ballistic missiles Bossi (1991), ceramic turbocharger blades, Arnold (1991), glass and graphite /epoxy aerofoils and panels for aircraft Georgeson (1991), Sheppard (1990, 1991), and the assessment of impact damage in aerospace composites, Potet (1988). On a more mundane level, and perhaps more appropriate to the materials of interest here, C.T. technology has been applied to the evaluation of porosity in portland cement, Draper (1994).

In collaborative efforts between computer scientists and material scientists the various theoretical aspects of computer analysis and display technology have been studied, Engler (1990), Crostack (1987), and algorithms have been developed to glean further useful information, for example the quantification of flaw volumes in ceramics, Stinson (1993).

X-ray tomographic microscopy (X.T.M.) is an advanced development of the C.T. technology already discussed, which allows the materials scientist to observe, in three dimensions and microscopic detail, the interior of materials, Ashley (1993), Ekenhorst (1993). The technique is nondestructive and non-invasive and as such does not interfere with

any forming processes and microstructural development, thus allowing observation and study of such processes. Ellingson and Co-authors, have applied 3D microfocus x-ray computed tomography technology to the task of mapping density and fibre distribution variations in chemical vapour infiltrated SiC/SiC continuous fibre composites and their effects on mechanical properties, Ellingson (1992a and b).

The technique has been used to observe the step by step fabrication of SiC/SiC composites by means of forces chemical vapour infiltration. Widespread use of these strong, refractory materials has been hampered by the high costs resulting from difficulties in controlling process parameters to reliably produce acceptable products. A knowledge of the composite's growth and consolidation should enable materials scientists to better control the process. Potential applications include not only ceramics and material science in general but also medical studies on bone diseases e.g. osteoporosis and bone development.

Throughout this section the C.T. techniques discussed have involved a collimated, flat fan shaped beam of X-Rays, together with rotational and translational movement of the subject relative to the X Ray source with either or both mobile. There exists an alternative technology in

cone-beam tomography which employs a divergent conical beam of X-Rays as in radiography, Smith (1990). The impetus for the application of this technique is its three dimensional data acquisition abilities, which results in a considerable time saving on acquiring sufficient data for processing into three dimensional representations, and the reduction in inaccuracies due to misalignment of sections. Due to the divergence, the theory and algorithms developed for fan beam and parallel beam C.T. is not totally adequate, and this fact has hindered its widespread application.

2.4.7 Nuclear magnetic resonance imaging.

Kudryavtsev and Pyatkova, studied the degree of hydration by means of N.M.R. relaxometer spectroscopy, but there are many techniques which can analyse samples to identify phases, Kudryavtsev (1989). However few methods exist to similarly analyse bulk material in artifacts or structures. Ultrasonic attenuation analysis, as discussed elsewhere in this thesis, offers some prospect of success but N.M.R. spectroscopy is a more established technique, although this technique is limited to small samples.

In such spectroscopy applications an accurately defined homogeneous fixed field is employed. If a field incorporating a gradient and a particular nucleus type, say hydrogen protons (often referred to as ^1H) in water, is present throughout the specimen in greater or lesser amounts then the frequency of the ^1H response would vary throughout the sample. Data gathered in such circumstances would contain information about the gradient and distribution of ^1H protons within it, thus encoded within the data is sufficient spatial information to produce an image mapping the distributions of such ^1H protons and hence water molecules within the specimen, Akitt (1992).

This development in N.M.R. techniques for obtaining spatially dependent N.M.R. information, has given rise to magnetic resonance imaging, (M.R.I.). This has made a particularly significant impact in medical applications, but the technique is also employed for the study of materials in general. N.M.R. microscopy is a development of M.R.I., and is a growing field where micron resolution is now feasible in suitable samples, Smith (1996).

The M.R.I. technique relies on spatial discrimination within a sample arising from the resonant frequency variation that occurs in the

presence of a magnetic field gradient G(xyz). The signal from resonant nuclei separated by a distance ∂z in a magnetic field gradient G(z) will differ in frequency by $\gamma G(z)\partial z$, where γ is the gyromagnetic ratio of the nuclei, and the resulting frequency spectrum will therefore provide a means of mapping the spin density. The spin density profile is thus determined along the direction of the applied gradient. A combination of slice selection, using an initial 90° pulse in the presence, say, of G(z) followed by a projection along G(x) can be extended to two- or even three-dimensional images by repeated measurements with different projection directions and then using back projection techniques to produce the image. More efficient methods using two-dimensional Fourier transformation are now more commonly used where back projection is no longer required for image reconstruction. This is probably more favourable since it can map space more evenly than the back projection method.

The medical application of M.R.I. has been greatly assisted by the liquid-like nature of the human body. Liquid state N.M.R., with its narrow resonance lines permits the sensitivity associated with narrow bandwidth techniques to be exploited. Mammalian tissue is largely water, about 55% overall in human tissues, and this is

distributed in different proportions in differing tissue types and furthermore its mobility varies thus making such managing techniques applicable to medical use, which was the first application developed and which remains perhaps the most important aspect of N.M.R. imaging technology. The relaxation times of water protons in living materials are, however, quite short and much signal intensity may be lost unless the signal intensity is enhanced using spin echo techniques such as magic angle spinning (M.A.S.) Akitt (1992).

In ceramics and other solid materials special techniques are required to deal with the associated broad resonance lines. Imaging resolution will be limited by the natural linewidth of the sample. The shorter the transverse relaxation time, T_2, the broader is the resonance line, and therefore a greater frequency separation is required to resolve spatially, signals from different groups of nuclei. The limit of resolution occurs approximately when $1/\pi T_2 = \gamma G(z)\partial z$. To image solid-like materials a solution usually relies on one or two approaches. Either special artificial line-narrowing techniques are used, or large field gradients and fast switching circuits are employed for both RF and possibly gradient systems. Both methods also require powerful RF pulses and any approach has so far been limited to small

samples (≈l cm^3) due to the heavy power requirement.

Although some success has been achieved in special cases using magic angle spin (M.A.S.) methods in solids, achievable M.A.S. rotation rates are insufficient to narrow the broadest lines, and multipulse methods are generally required. Perhaps the simplest and most direct technique is to use the very large field gradient (≈40Tm^{-l}) available in the fringing field of a superconducting magnet. An excitation pulse of duration t excites a bandwidth of $l/t = \gamma G(z)\partial z$ and spins within a slice ∂z. With a 90° pulse of 10 μs in 40Tm^{-l} a proton resolution ∂z of 15μm is predicted even in a solid. A stepper motor can be used to move the sample through the sensitive plane of resonance to produce stray field imaging. The method also renders internal background gradients negligible and is therefore valuable for very heterogeneous (e.g. porous) materials, as in this thesis, and those exhibiting large paramagnetic susceptibility. This method has provided the best resolution to date, but is very slow and requires physical movement (translation and rotation for three dimensional imaging) of the specimen. Techniques are now reasonably well developed but await exploitation for serious materials investigation.

Whilst three dimensional imaging information can be acquired by the methods outlined above, the data is generally displayed in a two dimensional format, and thus a plane is defined whose data is gathered and whose image is so displayed. Three dimensional images are built up plane by plane and by means of computer manipulation and graphical techniques a range of data for many planes is built up and can be displayed as a three dimensional projection in a two dimensional format. Further manipulation can result in other aspects or orientations and planes in alternative axes.

Gathering data to enable the production of such an image takes an appreciable time, several tens of minutes, depending upon the resolution and definition required. This necessitates a reasonably static subject. Rhythmic processes such as beating of the heart can be observed if the data gathering can be synchronised with the process.

To produce such an image the subject must be placed in a strong magnetic field and subjected to rapid changes in field gradient and to strong short radio frequency pulses. This has not been found to have any adverse effects upon human tissue and metabolism, and is thus in this respect far superior to X-ray examination and imaging.

The N.M.R. imaging technique is, as already indicated, capable of operation down to microscopic scales. The resolution obtained with such N.M.R. Microscopy is of the order of 30x30μm much less than that obtainable with optical microscopy but different materials are imaged by the two techniques and it is envisaged that living organisms may be imaged and things such as water uptake can be observed. This technology can also be applied to inorganic materials water or other liquid infiltration into porous materials can be images and studied. This would give much information on microstructure particularly the distribution of porosity.

The slip casting process in ceramics has been observed and studied using N.M.R. imaging techniques, Hayoshi (1988). Alumina slip cast in cylindrical plaster moulds was sequentially imaged, in a plane perpendicular to the central axis. The deposit was found to be clearly distinguishable from the slip and the mould due to differences in relaxation time and its thickness could thus be monitored with time.

With such a large number of organic chemicals present in the slurries of ceramic powders, these chemicals interact. The complexity of the bulk and interface interactions of powder water inorganic impurities,

and organic surfactants are not well-understood. These interactions lead to inhomogeneties in the suspensions and green body in the form of agglomerates, a non-homogeneous distribution of surfactants, voids and chemical segregation. These inhomogeneities, once formed in the green state, remain in the final ceramic; thus they form defects in the sintered ceramic. These defects are considered to be the main cause of the problems associated with the repeatability of the manufacturing processes. Wang (1993).

In advanced ceramic components, the failures often occur due to defects such as voids and large-scale chemical segregations undetectable by conventional methods. Nuclear magnetic resonance (N.M.R.) imagining is an emerging technology which provides a unique material-diagnostic technique by in situ, internal mapping. It can provide information not only on the material distribution (nuclear spin density), but also on the chemical and physical characteristics of these materials (nuclear spin relaxation times). In a ceramic green body, the binder distribution is a critical parameter that affects the final ceramic's mechanical, thermal and electrical properties, and its reliability. An understanding of the interfacial reactions between the binder and ceramic powders under various processing parameters is essential to alleviate binder distribution problems in ceramic

processing technology.

Most of the physical flaws in the vast range of fibre filled ceramic composites originate in the forming of the green compact. In addition, local variations in the distribution of fibres or whiskers in the matrix affect the densification behaviour of the green compact, and may cause large flaws in the material due to differential sintering. Therefore systematic inspection of the composite material in the green state is essential for the production of reliable components.

The application of non-destructive nuclear magnetic resonance (N.M.R.) imaging to slipcast samples of SiC fibre-reinforces ceramics for detecting physical flaws such as fibre agglomerates and open pores. Spatial resolutions of $70x70\mu m^2$ have been achieved by using high-field instrumentation and suitably selected signal acquistion and echo times, Karunanithy (1989a and b). Ellingson and various co-authors, Ellingson (1992 a and b), applied N.M.R. spectroscopy and multinuclear solid N.M.R. technology to the analysis of the surface condition of the fibres and that of the fibre-matrix interface in SiC/SiC continuous fibre composites.

N.M.R. imaging has also been used to obtain quantitative information regarding the bulk distribution of SiC whiskers in whisker-reinforces ceramics, in addition to detecting other physical flaws such as open pores or hard inclusions , that may inadvertently be included during sample preparation. Karunanithy (1991).

The considerable advancements which have been made in the medical and biological applications have been accomplished because the samples involved contain water in a mobile state. This is also the case for the slip casting process and to a lesser extent with green ceramic artifacts prior to firing, and as indicated some useful information has been acquired by exploiting this technology. However, due to the nuclear-dipolar broadening in solids, the development of N.M.R. imaging for application to solid materials has been difficult.

In hard solids like ceramics the linewidth due to nuclear-dipolar interaction is often a few thousand times larger than in mobile samples because of the restriction in atomic motion. Consequently, line narrowing and large field gradients are two factors critical to a successful N.M.R. imaging technique for solids.

Considerable efforts have been made to develop various techniques for

the improvement of line narrowing in N.M.R. spectroscopy. These techniques are readily applied to imaging so that a better resolved solid image can be achieved. They range from the development of a multiple-pulse sequence to multiple quantum coherence. However, line broadening still remains as an obstacle to N.M.R. spectroscopy in solids. Thus a large magnetic-field gradient is required to offset line broadening for a useful resolution in N.M.R. imaging, Wang (1993).

2.5 SONIC AND ULTRASONIC NONDESTRUCTIVE TESTING AND EVALUATION.

2.5.1 Acoustic emission.

Acoustic emission (A.E.) differs from the foregoing methods in that it is not an 'interrogative' technique. It is not possible to examine an unstressed component or structure, therefore it is necessary to stress the component in some fashion and monitor cracking which may occur. When a crack is initiated, a displacement wave is generated which propagates through the material and may be detected by a sensitive ultrasound transducer to yield a range of 'A.E. parameters'. Further emissions occur as the crack propagates. These parameters can be processed to yield useful information concerning crack damage to

ceramics.

Whilst there is considerable scope for developing the technique for ceramics, attempts to detect cracking or dislocations during the curing of chemically bonded ceramics, ie listening to the setting process, were inconclusive due to the lack of a lock out system to eliminate extraneous noise. Acoustic emission test methods would provide a way of improving the sensitivity of current proof-testing methods by providing information of sub-critical flaws.

2.5.2 Acousto ultrasonic methods

The acoustic emission method depends on loading to excite spontaneous stress waves such as those accompanying plastic deformation and crack growth. Acousto-ultrasonics, which term may be taken as a contraction of "acoustic emission simulation with ultrasonic sources," differs mainly in that benign ultrasonic waves are generated externally by a pulsed source, usually a piezoelectric transducer.

The general approach to acousto-ultrasonic testing is the use of a pair of ultrasonic piezoelectric probes in a send/receive configuration, a

pulsed sending probe, optimised for wave generation, and a receiving probe, optimised for signal sensing. The usual, and often most convenient, arrangement is to have the probes on the same face, coupled at normal incidence to the surface of a test piece. The receiver is displaced by a fixed distance from the sender, and in the limit of zero separation, this configuration reduces to conventional pulse-echo ultrasonics. The send-receive transducer pair is usually moved about as a unit and the test object is scanned to map material property variations, Vary (1989, 1991).

Acousto-ultrasonics differs from conventional ultrasonic methods primarily in the nature of the received signal. Once launched inside the material sample, the pulsed ultrasonic waves are modified by stochastic processes like those which affect spontaneous acoustic emissions from internal sources during stressing, deformation, etc. Moreover, acousto-ultrasonic waves are launched periodically at predetermined times and with predetermined repetition rates. Thus instead of well-defined wave reflection and propagation paths, as in flaw detection, the received signal will be the complex result of multiple reflections, and interactions with material microstructure and features, in a volume of material between the sending and receiving probes. Bulk and guided waves and several types of plate

waves can arise and flexural Lamb waves will tend to dominate in composite panels. In these cases, the wavelength will be comparable to or less than the major dimensions of the sample, such as thickness. Pure plate or Lamb waves are unlikely because wave generation is is broadband pulsing, not long-duration, single-frequency. Moreover, lamina and fibre-matrix interfaces will break up the wave-propagation paths, thus producing stochastic wave propagation, which is desirable because it ensures repeated wave interactions with microstructural features and diffuse flaws. For composite panels, this means that overlapping, scattered, and mode converted signals will arrive at the receiver.

Selection of the sending transducer centre frequency and the receiving transducer bandwidth and sensitivity are pivotal to successful evaluation. For composite panels, it is advantageous for the sender to produce wavelengths which are less than the thickness. This is to ensure that there are multiple wave interactions with diffuse flaws and microstructural features within the test volume. This may also entail high ultrasonic frequencies which are quite strongly attenuated, and the receiver must therefore be very sensitive, and have a bandwidth covering all of the frequencies passed by the sample.

For many graphite fibre polymer matrix composite laminates both the sender and receiver may be broadband 2MHz transducers. A bandwidth of about 1MHz may be adequate to characterise these materials, however, experimental determination of appropriate transducer properties should be made for each new structure. In highly attenuating materials the receiver may need to be a sensitive transducer of the type used for detecting acoustic emissions.

The acousto-ultrasonic technique depends strongly on establishing reproducible probe coupling. Otherwise, signal modulations due to material variations become confused with those due to coupling variations. Probes are usually coupled to a surface with a thin film of fluid, such as glycerin, gel, silicone grease, and shear wave couplants, and sufficient pressure must be applied to eliminate unwanted reverberations within the couplant. In addition, deleterious effects of surface roughness must be overcome. Similar precautions are needed with dry coupling which usually involves a thin elastomer buffer, e.g. silicone rubber, bonded to the transducer wearplate.

There are obvious disadvantages to the intermittent contact required with direct coupled (dry or liquid) probes. The potential need to scan large surface areas demands probes that can be readily moved about.

Using probes with the piezoelectric crystal mounted in the hub of a rubber-rimmed wheel allows continuous rolling contact scanning, rather than simply lifting and repositioning the probes. Even then, great care has to be taken to ensure that coupling variations are insignificant.

The prospect of contactless laser probes, particularly for scanning large complex surfaces, is very attractive. However the use of lasers to excite and acquire acousto-ultrasonic signals does not eliminate potential coupling problems because the signals are still influenced by surface roughness and also emissivity, reflectivity, and other thermal and optical factors.

In acousto-ultrasonics, quantification of information contained in the simulated stress wave is achieved by calculating a stress wave factor (S.W.F.). There are many ways to define and calculate the S.W.F. and this definition, in any particular case, depends on the nature of the signal, test piece (including material, size, and shape), types of flaws, damage states, and the nature of the mechanical properties to be assessed.

Because acousto-ultrasonic signals often resemble acoustic emission burst waveforms, it has been found to be practical to use

signal-analysis methods based on acoustic emission practice. For example, time domain quantities such as rise time, peak voltage, voltage decay or ringdown count, and root-mean-square voltage values tend to correlate with defect states and material properties. Spectrum analysis and statistical analysis on spectral mean values, second and third moments etc. can also form a basis for defining the S.W.F.

The techniques described above have been applied to various materials and situations including damage assessment of composites, Talreja (1989), monitoring thermal shock damage in alumina and zirconia toughened alumina, Konsztowicz (1990), Thompson (1991), porosity in glass systems, Aduda (1996), evaluation of cement quality in oil well installations, Gai (1993), modelling the mechanical responses of ceramic composites, Kautz (1989), Tiwari (1995), and the monitoring the effects of inclusions in glasses, Jen (1996).

Flaws common to ceramics such as inhomogeneities microcracks and voids together with poor interphase bonding, delaminations and disbonds, which are particularly problematical in ceramic composite materials, lead to a decrease in stress wave energy transmission. Acousto ultrasonic techniques have the potential to detect and

measure the sate of defect or damage in a material and thus offer a means of detecting the effects of these properties nondestructively.

Das et al have explored the potential of acousto ultrasonics to evaluate in a nondestructive manner the condition of aluminosilicate castable refactories based on fireclay grog and calcium aluminate cement subjected to thermal shock damage, Das (1991). These authors calculated a stress wave factor, and considered this as a measure of the efficiency of the stress wave energy transmission in thermally stressed material, and thus an indication of the continuous propagation of cracks in the cementitious materials.

These materials have much in common with the materials studied herein and these techniques could well prove useful in future N.D.E. strategies.

2.5.3 Resonant frequency techniques.

Many solids, including ceramics and composites can be made to resonate mechanically by vibrating them at specific frequencies depending on their physical properties and geometry. The resulting

spectrum of mechanical resonances contains a wealth of information about the sample's elastic properties, internal friction, structural integrity, and shape. With a recently developed technique called resonant ultrasound spectroscopy (R.U.S.), developed at Los Alamos National Laboratory, this information can be accurately obtained in a single measurement, Migliori (1993), Maynard (1996). This is of particular importance for the characterisation and nondestructive evaluation of many advanced materials such as polycrystaline ceramics, single-crystal materials, and anistotropic composites, which typically have more than one pair of elastic moduli. To fully characterise these materials using conventional dynamic modulus measurement systems, such as pulse echo techniques, requires multiple laborious tests on large samples, which are not always available.

An R.U.S. measurement is capable of the determination of all elastic moduli of very small (0.001 cm^3), possibly anisotropic, samples from 1.5-600 K. In addition, information is obtained concerning dimensional errors. Most simple solids require only two parameters to fully describe their elastic responses. Typical pairs of parameters include, for example, Young's modulus and the shear modulus, the bulk modulus and Young's modulus, or Poisson's ratio and the shear modulus.

However, many anisotropic materials require more than two parameters to adequately characterise their elastic response.

To make a measurement, the samples are first polished or otherwise shaped into rectangular parallelepipeds, right circular cylinders, or spheres with tolerances for parallelism, roundness, and the like, of about 0.1%. Such tolerances are readily obtained using an ordinary milling machine or surface grinder. The shaped sample is then mounted between two diamond/lithium niobate composite ultrasonic transducers, thus forming , in effect, an electromechanical bandpass filter for which sample resonances determine the pass frequencies. Optimal results are obtained if the sample contacts the transducers only at its corners and if the contact force is less than 10^{-3} N. The transducers are specially designed for this application. Coupling fluids are not required, an advantage where samples are porous or affected by water ingress, and the low contact pressures would be essential for weaker materials in the earlier stages of processing. This dry edge- or point-contact mount also eliminates any transducer bond correction or bond failures at nonambient temperatures.

The transfer function of the transducer/sample assembly (essentially it is sharply peaked at each resonance) is measured using an

automated, stepped, thermal-noise-limited superheterodyne detection system also designed specifically for this application. For maximum accuracy, processing algorithms are used to determine the centre frequencies and widths of each peak by using all the data points that trace out the peak shape.

The measured frequencies of the peak or resonances of the sample are determined by its geometry, density, and elastic moduli. Computer codes based on novel non-finite-element methods were developed to determine the resonance spectra for rectangular parallelepipeds, spheres and cylinders. These codes take very little computational time while providing high accuracy compared with conventional finite-element computational methods.

However, the inverse problem of finding moduli from resonances is much more difficult, particularly if some resonances are missed or if the sample has dimensional errors or high ultrasonic attenuation. The solution requires a sophisticated multidimensional non-linear optimisation scheme in which the elastic moduli are varied until the difference between the measured and fitted frequencies is made as small as possible.

Carbon-carbon (C/C) composites are particularly suitable for structural applications in high temperature environments. In comparison to conventional composites, the fabrication process of C/C composites is rather complex, due to the multiple steps involved in the carbonisation and densification cycles that the composite is subjected to after the initial impregnation of graphite fibres with the matrix precursor. While going through these cycles, the composite's microstructure and properties change resulting in the formation of a composite with wide ranging mechanical, physical and thermal properties.

In practice, the change in density of the composite during processing is used as an indicator of the change in material condition. An increase in density directly corresponds to an improvement of mechanical properties. Such an evaluation does not account for potentially problematical, localised variations in the material microstructure. Density variation is normally measured using destructive techniques, which are time consuming and expensive. There is hence a definite need to consider alternative means of assessing the integrity of C/C composites during the processing stages. The effectiveness of nondestructive vibration-based measurements in determining the changes in microstructure and

mechanical properties that occur during the processing of C/C composites has been demonstrated by Vaidya and Raju. The vibration-based parameters used by these authors were material damping and resonance frequency, Vaidya (1994).

In their technique, beam specimens were mounted at their geometric centre on an impedance head connected to an electrodynamic exciter, driven by a random noise generator. After the first carbonisation and densification cycle, the resonance frequency value increased and was found to be close to the value for the cured composite. In the successive processing cycles, the resonance frequency decreased with each carbonisation cycle while it recovered to higher values, approximating those ascertained for the cured composite with each densification cycle. After the fifth carbonisation cycle, it was observed that the values of the resonance frequencies did not change notably.

Measurements of damping were performed at the first four flexural modes of the specimens. For all processing stages of the composite, damping ratio values were found to be higher at higher flexural modes. The density of the composite was found to have decreased when compared to its value obtained in the previous stage, with each

carbonisation cycle, and was found to increase after each densification cycle. The maximum density attained at the fifth carbonisation cycle did not alter notably with further processing.

The vibration parameters, resonance frequency and damping ratio values, were found to be useful in determining changes in the material during processing. A strong qualitative correlation between different parameters, namely density, dynamic modulus, resonance frequency and microstructural changes of the composite during processing, was observed.

Another, apparently more simple, resonant frequency technique, J.W. Lemmen's grindosonic technique is an easily applied resonant frequency test using a point contact probe, again requiring no couplant. The specimen is set into various modes of vibration mechanically, by a blow from a suitable small hammer or rod, Wolfenden (1989), Lemmens (1991). The force of the blow is of such low magnitude that the stresses produced lie well within the tolerance of the materials. Any components damaged by such low levels of stress would be unfit for service and thus this risk of damage is of no consequence. The system determines the resonant frequency of vibration, and given the necessary parameters, of suitable cuboidal specimens, or other simple

regular geometric forms, the on board computer system gives a display of velocity. Both shear and compressional velocities, and hence elastic moduli, can be determined, and displayed, depending on the relationship between the point transducer and the location of the hammer blow.

For more complex shapes the system is applicable for a rapid pass/fail test based on experimentally determined parameters using specimens known to be of good and poor quality. Such a technique can be applied rapidly, by persons with minimal training, and a 100% testing of all components can be achieved at minimal cost. Indeed the level of expertise applied by selectors in the whitewares industry, tapping and listening to the sound produced and visually inspecting the pieces, exceeds that required for what is a much less subjective test.

There is currently much interest in the use of various thin film coatings, diamond for example, applied by chemical vapour deposition and sputtering etc. for various purposes. Such coatings are frequently impure, porous, of an unwanted phase, eg graphite rather than diamond, or otherwise imperfect. An important requirement in the application of such technology is a suitable means of characterisation, difficult when dealing with a coating. A measurement of the elastic constants

of a film would be ideal since all of the above faults would reduce the stiffness and affect their values. Theoretically the ultrasonic resonances in various modes can be manipulated mathematically to yield such a range of elastic moduli values, Kawishima (1992). Chandra and Clyne report on a simple method of measurement of these resonance values, by means of the Grindo-sonic equipment, on elongate subsrate samples before and after deposition of such coatings, with some success.

2.5.4 Ultrasonic testing.

To take a simplistic view at this stage, the velocity of sound in a solid material is a function of the square root of the ratio of an appropriate modulus of elasticity, E, to its density. Various relationships which can be used for the determination of the moduli of elasticity and Poisson's ratio, and hence as a means of checking the quality of the material, are discussed in chapter 3.

The apparatus generates a pulse of vibrations at an ultrasonic frequency which are transmitted by an electro-acoustic transducer held in contact with the surface of the sample under test. After

propagating through the material, the vibrations modified by their interactions with it, are received and converted to an electrical signal by a second electro-acoustic transducer, or the same transducer in many cases. The signal is fed through an amplifier to a cathode-ray oscilloscope for display and interpretation, or to data logging and other circuitry for more stringent analysis. The time taken by the pulse to travel through the material is measured by an electrical timing-unit with an accuracy of 0.l μs or better, and, knowing the length of path travelled through the material, the pulse velocity can be calculated.

It is necessary to have a high-energy pulse of vibrations to give a sharp onset waveform because the boundaries of the various material phases within the material cause the pulse to be reflected and weakened. At any interface mode conversions occur such that longitudinal or compressional waves, transverse or shear waves, and surface waves may all be produced. These may be monitored and data used to increase the range of parameters generated, see chapter 3.6.

For maximum sensitivity, the leading edge of the longitudinal waves is detected by a receiving transducer located on the face of the material

opposite to the emitting transducer; this is direct transmission, and is sometimes referred to as the pitch and catch method. An alternative method requires only one transducer, which operates as the transmitter and the receiver alternately, and interrogates the material by its interaction with the sound passing through the material twice, following reflection from the far boundary, or indeed any intermediate boundary. This method, often referred to as the pulse-echo method, gives extra information, particularly in relation to defect size and location, and can be used when access to two opposite sides of a specimen is not possible. The disadvantage of this method is that the energy received is lower than with direct transmission, and in grainy materials with poor propagation properties, such as the material with which this thesis is primarily concerned, noise due to backscatter can mask the doubly attenuated signal, making interpretation very difficult.

The basic ultrasonic pulse velocity apparatus is shown in figure 2.2 and more specific details and diagrams of the equipment employed during this research work are given in chapter 6.2.

In the case of cementitious materials both lack of compaction and a change in the water/cement, or other component ratios can be

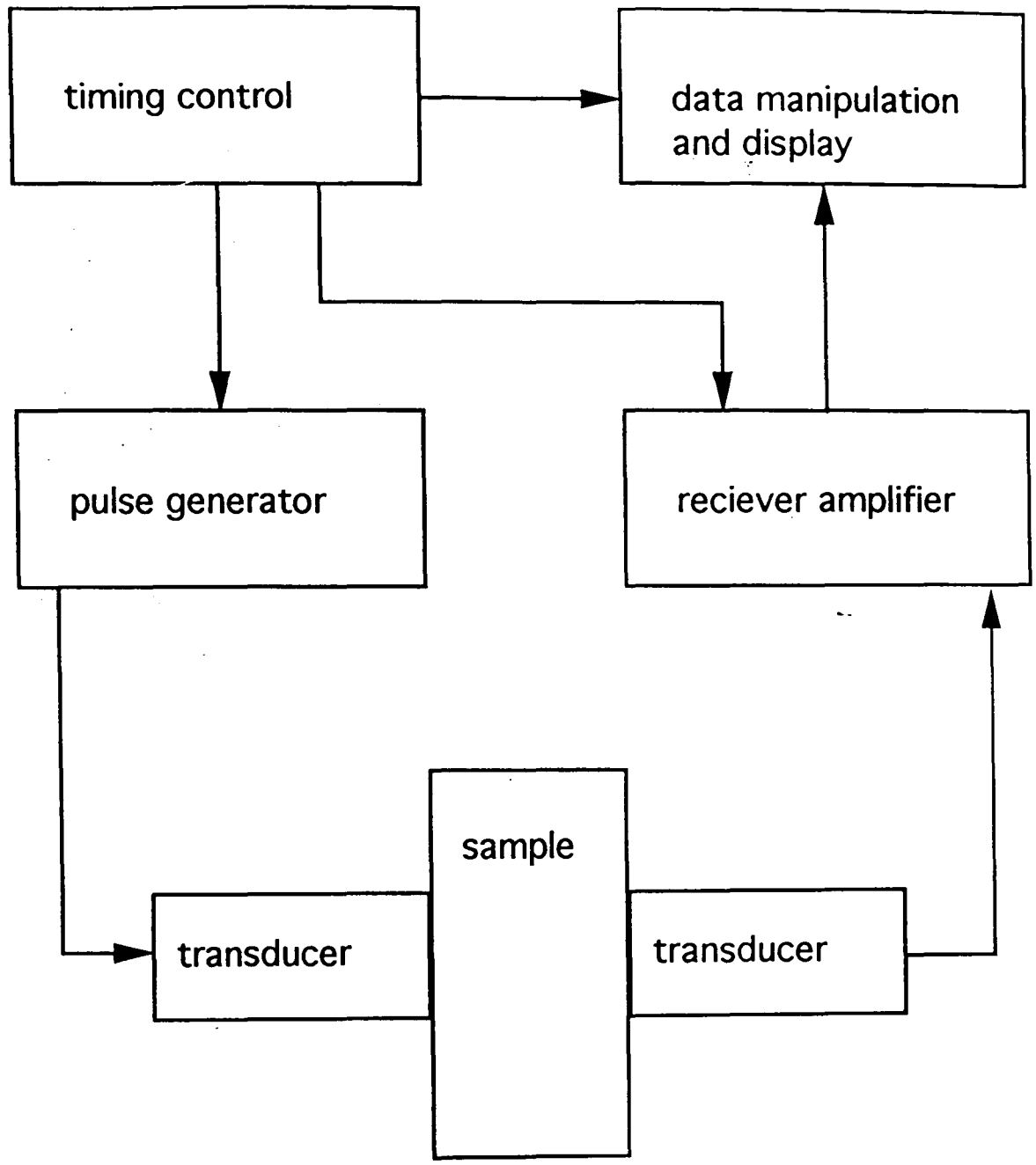

Figure 2.2 Block diagram of a basic ultrasonic apparatus capable of flaw detection and velocity or thickness measurement.

detected. Unfortunately the pulse velocity is difficult to apply as a general indicator of compressive strength because, for example, the type and grade of aggregate or filler and its content in concrete greatly influence the relationship between the pulse velocity and strength. Other factors affecting the relationship are the moisture content, age, presence of reinforcement and temperature. The pulse velocity technique finds important applications in bulk concretes for the detection of crack development in structures such as dams, and checking for deterioration due to frost or chemical action.

For fine or engineering ceramics ultrasonic tests offer the most promising methods for inspection of ceramics. Such fine ceramics have a lower attenuation coefficient for ultrasound than metals, though this is not the case for traditional ceramics and far from the situation with regard to the chemically bonded ceramics with which this thesis is concerned. The high impedance mismatch between voids and the surrounding ceramic material ensures high reflectivity of incident ultrasound pulses, although planar defects must lie in a plane near the perpendicular to the sound beam axis if they are to be detected. To refract the sound beam into a ceramic accurately is more difficult than with metals. The high acoustic velocity in ceramics angles the refracted beam sharply away from the normal

with only small changes in the angle of beam incidence.

2.5.5 Dry coupling techniques.

There are several difficulties associated with the ultrasonic evaluation of porous ceramic materials, and these are particularly problematical in green ceramics, or cementitious materials in the early stages of curing. For example, low-frequency sound waves are not scattered sufficiently to allow the detection of flaws much smaller than 1mm in size, on the other hand, sound waves with frequencies of 3MHz or greater generally undergo excessive attenuation in samples in excess of 3mm thick. Also, ordinary couplants (e.g. water or glycerol) are often absorbed by green ceramics, this not only mitigates their coupling function, but may also affect the subsequent fabrication process. This problem can be avoided by using pressure alone to couple the transducer to the specimen, but great care is required because the applied pressure can affect the data, or even result in sample breakage, Kupperman, (1984), Bhardwaj (1990).

In spite of these difficulties, studies of ultrasonic attenuation and

acoustic velocity in green ceramics may provide useful information related to density variations, porosity content, presence of agglomerates and delaminations, elastic anisotropy, and material quality in general. Further development of ultrasonic testing techniques, coupled with signal enhancement techniques, may lead to improved flaw detection sensitivity.

Dry coupling probes usually consist of a conventional transducer with a piezoelectric element and a plastic material in front of it which allows for a good sound transmission into the object under test. This plastic material must be selected carefully to achieve optimal probe features. Whereas at the transducer side it can be coupled by a fluid, on the side of the test object it must give good ultrasonic contact without any coupling medium. Therefore, the plastic material must be soft to conform closely to the surface of the test object by slight pressure, it must have low acoustic attenuation, and it must be strong enough not to wear off or to deform significantly under pressure. A soft silicon rubber was found to meet all the above mentioned conditions, and it can be cast into any shape and then fixed in front of the transducer by suitable means.

The dry coupling probes have been developed for three different types of operation: one single crystal probe in pulse echo mode; two single

crystal probes in through-transmission; and a twin crystal probe in pulse echo mode.

For normal incidence, the single crystal transducer has a silicon rubber delay line fixed to its emitting surface which is coupled to the transducer by a thin oil film. The delay line causes good near surface resolution, as the interface echo becomes small, when the probe is coupled to a material of low acoustic impedance. For the transmission of angle beams, a standard angle beam transducer is equipped with a thin foil of silicon rubber at its contact surface. The foil is also coupled with oil to the transducer and does not change its original angle of incidence.

These probes with a fixed delay line or foil can be used only for measuring at discrete points as the friction of the silicon rubber on the surface under test is normally too large to scan the probe continuously. A much better performance is obtained by the application of wheel-type probes. In such wheel probes, an ultrasonic transducer is placed inside the wheel and a thin oil film couples the sound to a special tyre on the wheel. The tyre is manufactured from silicon rubber and is sealed against a rim. The tyre is sufficiently soft to give a flat contact to the object under test for the whole

active area of the transducer, when the wheel probe is slightly pressed down. Using two of these wheel probes and arranging them properly in a fixture on both sides of the test specimen, a continuous scanning in through-transmission is easily accomplished. The diameter of the wheel for a 1MHz probe is about 50mm and the width of the tyre is 12mm.

If the access to the material under test is only possible from one side and continuous scanning with good near surface resolution is required, then a dual crystal, wheel probe is the best solution. This type of probe consists of dual transducer elements inside the wheel which has its acoustic barrier arranged perpendicularly to the wheel axis. Care must be taken to ensure that the acoustic isolation between the transmitter and receiver crystals is not impaired by the tyre in front of the dual element transducer. With good design, the crosstalk level could be kept sufficiently low to detect small delaminations close to the surface of the test object. The wheel diameter of a 4MHz probe is likely to be around 50mm and the width of the tyre is likely to be around 20 mm.

Attempts to link the pertinent material properties of finished sintered ceramics to those of the green formed piece have been made in order to

enable manufacturers to eliminate poorly formed pieces prior to further costly processing, Jones (1985). Kulkarni, (1994a, 1994 b).

In order to avoid sample contamination by couplant absorption these authors developed dry coupling techniques for both longitudinal and shear waves, using an elastomer as a coupling agent, thereby considerably reducing the applied pressure, from the values required by Kupperman, to acceptable values, which are well within the tolerance of the material. Order magnitude differences were thus observed between green and sintered materials. The presence of hard agglomerates could be detected in the green and partially densified states, but not in the fully dense state, Jones (1986).

Paper products can be affected by liquid couplants more severely than ceramics thus prompting the use of dry contacted techniques, one of which, the use of fluid filled wheel probes offers the prospect of easy examination of large structures and possibly a technology transfer to the monitoring of tape cast ceramic substitutes etc. Brodeur (1994).

In this technique probes are set in the centres of fluid filled flexible rubber tyres as described previously, a pair of matched probes being placed on opposite sides of the paper sheet.

The data collection techniques and subsequent analysis effectively eliminate the tyre thickness and fluid thickness. This technique could be modified to examine cast tapes and a single probe method could be applied to the scanning of larger ceramic and cement structures where access is available on one side only.

As an alternative to techniques involving dry contact probes it is possible to protect the material using some kind of impermeable barrier. Initial evaluation on the phosphate bonded samples was effected with a grease as the couplant, which then became a barrier and thus enabled the use of aqueous gel couplants. However this altered the surface of these samples and could not be considered truly nondestructive, and is certainly not noninvasive.

Some success has been achieved in coupling ultrasonic transducers to alumina samples using a fluid couplant and an adhesive tape as a barrier, Yamanaka (1988).

This method was indeed tried, but with little success because the surfaces of the samples were not sufficiently smooth to eliminate any air gap, the attenuation in the signal was thus too high for adequate

sound propagation.

Another barrier technique involving the packaging of the sample in an evacuated polymer film enclosure has been developed, Roberts (1987), Fraser (1991). This enables fluid coupling and even immersion techniques to be applied. The disadvantage is the inability to package large items and monolithic castings.

Dry contact probes have also been used for ultrasonic C-scan imaging, for moisture sensitive aerospace components where moisture contamination could adversely affect the material properties, Rogofski (1991).

Amorphous silicone based gels are acoustically similar to water yet sufficiently rigid to maintain a shape and remain non wetting. These can be used as couplants for ultrasonic transducers, particularly where aqueous couplants are inapropreate in porous materials and materials prone to such degradation in the presence of water. This method of coupling thus lends itself to examination of green ceramics, porous ceramics and chemically bonded ceramics prone to such degradation as indeed are the phosphate bonded materials in this study.

This silicon gel coupling medium can be applied to C-Scan techniques whereby a block or sheet of the silicon material is placed in contact with the porous ceramic material. The probe is coupled to this material with a thin layer of aqueous couplant in order to allow sliding contact during scanning, Wright (1995).

As already mentioned grease was used but found to be messy and difficult to remove from the sample. Some types of rubber were tested but the signal attenuation was increased in comparison to grease. Silicon sealing mastic was found to be the best of these materials in this respect. It was decided that whilst messy grease worked well in the first instance, subsequently it was possible to utilise aqueous couplants with the remnant layer of grease acting as a surface barrier preventing fluid absorption. However for a production situation the silicone couplant would probably be preferable as grease would be unacceptable. Finished samples with surface coatings would not present such problems and aqueous gels would suffice.

Capacitance transducers have been developed as receiving transducers, Hutchins (1985), whereby the probe is one plate of a capacitor. This is located above the material under evaluation any ultrasonic displacements adjust the air gap and hence the capacitance of the

system.

The air gap capacitance transducer has more recently been demonstrated to act as a generator of ultrasound, and contrary to popular belief has been shown by Schindel and Hutchins to be capable of operation with dielectrics, Schindel (1995). The sensitivity with metals is low and in the case of dielectrics the sensitivity is two orders of magnitudes less, thus limiting the application possibilities.

2.5.6 Ultrasonic imaging.

Ultrasonic C-scan inspection is an important tool for the NDE of these structures since it allows high-resolution imaging of subsurface regions, which would otherwise be inaccessible with the conventional techniques of optical or scanning electron microscopy.

Essentially , a C-scan image provides a two-dimensional view of a specimen in which differences in image contrast from the object's interaction with an impinging acoustic wave.

Various techniques such as ultrasonic holography, interferometry,

acousto-optic scattering of light , one and two-dimensional arrays and scanning laser acoustic microscopy have been used to generate C-scan images, Gordon,(1993).

The acoustic energy is coupled from the transducer into the sample by a liquid, usually water. A number of techniques to avoid immersion have been tried, including the use of elastomer probe faces, vacuum packaging of test specimens in elastomer membranes, Roberts (1987), and the use of silicon rubber sheets in conjunction with liquid film couplants, Wright (1995), as discussed in relation to dry coupling techniques.

Data, in the form of returned signal amplitudes, are collected along a two-dimensional grid as the transducer is raster-scanned over the specimen. Electronic gates can be set to extract selected echoes from the entire return signal, and these data are then used to vary the intensity on a monitor, which can be printed to paper. Magnification or reduction can be achieved by scaling the scanning grid.

The sample surface should preferably be smooth to within a wavelength of the interrogating beam. At high frequencies, this means that the samples are typically polished to optical flatness.

To eliminate inclination problems, many commercial C-scan software packages offer a surface following routine. This feature can be used to adjust dynamically the gated return from an inclined sample, so that variations in path length between the sample and transducer are removed from the data. Even more sophisticated scanning systems can control the transducer movement through many degrees of freedom and enable the transducer to follow curved surfaces. Most such scanning systems employ guides and actuators enabling movement in three axes independently or in combination, in the fashion of an overhead factory crane. Manipulation of the probe to adjust its aspect to the aspect of the surfaces under scrutiny is also frequently necessary. Another method of obtaining a scan is by the use of a serial link robotic arm, after the fashion of a JCB agricultural trench digging and loading machine. This technique is particularly suited to mounting on a remotely controlled roving vehicle for NDE of large structures, Fan (1995).

C-scan systems can be configured in a variety of modes such as a pulse echo, through transmission, and angle beam using either plane or focused wave transducers. The pulse echo mode employs a single transducer to send and to receive an acoustic wave, the image that is

developed depends on the variation in acoustic impedance experienced by the wave.

When the electron gate is set to collect echoes corresponding to a certain depth, or perhaps an interface, the C-san image becomes a plane view of a slice of the specimen where the slice thickness is proportional to the width of the gate.

In the through transmission mode, two con focally (focused) or con axially (plane) mounted transducers are used, and the image contrast is derived primarily from differences in attenuation experienced by the acoustic wave as it passes through the entire sample.

Clearly, if a pulse echo image is made from a back wall reflection, then the image is analogous to a through-transmission image. However, in the pulse echo case, the wave has passed through the sample twice, and is therefore more attenuated, and is more sensitive to irrelevant sources such as backwall roughness and geometry.

Using high frequency ultrasonic transducers operating at frequencies of the order of 100MHz, and precision X-Y-Z scanners to give high resolutions, small ceramic products such as integrated circuit chips

and their mountings can be imaged. Such techniques are capable of imaging disbonds, delaminations and holes with diameters of the order of 10μm, in ceramic metal interfaces, electrical connections etc. in such integrated circuit chips, and other composite components, Nonaka (1989).

Such techniques are also capable of imaging fine porosity in advanced ceramics such as silicon nitride and silicon carbide, and have been applied not only as an N.D.T. technique but also as a means of monitoring the densification as sintering proceeds, Generazio (1989).

Ultrasonic velocity C-scans complement conventional defect and amplitude C-scans. Velocity scans display elastic modulus variation caused by non-uniformly distributed microporosity within ceramics. With composite materials, velocity C-scans can also provide information concerning percent fibre volume and matrix porosity.

In many cases, the information derived from velocity C-scans cannot be derived from amplitude C-scans or from radiography. Also , velocity C-scans are more repeatable and less sensitive to material surface roughness and transducer frequency than are amplitude

C-scans. Furthermore, velocity C-scans often require less calibration and setup time than amplitude C-scans.

Using a pulse echo technique it is possible to produce longitudinal wave velocity C-scans in one scanning operation when the test specimen has uniform thickness. The time of flight is measured within the specimen, and the ultrasonic velocity is simply twice the thickness of the part divided by the ultrasonic time of flight. When the specimen does not have a uniform thickness, the longitudinal-wave velocity C-scan is produced by dividing a specimen-thickness C-scan by the time-of-flight C-scan.

Thus when a part has nonuniform thickness, a velocity image cannot be directly constructed from its time-of-flight C-scan without first constructing a thickness-variation C-scan. To measure thickness variation within parts with inhomogeneous composition, the distance between the transducer and the specimen surface is estimated by measuring the water-path flight time. Shear wave velocity C-scans can also be made by rotating the specimen through 30-50° to produce shear waves by mode conversion.

Combining shear and compressional velocity C-scan data by suitable computer aided techniques allows the production of C-scan maps of

elastic moduli, local material density and elastic module values being estimated from longitudinal velocity C-scans. Fibre volume fraction and porosity maps of uniaxial fibre reinforced graphite epoxy composites have also been produces using dual velocity C-scans. This technique has been applied to produce velocity C-scans of hot pressed titanium diboride and sintered silicon carbide, Gruber (1988), Kunerth (1989).

Ultrasonic velocity C-scans have also been applied to slip cast silicon nitride ceramics in the green state. This required a dry contract technique involving a silicon rubber protective layer enabling sliding contract with a thin layer of couplant, Wright (1993, 1995)

Progress in ultrasonic imaging depends not only on the advancement of ultrasonic techniques and technology but also upon advancement in signal processing and computer technology. Such techniques serve to enhance the image whilst maintaining processing times at reasonable values. Scanning can be eliminated by the use of transducer arrays at the expense of more complex processing techniques with algorithms to reduce the processing time, Ozaki (1987), Paradis (1987).
Other workers have applied these techniques towards enhanced images, optimising the ultrasonic techniques employed and using more

effective processing techniques to derive more information from fewer data taken over reduced times, Crostack (1987), Hanstead (1987).

2.5.7 Laser generation and detection of ultrasound.

Recently much effort has been expended on the development of lasers as sources and receivers for nonconducting ultrasonic measurements. Telschow (1990a). In order to use ultrasonics for characterisation of microstructural features in ceramics, high frequencies (short wavelengths) must be employed to obtain sufficient scattering from the often small grains and porosity. Also it is often necessary to have highly distinguishable features in the ultrasonic waveform to use for velocity and attenuation measurements, such as well separated wave pulses or sharp spikes. When a pulsed laser is used to generate ultrasonic waves in solids by the thermoelastic mechanism, the resulting elastic displacement waveform is wideband, and contains such distinct features only at the times of arrival of the longitudinal and transverse components of the initial thermal expansion.

The use of laser ablation as an ultrasound source produces a high amplitude, sharp spike waveform with large bandwidth, which appears

at the longitudinal arrival time. This spike is readily used for both velocity and attenuation measurements. Unfortunately the ablation method can cause surface damage, although sometimes this can be alleviated by ablating a surface coating, such as oil, from the sample. However, this is not always feasible, especially in the processing environment, where the noncontacting nature of the laser ultrasonic technique is particularly useful, and may well be the major consideration in the choice of this method.

Under appropriate conditions, a small, but relatively sharp, spike has been observed involving only the thermoelastic generation regime. The source of this spike , which has been termed a precursor, has been attributed to thermal diffusion from the source point. Dewhurst (1982). This was verified by doyle who provided a qualitative explanation for its occurrence, Doyle (1986).

Most ceramics have a significant optical penetration depth, which alters the thermoelastic generation mechanism. This can be used to advantage. Thermoelastic generation at the surface produces an elastic wave radiation pattern with large directionality away from the surface normal, whereas ablation produces its largest wave motion in the direction of the surface normal. Therefore, for through

transmission or pulse echo measurements the ablation mechanism is preferred, and is easily produced in ceramics due to their small thermal diffusivity compared to metals, but at the expense of undesirable material surface damage. However, in ceramics which exhibit a large optical penetration depth, the thermoelastic mechanism itself produces a significant component of the ultrasonic wave in the direction of the surface normal because the thermoelastic expansion extends into the material. This subsurface expansion produces a significant normal surface motion, Telschow (1990b).

Telschow et al applied laser generation and detection of ultrasound to the monitoring of sintering of ceramics using a conical, Fabry-Perot interferometer, to detect the ultrasonic waves on the surface of the samples. Such a detector is sensitive to the Doppler shift of light, reflected from the sample surface, which is moving due to the ultrasonic wave. An argon ion continuous laser was used to illuminate the sample surface, a small portion of which was diverted for electronic stabilisation of the Fabry-Perot cavity length with respect to the laser frequency, such that the operating point was maintained on the side of the interferometer transmission curve.
The output of the interferometer was detected by a photodiode which yielded a signal proportional to the frequency shift of the light

scattered from the moving surface with respect to the stabilisation point. The electronic stabilisation corrected for the laser drift and low frequency instability due to ambient vibrations of the apparatus.

Such a detection scheme is self referencing, i.e., the photodiode signal originates from the interference of light scattered from the sample surface and delayed portions of that light within the Fabry-Perot interferometer. Since all of the optical wavefronts are nearly identical to those scattered from the sample surface, light from a relatively large surface area (about 4mm^2) including many speckles is collected efficiently. The detection scheme thus has the sensitivity required for detection from rough and/or optically diffuse material surfaces, such as are encountered in ceramic materials in general and "green" state ceramic materials in particular. Increasing the detection laser power can compensate for much of the lack of specular reflection due to this rough sample surfaces

Telschow et al undertook studies of the sintering of zinc oxide, starting with green state samples which were pressed to approximately 47% of theoretical density in disks 25mm in diameter and 8-10mm thick. The green state samples were ablated significantly by the source laser at the energy levels required for

adequate detection signal to noise ratio. Therefore, the ultrasonic response of the green state samples was recorded with a minimum of signal averaging, usually 10 pulses.

Their measurements were of the time of flight of longitudinal ultrasonic waves propagating through the sample, as it sintered. In order to determine the sample average density from these measurements, it was necessary to know the sample thickness and the effect of density and temperature on the ultrasonic velocity. Since heating in the sintering process generally takes place from the surface towards the centre, the internal temperature gradient would tend to cause nonuniform density during the sintering process. The time of flight of the ultrasonic wave would thus be an average value, over this nonuniformity, and could not resolve the density variations.

During the sintering process, the ultrasonic measurements could be used to determine the average density of the sample in real time. With an assumption of uniform, isotropic shrinkage, the sample thickness can be taken to be directly dependent on density during sintering, thus allowing the calculation of both average density and shrinkage of the sample as it sinters. During sintering, the ultrasonic time of flight and material dimensions decreased significantly as the

material's density and wave velocity increased.

From measurements made on fully sintered samples, these authors found that the longitudinal wave velocity is essentially temperature independent (to within 5%) over the range of temperatures from ambient to 1100 ^{0}C. Therefore, no correction for temperature was considered necessary.

Ultrasonic velocity measurements thus provide a direct measure of the densification of the material during sintering which can now be easily and quickly determined by use of the noncontacting laser ultrasonic measurement of densification. This then allows the direct monitoring of the sintering process as a function of both time and temperature.

During investigations on ceramic components at Rolls Royce, using ultrasonic technology capable of finding defects of the order of 50μm, to a depth of some 25mm, in advanced ceramic material, it was found that many of the test pieces had experienced cracking during the actual test process itself, Butcher (1993). This problem was not, however, confined to locations which had encountered particularly high stresses during the testing procedure. Significantly, the defects were

located at points were the artifact had been clamped, or had been subjected to a high contact load during the post forming machining process.

Thus it was assumed that residual stresses developed during the machining process, and not subsequently relieved were at the root of the problem. When during the test process, the component had been heated, the stresses were redistributed, and the material cracked as a consequence of these differing stresses. The defects were therefore not, in fact the cracks, but the residual stresses which had caused them. The crack depths in fact proved modest, not more than 5 microns, but they nevertheless propagated to swiftly cause failure.

Ultrasound and laser technology can be combined to provide an efficient means of inspection and detection. With ultrasonics it is possible to fine-tune control of the depth of penetration by altering the magnitude of the acoustic wavelength. Laser technology, as discussed above, can generate a high frequency ultrasonic wave of great constancy,

Thus when a laser is beamed across the surface of the material to be tested, the acoustic waves which it generates increase in speed over

the defective areas. A second laser can be employed to monitor the increases in wave speed and thereby record the location, depth and level of residual stress in the material under examination.

One of the big advantages in using lasers for the propagation of acoustic waves is that they obviate the need for piezoelectric materials; sonic energy can be introduced into the test material directly, avoiding the hazards of inaccuracy which can be encountered in couplings using more traditional methods. Thus high quality evidence can be collected with relative simplicity. There have been other applications of similar techniques to ultrasonic measurements at high temperatures, see for example Dewhurst (1988).

Linking laser generation and detection of ultrasound with fibre optics technology could overcome problems associated with the mechanical vibration of the object under test, control of the ultrasonic beam characteristics, and ease problems of access in larger components and structures. Vogel and Bruinsma have discussed such a fibre optic laser ultrasound system to address these problems and others associated with imaging techniques, Vogel (1987).

2.6 APPLICATION OF NONDESTRUCTIVE TEST METHODS TO CERAMICS.

2.6.1 Nondestructive evaluation of green and sintered ceramics.

Bell, in a review of nondestructive testing of refractories, Bell (1989) suggests that when embarking upon any kind of programme designed to improve service performance by materials testing (either destructive or nondestructive), a clear-minded approach is necessary. NDT can provide a great deal of interesting information but only some of this is useful. Basically, there are two approaches which are employed. The first is to establish which properties are important and then devise a nondestructive method to measure those directly. A good example is crack detection by ultrasound.

Such a simplistic approach can seldom be employed and the inference of an important property from measurement of a related parameter is much more common. Examples include strength prediction from resonant frequency measurements, and density estimation from X-ray or gamma-ray absorption or back-scattering. Such an approach is clearly much more practicable but requires extensive background work and theoretical knowledge in order to succeed. The best results will be obtained where the property measured or inferred is particularly relevant to the application. Cold crushing strength or

flexural test results (frequently referred to as modulus of rupture, MOR) are often quoted on data sheets supplied by virtually all manufacturers of ceramic materials. They are clearly of little relevance for refractory materials designed (and defined) to be used at high temperatures, and the loading of any component is unlikely to correspond to that experienced in the flexural test. Such measurements of "strength" are however widely accepted as a "quality control parameter", where a value close to the expected value is taken as indicative that other diverse properties such as density, thermal conductivity, hot strength, porosity, hardness, will lie within acceptable bounds. In this way, simple and relatively cheap tests can be used to gain information about properties which would be much more difficult to measure. It should be noted that a "strength" value higher than expected is as indicative of property variation as a value lower than expected. Furthermore, since in many cases an improvement in one parameter is obtained at the expense of detrimental effects upon others, variations above or below accepted bounds should be treated with equal scepticism. NDT methods currently available can be indicative of strength, density, crack location, abrasion resistance, structural integrity and permeability to air.

Bell asserts that in general it is not possible to locate flaws in refractories by the pulse-echo technique, although many attempts have been made, including successfully measuring the thickness of paving flags. Ultrasonic examination undertaken at British Ceramic Research Ltd (now Ceram Research), using 1 MHz high power signals gave acceptable results for fired products under ideal conditions, but no clear back wall echo could be detected with castables. Bell concluded that this technique was not suitable for use in the field to detect cracks, voids, etc. The refractories of interest to Bell are very similar acoustically to the chemically bonded ceramics with which this thesis is concerned, making his observations particularly relevant, although I would not altogether dismiss the pulse echo technique having achieved some success, albeit in small samples. He observes that correlations between ultrasound velocity and crushing strength are often very good, and that the technique is applicable as a control test for strength estimation. Accuracy in strength estimation can be improved if ultrasound measurements are combined with density measurements, Reynolds (1984 a).

Cracks and larger defects may be detected by the through transmission technique, which is more suited to porous grainy materials. There are two reasons for this, firstly the path length is halved, and secondly,

and perhaps more importantly whilst the sound wave is attenuated due to scattering the scattered sound does not give rise to noise as it does in the pulse echo technique, where the doubly attenuated backwall echo is masked by echoes due to scattered waves returning to the transducer, now in receiving mode.

Various workers have developed techniques for particular applications, both for research and quality assurance purposes. Some of these are briefly discussed below, begining with the use of ultrasonic techniques to study the slip casting process, through to automated on line technology.

Slip casting is a commonly used forming technique found throughout the ceramics industry from earthenware to advanced single oxide and nitride ceramics. The ceramic material in the form of colloidal particles is dispersed in water and poured into a mould made of plaster in most cases. The mould being porous removes the water from the slip causing a build up of a cake, the square of whose thickness is proportional to the casting time. The constant of proportionality is highly variable even from cast to cast in the same mould. Thus it would be useful to monitor the casting process on line. This has been accomplished by Hutchins and co authors, using an

ultrasonic immersion probe to monitor the thickness of a flat bottomed cast, Hutchins (1989), Appleton (1991).

The casting thickness as a function of pH was also investigated, this being a factor on the flocculation or deflocculation state of non-clay ceramic materials, and thus affects the rheological properties of immense importance in ceramic casting processes. The cake structure, porosity and permeability have also been studied by a similar technique, Haerle (1995).

As already mentioned the immersion probe is immersed in the slip and monitors the thickness of the bottom section of the cast. In commercial slip casting process such access is not always possible and bottom sections are not always flat. It would thus be useful to monitor the cast thickness from without, though preferably through the bottom of the mould such that moulds passed over a fixed transducer as part of an automated controlled sequence in a production line.

Sintered structural ceramics are susceptible to thermal shock damage in the form of microcracks which can propagate leading to eventual failure. There is a critical temperature difference for the initiation

of thermal shock damage, beyond which there is an increase in the severity of the damage with an increase in the magnitude of the thermal shock, as measured by the magnitude of the abrupt temperature change. Such thermal shock damage has been estimated by the use of ultrasonic amplitude and shear and compressional velocity measurements, Hefetz (1992). Elastic anisotropy due to preferred crack orientation could be estimated along with the critical temperature difference for the particular material under examination.

Another area of application of ultrasonic NDE is in the detection and evaluation of surface breaking defects, for example following machining. Such defects even when very small, 50-100μm, can prove critical to the survival of highly stressed, specialised components in crucial situations. These defects are smaller than those deemed to be critical in similar metal components, due to the different elastic behaviour of the materials and also to the fact that ceramic components tend to be developed where metallic components prove to be inadequate. The machining process whilst problematical in providing a further source of defects is of great importance in the production of ceramic materials to precision engineering tolerances. Ultrasonic investigations on sintered silicon carbide and hot pressed silicon nitride, using Leaky surface waves, have shown that the

probability and ease of detection of such defects depends upon the type of material under test and the inhomogeneities in the surface, such as porosity and surface roughness, in relation to the size of the defects, Winterfeld (1993). This type of evaluation tends to require high frequencies, of the order of 10-100MHz, hence short wavelengths of the order of the defect size or smaller, to increase the resolution to cope with such small defects. However a simple increase in the ultrasound frequency does not automatically lead to certainty of location of very small defects, due to the inhomogeneities discussed above, thus it may be necessary to determine, empirically, the probability of defect detection for different materials and surface conditions. Winterfeld et al concluded that that the testing frequency for surface defect evaluation should be selected such that it is sufficiently high as to detect the critical defect size with the required degree of certainty so that an optimal testing frequency is used.

Whilst a considerable amount of research effort has been applied to the nondestructive testing of advanced ceramics and composites, and to the nondestructive evaluation of novel ceramics and composites to facilitate research into various aspects of their formation, processing

and property development there has been comparatively little development or application in the traditional clay based ceramics, and this has been largely confined to the refractories sector, Bell (1989). This is understandable in terms of their cost and non-critical applications, however since the technology exists, following development elsewhere, ultrasonic NDE is being applied, increasingly more frequently and successfully to these materials. Ultrasonic shear and compressional velocity measurements have been used for the characterisation of sintered clay based porous ceramic materials, and the variation in shear and compressional velocity with porosity determined, Roth (1991), Panakkal (1992). From these the elastic moduli and poissons ratio were evaluated, and the variation of these parameters with porosity compared with values derived theoretically from elasticity and scattering models. The approach of these authors to these studies was substantially similar to that taken here in relation to the cementitious materials of interest.

Edwards describes two ultrasonic test systems developed for inspecting ceramics: a high frequency immersion testing system and a computerised ultrasonic system, Edwards (1988).

The ultrasonic immersion testing system with a capability for testing

ceramic turbine blades employs ultrasound at a frequency of 50 MHz. Magnification is achieved by spacing the raster scans made by the probe across the test surface at only 2 μm apart and then expanding the C-Scan image on a video screen. The C-Scan is a sound amplitude map of the test object created by monitoring the amplitude of a reference echo from a glass plate placed beneath the object. Problems with curved specimens, eg turbine blades can be ameliorated by the use of a computer-controlled scanning table which has three axes of translational and one of rotational movement.

The computerised ultrasonic test facility has recently been installed at Toyota Motors to inspect a ceramic precombustion chamber. The system is totally automated. The components drop on to a turntable on which they rotate inside an assembly of ultrasonic probes. The component and probe assembly are immersed in water to give an ultrasound coupling medium between transducers and component. As the component rotates, one set of probes moves axially down the cylindrical sides of the component and another set moves radially across the flat end surface. The defects sought are pores on the external and internal surface of diameter greater than 50 μm. Five ultrasonic probes cover the critical areas. They propagate ultrasound with a frequency of 15 MHz, providing adequate sensitivity

to detect small defects. Some are focused and others have collimated sound beams to improve spatial resolution and reduce echoes from geometric features in the component.

Control of the test sequence is by computer. The axial scans are made at 0-5 mm increments. The data are taken from the A-Scan at each 1-6° angular displacement. A total of 19,350 data points is thereby collected in 8.8 s. For the radial scans, the increments are 0.25 mm per revolution with a similar 1.6° angular displacement between readings of the A-Scan. This results in a further 21,725 data points acquired in 9.9 s.

The data from each of the five probes are processed and the results displayed as either a C-Scan image or a line scan. The information can be used for statistical quality control of the manufacturing process.

Neither of these techniques, and there are many other examples, would be applicable to the chemically bonded ceramics of interest as they are too costly, the envisaged components are too large, they would be harmed by prolonged exposure to water, and a drying station would be required.

The ultrasonic testing of dense advanced ceramics is generally accomplished using test equipment operating at frequencies of 10-50MHz. The method is sensitive to most defect types, particularly planar ones, as long as the sound beam is incident along the normal to the defect plane. Material properties present few problems because of the low ultrasound attenuation coefficient. The geometry of the component can make ultrasound coupling difficult and it may not be possible to scan over complex surfaces. Defect resolution is poor if the defect lies within a few microns of the surface. Computer aided signal processing makes the method suitable for application to on-line inspection.

2.6.2 Nondestructive evaluation of chemically bonded ceramics.

As technology advances and ceramics enter more critical fields of application, quality control of their manufacture will become more important. As part of this quality control, NDT has a role to play but perhaps more important is nondestructive evaluation (NDE). NDE extends beyond the physical test methods and includes an evaluation of all the parameters which affect component performance, both in the manufacturing processes and the service conditions.

The quality of engineering ceramics is generally susceptible to subtle and minute changes in chemistry and microstructure during processing and therefore NDE methods with a high level of defect sensitivity are needed. Chemically bonded ceramics are even more susceptible to chemical and physical inhomogeneities and variations from day to day and structure to structure, governed in ways currently poorly understood, and dependent upon, amongst other factors, moisture content, humidity, temperature, and process parameters. Conventional NDT methods cannot provide this level of sensitivity without considerable refinement of the techniques. This may be accomplished for example by using microfocus radiography or ultrasonic immersion tests at frequencies of 50 MHz.

However the most versatile and most promising evaluation techniques employ ultrasound, with current applications ranging from metallurgy to maternity and electronics to elephants, why not carbides to concrete. Ultrasonic test methods are the most sensitive to cracks and delaminations but clusters of small defects can be difficult to resolve. By increasing the test frequency, defects of small size can be detected, but with a loss of penetrating power of sound below the surface. With porous and grainy materials this is not an option as

scattering and wave attenuation become problematical, and limit the frequencies used to 5MHz and preferably lower.

Ultrasonic techniques have, in fact, been applied to concrete structures for some three decades or longer, with various reviews and appraisals, Knab (1983), Reynolds (1984 b). Reynolds concluded that the degree of correspondence achieved between the simple theoretical model proposed and the wide range of experimental data presented shows that attempts to correlate ultrasonic wave velocity or density measurements with strength are subject to inherent ambiguities. Where the quality of the aggregate and formulation can be guaranteed constant these ambiguities may be reducible within acceptable limits for specific purposes, which is the real object of establishing on-site correlations. If the types of aggregate present are variable, some other measurement is needed to narrow the limits and it has been shown that density is a suitable parameter in this context. Measurement of density may be made by coring, gamma-ray attenuation or backscatter, or indirectly by surface rebound tests.

Through transmission ultrasonic pulse measurements for the nondestructive estimation of concrete strength are performed today

in the same manner as they were at their introduction more than 40 years ago. Current pulse velocity measurements, do not therefore correlate much better with concrete strength than in the past. In fact, this pulse velocity method, even when used in conjunction with preestablished calibration curves, is accurate to a degree of 20% error. If such a calibration is not available, which is the typical case in practice, the strength estimates are less reliable because different concretes have different calibration curves. This is so because the pulse velocity is controlled primarily by the young's modulus of the material and not by its strength and the two parameters are affected differently by changes in the composition of a concrete. As an example, the strength of concrete is drastically decreased by increasing water-cement ratio whilst little change is observed in the pulse velocity.

This does not mean that there is no relationship between propagation parameters and concrete strength, but rather that such a relationship would be quite complex and the details of this have not yet been established. The view that concrete strength is proportional to the fourth power of the pulse velocity is an empirical oversimplification that does not always work, Popovics (1990). The "theoretical" basis of this simplistic view is that, according to the Poisson's formula, the

modulus of elasticity is proportional to the square root of the pulse velocity. This relationship was obtained from the assumptions that the material is homogeneous, isotropic and linearly elastic, and concrete is none of these, thus, the Poisson's formula is not strictly applicable to concrete. The modulus of elasticity is also assumed, in an empirical manner, to be proportional to the square root of the compressive strength of concrete. The combination of these two formulae gives the spurious fourth power relationship, however it is not sound practice to combine a theoretical formula with such a rough empirical formula. Most experimental data do not support any fourth power relationship between concrete strength and pulse velocity with acceptable degree of fit, generally a second power is closer. This means that the pulse velocity method , in the present form, cannot be used accurately for in-situ determination of concrete strength.

Popovics et al have reviewed these theories, and following experimental determinations, report their findings. The pulse velocity in the longitudinal direction of a concrete cylinder differs from the velocity in the lateral direction, at low velocities the longitudinal velocities are greater, whereas at high velocities the lateral velocities exceed the longitudinal velocities. This difference is more pronounced with lower frequencies, and the pulse velocity in

concrete increases with higher frequencies, that is, concrete is a dispersive material, the dispersive nature of concrete decreasing with age. This is commensurate with low frequency velocity variations observed in this study, as discussed elsewhere in this thesis. The pulse velocity is also largely independent of the stresses in concrete. A feature-based computer system can be made applicable to concrete, and is probably the most promising method of obtaining meaningful strength evaluations and predictions.

Berthaud discussed and reported on investigations into the possible correlations between the mechanical and acoustical consequences of damage in concrete, Berthaud (1990). Microcracks or micropores either initially existing in the virgin material or created by mechanical loadings, or chemically in the case of concrete, are responsible for the strong variations of the elastic constants and therefore the acoustic properties of the material.

Data was gathered using transducers affixed to specimens under compressive stresses to monitor the acoustic consequences of increasing damage levels. To ensure the test to be meaningful for heterogeneous materials, the size of the specimen must be much larger than the maximum aggregate size, ratio of 10 being a valid lower

bound. The material must be seen by the wave as homogeneous and that requires a ultrasonic transducer larger than the maximum aggregate size, or maximum pore size. The small samples used in the experimental work reported in this thesis also proved problematical in this regard.

Our dependence upon the national concrete-based infrastructure is obvious, as is the fact that many traditional analytical techniques currently being used have not been adequate in predicting the premature deterioration of these structures or, in some cases, in recommending the proper courses of action for remedial action. Because concrete is of such a complex and dynamic nature, we need to employ all the means at our disposal in order to understand how it responds to its environment and to predict how it will perform. Once we are able to accomplish this, we can use this knowledge to design concrete structures which do not begin to "self-destruct" after only a few years of service. Methods and analytical techniques traditionally developed for materials analysis can be used with excellent results when evaluating concrete, especially when used in conjunction with each other. Computer programmes and computer-controlled equipment designed to maximise and complement each instrument's capabilities are essential for efficient acquisition of the data, Lee (1992).

X and gamma radiography are particularly attractive because of the directly accessible and quantitative information they yield about an object. Unfortunately, the physics of basic film radiography dictates that the images produced by the passage of x and gamma rays through an object result in a complete projected view of the object. This may not be a problem if the object in question is of a homogeneous nature such as a steel alloy or ceramic. However, in nonhomogeneous materials such as concrete with emplaced rebar, the images resulting from this method are often difficult to interpret and do not allow the investigator to isolate and examine a particular area of interest within an object.

Computer aided gamma ray tomography is potentially a very powerful diagnostic tool for the evaluation of concrete and has been used recently with some success by Lee et al at the Lawrence Livermore National Laboratory.

Low frequency techniques and equipment developed for concrete structures would seem promising but difficulties arise with small samples due to uncertain modes of ultrasound propagation. Low frequency ultrasonic NDE was therefore considered to be the most

promising technique for the chemically bonded ceramics under investigation, together with radiography for corroboration where appropriate. It was also decided to attempt to achieve some understanding of the problems encountered with small specimens at low frequencies, and to determine the most suitable techniques and frequencies for routine application in the commercial production of articles using these materials.

The greatest drawback to ultrasonic methods, however, lies in the need to couple the transducers ultrasonically to the surface of the ceramic. This is most satisfactorily accomplished by immersing the test component in water, which is not always acceptable, and was not attempted in this study. With the porous samples used, considerable effort was expended investigating coupling techniques, particularly for shear wave determinations. The main problem was the absorption of the couplant into the pores, and the commercial solution to this is to test the finished product following the application of the surface coating, despite the increased costs incurred by the coating of substandard articles.

2.7 THE EVALUATION OF ELASTIC MODULI.

Techniques for the measurement of the velocity of sound through a medium, and the relationships of those velocities to the elastic moduli and other material properties are discussed in chapter 3.6. The reader is also referred to the works of Gooberman (1968), Szilard (1982), Halmshaw (1987) and Kolsky (1963). The moduli so determined apply to the bulk material rather than to any particular phase and are best regarded as an effective modulus for multiphase materials. Hashin, Hashin (1962), and Hashin and Shtrikman, Hashin (1963), considered composite materials with an assumption of a uniform matrix with spherical inclusions, homogeneously dispersed in such concentration as to remain discrete. They viewed each inclusion surrounded by a section of matrix as two concentric spheres (with conservation of volume) and considered them to be individual spherical composite elements in an array of such elements. The volume of matrix remaining between these elements was considered to be under constant stress and small strain due to perfect packing of a range of sizes, see figure 2.3.

Hashin and Shtrikman derived for this idealised system a relationship between the actual moduli and Poisson's ratio of the matrix and

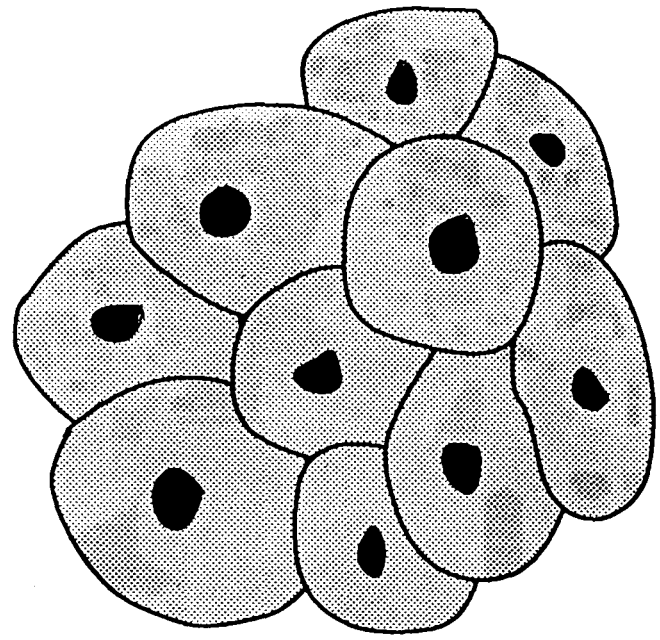

a

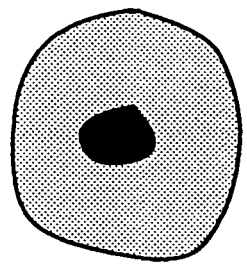

b

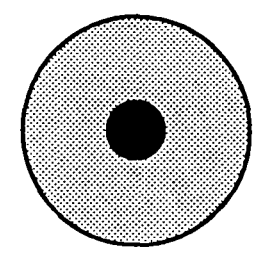

c

Figure 2.3 a. Composite material divided into elements consisting of a filler particle surrounded by a section of matrix.
b. An element with mean volumes of matrix and filler particle.
c. A spherical element with same volumes of filler and matrix.

disperse phase, or filler, on the one hand, and the maximum and minimum values of the effective moduli on the other. Where the bounds are close together their mean values would, in most cases, be a close approximation of the effective moduli of the material. Where this is not so, as in the case of the disperse phase and matrix having very different moduli, the bounds are not suitable for such an estimate. They would, however, still be useful as an indication of this fact and would allow inferences as to packing and homogeneity to be made.

To apply the formulae of Hashin and Shtrikman, discussed in chapter 3.6, it is necessary to know the values of the elastic constants of the components of the two phase material. For pure materials of known composition and structure this information may be available in tables or published literature, otherwise, if samples are available it may be obtained by measurement. Of course, the elastic data required are unlikely to be available for obscure crystals, amorphous phases and solid solutions, all of which are likely reaction products.

It is therefore useful to be able to predict the elastic properties of polycomponent systems solely from a knowledge of the system composition, density and well-known tabulated physical properties.

Makishima and Mackenzie, Makishima (1973, 1975), proposed expressions relating the elastic moduli of glasses to the dissociation energies of the constituent bonds, and the packing density of atoms expressed as a summation function of their Pauling radii. These semi-empirical formulae use known elastic data on silicate and borate glasses.

In an extensive range of papers, O.L. Anderson and co-workers, Anderson (1965), Soga (1966), Anderson (1971), related the bulk modulus of isostructural, multicomponent crystalline oxides to the packing density of atoms, and a summation over the valence charge products and ionic character of the various bonds. In contrast to the work of Makishima and Mackenzie, packing density was defined in terms of the molar volume per ion pair.

More recently, Bridge and Higazy, Bridge (1986a), proposed a model in which the elastic moduli of polycomponent oxide glasses were expressed as a summation over the number of network bonds per unit volume, the cross-link densities per cation, and the stretching force constants, for each bond type. The model was tested on a range of phosphate glasses, the force constants being estimated from electronegativity data when unknown.

The common feature in all of these models is that elastic moduli are, in effect, related to the number, and arrangement, of network bonds per unit volume, and the magnitude of their force constants. In the Makishima and Mackenzie model, bond dissociation energies are assumed to correlate with force constants. The models differ substantially in the calculations required and in the results produced.

Bridge with other co-workers, Bridge (1983, 1986b, 1988a), extended the range of application of this model and derived a simpler one. In the model of Bridge and Higazy, Bridge (1986a), the important variables were the coordination numbers, ie the number of atoms of a particular species coordinated or bonded with the atom in question, and first order stretching force constants. There is a linear dependence of bulk modulus on coordination numbers and all other interactions as well as nearest neighbour interactions, are subsumed in the values of stretching force constants to be used in the model. The experimental values of these constants are therefore the net results of combined long-range and nearest neighbour interactions. Long-range effects are thus allowed for in these values which, one may anticipate, will tend to become smaller with increasing coordination numbers.

2.8 MATERIALS CHARACTERISATION USING ATTENUATION SPECTRA.

For the determination of ultrasound attenuation as a means of material characterisation Papadakis, Papadakis (1972, 1984), suggested the use of liquid or solid buffers to separate the specimen and transducers, as shown in figure 6.3. This not only precluded any influence of the transducer on signals in the specimen but for this research provided a useful reference signal through the buffer alone. A graph of attenuation in the specimen could thus be derived from the difference between this reference signal, and the signal after transmission through the specimen, see chapter 7.3 and figures 7.5-7.9.

Reynolds and Smith, Reynolds (1984 a), Smith (1987), developed a model for the analysis of attenuation spectra based on the accepted treatment of grain scattering valid in the Rayleigh, stochastic and diffusive regions. At low frequencies the scattering is proportional to the fourth power of the frequency, whilst at higher frequencies the scattering is in direct proportion to the square of the frequency. As the frequency increases attenuation eventually becomes independent of the frequency.

In this model the frequency at which each scattering mechanism becomes dominant depends upon the ratio of the grain size to the wavelength. In the case of a real material with a grain size distribution about some mean it is possible to observe all three mechanisms simultaneously at a single frequency within some frequency range. There will usually also be a frequency range where all grains will scatter in a fourth power Rayleigh mode.

Reynolds and Smith with other co-authors applied the model to a variety of metallic systems, Smith (1984), Reynolds (1985), Sayers (1985) , to polymers, Reynolds (1986), composites and ceramics, Smith (1985), Reynolds (1989). It was reported that fibre reinforced composite materials presented difficulties in measurement and analysis due to fibre boundary porosity and disbonds.

2.9 ULTRASONIC MONITORING OF CURING.

All of the foregoing discussion on nondestructive evaluation and the theory behind it is concerned with the analysis of solid specimens which were chemically inactive, or assumed to be so in view of the slow rate of reaction in their advanced stage of curing. As previously

discussed with cementitious materials the strength develops over a greater or lesser period as a result of chemical reactions and the development of elastic moduli can be studied nondestructively. Such studies were undertaken by Lawrence et al, Lawrence (1974), who monitored the sound velocity changes in calcium silicate pastes and studied the effects upon the reaction kinetics of such pastes containing various admixtures. The hydration and other types of chemical reactions involved in the setting and hardening of Portland cements and other cementitious systems are discussed in chapter 2.1.2. The chemical reactions and phase changes involved in the preparation and curing processes of the materials studied in this thesis are considered in detail in chapters 4 and 5.

Further studies were undertaken by Stepisnik et al, Stepisnik 1981, who used measurements of the reflection coefficient for ultrasonic waves to follow hydration kinetics of Portland cement pastes under various conditions. The development of the shear modulus of elasticity and dynamic viscosity were determined, together with the geometry of the grain growth.

These studies inspired the research into the reaction kinetics and strength development of the newberyite materials under discussion,

although the methods employed here differ considerably from those used by either of the above authors.

3. THEORETICAL CONSIDERATIONS.

3.1 TRANSMISSION THROUGH MULTIPLE BOUNDARIES.

A plane wave incident on an interface between two media will have reflected and refracted components governed by the nature of the interface and the boundary conditions to be met. The specific acoustic impedance, Z, can be defined as the acoustic pressure, p, divided by the acoustic velocity, u, such that $Z = p/u$. The first boundary condition is that the algebraic sum of the acoustic pressures of the incident and reflected waves, the waves in the first medium, is equal to the acoustic pressure of the transmitted wave in the second medium. The second boundary condition is that the algebraic sum of the particle velocities of the incident and reflected waves is equal to the particle velocity of the transmitted wave or the media would not remain in contact. Using subscripts i, r and t to denote values for incident, reflected and transmitted waves the first condition gives :

$$p_i + p_r = p_t,$$

and since $p = Z.u$ this gives:

$$Z_i u_i + Z_r u_r = Z_t u_t \qquad (5)$$

The second condition gives :

$$u_i + u_r = u_t \qquad (6)$$

Denoting the first medium by subscript 1 and the second medium by subscript 2 then $Z_i = Z_1$, $Z_r = -Z_1$ and $Z_t = Z_2$.

Multiplying equation (6) by Z_1 gives :

$$Z_1 u_i + Z_1 u_r = Z_2 u_t \qquad (7)$$

Addition of equations (5) and (7) then gives :

$$u_t/u_i = 2 Z_1/ Z_1 + Z_2 = t$$

where t is the amplitude transmission coefficient.

Multiplying equation (6) by Z_2 gives :

$$Z_2 u_i + Z_2 u_r = Z_2 u_t \qquad (8)$$

Subtraction of equation (5) from equation (8) then gives :

$$u_r/u_i = (Z_1 - Z_2)/(Z_1 + Z_2) = r \qquad (9)$$

where r is the amplitude reflection coefficient.

Acoustic intensity reflection and transmission coefficients (R and H respectively) can be similarly derived denoting acoustic intensity by η with subscripts as before.

For the transmission coefficient.

$$H = \eta_t/\eta_i = Z_2 . u_t^2 / Z_1 . u_i^2 = Z_2 . t^2 / Z_1$$

$$H = 4 . Z_1 . Z_2 / (Z_1 + Z_2)^2$$

For the reflection coefficient :

$$R = \eta_r/\eta_i = Z_1 . u_i / Z_1 . u_r = Z_1 . r^2 / Z_1$$

$$R = (Z_1 - Z_2)^2 / (Z_1 + Z_2)^2$$

These formulae would also apply to a probe which has a buffer rod attached to the front face of the transducer, providing that the thickness of the buffer is greater than the pulse length.

For the case of a wave incident upon a series of media with a pulse length in excess of the thickness of laminations the situation is much more complicated. The various boundary conditions become independent and so both H and R become complicated periodic functions of the media thickness relative to the wavelength. The subscript Considering a simple case, that of three media with parallel interfaces, and the most commonly encountered example of transducer, coupling fluid and specimen, denoting these as media 1,2, and 3, respectively, then their specific acoustic impedances are such that $Z_1 \gg Z_2 \ll Z_3$. If $Z_1 \approx Z_3$ and $\lambda \ll l$ then the transmission coefficient, H, of the pulse through the fluid of thickness l is given by :

$$H \approx 4.Z_2^2 / Z_1^2 \cdot k_2^2 \cdot I^2$$

When wave energy is transmitted into a material some of the energy is scattered in all directions by the inhomogeneities in the material such as grain boundaries, dislocations, small defects, and residual stress distribution caused by variations in interatomic spacings.

Part of this scattered energy travels backwards along the beam eventually returning to the probe and is called backscatter. This is seen on the display as spiky noise, usually referred to as grass.

In most metals this is of a lower amplitude than the signal but in polycrystalline materials such as the ceramic materials in this study backscatter amplitudes, particularly from grain boundaries, are often greater than those of the reflected signals which are highly attenuated. Where materials evaluation is the aim, a two probe technique is frequently more effective since the receiver does not collect the backscatter noise and the one way signal is attenuated to a much smaller degree. Unfortunately, information on faults is minimal and limited to comparison of signal amplitudes and wave velocities with standards or in different locations on a specimen. This was investigated and published, Round (1988a).

If there is a residual stress distribution, the velocity , c , varies spatially which gives rise to impedance variations, and if these variations are sharp, scattering will take place. This effect leads to the use of backscatter as an evaluation technique. However in the polycrystalline materials under discussion this effect is masked by scatter from grain boundaries.

3.2 RELATIONSHIPS BETWEEN WAVE VELOCITY AND MATERIAL STRUCTURE.

Whilst the idea that elastic moduli should be directly proportional to interatomic forces is attractive, it is not supported by observations. Elastic moduli of materials like steel exceed those of plastics by a factor of 100 or more yet the atomic bonds in plastic (strong covalent bonds) along the chain are much stronger than the metallic bonds in steel. Similarly P-O bonds are rather stronger than Si-O bonds, yet the elastic moduli of SiO_2 glasses are approximately double those of P_20_5 glasses.

The reason for these anomalies is that the nature of the atomic configurations determines the macroscopic elastic moduli, rather than the magnitude of the inter-atomic forces. If, when a material structure is compressed, all atomic bonds are uniformly reduced in length, without bond angles being changed, then for a simple structure, with one kind of bond only (eg. any metal or simple oxide like FeO, Fe_20_3, Al_20_3, and SiO_2) the bulk modulus, K, would be given by, Bridge (1986a) :

$$K = n.r^2.F/q \qquad (10)$$

Where :

n is the number of bonds per unit volume,

r is the bond length,

and F is the bond stretching constant.

In a few materials,eg. diamond, this formula gives approximately the right answer, but in most cases (eg.in many plastics, glasses, etc) the bulk modulus predicted by the bond compression model, K_{bc}, is greater than the experimental bulk modulus, K_e, by a factor of 3-10. This suggests that isotropic compression involves a process taking much less energy than bond compression, ie. that some bond bending is

taking place (typically bond stretching force constants are 10 to 20 times greater than bending force constants).

The extent of this bond bending will increase, ie. K_{bc}/ K_e will increase, as the size of the atomic rings increases and the atomic structure becomes more open.

The term atomic ring can be applied to the shortest closed circuit of atomic bonds. Diamond has small rings of six carbon atoms all with the same force constants and bond lengths. This structure is three dimensional with similar rings in all three axes. The values of bulk moduli calculated from the bond compression model and the experimentally observed values are in agreement and $K_{bc}/ K_e \approx 1$. In the case of larger rings of silica tetrahedra, consisting of six silicon atoms and six oxygen atoms, which are more easily compressed, K_{bc}/ K_e is approximately 3.5.

In contrast, polymers consist of hydrocarbon chains with strong C-C bonds along the chain and very weak hydrogen bonds between chains with force constants perhaps a thousand times smaller than those of the C-C bond.

For forces applied parallel to the chains, the elastic moduli of polymers can be very high. Usually, polymers consist of randomly oriented chains; thus isotropic compression results in some bending of C-C bonds, together with some compression of the much weaker H-H bonds.

The effect of the hydrogen bonds is to produce quite small rings of alternating strong C-C and weak H-H bonds. So isotropic compression produces fairly direct compression rather than bending of these bonds. As a result, the observed modulus K_e for unbranched chain polymers (ie.high density polymers) lies between the values of K_{bc} calculated for C-C bonds and for H-H bonds.

In crystals held together by Van der Waal's forces, small atomic rings are obtained, and therefore $K_{bc}/ K_e \approx 1$, ie. isotropic compression produces bond compression rather than bending. Such crystals have very low moduli because Van der Waal's force constants are small. As a general rule, for covalent bonds, Poisson's ratio (σ) increases as the crosslink density per cation decreases. Crosslink density per cation is the number of network bonds minus two. With 4 bonds per silicon atom the crosslink density is 2, and Poisson's ratio is 1.5.

3.3 RELATIONSHIPS BETWEEN WAVE VELOCITY AND ELASTIC MODULI FOR MULTIPHASE MEDIA.

For an isotropic polycrystalline material the ultrasonic compressional and shear wave velocities are related to the elastic moduli by the equations,Halmshaw(1987), Bridge (1987a,1987b) :

$$G = c_T^2 \rho \qquad (11)$$

$$L = c_L^2 \rho \qquad (12)$$

$$K = \rho (3c_L^2 - 4 c_T^2)/3 \qquad (13)$$

$$E = \rho c_T^2 (3c_L^2 - 4 c_T^2)/ (c_L^2 - c_T^2) \qquad (14)$$

$$\sigma = (c_L^2 - 2 c_T^2)/2(c_L^2 - c_T^2) \qquad (15)$$

where c_L is the compressional wave velocity, c_T is the shear wave velocity, ρ is the density of the specimen, G is the shear modulus (Pa), L is the longitudinal modulus (Pa), K is the bulk modulus (Pa), E is Young's modulus (Pa), and σ is Poisson's ratio.

Comparison of experimental elastic moduli with the theoretical bounds of these moduli for a two-phase material can provide certain information about defects which may be present in the material. The closest set of theoretical bounds of bulk and shear moduli of a

two-phase material, in which the second phase is in the form of a particulate filler, are given by the well known formulae originally attributable to Hashin and Shtrikman, Hashin (1963) :

$$K_U = K_2 + \frac{(1 - V_2)}{\left(\frac{1}{K_1 - K_2} + \frac{3 V_2}{3K_2 + 4G_2}\right)} \tag{16}$$

$$G_U = G_2 + \frac{(1 - V_2)}{\left(\frac{1}{G_1 - G_2} + \frac{6(K_2 + 2G_2) V_2}{5G_2(3K_2 + 4G_2)}\right)} \tag{17}$$

$$K_L = K_1 + \frac{V_2}{\left(\frac{1}{K_2 - K_1} + \frac{3(1 - V_2)}{3K_1 + 4G_1}\right)} \tag{18}$$

$$G_L = G_1 + \frac{V_2}{\left(\frac{1}{G_2 - G_1} + \frac{6(K_1 + 2G_1)(1 - V_2)}{5\, G_1 (3\, K_1 + 4\, G_1)}\right)} \tag{19}$$

where the subscripts U and L denote upper and lower bounds respectively, subscripts 1 and 2 denote the matrix and the particulate phase respectively, and V_2 is the filler volume fraction which is

given by, Bridge (1987c) :

$$V_2 = \frac{\rho - \rho_1}{\rho_2 - \rho_1} \qquad (20)$$

where ρ is the density of the sample, ρ_1 is the density of the matrix and ρ_2 is the density of the filler.

It is important to note that the above equations apply even for two end members, ie. matrix and filler (particulate) components consisting of multiple phases. Thus, equations (16)-(20) will be applicable to the materials under discussion, taking the reaction products as the matrix component and the alumina as the particulate filler component. If these equations are to be practical for the prediction of the volume fraction dependence of moduli bounds one has to assume that the elastic moduli of the end-members are themselves independent of volume fraction. This assumption can be justified if the proportions of any multiple phases present in the end members are independent of volume fraction. This condition will doubtless hold for the non-reactive filler. There is some doubt in the case of the matrix because reaction rates and temperatures during the reactions were dependent on volume fraction. Nevertheless, to allow an analysis of

the composition dependence of elastic properties, it is assumed that the elastic properties of the fully cured matrix are relatively insensitive to filler volume fraction.

Upper and lower bounds for Young's modulus, E, and Poisson's ratio, σ, are obtained by combining equations (16) to (19) with equations (14) and (15). The Hashin and Shtrikman bounds apply for an arbitrary phase geometry ie; the size, shape, and spatial distribution of the filler particles. The only restriction of the theory is that there should be a reasonable number of particles in any layer of the sample running perpendicular to the wave propagation direction, and one wavelength thick. When particles are exactly spherical, the lower theoretical bound for each modulus should apply exactly. Finally there is an implicit assumption in the Hashin and Shtrikman theory that there is good bonding between the filler and matrix.

3.4 MODES OF PROPAGATION.

In rods, an infinite set of compressional wave modes (which one can label by n, where n=1,2,3...) is possible, see figure 3.1, each one having

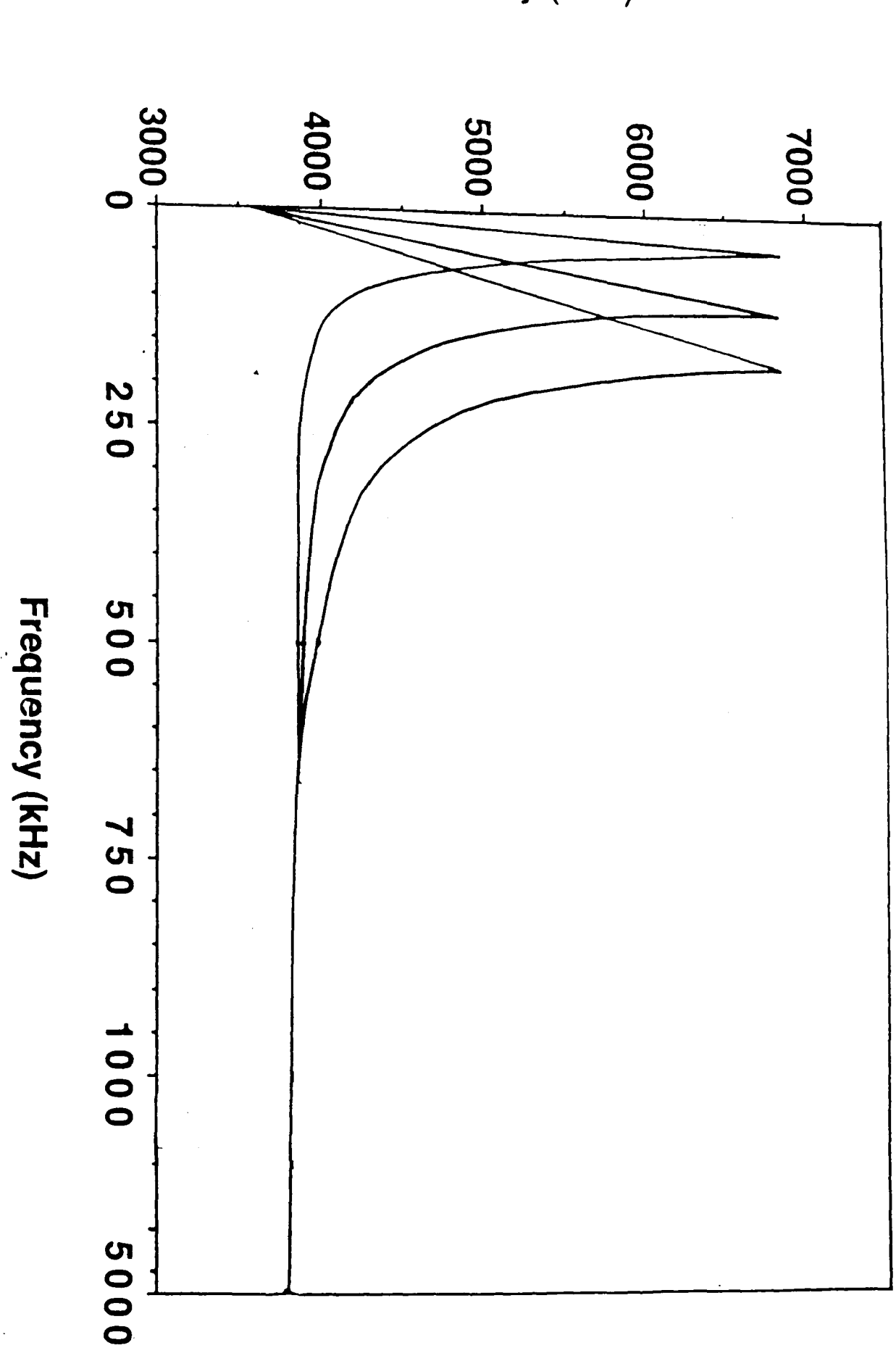

Figure 3.1. Theoretical frequency dependence of phase velocity of a longitudinal wave pulse. The three curves correspond to propagation consisting of the rod wave mode combined with the 1st 2nd and 3rd c_n for a 1.5 x 6cm section.

a dispersion relationship which depends on the dimensions of the sample perpendicular to the propagation direction, and a peak amplitude which decreases as n increases. In each mode the pressure distribution perpendicular to the rod axis is not uniform. Thus, to propagate a pure mode, a non uniform pressure distribution across the couplant-sample interface is required and it follows that a uniform pressure distribution in the couplant will necessarily lead to mixed mode propagation. This condition almost certainly applied throughout this research because the transducers were too rigid to permit the formation of meniscus-shaped coupling films to produce non uniform pressure distributions.

The above description describes qualitatively the solutions to the general wave equation subject to the boundary condition that the stress over the sidewalls of the rod must vanish. Quantitatively the solutions are exceedingly complicated. As a first approximation a simplified quantitative picture can be obtained as follows. Each mode consists of two compressional plane waves which travel back and forth across the sample at such an angle, a, that the boundary conditions can be satisfied. Divergence of the beam generated by the transmitting probe provides the necessary mechanism to launch the

modes. It is obvious that an oblique motion of plane waves will lead to a non uniform pressure distribution in cross sections at right angles to the rod axis, although this distribution is only approximately similar to what is predicted from an exact solution of the wave equation. The non-uniform transverse pressure distribution and the zig-zag motion of plane waves both imply that there are transverse as well as axial components to the particle displacements, ie wave modes propagating axially in rods cannot be purely compressional exhibiting axial motion only.

The angle, a, is given by the equation, Kolsky (1963) :

$$\cos a = (J_o)_n c_L / D\omega \qquad (21)$$

where $(J_o)_n$ is the appropriate root of the Bessel function J_o, c_L is the longitudinal wave velocity, and D is a term related to the dimensions of the specimen.

This leads to a phase velocity along an axis given by;

$$c_n = c_L / \sin (a_L)_n = c_L / \left\{ 1 - (J_o)_n^2 c_L / D^2 \omega^2 \right\}^{0.5} \qquad (22)$$

For a cylindrical rod, D is the radius. For other geometries, D is more complex and, for a rectangular cross section, Kolsky advocates using:

$$D = (d^2/3)^{0.5} \tag{23}$$

as the dimensional term in equation (22), where d is the diagonal of the rectangular cross sectionperpendicular to the axis of ultrasound propagation.

It will be noted that there is a low frequency cut off, ω_c,where c_n rises asymptotically to ∞ and below which no propagation is possible (imaginary c_n values). Above the cut off, c_n decreases monotonically and asymptotically to c_L as ω tends towards infinity. Because of the finite bandwidth of the pulses, infinite phase velocities are not observable in practice. If the bandwidth of the pulse encompasses the cut-off frequency, because of the variation of c_n close to the cut-off, the proportion of the pulse energy which travels at velocities approaching infinity is infinitesimal, so that the leading cycles in the pulse are too small to be observed. In practice, the velocity of a mode will be seen to rise to a high but finite value in the vicinity of the cut-off.

There is an additional longitudinal wave mode called the rod wave mode, whose velocity can be denoted by c_E, which has no low frequency cut-off but exhibits a maximum of;

$$c_E(0) = (E/\rho)^{0.5} \tag{24}$$

where E is Young's modulus, as ω tends towards 0. As ω increases, c_E falls continuously, approaching the surface wave velocity as ω tends to infinity. Now $c_E(0)$ is always less than c_L so that c_E is always less than c_n. Thus, if a pulse consists of a mixture of the rod wave mode with one or more c_n modes, the plot of the frequency dependence of the fastest observable phase velocity in the pulse will exhibit maximum and limiting values of $c_E(0)$ and c_L as ω tends to 0 and ∞ respectively. The maximum will lie somewhere within the range of cut-off frequencies for the different c_n modes present. As ω drops below the cut-off point ω_c the velocity will not drop suddenly to c_E (which is $<c_L$). Instead, because of the finite bandwidth of the pulse extending to $\omega>\omega_c$ the velocity will fall off continuously from a maximum value , to $c_E(0)$ as ω tends towards 0.

Using the above model an apparent frequency dependence of velocity

and certain other questionable, but repeatable, low frequency observations can be explained. Typical cases of the theoretical frequency dependence are plotted in figure 3.1, for the fastest observable phase velocity (ie the speed of the first quarter cycle to be visible) of a longitudinal wave pulse. The three curves correspond to propagation consisting of the rod wave mode combined with the 1^{st} 2^{nd} and 3^{rd} c_n respectively. Velocities above the cut-off frequency are obtained from equation (22) substituting the appropriate value of n, calculated from equation (23) and using for c_L the experimental compressional wave velocity at a frequency of 5MHz.

At the cut-off frequency, ω_c, a finite value of c_n has been derived from the following argument. To a reasonable approximation, a pulse of centre frequency ω has a spectrum bandwidth of $\omega \pm \omega_{c/p}$ where p is the number of cycles in the pulse, assumed of equal amplitude. Thus to a first approximation, because of finite bandwidth, the velocity at the cut-off frequency, $c_n(\omega_c)$ may be taken as the velocity evaluated at the frequency $\omega_c + \omega_{c/p}$ i.e.

$$c_n(\omega_c) \approx c_L \Big/ \left\{1-1/(1+{}^1/_p)^2\right\}^{0.5} \qquad (25)$$

Taking p = 5 as reasonable for the probes employed, one obtains :

$$c_n(\omega_c) \approx 1.8\, c_L \qquad (26)$$

Finally, velocities below the cut-off frequency are obtained by linear extrapolation between the value $c_n(\omega_c)$ from equation (26), and c_E obtained from equation (24) with E obtained from the compressional and shear wave velocities (equation (14)).

It would thus appear that at 220kHz the peak in the velocity dispersion curve has been passed, and at 2MHz a steady velocity, independent of frequency and sample parameters obtains.

4. MATERIAL PREPARATION.

4.1 CHEMICAL REACTIONS.

When MgO powder reacts chemically with a solution of $Al(H_2PO_4)_3$ (Cassidy1977, Taylor 1981, Green 1987), in the presence of Al_2O_3, a multiphase ceramic, consisting of several polycrystalline magnesium and aluminium phosphates with water of crystallisation in specific crystalline planes, is produced. This material, which is almost as easy to mould as a polymer, is suitable for structural applications without the need for sintering. Carbon or glass fibres can be incorporated to impart stiffness, fracture toughness and forgiving fracture. The reaction sequence is complex and the main reactions are essentially as follows.

Gibbsite and phosphoric acid react to produce aluminium orthophosphoric acid :

$$\underset{\text{Gibbsite}}{Al_2O_3.3H_2O} + \underset{\text{phosphoric acid}}{6(H_3PO_4)} \rightleftharpoons \underset{\substack{\text{aluminium} \\ \text{orthophosphoric acid.}}}{2Al(H_2PO_4)_3} + 6H_2O$$

The aluminium orthophosphoric acid is allowed to retain water, and more is added, to produce a 48% by weight solution which reacts with magnesia in the presence of alumina thus :

$$2MgO + Al(H_2PO_4)_3 \xrightarrow{H_2O} \underset{\text{crystalline newberyite}}{2MgHPO_4.3H_2O} + \underset{\text{amorphous}}{AlPO_4.xH_2O}$$

In the composites discussed here the dimensions of the alumina and magnesia powder particles were 0.5-10μm and 3-40μm,respectively, whilst the milled fibres were approximately 150μm in length and 10μm in diameter. The final phase assemblage for the reaction bonded material would be a matrix consisting ideally of about 70% crystalline newberyite, and 30% aluminium phosphate by weight, the exact proportions depending on x, the hydraton level of $AlPO_4$ in the above equation. Whilst the prevailing reaction is as stated, others also occur leading to the formation of other magnesium phosphates, so that in practice small amounts of MgO, $Mg(PO_3)_2$ and $MgH_2P_2O_7$ will be present. The filler, alumina and any fibre, 55 to 60% by weight, is dispersed throughout the matrix. Taking the alumina content to be 55% by weight there would be 31.5% newberyite and 13.5% aluminium

phosphate by weight ignoring minor phases.

Throughout this thesis the residual alumina is defined as the filler whilst the matrix is formed of the reaction products. Thus the matrix might consist of two phases with newberyite predominating, as described in the equation. Alternatively, since the equation is only an approximate description of the chemical process occurring, the matrix will probably consist of more than two phases.

4.2. AGGLOMERATION AND MIXING OF POWDERS.

In September 1986, work started at THORN EMI Central Research Laboratories, with trials undertaken by co-workers from Thorn-EMI at Baker Perkins Chemical Machinery, Stoke-on-Trent, on the investigation of a suitable formulation and production process for moulded phosphate bonded ceramics, Green (1987).

The process commences with a mixture of two powders, alumina and magnesia, dispersed in and 'wetted' by an aluminium orthophosphate acid solution. Samples in which the powder components are not fully 'wetted' are of lower strength and the mixing technique must therefore

ensure the 'wetting' of the powders by the acid solution and overcome any tendency of the powders to agglomerate.

Powder particles agglomerate or stick together by three main mechanisms :

I) Solid Bridging which may come about as the result of sintering, solid diffusion or chemical reaction.

2) Liquid bridging, which is the presence of a liquid phases between the particles. Small amounts of the liquid may concentrate in saddles lying between the particles, greater quantities may form a continuous network, eventually completely coating the particles, and finally filling the interstices. Surface tension forces on the outside of the drop keep the particles together. With the earlier stages there is a negative capillary pressure in the filled saddles, and subsequently surface tension causes the bonding between grains.

(3) Attraction between particles due to Van der Waal's forces.

The mixing process must overcome these mechanisms and break up the agglomerations in order to ensure that each particle is 'wetted' by the

acid solution. Thorough 'wetting' in necessary to maximise the rate of reaction between orthophosphoric acid and the magnesium oxide. Imperfect 'wetting' of either of the powder components causes agglomerates within the matrix, which reduces the mechanical strength.

The material, as it undergoes processing, also varies in viscosity as the MgO/acid reaction proceeds. The mixing equipment must therefore be able to handle materials of different and varying viscosities. The MgO/acid reaction is exothermic which necessitates cooling, and furthermore the incorporation of temperature control would enable the control of reaction or setting time. Ease of cleaning and the ability to withstand corrosive and abrasive conditions are also important considerations.

For volume production of the phosphate ceramic material in both research and production environments batch mixing and continuous extrusion could be considered.

4.2.1 Batch mixers.

These generally consist of two contra-rotating blades or cylinders

which are set on parallel shafts along a trough. The blades are designed to draw the material down between them, thus working it between the blades and the trough wall, which is usually shaped to the contour of the blades or cylinders for greatest efficiency. The mixers work a small proportion of the batch at a time which leads to long mixing times to ensure a uniform product.

Long mixing times do not pose a problem unless, as with these composites, the time available to work the material is restricted by setting reactions. Cooling of the phosphate composites can delay setting, but where there is a large bulk of material, efficient removal of heat is difficult. Problems encountered with overheating of the material would only be intensified as batch sizes increase, necessitating the dissipation of extra heat from a proportionately lower surface area. Trials using a Z-blade mixer by co-workers from Thorn-EMI at Baker Perkins Chemical Machinery, Stoke-on-Trent met with little success.

4.2.2 Extrusion / Injection moulding

This is a continuous production method widely applied to the plastics

industry and the most likely method for the commercial production of artifacts from the ceramic composite. An extruder is used to compound material and pump it into a die. The extruder alone produces a continuous length of constant cross section, which would be inappropriate for this material without initial support. Clearly, if the material is sufficiently viscous to support its own weight immediately on exit from the extruder, there is a strong probability of the material setting within the machinery with little safety margin. The advantages of extrusion are continuous production, accurate temperature control and effective transport of difficult materials. Single screw machines impart high degrees of shear, but are less intense mixers than twin screw machines which can be co-rotatory or counter-rotatory.

The differences between the two types of twin screw machines are the methods by which they transport and mix the material. Co-rotating extruders, have inter-meshing screws which are self wiping. Material moves helically along the inside barrel wall in a figure of 8 path from the feed section to the discharge point. The screw design is such that the root of one screw is constantly being wiped by the flight tip of the other, with a uniformly small distance between them. This eliminates dead spots and the residence time of each mix component is

uniform. Clearly this is of great advantage with chemically setting material.

In the counter-rotating type of twin screw extruder the mixing operation is accomplished by the screw flights, which carry the material, forcing it towards the point where the two screws meet, or are at their closest proximity to each other. This is often referred to as a 'nip'. Contra-rotating extruders can put the material through high degrees of shear by means of this nip. The degree of shear can be controlled by narrowing or increasing the clearance between the screws, but only a proportion of the material is subjected to the high shear present at the nip and contra-rotating twin screws are not totally self cleaning.

Single screw extruders are not generally used for compounding operations requiring a high degree of mixing. In view of the problems outlined above the counter rotating twin screw machine also seems inappropriate for phosphate bonded ceramic material.

Two co-rotatory extruders were used as compounding mixers for the manufacture of prototype moulded ceramic items in trials undertaken by co-workers from Thorn-EMI. These were a Baker Perkins twin

screw extruder and a Werner Pfleiderer compounding extruder, modified to run in a horizontal mode.

4.3 SAMPLE PREPARATION.

The silicone rubber moulds for producing l5xl5x220mm^3 test specimens were made using Silastic grade E RTV from Dow Corning, this was degassed under a slight vacuum for 30-40 minutes before being cast around the wooden formers and cured over 24 hours at 60°C. The softness of the rubber caused non-uniformity of some samples and mismatch at the mould join led to poor sample geometry in several cases. A wide selection of mechanical test specimens were, however, successfully moulded.

The mixture was extruded under vacuum, vibrated into moulds and set at 100°C or 20°C. After mechanical testing by workers at Thorn-EMI the fragments of these test pieces (now approximately 15x15x55mm) were made available for use in the research project herein reported.

The compositions of the various samples produced are given in table 4.1 below. The compositions in columns 1-3 were produced as

mechanical test pieces of dimensions 15x15x220mm, in the production trials described, using the Baker-Perkins co-rotatory extruder as a compounding mixer. These differ mainly in the type of fibre reinforcement if any. The composition in column 4 was produced in house, using a small batch mixer, without filler or reinforcement.

Table 4.1 Starting compositions in wt%

Al_2O_3	55.5%	58.82%	57.92%	0%
$Al(H_2PO_4)_3$ in H_2O	33.43% 48% solution	33.40% 48% solution	33.80% 60% solution	82.63% 48% solution
MgO	6.07%	6.15%	8.28%	17.37%
Fibre	5.0% Glass	1.63% Carbon	nil	nil
Mean Density (kg/m^3)	2356	2385	2326	1561
Setting Temp (°C)	100	100	20	20

For the monitoring of the setting material the samples were of necessity mixed immediately prior to the commencement of monitoring. This was carried out as rapidly as possible commensurate with achieving an intimately mixed homogeneous paste.

Initially 59.80 wt.% of MA95 calcined α-alumina , 6.25 wt% of HMD4 magnesia and 33.95 wt.% of the 48% w/w solution of aluminium orthophosphoric acid ($Al(H_2PO_4)_3$) were hand mixed in a glazed earthenware bowl, the dry ingredients being intimately mixed by means of a pestle prior to the addition of acid, until a consistent paste was achieved, in most cases after approximately 3 to 4 minutes. The paste was then transferred into the prepared cell. All elapsed times were measured relative to the time at which the acid was added.

The MgO used in this work was obtained from Steetley Chemicals, Hartlepool, under the trade name HMD4. It consisted of 96% MgO, dead burnt, with 65% of the particles being less than 53 μm diameter. Where the term "AOP" is used in the text, it refers specifically to a solution obtained from Albright and Wilson, Oldbury. This is a 48% wt/wt solution of AOP in water where "AOP" has the nominal composition of $Al(H_2PO_4)_3$, although some variation in P:Al ratio may occur between batches.

Any given batch is probably comprised of a number of different aluminium acid phosphates, for example:

$Al(H_2PO_4)_3$ (P:Al = 3:1)

$AlH_3(PO_4)_2 . 3H_2O$ (P: Al = 2: 1)

$Al_2(HPO_4)_3$ (P:Al = 3:2)

Phosphoric acid was obtained from Albright and Wilson, Oldbury and consisted of 85.3% wt/wt H3 P04 in water, with a specific gravity of 1.70.

Gibbsite was obtained from B.A. Chemicals, Gerrards Cross under the trade name FRF85, with a purity of 99.6% wt/wt $Al(OH)_3$, and a mean particle diameter of 5μm.

5. MATERIAL CHARACTERISATION.

5.1 PHASE IDENTIFICATION.

Chemical and structural analysis would normally have been undertaken as part of a research programme of this nature, however since co-workers at Thorn-EMI, in conjunction with Sheffield University, had already undertaken this work on similar samples produced from the same batches of raw materials this was not necessary. Their results have been published, Finch (1989), and their main findings are discussed below.

Using X-ray diffraction analysis (XRD) Finch and Sharp found that these phosphate cements appear to contain both crystalline and amorphous phases, the presence of an amorphous phase being clearly indicated by a hump in the XRD pattern at values of 2θ between 20° and 35°. Sharp peaks on the XRD trace were identified as due to the presence of two distinct crystalline phases, newberyite, $MgHP0_4.3H_2O$, and MgO.

The relative amounts of the crystalline materials present in the set

cements depended largely on the molar ratio of MgO: AOP used as starting materials. A maximum amount of newberyite is associated with a molar ratio of about 4:1.

As the molar ratio MgO: AOP is increased, the cement sets faster and with a larger evolution of heat. From analysis of the time taken to reach the maximum exotherm temperature (which provides an estimate of the setting time) it was found that mixtures with an MgO: AOP ratio of less than two failed to produce set cements. At a ratio of exactly two, the mixture "set", but only slowly and always remained tacky.

Varying quantities of magnesium can be accommodated in the amorphous material, saturation being reached when the atomic ratio in this phase is around Mg:Al = 1:1. The exact amount of magnesium which appears in the form of newberyite, magnesia or in the amorphous phase depends on a number of factors, such as the molar ratio MgO:AOP, the particle size and reactivity of the starting materials, and the intimacy and duration of mixing.

Hence the most accurate equation for the reaction is

$$pMgO + Al(H_2PO_4)_3 \xrightarrow{+\,H_2O} qMgHPO_4.\,3H_2O + [1/2Al_2O_3.\,rMgO.\,2P_2O_5.\,sH_2O] + tMgO$$

where r≤1, t = 0 until p > 3, and p must ≥ 2 to produce a set cement. Phosphorreslerite, MgHP04 7 H_2O, can be formed in the presence of excess water, but readily transforms into the trihydrate, newberyite, at ambient temperatures. This may be an intermediate phase and could produce anomalies.

Acids with lower water contents can react to form a new hydrate called "hayesite" by Finch and Sharp which is probably a lower hydrate of $MgHP0_4$ than newberyite, perhaps $MgHP0_4.H_2O$ or $MgHPO_4.2H_2O$.

5.2 MATERIAL STRUCTURE AND MICROSTRUCTURE.

Simple observation of the surface shows that the material suffers from serious void defects which can be several millimetres in diameter in extreme cases, and arise from gaseous reaction products, mainly water vapour, and air incorporated during mixing and moulding. Hand lens observation of fracture surfaces reveals a coarse texture, with grain dimensions on a millimetre scale. Therefore another possible defect is poor intergranular bonding (which may be related to grain dimensions) due to departures from the intended chemical

reaction route. This may stem from local variations in proportions and/or conditions. Such inhomogeneities are more likely with these multiphase composites than with simpler two phase composites.

Samples were finely ground and examined under oblique illumination adjusted to give the greatest possible contrast between the two major phases. The photomicrographs are shown in Plates 1, 2, and 3. There are differences in the microstructures of the samples with grains of up to 2mm in the 5% glass fibre samples (Plate 1), grains up to 1mm in the 1.5% carbon fibre sample (Plate 2), and grains up to 0.7mm in the fibre-free samples (Plate 3).

In all samples there are two main phases visible, with the softer phase, containing the majority of the porosity, effectively forming a matrix between the regions of the harder phase. The softer nature of this face resulted in the breaking away of surface particles during the grinding and polishing process. This effect did at least increase the contrast between the phases when illuminated obliquely. In the case of the no fibre sample there is little contrast between the two phases, their presence being indicated by the arrangement of pores.

In the case of the fibre reinforced ceramics the individual fibres are

visible in all phases and the differences in microstructure would not appear to be related to fibre content.

The overall structure of the basic materials can therefore best be described as a two phase material, each phase being composed of a complex mixture of other phases: alumina, aluminium phosphate, newberyite, and any fibres present. The extent to which the proportions of these phases differ from the theoretical proportions described earlier is unknown.

The foregoing low power optical observations confirm the conclusions of the attenuation analyses, with regard to the dimensions of the major scatterers, which are discussed in chapter 7.3. Unfortunately they do not confirm the presence of flattened crystals indicated from a consideration of the values of theelastic moduli with respect to the Hashin and Shtrikman bounds, a theoretically derived set of limits, which is discussed in chapter 8.2. In fact the grains appear to be somewhat rounded, and therefore at odds with the above prediction.

However the grains so far observed are agglomerations of various crystals produced from the reactions, alumina filler particles and in some cases fibre for toughening purposes.

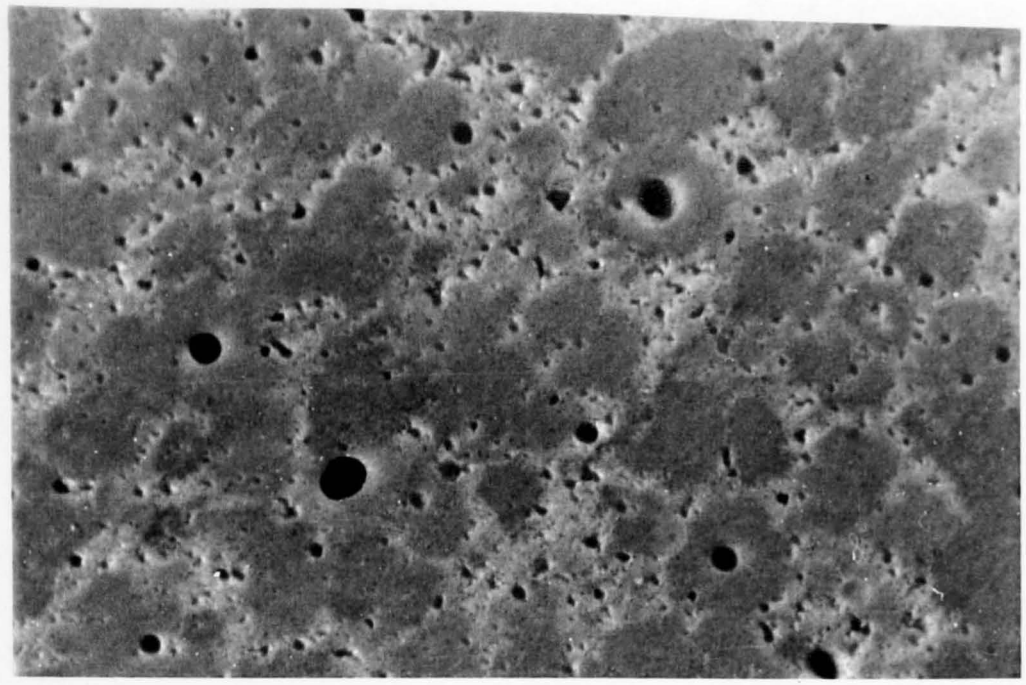

Plate 1.
Photomicrograph of the material containing glass fibres, taken using oblique illumination. The field width is 7mm. Grains or agglomerations with dimensions approaching 2.0mm are shown.

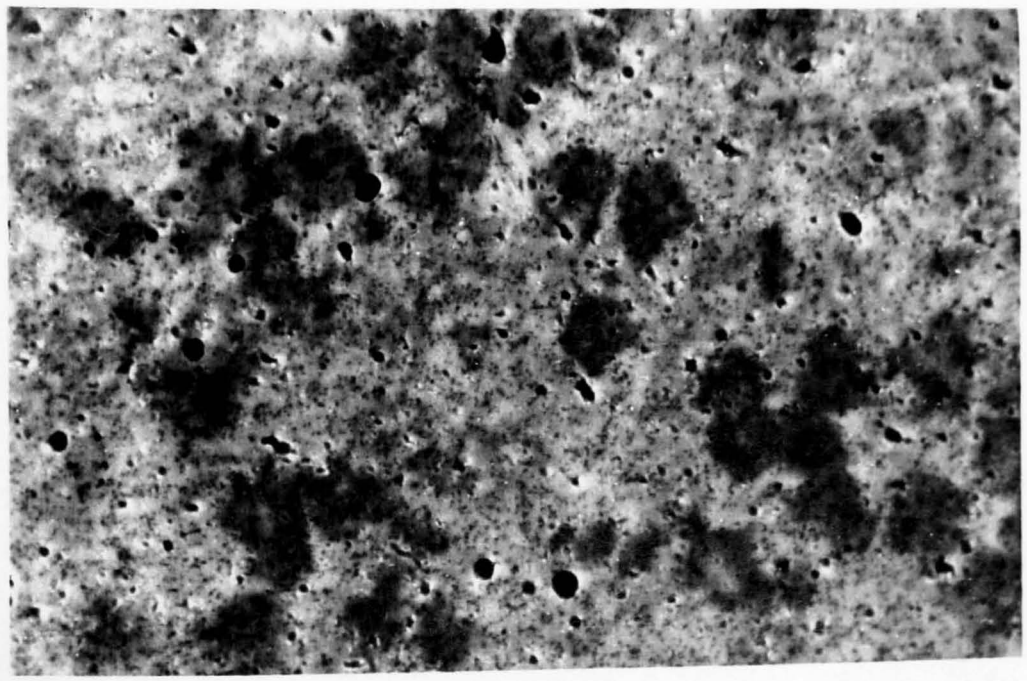

Plate 2.
Photomicrograph of the material containing carbon fibres, taken using oblique illumination. The field width is 7mm. Grains or agglomerations with dimensions approaching 1.5mm are shown.

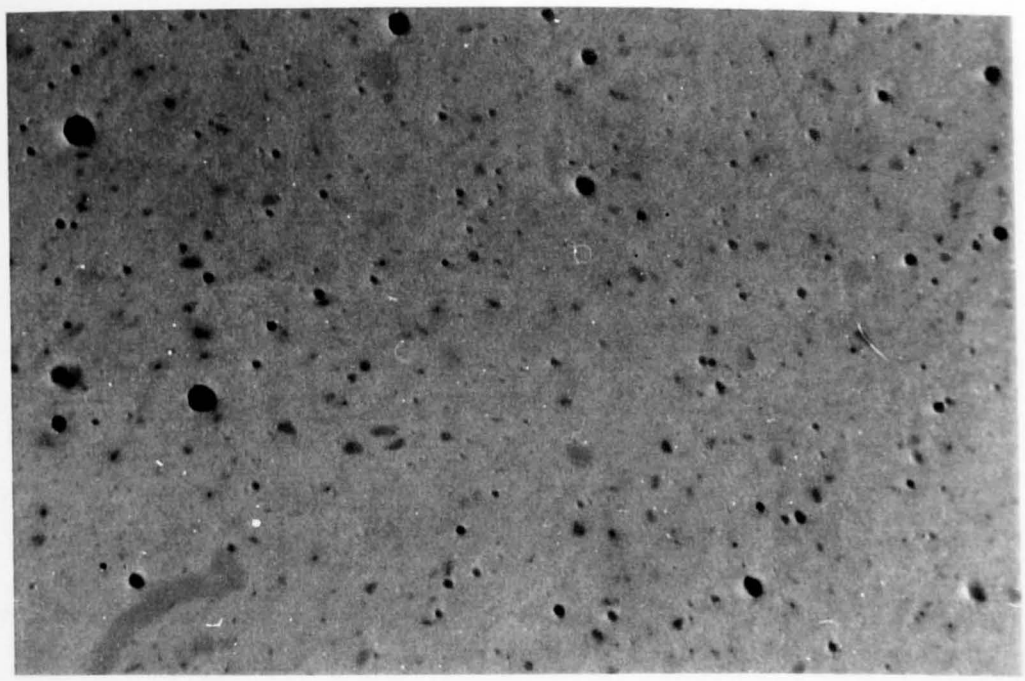

Plate 3.
Photomicrograph of the material containing glass fibres, taken using oblique illumination. The field width is 7mm. The presence of grains or agglomerations with dimensions approaching 0.7mm is suggested by the distribution of porosity.

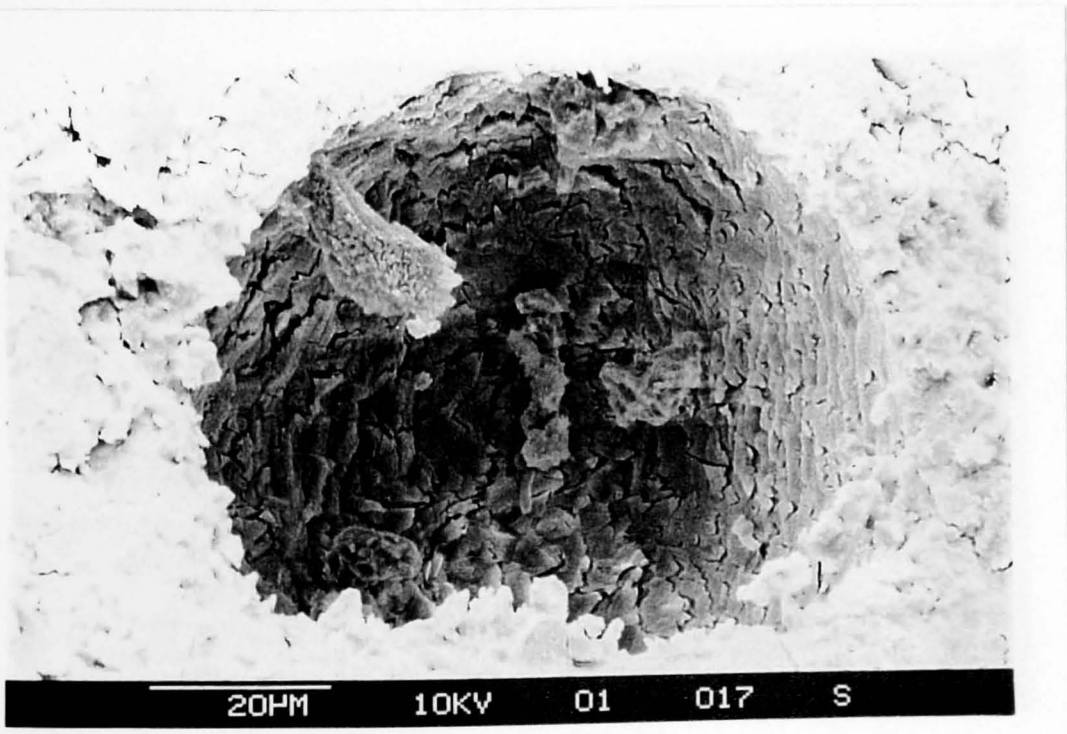

Plate 4.
Scanning electron micrograph of the material containing 0% alumina showing flat and leyered structures in a pore. The scale is given by the bar.

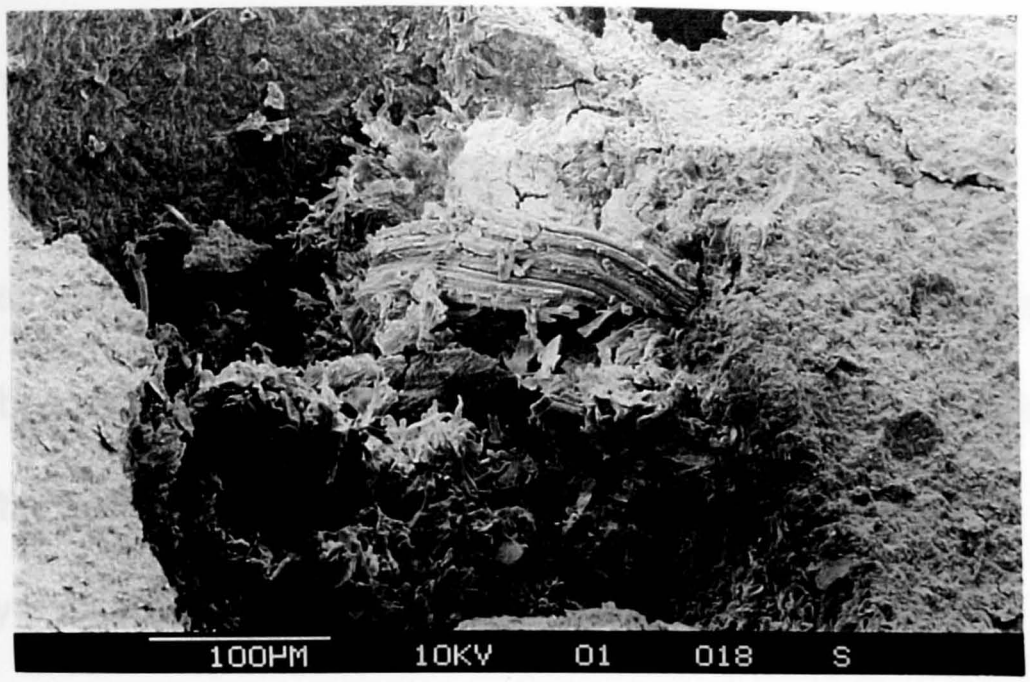

Plate 5.
Scanning electron micrograph of the material containing 50% alumina showing a variety of irregular flat cristallites. The large leyered structure at the edge of a pore may have been dislodged from the surface by a gaseous eruption. The scale is given by the bar.

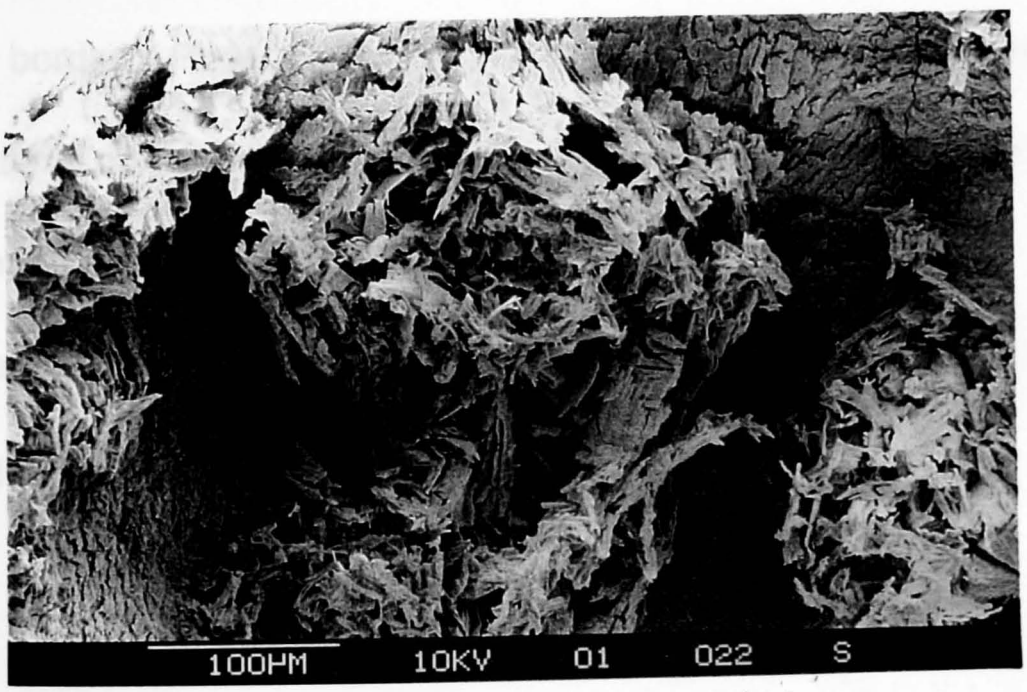

Plate 6.
Scanning electron micrograph of the material containing 50% alumina showing a variety of thin, flat interlocking cristallites with irregular, jagged shapes. The scale is given by the bar.

High magnification examination by scanning electron microscope (SEM) revealed the presence of very much smaller flat crystals, approximately 1μm thick, of irregular shape some 10-20μm across. In the bulk of the material these crystals are aligned and well packed, but in the surfaces of the pores they are randomly orientated and loosely packed, thus enabling their examination by microscopy. Some photomicrographs are shown in Plates 4, 5, and 6.

Plate 4 is a scanning electron micrograph of the material containing 0% alumina showing flat and layered structures in a pore. The scale of all the scanning electron micrographs is given by a bar in the bottom border. Plates 5 and 6 are scanning electron micrographs of the material containing 50% alumina showing a variety of irregular flat interlocking cristallites with irregular, jagged shapes. The large laminar structure at the edge of a pore in Plate 5 may have been dislodged from the surface by a gaseous eruption.

6. EXPERIMENTAL METHODS.

6.1 GENERATION OF ULTRASOUND.

Electromechanical transducers operating on the piezoelectric effect are the usual means by which ultrasound is generated for application in nondestructive testing (NDT), and nondestructive evaluation (NDE) of materials.

Consider a disc of piezoelectric mineral which has been cut along an appropriate crystal plane, or a polycrystalline ceramic which has been poled by an applied electric field with suitable thermal treatment, so as to exhibit the desired piezoelectric properties in an appropriate plane or axis. When excited by an alternating voltage applied to electrode plates on opposite faces of the disc, the thickness increases and decreases cyclically such that the surface of the disc vibrates. This will cause similar vibrations in materials with which the disc is in contact. The frequency of vibration is the same as the electrical excitation frequency but its amplitude is only appreciable when the applied frequency matches a natural frequency, f, of the crystal. This will occur when the thickness, t, of the crystal is an exact multiple of

half wavelengths such that

$t = n\lambda/2$. and since $f = c/\lambda$, then $f = cn/2t$

where λ is the the wavelength of the acoustic wave in the crystal, c is the acoustic velocity and n is an integer. This is known as harmonic excitation.

Shock excitation, which produces short, fast rise-time pulses, is the normal method used in commercial flaw detectors. Here, a spike voltage pulse excites the crystal into vibration which decays in a few cycles. The frequency of these vibrations is the crystal's fundamental frequency, such that :

$t = \lambda/2$. and $f = c/2t$.

Harmonic excitation tends to be used mostly in NDT research laboratories, rather than in 'field work' for which shock excitation is normally used.

Common piezoelectric and electrostrictive materials include quartz crystal which can be naturally occurring or manufactured, and polarised ceramics such as lead zirconate titanate (PZT), lead niobate,and barium titanate.

Ceramic transducers are very delicate and therefore they need to be mounted in a robust manner for practical NDT use. For research purposes, electroded crystals are bonded to test specimens, thereby eliminating losses and errors caused by protective housings. This technique was tried but found to be unsuitable for the materials under scrutiny and the data were gathered using commercial probes. This was in any case more in keeping with the purpose of the research, which was to assess the suitability of various methods of nondestructive evaluation and testing of the materials for quality assurance purposes.

An ultrasonic 'probe' is a transducer disc conveniently mounted in a protective housing which also has integral coaxial electrical input/output socket or sockets, see figure 6.1. Usually, but not always the transducer is mounted on a backing material which acts as a damper.

When the probe face is coupled to a material or component, via a thin film of coupling fluid, the mechanical vibrations of the transducer disc are transmitted into the material as waves. Conversely, if the probe face is coupled to a material supporting an ultrasonic wave, an alternating voltage waveform appears across the coaxial connector.

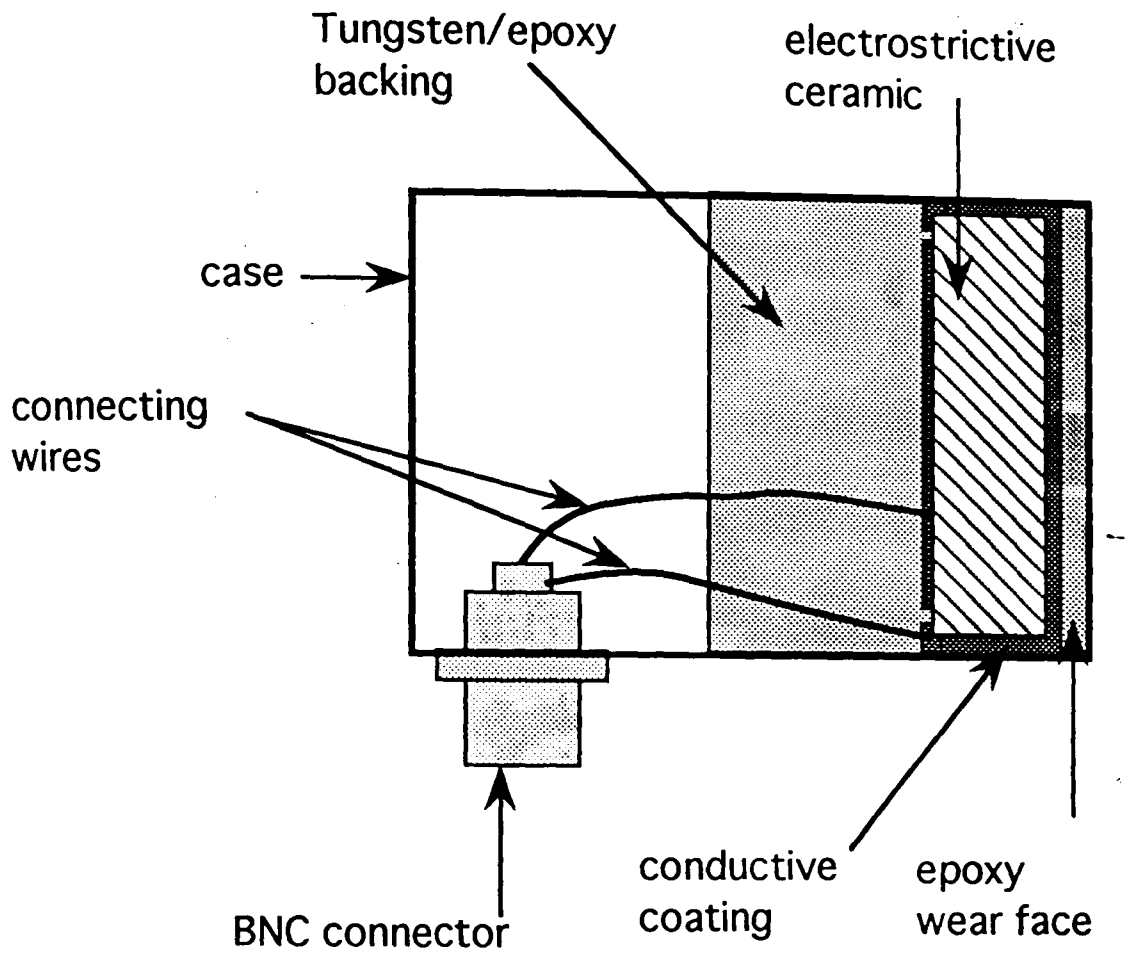

Figure 6.1 Typical ultrasonic probe, diameter could be from12mm to 12cm, tending to larger probes for lower frequency operation

Ultrasonic waves having frequencies suitable for use in flaw detection (typically 0.5 MHz and above) cannot be propagated efficiently across an air gap, no matter how narrow, because of the large difference in specific acoustic impedance of the probe and the air. The specific acoustic impedance, Z, is defined as the acoustic pressure, p, divided by the particle velocity, u, so that $Z = p/u$, Pain (1983). It is a quantity which changes sign with the direction of the wave and can be regarded as the impedance per unit area and is broadly analogous to electrical impedance. As explained in detail in section 3.1 a mismatch of specific acoustic impedances at an interface will increase the proportion of sonic energy reflected at the expense of that which is transmitted. There is an almost total reflection of sound wave energy at an air-water or air-solid interface, regardless of the medium through which the boundary is approached. A solid or liquid coupling medium must therefore be introduced between a transducer and a solid sample in order to produce a permanent or temporary bond and to minimise the mismatch of specific acoustic impedances, thus increasing the efficiency of wave energy transfer. A transmittance of approximately 0.15 giving an attenuation of approximately 16.5dB at a solid-liquid boundary is typical.

There will be some attenuation within the couplant and consequently

the coupling medium should be maintained as thin as possible. The couplant will have a finite but variable thickness and the ultrasonic beam will propagate across the couplant layer in a significant time which must be considered during data analysis. It is possible to eliminate the transmission time of the beam through the couplant by taking data for second and subsequent echoes where conditions allow this. Unfortunately, the ceramic specimens under discussion were highly attenuative and this was not always possible. An alternative technique is to calibrate the timebase to zero using probes coupled face to face. This may result in errors due to the slight variation in the thickness of the couplant layers from specimen to specimen. Taking the mean of several readings on each specimen minimises this source of error. Rough specimens require thicker films than polished ones and consequently the error is increased. Where the specimen is porous there is a tendency for the coupling medium to be absorbed. The timing error decreases as the film becomes thinner and the signal amplitude decreases as the quality of the coupling deteriorates. It was observed that this problem diminished as the couplant filled surface pores but the surface had, of course, been altered by the absorption of couplant.

6.2 INSTRUMENTATION.

6.2.1 Low Frequency Measurements 24-500kHz.

Measurements were made at 24, 37, 54, 82, 150, 220 and 500kHz using the C.N.S. electronics PUNDIT (an acronym : Portable Ultrasonic Nondestructive Digital Indicating Tester). This equipment uses two probes, one to transmit and the other to receive the ultrasonic pulse, and gives a digital readout of the transit time of the pulse through the sample. From these measurements and thickness data, measured by micrometer, the ultrasound velocity was calculated. The clock circuit measures the arrival time of the earliest negative going quarter cycle of the pulse to exceed the trigger threshold of 200μV. If the sample attenuation is so high that the threshold is not reached then no time measurement at all is obtained. Thus it appears that the fastest 'observable' phase velocity in the received wave group is usually measured rather than a group velocity, which is the velocity with which the energy in a pulse of waves is transmitted, Kolsky (1963).

'Observable' , as implied earlier, means that the waveform must exceed the trigger threshold. Thus depending on attenuation levels and the spectral energy distribution in the pulse, the fastest observable phase velocity is not necessarily the fastest phase velocity

in the wave components of the pulse.

Ultrasonic coupling between the probes and the sample was achieved using Castrol water pump grease. Whilst the grease is difficult to remove from the ceramic surface it has proved superior to an aqueous gel couplant (KRAUTKRAMER ultragel II) since the latter is absorbed by the porous ceramic, leading to loss of adequate coupling and probably degradation of the ceramic in time. Care must be exercised when applying the grease since excessive amounts result in a thick layer of couplant and low velocity values. Insufficient grease causes inadequate coupling which also leads to low values of sound velocity. Repeated use of grease for coupling sealed the ceramic surface to some extent and it was then possible to use ultragel II where prolonged coupling was not required.

A delay circuit is incorporated in the instrument to enable calibration against a standard test block thereby eliminating the time delay introduced by the probe faces and couplant.

6.2.2 High frequency velocity and narrow band attenuation measurements.

A broadband Pulser-receiver (PANAMETRICS 5052 PR) was employed to generate and amplify ultrasound echoes by 40 dB before display on a 150 MHz oscilloscope (TEKTRONIX Model 2445). The receiver bandwidth of 10 kHz- 35 MHz allowed the first quarter cycle of the first echo to be readily identified on a second CRO channel. The output of a digital delay generator, (BERKELEY NUCLEONICS Model 7030), triggered synchronously with the transmitter pulse, was also displayed. This instrumentation is shown schematically in figure 6.2, and figure 6.3 which is a simplified arrangement also illustrating the probe switching circuitry essential for the timed monitoring of setting samples, see chapter 6.2.4.

By triggering the oscilloscope from the second channel and using time base expansion and adjustment of the delay time, the peak of the first quarter cycle of the first echo was made to coincide with a fixed peak in the delay pulse. This adjustment was carried out both with and without the presence of the ceramic (with the mould cell outer plates in contact for the monitoring trials). By taking the difference in the two delay settings, the travel times in the protective buffers and any

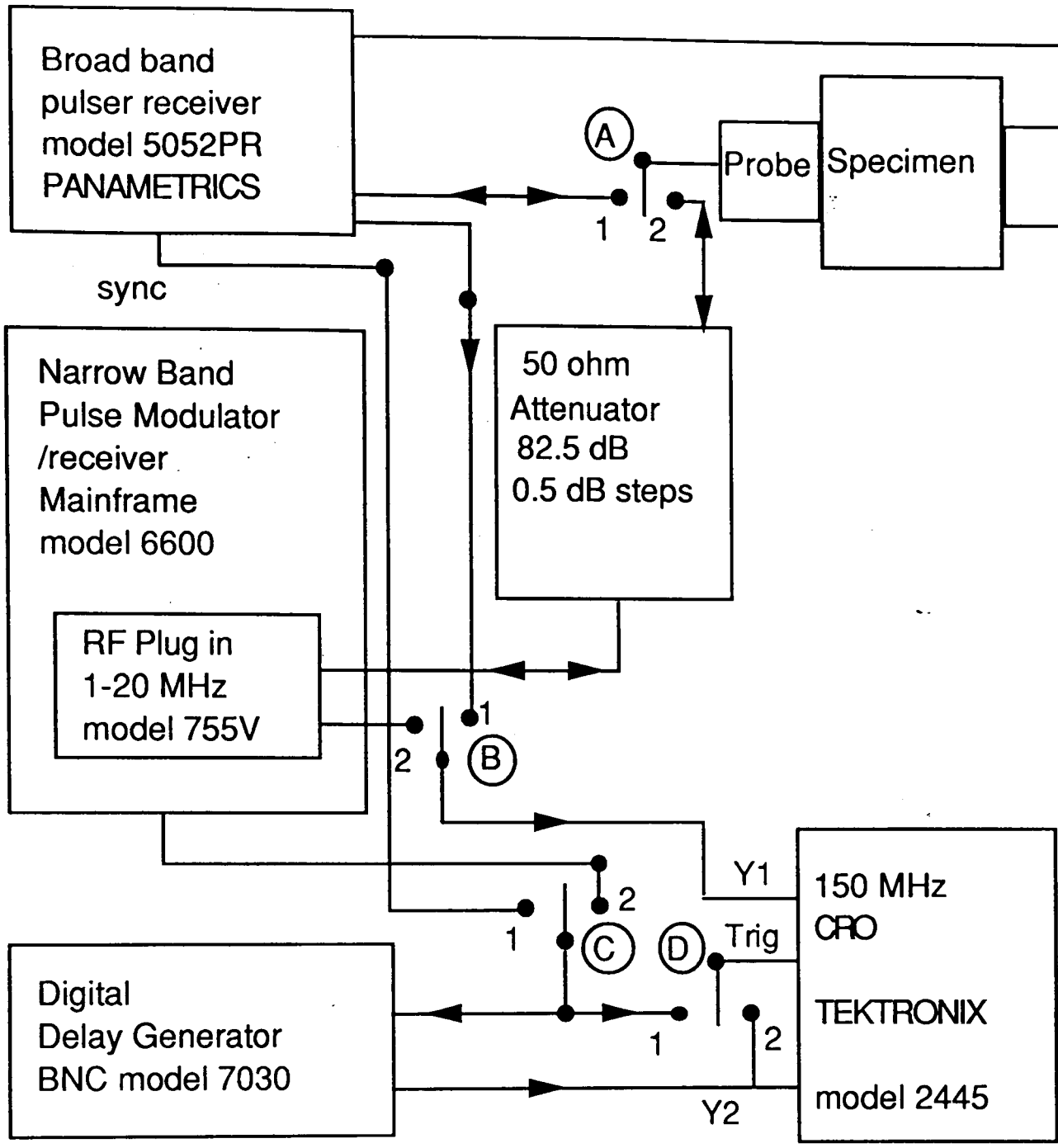

Figure 6.2 Velocity measurement equipment incorporating a digital delay generator. The Cathode ray oscilloscope can be triggered from either channel 1 or channel 2, the transmitted pulse,Y1, and the delayed pulse can be simultaneously displayed.

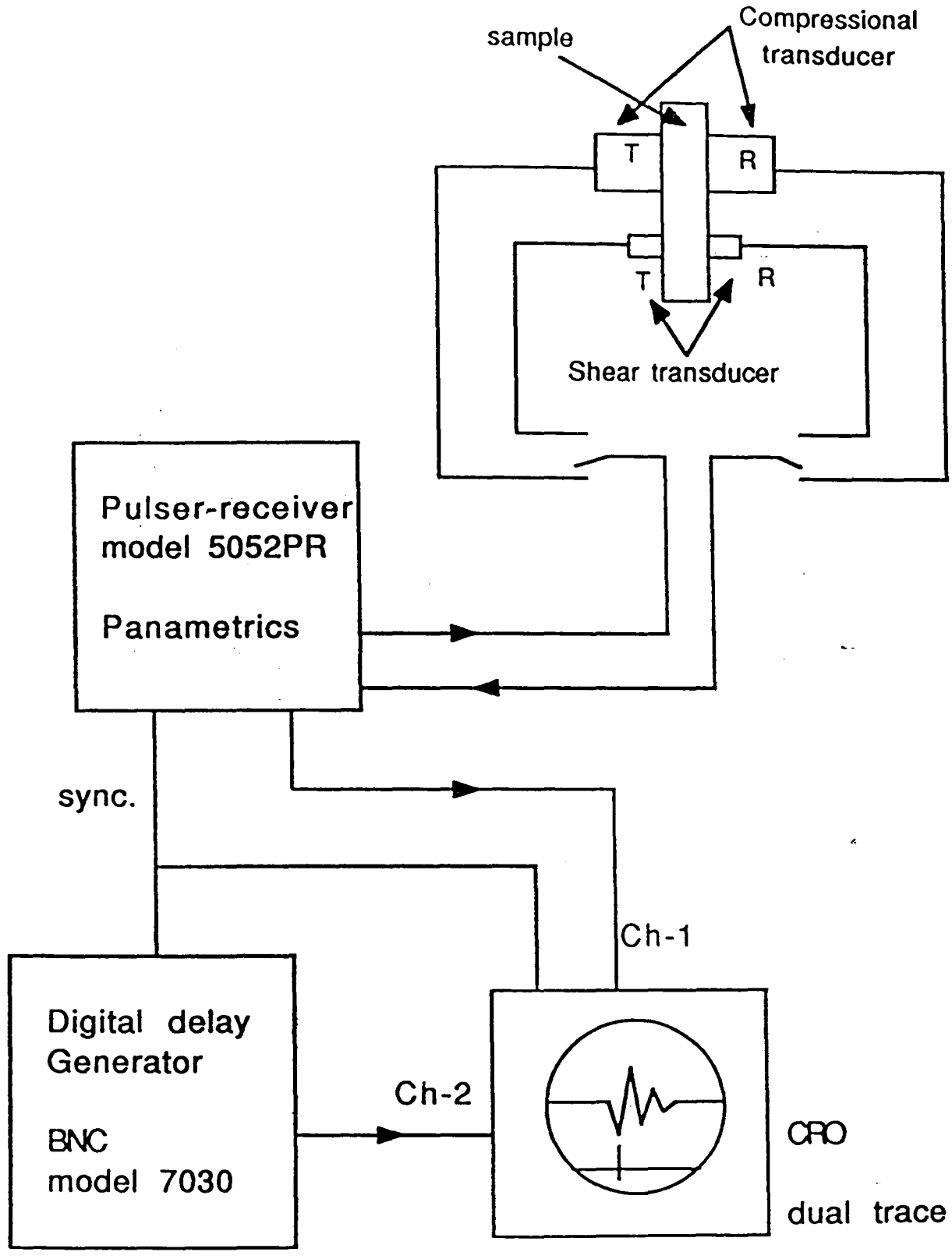

Figure 6.3 Velocity measurement equipment incorporating a digital delay generator and switched shear, and compressional, probes.

possible small delay between the start of the transmitter pulse and the triggering of delay generator and the oscilloscope, all cancel to yield the transit time τ in the specimen. With interpolation between 1ns intervals the instrumentation error for time differences is only ±100ps, the specified time jitter. Timing errors due to other causes such as sample wedging effects, bond thickness variations, and location of cycle peaks on the CRO are, of course, much larger. Setting the sample between the probes, an optimal signal was obtained, the peak height being marked by the cursor trace. With all equipment settings remaining constant, a reference signal obtained with the probes in direct contact was reduced by the attenuator such that the peak height was the same as the sample peak height, as indicated by the cursor. This procedure was repeated several times for each piece at frequencies of 0.25, 0.5, 1.25, 2.25, 5 and 10MHz, for all material variations.

This equipment can be used in single probe or dual probe configuration, but for these samples the single probe technique was, in general, inadequate for frequencies above 2 MHz.

Some velocity and attenuation measurements were repeated using

pulses of narrower bandwidth from the MATEC pulse modulator. This data confirmed that errors in the original measurements with broader pulse bandwidths were negligible compared with other sources of experimental error.

The pulser/receiver was linked via a high gain amplifier to the dual channel oscilloscope, the second channel of which was used as a cursor. A switched attenuator, variable from 0 - 82.5 dB in 0.5dB increments, was incorporated in the circuit.

6.2.3 Spectrum analysis.

Spectrum analysis was carried out using a Marconi Instruments spectrum analyser 2382 with display unit, together with Panametrics pulser-receiver PR 5052, gated peak detector GPD 5052, and 5MHz broad band probes, as shown in figure 6.4. Again a dual probe technique was used. The amplitudes may be in volts or dB with various standards. These can be subtracted and the difference displayed, thus giving a plot of frequency versus attenuation in dB in the latter case.

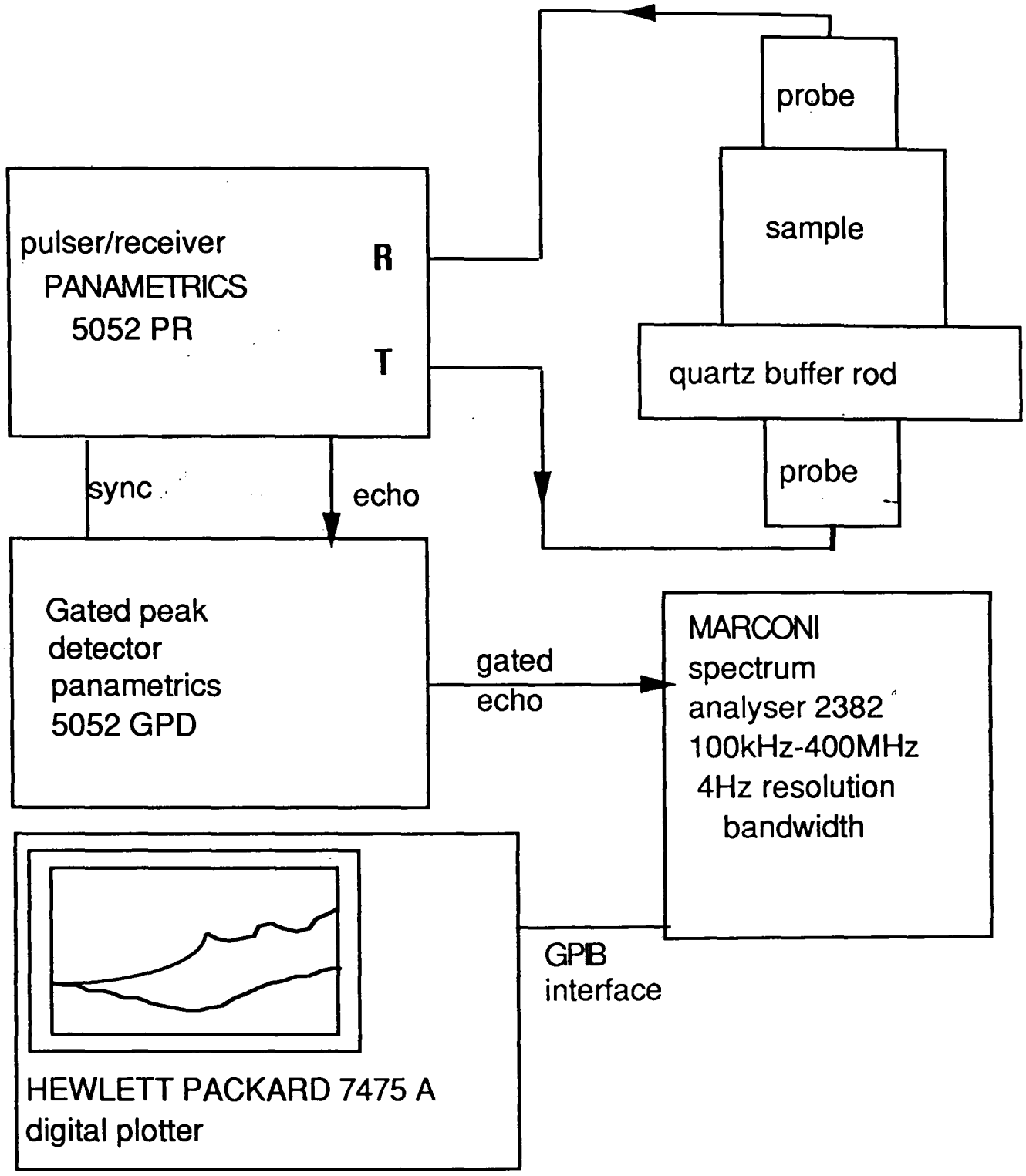

Figure 6.4 Instrumentation for the spectrum analysis attenuation measurements. The analyser plots the difference spectrum between the signals transmitted through the sample and the reference specimen, common errors are thus eliminated.

The best results were obtained using a quartz disc as a buffer rod, taking as the reference the signal through the quartz, and subtracting from this the signal through the specimen and the quartz, to give a plot of attenuation versus frequency. The buffer rod introduced the delay required to enable a correctly gated reference pulse to be obtained, the low level of attenuation introduced by the quartz was negated by the subtraction process. The grease proved to be the most suitable couplant being capable of maintaining constant bonds throughout the analysis process. Six repeat plots were made for every sample, each obtained with independent probe-sample bonds. These were superimposed on the same plot in different colours thus facilitating the reading of attenuation data for analysis.

6.2.4 Simultaneous shear and compressional velocity measurements on setting material.

For the simultaneous shear and compressional velocity measurements on setting material the instrumentation described in 6.2.2 was used. To enable both modes of propagation to be monitored on one sample a switch box was incorporated to switch between the two pairs of

normal incidence shear and compressional wave probes.

Compressional wave probes of diameter 28.50mm with nominal transmitting frequencies of 1.25MHz and 2.25MHz and shear wave probes, each 9.00mm in diameter, with nominal transmitting frequency of 2.0MHz were used, with initially a separate experimental run for each frequency. The receiving ultrasound probe for the two compressional wave frequencies has a diameter of 28.50mm and a nominal frequency of 2.25MHz whilst that for the shear wave has a diameter of 9.00mm and a nominal frequency of 5.0MHz. The frequency bandwidth of the higher frequency probe used as a receiver covers the frequency spectrum of the transmitting probe. At these higher frequencies beam divergence problems were eliminated, but unfortunately high attenuation during the first 30-50 minutes of the setting process prevented data acquisition during this time.

6.3 MEASUREMENT PROCEDURE.

6.3.1 Measurements on precast reinforced samples.

The mechanical test specimens for ultrasonic moduli measurements were, as already stated, fragments some 15x15x220mm with at least

two parallel long faces. In order to ensure repeatable results the samples were marked at various points so as to indicate direction of measurement and measured with a digital micrometer and examined ultrasonically at these same points. A simple jig was constructed to support the samples and probes to ensure accurate placement and parallelism. A constant contact pressure was arranged for each set of probes by the application of a fixed mass to the upper probe which was free to move in a vertical axis only. This arrangement shown in figure 6.5 provided adequate rigidity and accuracy for measurements together with a quick and simple operation.

6.3.2 Continuous monitoring of setting samples.

A mould cell to retain the ceramic ensuring a constant thickness of material for ultrasonic monitoring was made of perspex and is illustrated in figure 6.6. The ultrasound probes were aligned in contact with opposite sides of the perspex walls. Pressure on the walls was kept to a minimum to prevent flexing of the thin walls causing loss of parallelism. Cavities of suitable dimensions were machined into the perspex both to locate the probes and minimise the thickness of perspex at the measuring points. Screw clamps to fix the

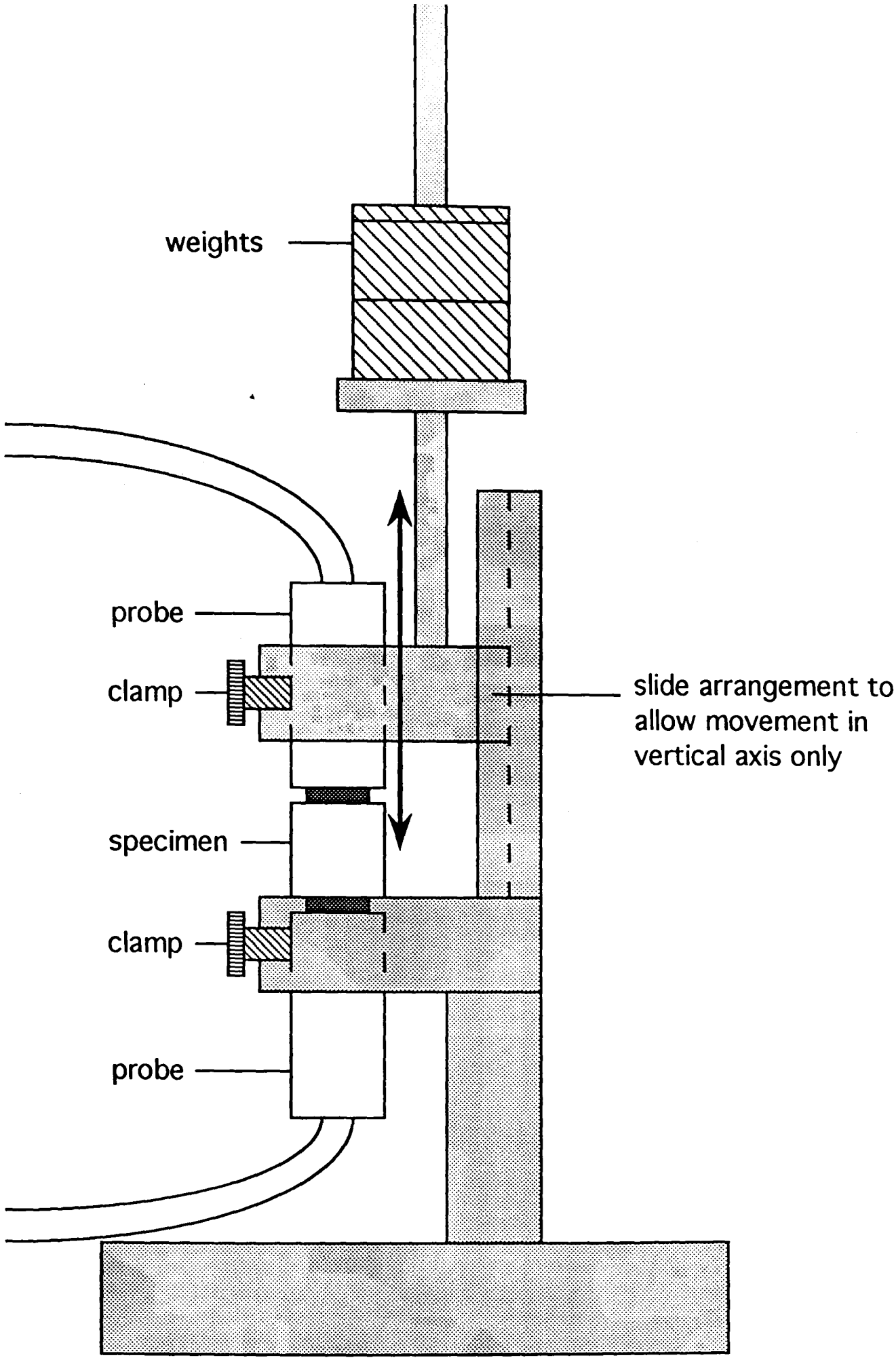

Figure 6.5 Jig for maintaining steady probe /specimen contact
The lightly stippled part complete with attached probe is free
to move in a vertical axis against the fixed heavily stippled part.

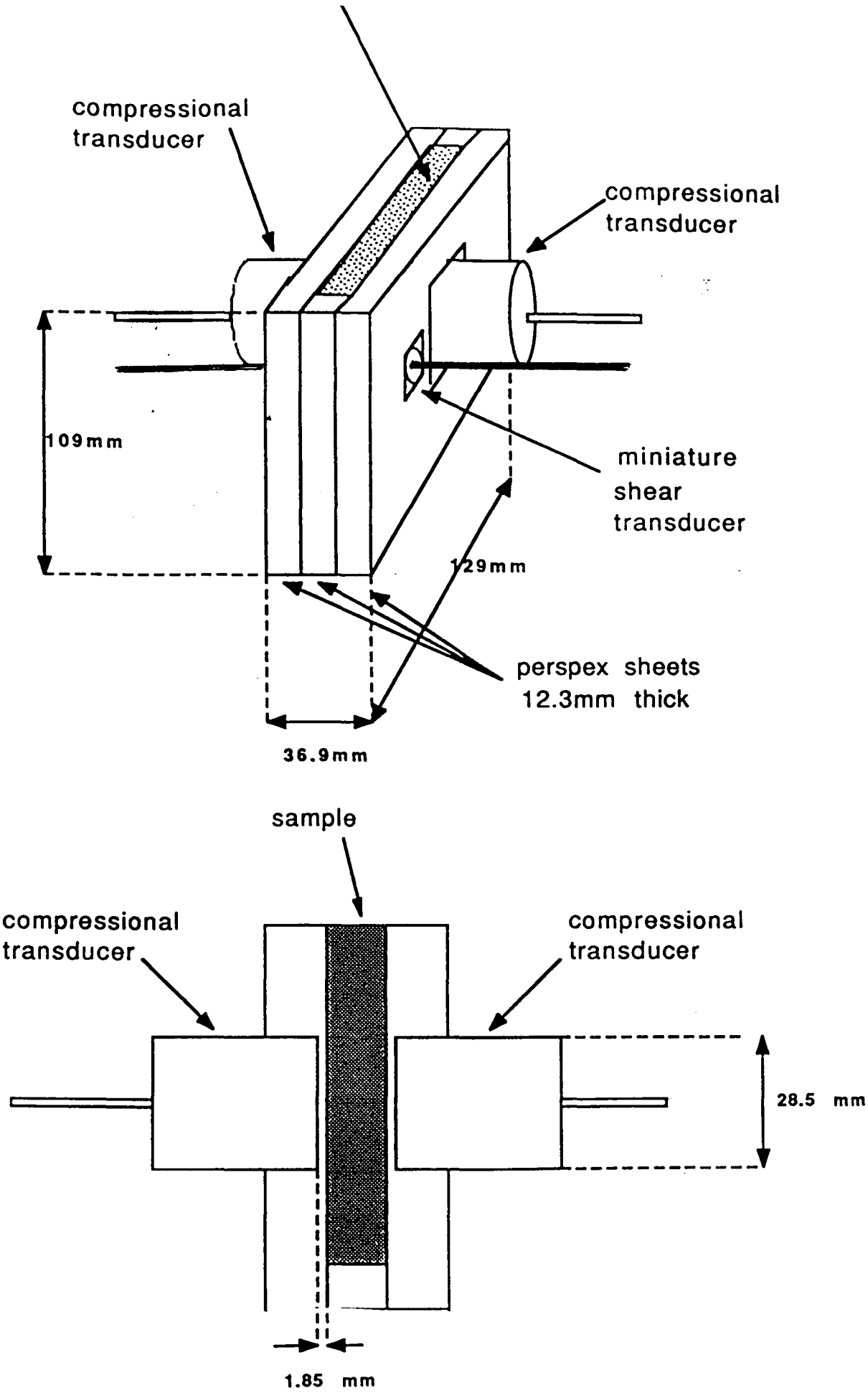

Figure 6.6. Sample mould and transducer assembly. Both the compressional and shear transducers locate in carefully aligned slots, milled to give an exact fit, and are secured by integral clamps . The lower diagram shows a cross section of the mould system.

probes in position were incorporated into the design.

Due to the high attenuation of the transmitted pulse in the sample, the optimum thickness of the mould, for the high frequency measurements, was found to be rather small (13mm). This was the minimum thickness at which the received transmitted pulse could just be separated from the pulse electromagnetically radiated directly from the transmitting to the receiving probe.

The probes were aligned and clamped in position. Acoustic bonds between the transducer buffers and the specimen were made using Castrol water pump grease, (for compressional waves) and Panametrics SWC supplied by Diagnostic Sonar Ltd (for shear waves). Measurements were made on the first quarter cycle of the first transmitted pulse to minimise any ambiguity, and monitoring continued for approximately eighty hours. They were made at five minute intervals for the first one hour and at half-hour intervals until approximately twenty hours had elapsed when measurements at approximately five hour intervals were adequate.

At a particular stage in the curing process the amplitude of the transmitted ultrasound pulse decreased abruptly. This was attributed

to the hardened material becoming detached from the cell walls thus breaking the ultrasonic bond. The ceramic was at this stage strong enough to be removed from the cell without damage, and the sample was then monitored with the probes in direct contact with the same faces of the sample.

The surface roughness of the ceramic necessitated a thicker layer of couplant than that required to couple two probes in direct contact, which meant that a simple correction for the probe buffers by difference between the delay settings with and without the specimen was not valid. The difference between the corrected transit time immediately before the loss of signal, and the measured time immediately after the removal of the sample from the cell (demoulding) is almost entirely due to the transit time of the probe buffers and the couplant. Taking the difference between this change in transit time, and the measured delay setting, yields the transit time for the ultrasound beam through the ceramic alone.

At the end of each monitoring period, the bulk density of the sample was measured using Archimedes' principle. After the initial weighing the sample was given a thin coating of grease to prevent the absorption of water by the ceramic. The error due to absorbed water

would invalidate the density value obtained, whilst that due to the presence of the grease was considered negligible, approximately 0.3% at worst. The density calculated for the basic composition, with approximately 60wt% alumina filler, was 2300 ± 100kgm^{-3} over the range of samples. Those prepared in the laboratory were generally at the lower extreme due to lack of vacuum during preparation. The variation in filler volume fraction resulted in a range of densities down to 1561kgm^{-3}. The density of the ceramic in its initial paste state was also calculated from the mass of the paste in the cell and the volume of cell filled by the paste. There was no detectable change in density between the initial and final state of the ceramic within the experimental error given above. This implies that practically all of the water present in the original mix is taken up as water of crystallisation during the course of the reaction. However the fact that the material becomes detached from the mould indicates that there must be some shrinkage taking place.

The time of flight values ranged from several microseconds to several tens of microseconds for samples ranging from 6-15 mm. The sample thickness was generally as high as possible commensurate with adequate propagation of the ultrasonic pulses. The absolute timing errors due to sample wedging effects and bond thickness variations

were estimated to be approximately 0.75% and 1% for the compressional and shear wave velocities respectively. Thus, the changes in longitudinal and shear elastic moduli with composition are accurate to within 1.5% and 2% respectively, whilst those of Poisson's ratio are accurate to within 4%. The changes in elastic moduli with time are known to a much greater accuracy because of the high precision of the timing circuitry, as implied earlier. Using the digital delay generator, and spreading out the the waveform it is reasonable to assume that the position of the peak of any cycle in an ultrasonic echo can be spatially located on a CRO screen to a precision of about 1/100 of the wave period. This corresponds to a timing error of 5ns, and it is clear that for the relative measurements under discussion the precision is limited by the operating frequency employed (which was as high as feasible given the high attenuation levels encountered) rather than by the timing instrumentation.

7. EVALUATION OF PRECAST, FULLY CURED CERAMIC SPECIMENS.

7.1 LOW FREQUENCY VELOCITY MEASUREMENTS.

As was established in section 3.4 an infinite set of compressional wave modes of decreasing amplitude, (labelled by n, where n=1,2,3...) are possible in the specimens, each one having a dispersion relation which depends on the dimensions of the sample perpendicular to the propagation direction. In each mode the pressure distribution across a section perpendicular to the rod axis is not uniform. Thus to propagate a pure mode a non uniform pressure distribution across the couplant-sample interface is required, and it follows that a uniform pressure distribution in the couplant will necessarily lead to mixed mode propagation.

The experimental data measured at various frequencies up to 5MHz show apparent variations in the longitudinal wave velocity in the three samples. Figure 7.1a-c shows a number of theoretical velocity frequency curves with these data superimposed. The data generally lie within the bounds of the peaks prescribed theoretically, and some

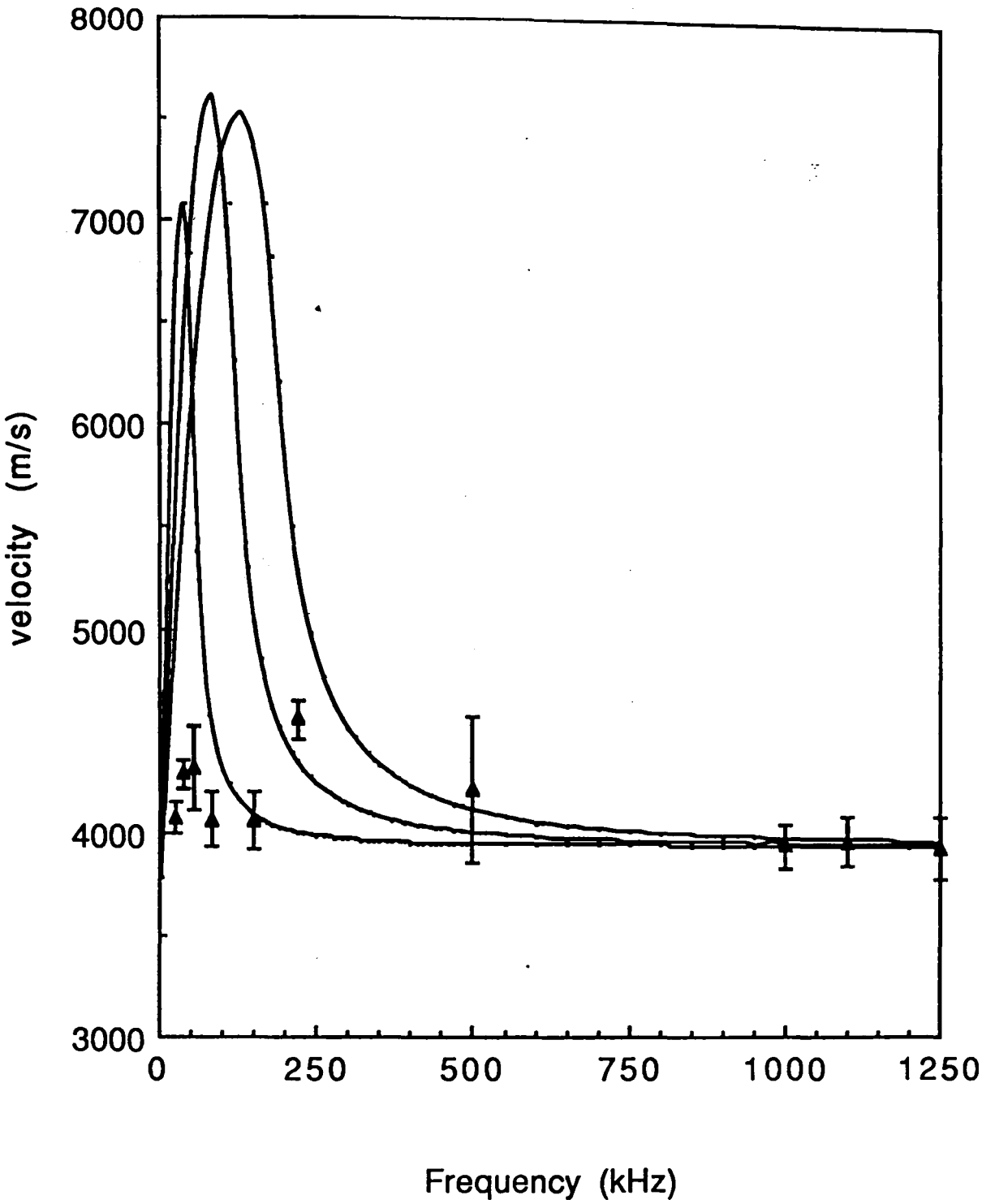

Figure 7.1. Actual and theoretical frequency dependence for the fastest observable phase velocity of a longitudinal wave pulse. The three curves correspond to propagation consisting of the rod wave mode combined with the 1st 2nd and 3rd c_n for a 1.5 x 6cm section, with c_L measured at 5MHz.
7.1a, 5% glass fibre, above
7.1b, 1.5% carbon fibre; 7.1c, no fibre content, on following pages.

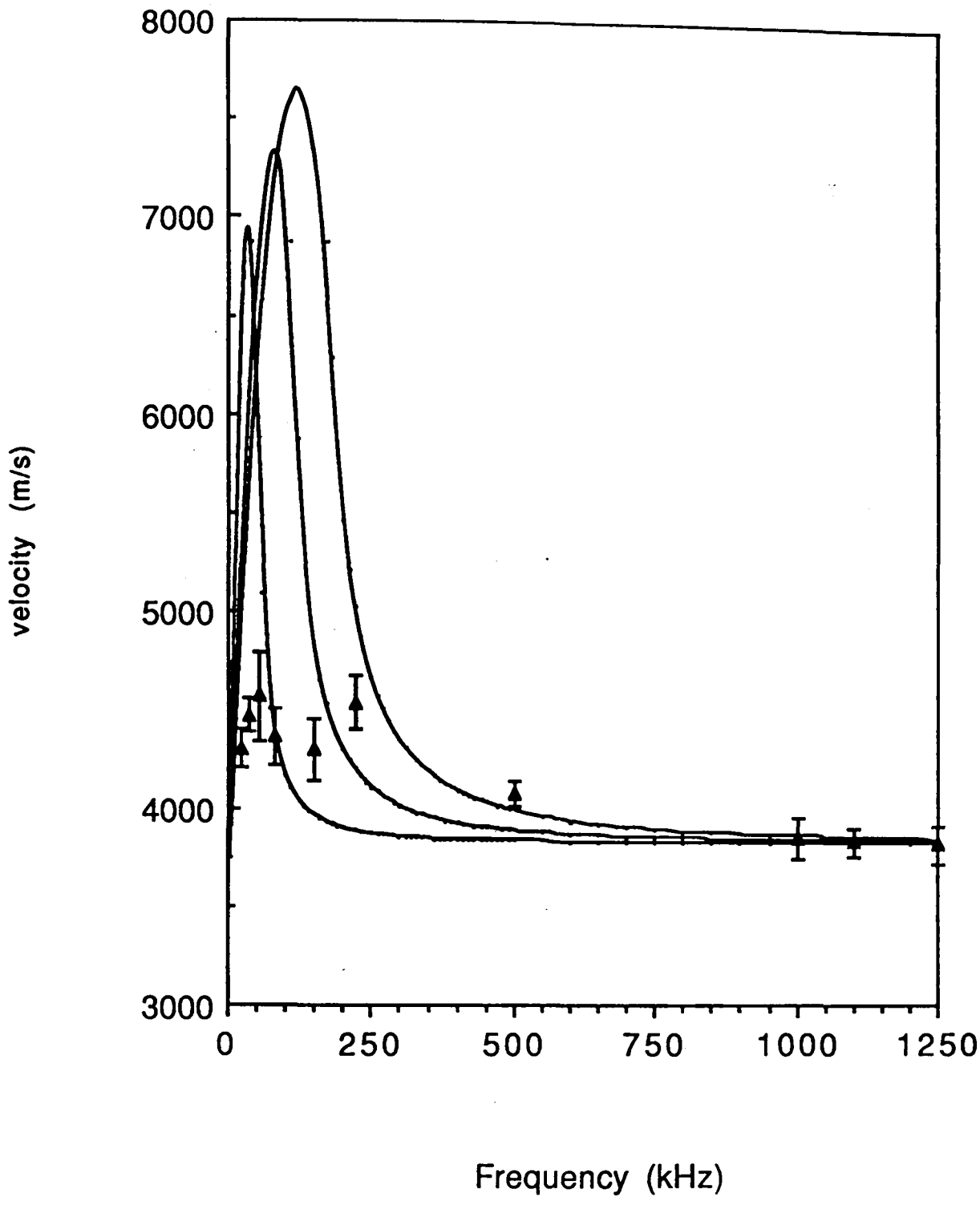

7.1b, 1.5% carbon fibre;

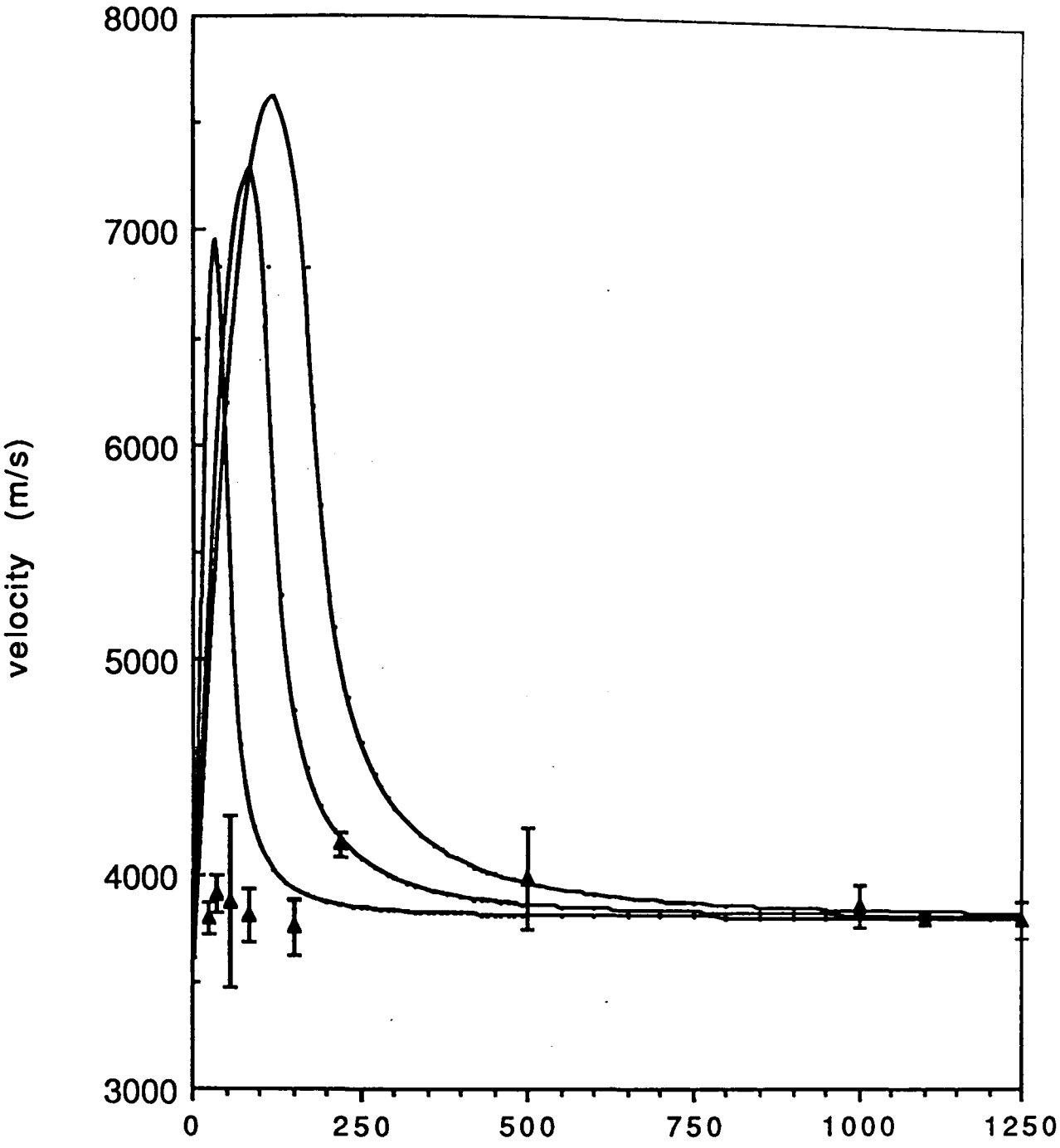

7.1c, no fibre content.

coincide approximately with the theoretical curves. However they do not correspond to any specific mode nor do they approach the theoretical maxima. The presence of a mixture of c_n modes of low n values (1,2,3) together with the rod wave mode at the lower frequencies would explain the apparent variation in velocity with frequency. These velocity data are derived from a digital indication of time corresponding to that of the fastest mode having a pulse amplitude in excess of of the equipment's trigger threshold. It is possible that different mixtures of modes are propagated over this range of frequencies thereby leading to inconsistent velocity values.

The use of these low frequency methods would seem to be limited by specimen parameters but possibilities exist for their use where samples are large and other methods are suffering from attenuation problems. In this circumstance the uncertainties about the mode of propagation and the apparent inconsistency of the velocity values will diminish as the thickness of the specimen increases. In the case of a particular component a specified measurement can be compared to predetermined values particularly where accept/reject decisions are all that is required.

7.2 HIGH FREQUENCY ELASTIC MODULI.

The data in section 7.1 demonstrate that any inconsistency in the measured velocity values occur at frequencies of about 500kHz and lower. Above this frequency the measured velocity values become independent of frequency.

A comparison of ultrasonically measured elastic moduli with theoretical bounds for 2-phase materials, Bridge (1986a, 1987c) as discussed in chapter 3, can provide information about the material.

The Hashin and Shtrikman bounds are valid for an arbitrary phase geometry (ie any particle size and shape distribution and any spatial distribution of particles) providing that certain conditions hold. These are :

(i) the particle dimensions are small with respect to $\lambda/4$,

(ii) adhesion between the filler and the matrix is good,

(iii) there are no voids in the matrix.

If an additional condition holds, namely that the particles are spherical, then the experimental data should lie exactly on the lower

bound.

It is clear that the types of defects likely in this material may be signalled by the departure of experimental moduli from the Hashin and Shtrikman bounds. For example, poor filler matrix adhesion may cause ultrasound to propagate only in the matrix so that the experimental moduli lie much lower than the lower bound. Voids produce a similar effect by lengthening the effective path length of ultrasound in the matrix.

Agglomeration will cause the experimental moduli to be frequency dependent, Bridge (1987c) if the size of the agglomerates becomes comparable with or larger than $\lambda/4$. Since, for typical fillers, the Hashin and Shtrikman bounds will be quite broad, the technique will work best when spherical particles are present so that only the lower bound need be considered as a quality indicator for the sample.

The experimental moduli were obtained from the relationships given in chapter 3 equations 11-14, and are given in table 7.2.

Table 7.2 Elastic constants measured at 5MHz

	5% Glass	1.5% carbon	no fibre	no alumina
Shear modulus (GPa)	14.33	14.77	12.66	2.30
Bulk modulus (GPa)	17.33	15.12	16.67	5.20
Young's modulus (GPa)	33.70	33.42	30.30	6.01
Poisson's ratio	0.18	0.13	0.19	0.30

The most striking feature of these results is that the bulk modulus of the fibre-free ceramic is a factor of 10 less than the bulk moduli of the constituent oxides, magnesia and alumina, which are 162 and 252GPa respectively. When such a large change of modulus occurs during a manufacturing process there are obvious prospects of using this property for non destructive process monitoring, since only a slight departure of the final material from its intended composition may produce substantial modulus variations. It is interesting to note that the elastic moduli of the three finished samples differ by less than 10%, notwithstanding the order of magnitude change in modulus during processing mentioned previously. Therefore it seems

reasonable to assume that the final modulus achieved is the norm to be expected when the chemical reactions proceed as intended, (it is assumed in this argument that the contribution of the fibres to the modulus at MHz frequencies is small due to the low filler volume fraction).

As will subsequently become apparent, the reason why the modulus of the final product is so much less than that of the starting oxides is not the weak hydrogen bonding in the waters of crystallisation. The magnesium and aluminium phosphate structures in the matrix consist of three dimensional closed rings of strong metal (Al, Mg and P) -oxygen bonds (figures 7.2 and 7.3). These rings and not the hydrogen bonding govern the elastic constants. However these rings have diameters almost twice as large as those occurring in the starting oxides, and, assuming an approximate inverse fourth power law relationship, Patel (1983), between ring diameter and bulk modulus, it is not surprising to find moduli values in the final product up to 16 times smaller than values obtaining in alumina and magnesia. Further reductions in the final modulus would be caused if free water (rather than just bound water) were still present because the former would constitute an additional phase of very low modulus.

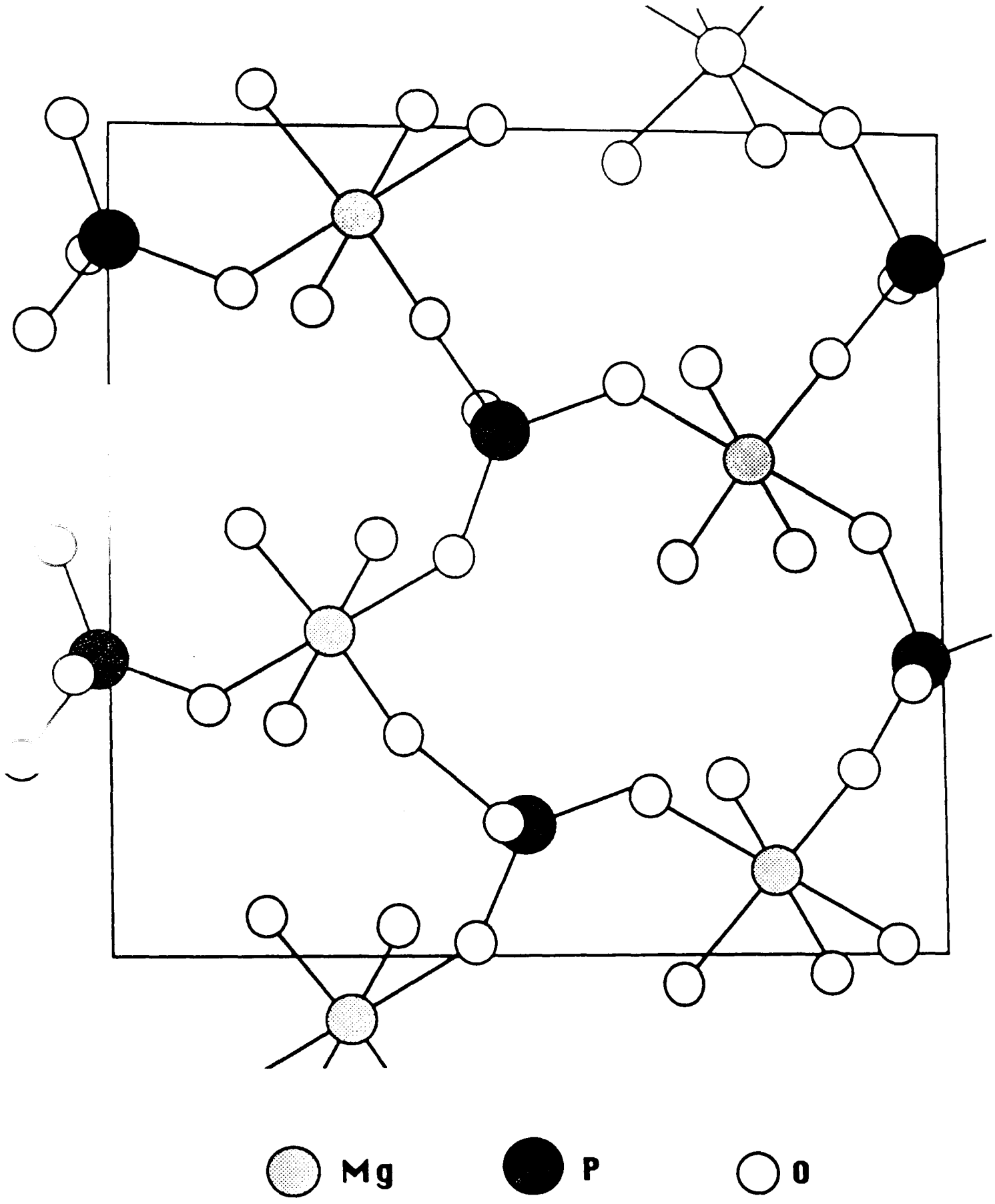

Figure 7.2. Unit cell structure of crystaline newberyite after Sutor,1967. The magnesium atoms are approximately coplanar and lie between two planes of phosphorus atoms. They are co-ordinated octahedrally by the oxygen atoms from the phosphate groups and the three water molecules, the hydrogen atoms have been ommitted for clarity.

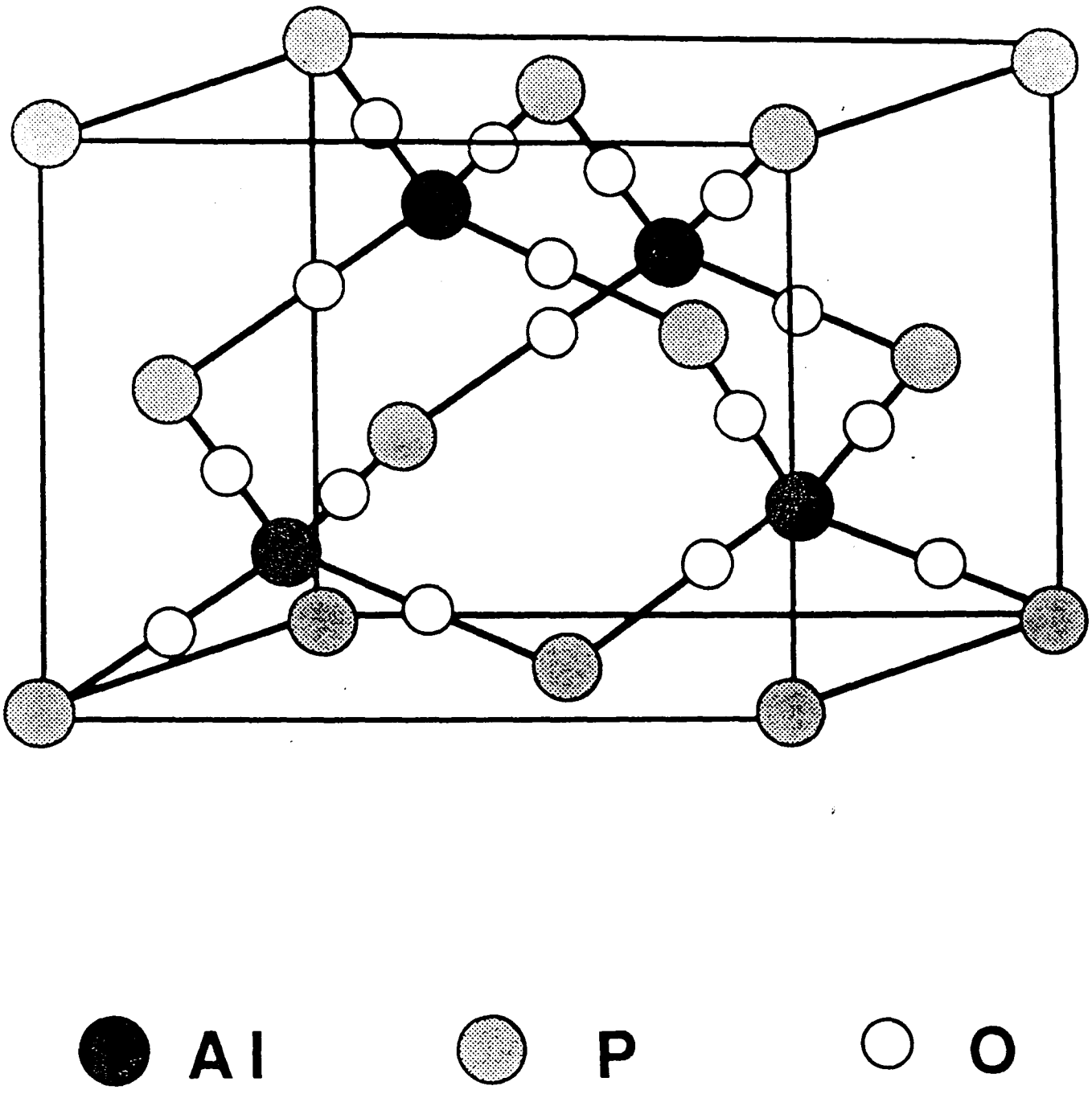

Figure 7.3. Unit cell structure of crystaline berlinite.

A sample of material with the same aluminium acid phosphate : magnesia ratio but devoid of alumina was prepared. This was found to have a density of 1561kgm^{-3}, and elastic constants as given in table 7.2. Substituting this density and those of the filled sample and alumina, 2356 and 3980kgm^{-3}, Kingery (1950), respectively, into equation 20, chapter 3, a matrix volume fraction of 0.67 is obtained. This is in good agreement with the matrix volume fraction of 0.70 obtained from consideration of the starting composition, and implies that the alumina is simply a space filler and takes little part in the reaction. It would therefore seem reasonable to assume that the elastic constants of the matrix in the filled composite are very similar to those obtained for the unfilled sample.

Proceeding on this assumption, Hashin and Shtrikman bounds were calculated considering the unfilled material and alumina as the end members such that :

$K_1 = 5.2$ $K_2 = 251.2$ $G_1 = 2.3$ $G_2 = 163.4$ $V_1 = 0.67$ $V_2 = 0.33$

Substituting in equations 16-19 from chapter 3 one obtains bounds for the bulk modulus of 9.32 and 52.09GPa, and for the shear modulus of 4.42 and 34.75GPa. The actual measured values lie between these two

bounds towards the lower bound and thus one can conclude that there is no definite layer structure, nor are the particles spherical, since the moduli are not at the lower bound. It would be reasonable to assume therefore that the particles are flattened or plate like. This assumption has since been confirmed by scanning electron microscopy.

The structure of newberyite, one end product of the reaction, was documented by Sutor, who worked on crystalline material from Skipton caves, Australia, Sutor (1967). The structure is illustrated in figure 7.2 after Sutor. Using this structural data a theoretical value for the bulk modulus was calculated, using the model of Bridge and Higazy, Bridge (1986a) discussed in chapter 2.7, from the relationship :

$$K = S \sum_{i=1}^{n} \frac{n_{fi} N_{fi} r_i^2 F_i}{9} \qquad (27)$$

Where for bond type i, N_{fi} is the number of formula units in which the bond resides per unit volume, n_{fi} is the number of network bonds per formula unit, r_i is the network bond length, and F_i is the first order stretching force constant. The factor S is less than unity and decreases with the extent to which isotropic elastic deformation leads to bending rather than direct compression of

bonds, Patel (1983). The summation function, conveniently abbreviated to K_{bc}, represents the bulk modulus that would obtain if no bond bending takes place. Values of F_i can be estimated from the empirical relation:

$$F = 5.28N \frac{(X_a X_b)^{3/4}}{r^2} + 30 \text{ Nm}^{-1} \qquad (28)$$

where r is in nm, N is the bond order, and X_a and X_b are the electronegativities of the two atoms.

Denoting i = 1 and 2 for Mg-O and P-O bonds respectively, and neglecting the weaker H-O-H bonds, the following list of values can be drawn up, taking the unit cell as shown as the formula unit.

1	Mg-O	nf_1	= 3	r_1	= 0.204 nm	F_1	= 198 GPa
2	P-O	nf_2	= 3	r_2	= 0.153 nm	F_2	= 424 GPa

The values for r being the mean of the reported values, and the values for F have been obtained from equation, Reynolds (1984), by the use of electronegativity values (Allred-Rochow scale), of 1.2, 2.1 and 3.50 for Mg, P and O, respectively, Cotton (1972). We also

have in this case

$$N_{f1} = N_{f2} = N_A\rho/M \qquad (29)$$

where N_A is Avogadro's number, ρ is the density, and M is the molecular weight.

The theoretical value for the density reported by Sutor is 2119 kgm^{-3} so that $N_f = 7.32 \times 10^{27} m^{-3}$. Substituting this and the other data above into equation (27), one obtains :

K_{bc} = 44.31 GPa (for a single crystal)

A value for S can be arrived at by the use of figure 7.4, Bridge (1986 a) which presents a systematic relationship between atomic ring size (i.e. the shortest closed circuit of bonds) and K_{bc}/K_e (where K_e is the experimental modulus) for simple oxide structures. The smallest mean ring diameter (circumference/π) in the unit cell of newberyite is 0.68nm, so that from figure 9 S $\approx$ 0.2 and:

$K = 0.2K_{bc} = 8.86$ GPa

The other end member of the reaction, aluminium phosphate can crystallise in several forms, some with various degrees of hydration. The anhydrous form stable at ambient temperatures is berlinite which

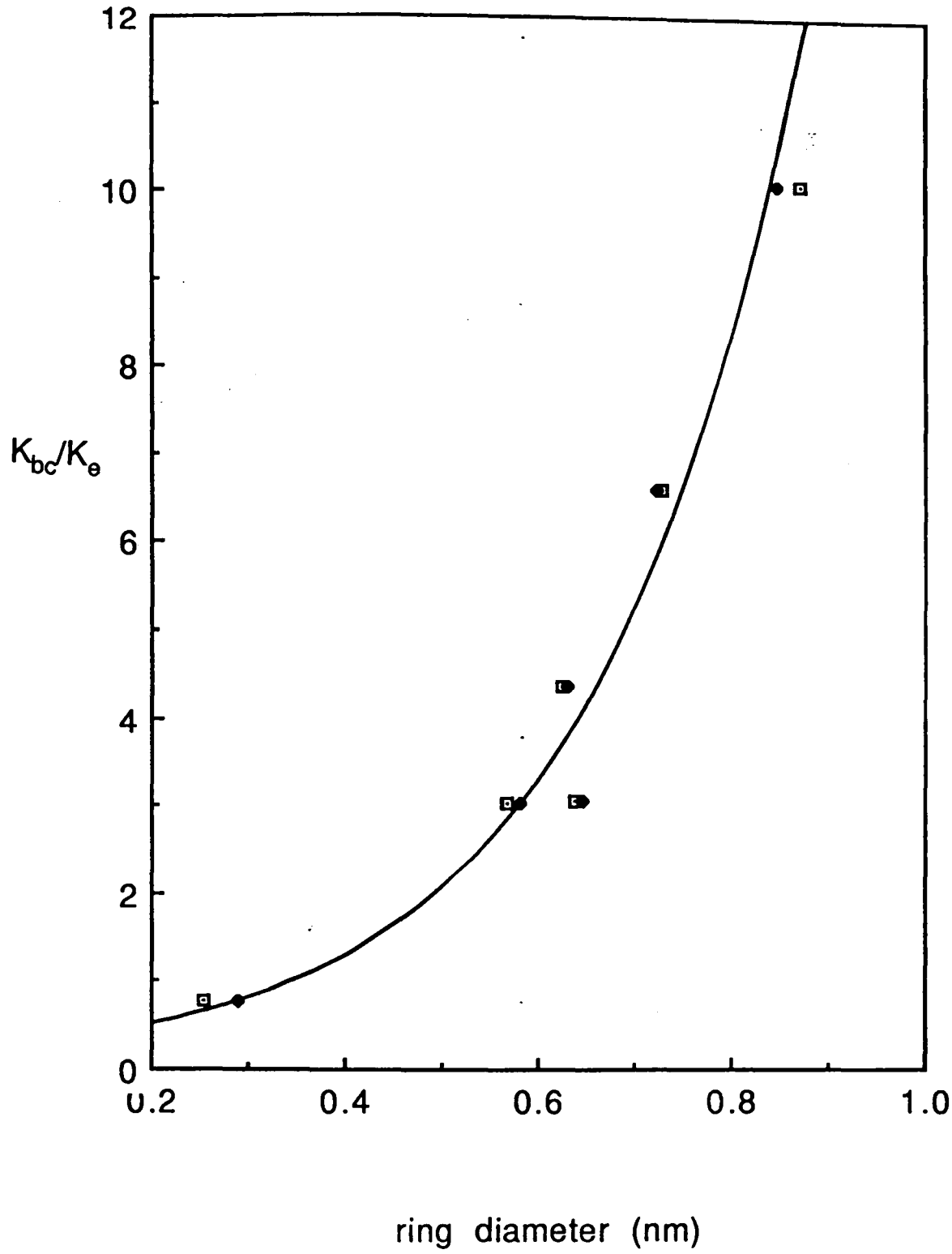

Figure 7.4. Dependence of K_{bc}/K_e on the mean atomic ring size in pure oxide glasses, where k_{bc} is the theoretical bulk modulus that would arise if bonds did not bend during isotropic deformation, and K_e is the experimental modulus.

has the structure illustrated in Figure 7.3, Kingery (1950), Wyckoff (1965), and a density of 2566kgm-3, CRC Handbook (1989). The aluminium and phosphorus have, respectively, electronegativities of 1.5 and 2.1, bond lengths with oxygen of 0.156 and 0.170nm, Wyckoff (1965), Sutor (1967), and co-ordination number of 4.

Thus from equations 28 and 29 one can derive the following values:

1	Al-O	nf_1	=	4	r_1	= 0.170 nm	F_1	= 291Nm^{-1}
2	P-O	nf_2	=	4	r_2	= 0.156 nm	F_2	= 413Nm^{-1}

Substituting the data above into equation (27), and taking Nf_1 and Nf_2 (from equation 29) to be 1.26 x 10^{28}m^{-3} one obtains :

K_{bc} = 93.6 GPa (for a single crystal)

The mean atomic ring size of 0.622nm gives from figure 7.4 a value for S of 0.29 and ;

$K = 0.29\ K_{bc}$ =27GPa

Given the reaction proposed earlier the volume fraction of newberyite in an unfilled ceramic is about 80%. Thus, given the theoretical estimates for the bulk moduli of newberyite and aluminium orthophosphate, 8.9 and 27GPa respectively, the Hashin and Shtrikman

formulae (equations 16 and 18, chapter 3) can be applied to compute theoretical bounds on the bulk modulus of this unfilled ceramic product. In the absence of a theoretical computation of shear moduli for newberyite or aluminium orthophosphate the approximation that G_1 and G_2 (equations 17 and 19, chapter 3) are equal to the experimentally determined shear modulus of the ceramic product 2.30GPa has been made. The result is:

K = 10.4GPa (theoretical estimate for non-porous unfilled ceramic)

there being no difference between upper and lower bound within the first 3 significant figures.

So far we have only considered ideal pore-free samples. Substitution of the theoretical (unit cell) density of newberyite (2111 kgm^{-3}) and aluminium orthophosphate (2566 kgm^{-3}) into equation 20, chapter 3, with an assumed volume fraction of newberyite of 0.8, the theoretical density of the non-porous product is 2208 kgm^{-3}. The density of the actual product was, however 1561 kgm^{-3}. Substitution of these two densities in equation 20, and taking the density of the pores to be zero, the volume fraction of porous voids is established to be 0.29. If the

pores are assumed to be spherical and much smaller in diameter than the ultrasonic wavelength then the elastic moduli of the porous material are given by, Kreher (1977).

$$K = K_o (1-V)/(1+f_1 V) \quad (30)$$

$$G = G_o (1-V)/(1+f_2 V) \quad (31)$$

where

$$f_1 = (1+ \sigma_o)/2(1-2 \sigma_o) \quad (32)$$

$$f_2 = (4-5\sigma_o)/2(7-5\sigma_o) \quad (33)$$

V denotes the volume fraction of pores, and the subscripted K, G and σ values denote values for the ideal pore-free material ie. the matrix.

Since f_1 varies slowly with realistic values of σ_o , in the absence of a theoretical value for Poisson's ratio, the value measured for the unfilled ceramic, 0.30, will be assumed correct.

Taking V = 0.29 and K_0 = 10.4, (our theoretical value for the ideal ceramic), substitution in equations (30) and (32) gives

K=5.0 GPa (theoretical estimate for actual unfilled ceramic)

in reasonable agreement with the experimental value of 5.20. This supports the hypothesis that newberyite is the main reaction product.

In the above model of the elastic behaviour of the ceramic matrix, starting with equation (27), an implicit assumption has been made that the presence of hydration does not affect moduli values dramatically. This seems a reasonable assumption when one considers that in both the newberyite and aluminium orthophosphate structures there are closed ring networks comprising Mg-O or Al-O, and P-O bonds so that there is no question of weak hydrogen bonds breaking what are essentially 3-dimensional networks of strong and relatively directional bonds. If such an effect had been present the K_{bc}/K_e - ring size relationship used would have been invalid.

The excellent agreement between theory and experiment achieved in the above analysis provides an example of how ultrasound -based moduli measurements can be used for quality control and assurance purposes. Comparison between experiment data and theory may allow one to decide non-destructively ie. without sectioning or chemical analysis, whether the level of porosity in the matrix is within

tolerable limits.

Certain of the above theories were applied to various compositions of barium-yttrium-copper oxide high T_c superconductors shortly after their discovery. The data were obtained from samples made in house and donated from other sources, together with published elastic data and resulted in the publication of a number of papers, Round (1987), Bridge (1988b, 1989).

7.3 ATTENUATION DATA.

The attenuation data obtained by narrow band and spectrum analysis techniques are shown in figures 7.5 and 7.6. These graphs were manually curve fitted, with estimated peaks drawn assuming the theoretical analysis to hold, a reasonable assumption in view of the spectrum analysis plots. These were obtained from the Hewlett-Packard spectrum analyser, which can display and plot the difference between any two spectra of interest, printing the spectra displayed on the VDU by means of a digital plotter, via the general purpose interface bus (GPIB). Difference spectra between samples and a

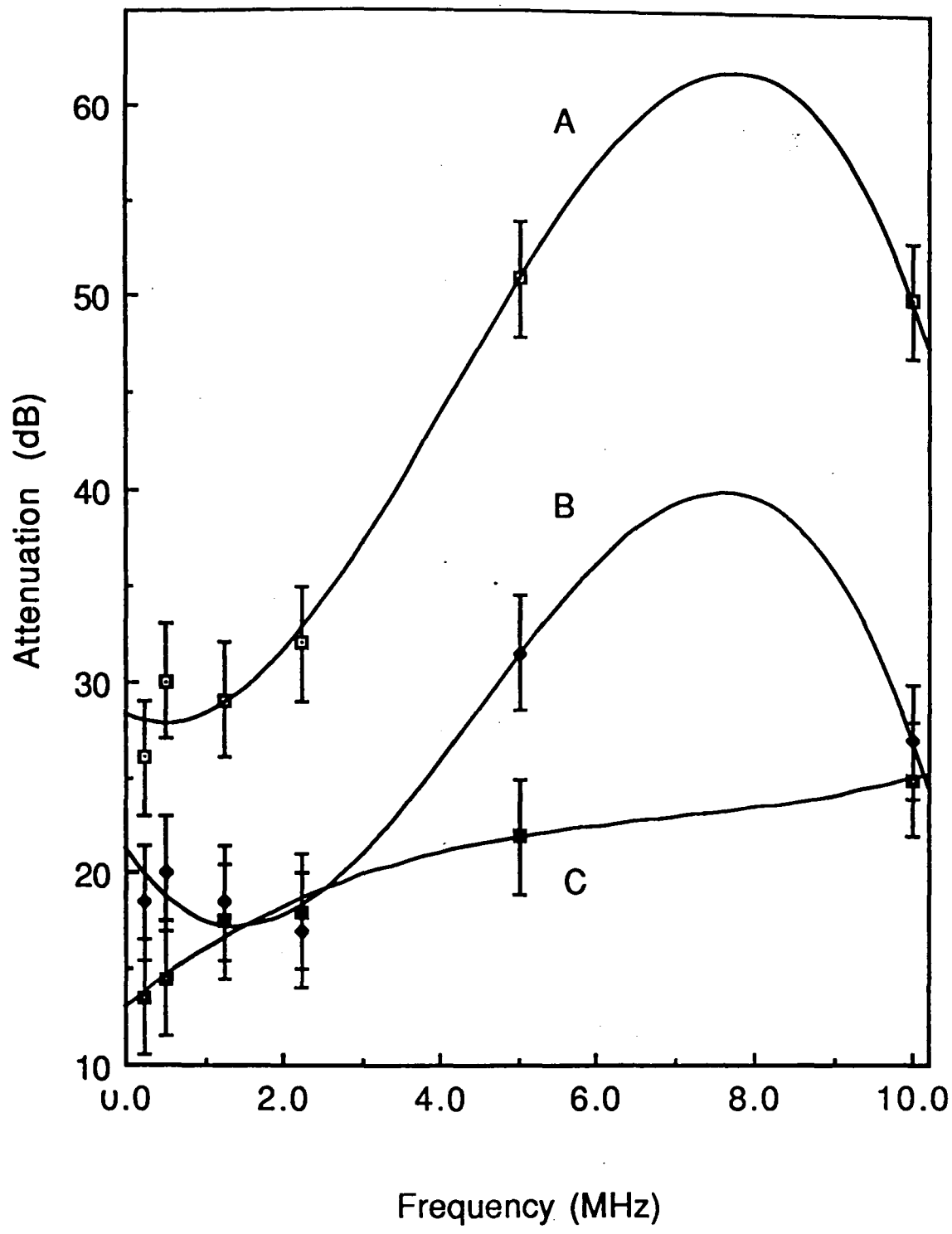

Figure 7.5. Plot of attenuation versus frequency determined by the narrowband technique on 1.5cm ceramic blocks with various fibre contents :
A, 5% glass fibre; B, 1.5% carbon fibre; C, no fibre content.

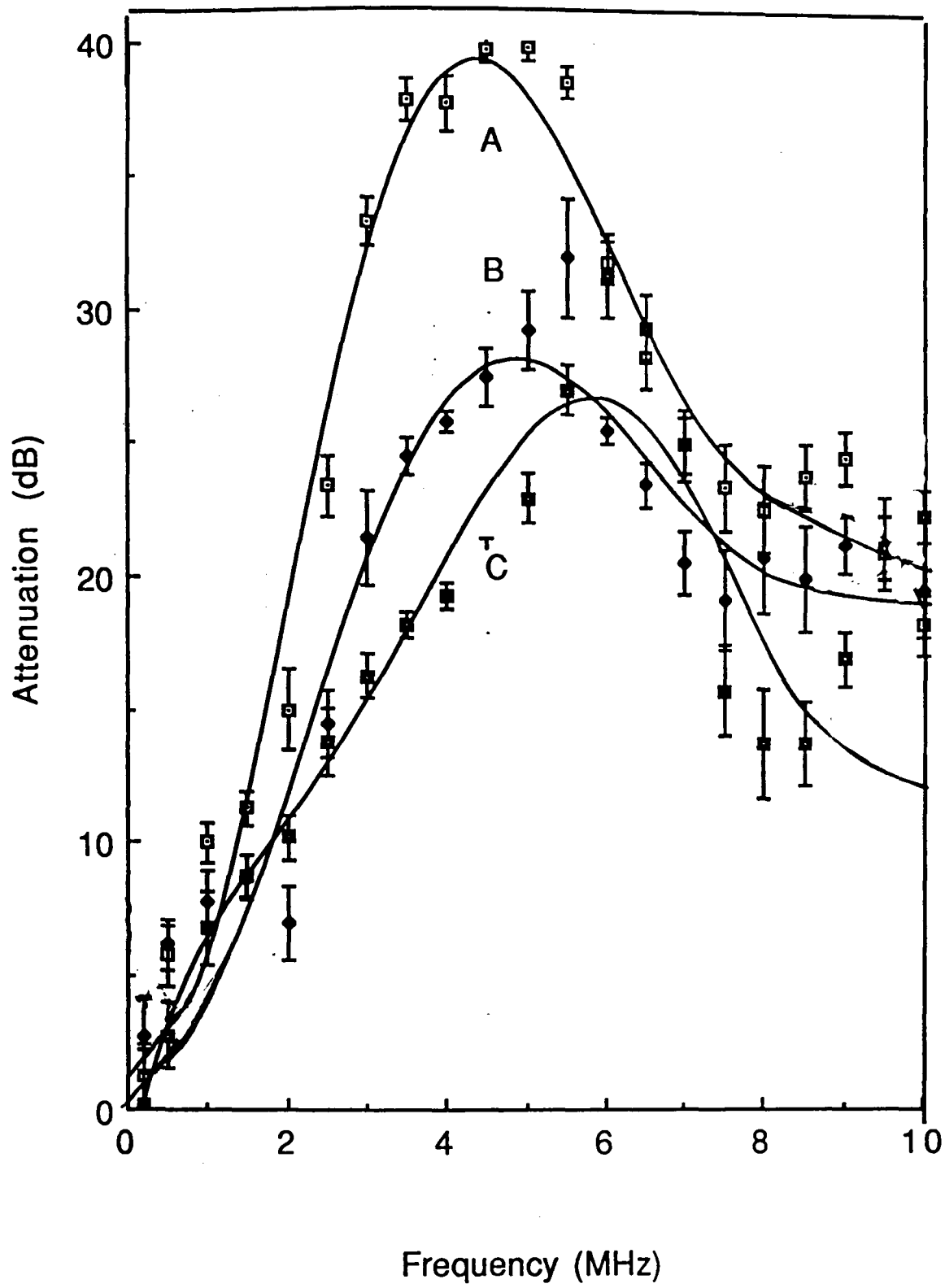

Figure 7.6. Plot of attenuation versus frequency determined by specrum analysis using 5MHz probes on 1.5cm ceramic blocks with various fibre contents :
A, 5% glass fibre; B, 1.5% carbon fibre; C, no fibre content.

quartz buffer rod reference were plotted. Six repeat plots were made for every sample, each obtained with independent probe-sample bonds, and from these the data and error bars for figure 7.6 were derived. Plots for the three samples under discussion are given in figures 7.7-7.9. The attenuation data show considerable differences in the frequency dependence of the three samples indicating a considerable potential of the measurements for materials sorting. They also show pronounced maxima indicative of the transitions between Rayleigh, stochastic and diffusive scattering modes, potentially useful in grain size determination. Differences between the narrow band and spectrum analysis techniques used would necessitate the adoption of one technique as standard, and spectrum analysis would be the most suitable commercially.

Examination of the frequency regime in which the data are most reliable (2 - 4MHz) indicates that the attenuation of all samples varies approximately as the first power of the frequency. This could be due in part to a hysteresis or multi-relaxational loss, but if there is a scattering contribution (α_s) it must be of the stochastic type, i.e. $\lambda/3 < d < 3\lambda$ and $\alpha_s \approx const_2.df$. Given the typical wave velocity of

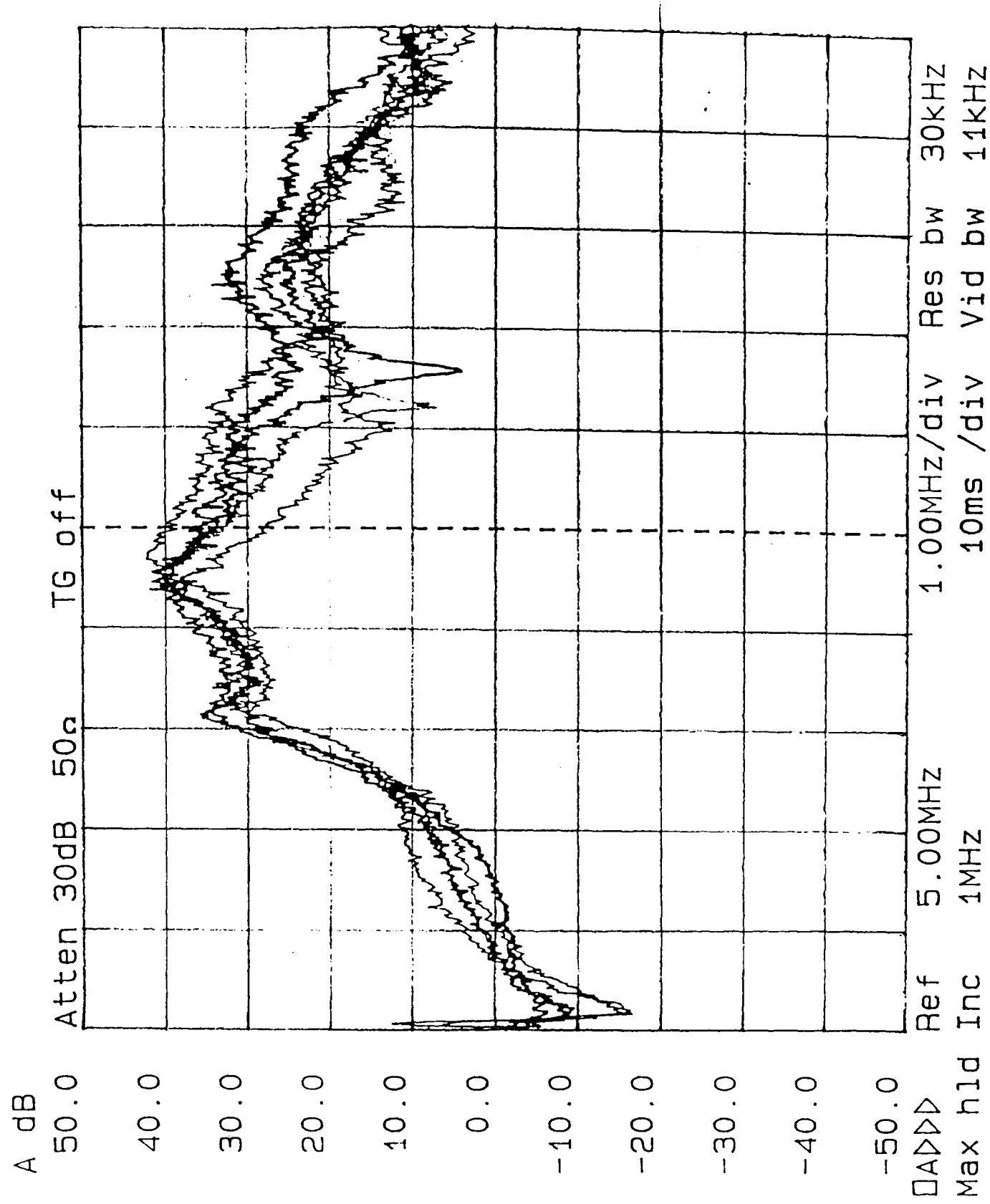

Figure 7.7. Difference spectra between ultrasonic pulse amplitude through 1.5cm thick ceramic samples and a quartz buffer rod direct to probe reference as plotted by digital plotter for ceramic composite containing 5% glass fibre.

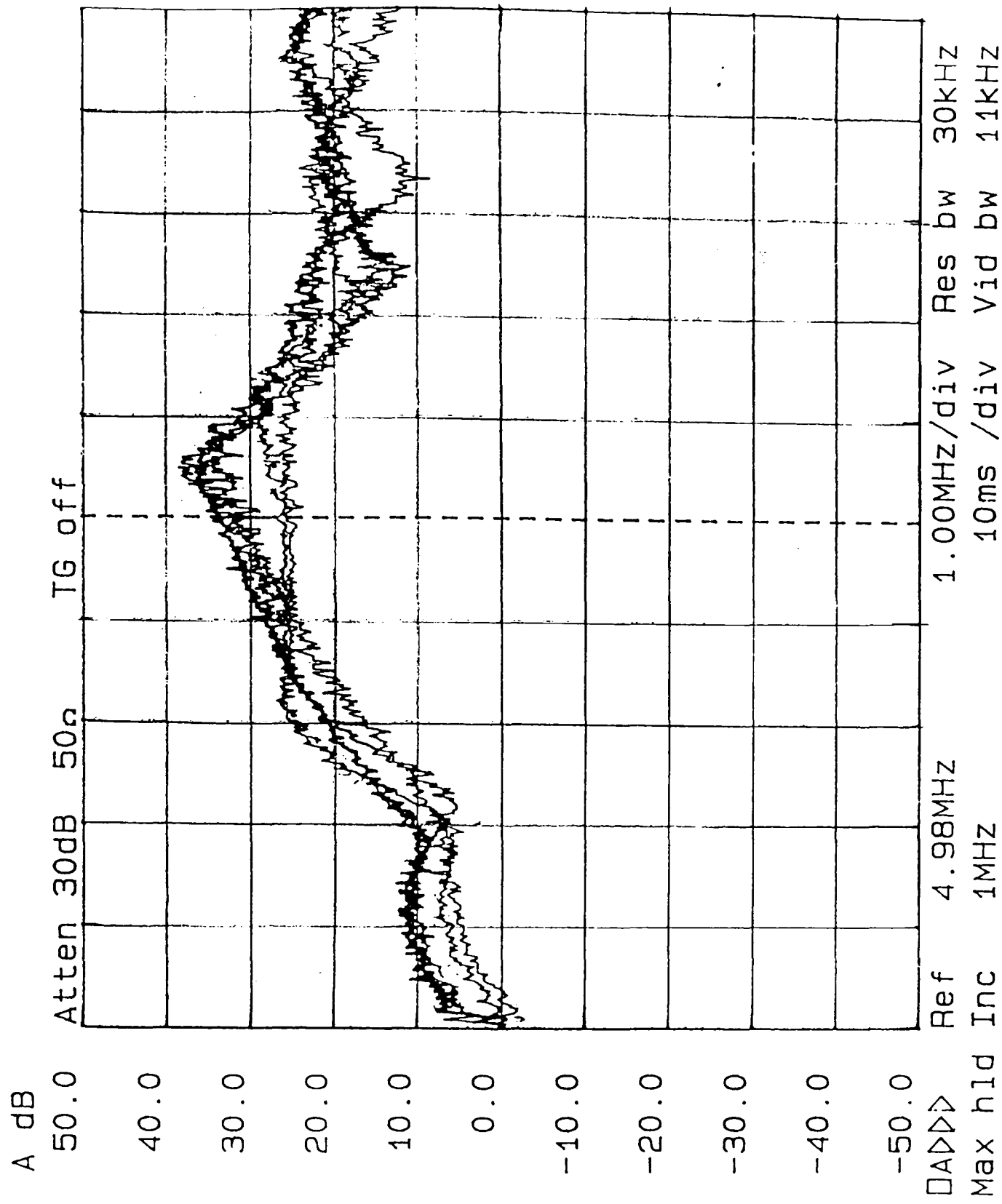

Figure 7.8. Difference spectra between ultrasonic pulse amplitude through 1.5cm thick ceramic samples and a quartz buffer rod direct to probe reference as plotted by digital plotter for ceramic composite containing 1.5% carbon fibre.

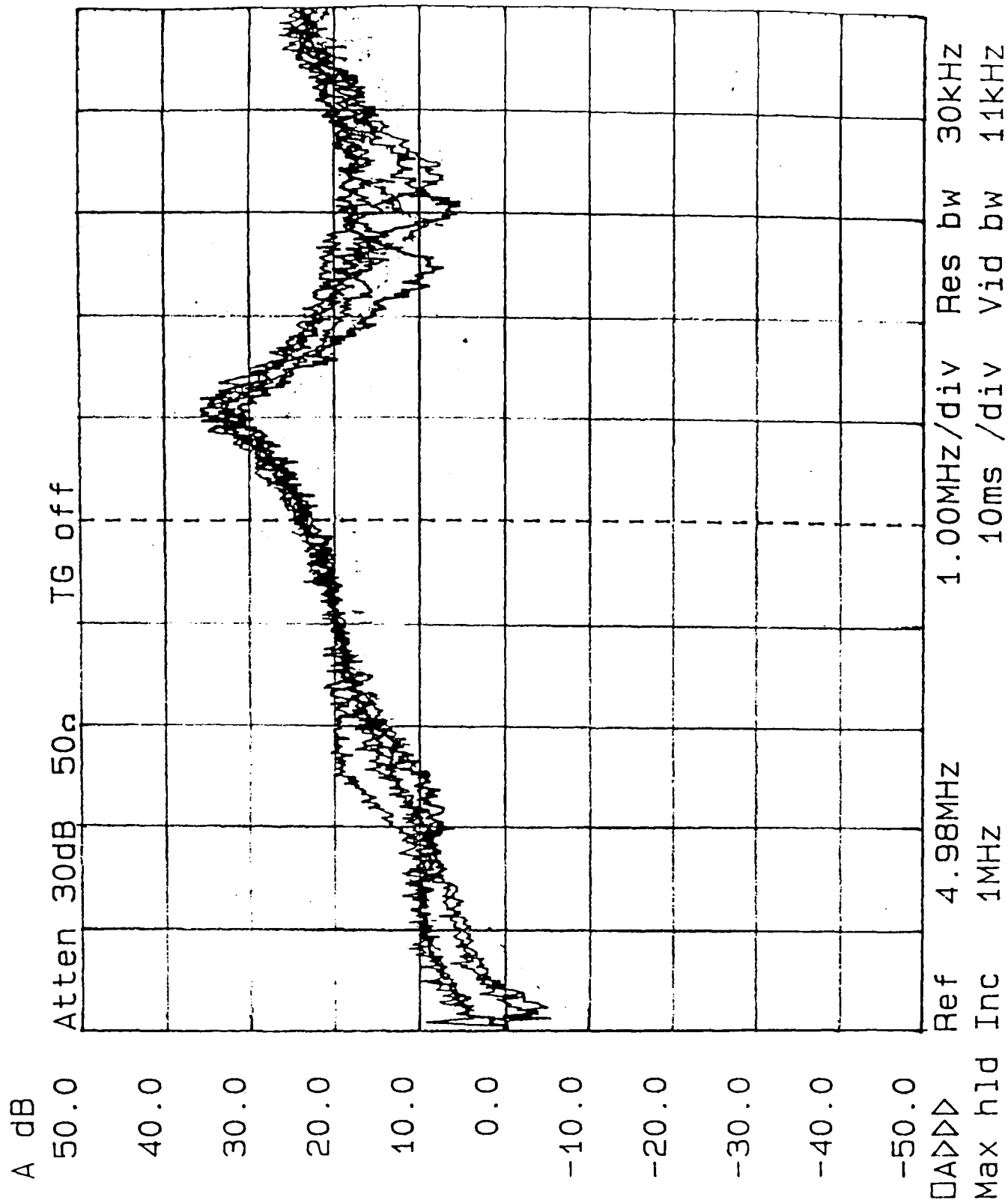

Figure 7.9a Difference spectra between ultrasonic pulse amplitude through 1.5cm thick ceramic samples and a quartz buffer rod direct to probe reference as plotted by digital plotter for ceramic composite containing no fibre. Figure 7.9b overleaf.

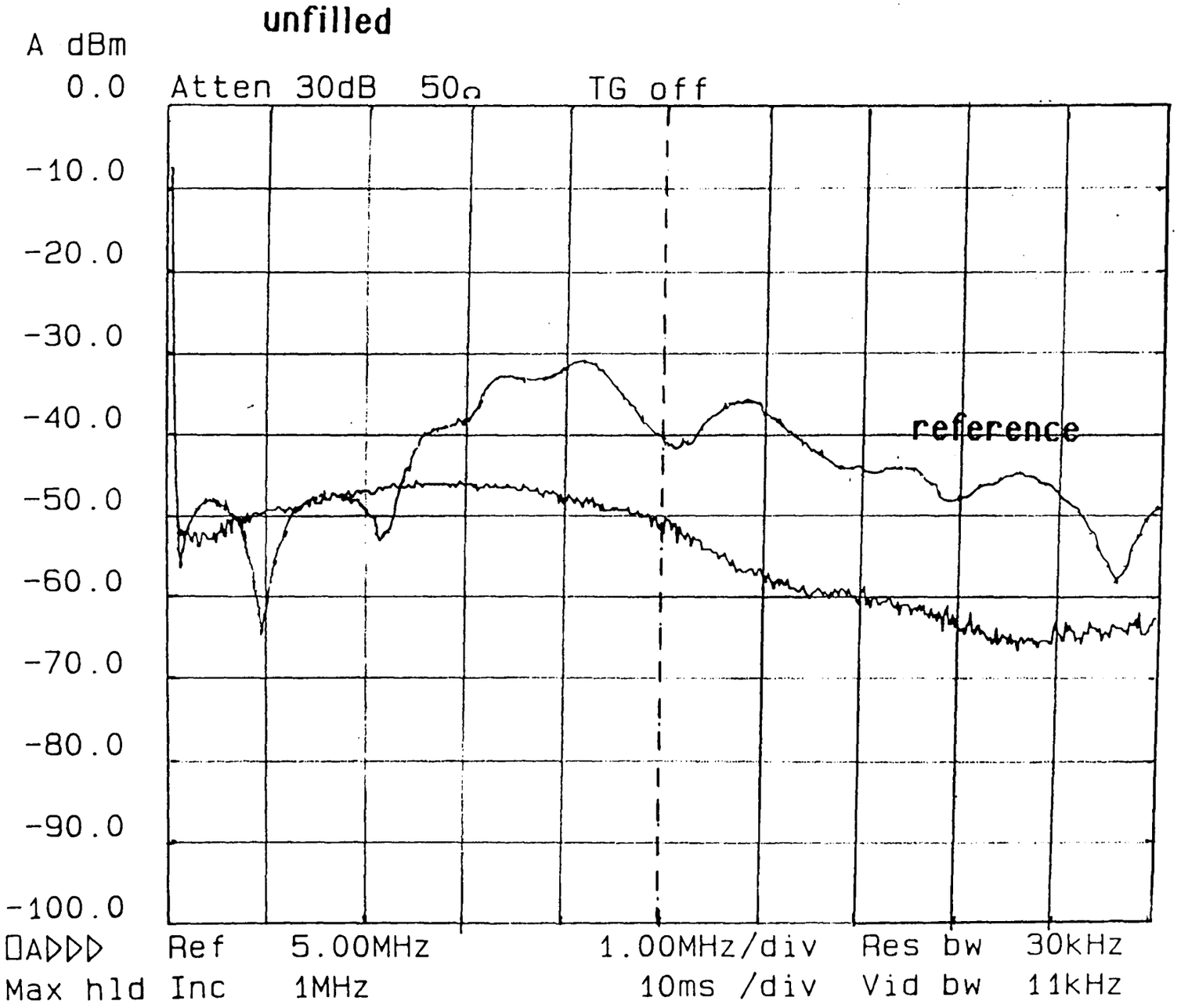
unfilled
A dBm
0.0
Atten 30dB 50Ω
TG off
-10.0
-20.0
-30.0
-40.0
-50.0
-60.0
-70.0
-80.0
-90.0
-100.0
reference
□A▷▷▷ Ref 5.00MHz 1.00MHz/div Res bw 30kHz
Max hld Inc 1MHz 10ms /div Vid bw 11kHz

Figure 7.9b

4000 ms^{-1}, λ lies in the range 1-2 mm, implying extreme bounds of the mean diameter of scattering grains of 0.3-6.0 mm.

Thus, scattering from fibres cannot account for the observed frequency dependence, since the geometrical mean of their cross-section is only 0.04mm. As a result $d \ll \lambda$ which would be expected to lead to a d^3f^4 term in the attenuation coefficient, i.e. Rayleigh scattering, which is not in evidence. Thus grain boundaries, rather than the fibres, must be the dominant scatterers in the frequency regime under discussion. For the glass fibre filled sample the attenuation became frequency independent above about 6MHz, implying that diffusive scattering conditions hold, that is $d > 3\lambda$ and $\alpha_s \approx const_2./d$. Since λ is 0.6mm at 6MHz the scattering particles can be expected to have dimensions of approximately 1.8mm. Taking attenuation data at 3MHz, and ignoring the possible presence of an absorption contribution, one can estimate the dimensions of the scatterers in the samples which do not exhibit a plateau in the attenuation versus frequency plots. This gives values for d of 1.2 mm and 0.5 mm for the carbon fibre filled sample and the fibre-free sample respectively. The above three estimates are in rather good agreement with the results of microscopy on polished specimens, see photomicrographs, chapter 5.

At frequencies higher than those presently investigated the Rayleigh scattering contribution from the filler particles would begin to become relatively strong compared with the diffusive scattering from grains and the multi-relaxational and/or hysteresis losses. However the high level of these "background" losses will require thinner samples or increased probe output power for filler scattering to be detectable.

The reseach data from samples made in house and supplied by Mr A. Green of Thorn E.M.I., and interpretation leading to possible materials evaluation strategies, discussed in this chapter, have since been published, Round (1988a, 1988b), Bridge (1991).

8. COMPRESSIONAL AND SHEAR WAVE VELOCITY MEASUREMENTS ON SETTING MATERIAL.

8.1 VELOCITY MEASUREMENTS.

By monitoring the transit time through a standard thickness of ceramic the compressional and shear wave velocities for seven samples were obtained over a period of 100 hours in each case. The compositions used are given in table 8.1 and the values of sound velocities and elastic moduli are given in table 8.2. The measured compressional and shear wave velocities plotted against the elapsed time for different alumina contents are shown in figures 8.1 and 8.2.

At some stage during each run, contact between the perspex and the sample was broken, due to a slight shrinkage of the sample resulting in a loss of signal. At this point the central piece of the mould was removed, and, ensuring that the ceramic remained in the correct location, both covers were again fixed in place, making new bonds. Additional time delays were introduced by the new couplant layers and slight changes in geometry, which led to an apparent fall in velocity through the specimen. This delay was noted and used as a further

TABLE 8.1

The composition of alumina, magnesia and acid phosphate in weight % .

Sample	Al_2O_3	MgO	$Al(H_2PO_4)_3$
A	0	15.55	84.45
B	10	13.99	76.01
C	20	12.44	67.56
D	30	10.88	59.12
E	40	9.33	50.67
F	50	7.77	42.23
G	60	6.22	33.78

TABLE 8.2

SAMPLE :	A	B	C	D	E	F	G
Density (kgm^{-3})	1561	1641	1706	1775	2058	2260	2369
Porosity (%)	32.6	28.4	23.2	18.9	21.0	16.6	13.9
Volume fraction	0.000	0.033	0.060	0.089	0.205	0.289	0.334
Youngs Modulus (GPa)	6.0	7.5	8.5	12.0	14.2	21.7	26.0
Shear Modulus (GPa)	2.3	2.9	3.4	4.9	5.8	9.0	11.0
Bulk Modulus (GPa)	5.2	5.9	6.0	7.5	9.0	12.5	13.7
Poisson's Ratio	0.305	0.285	0.265	0.236	0.234	0.213	0.182
Reaction Rate Index, n_1	1.643	1.093	1.187	1.222	1.657	1.859	1.475
Reaction Rate Index, n_2	0.317	0.254	0.361	0.387	0.434	0.533	0.780
Time constant 1 (hours)	0.882	0.665	0.861	0.566	0.483	0.380	0.203
Time constant 2 (hours)	1.782	1.286	0.643	0.174	0.339	0.134	0.110

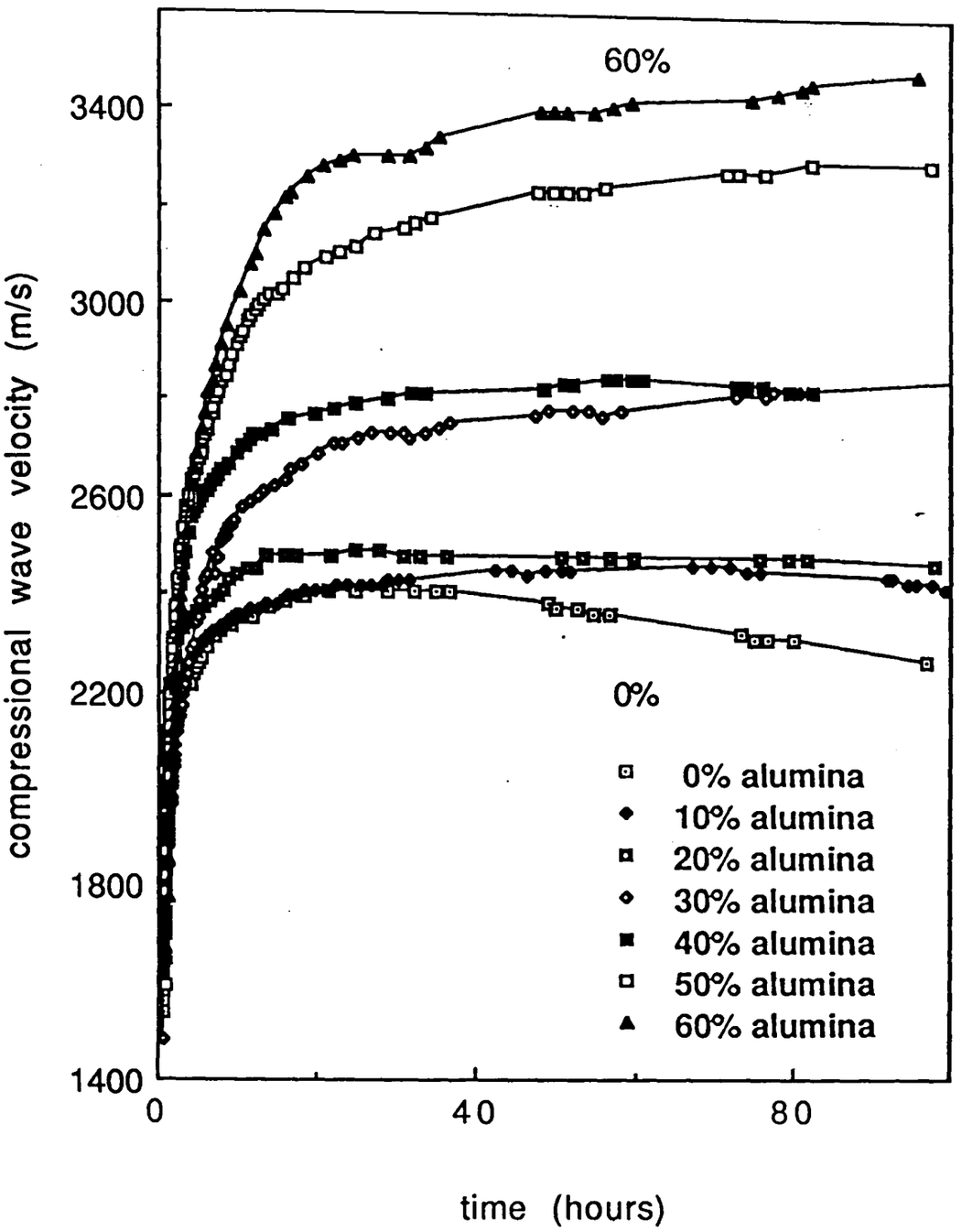

Figure 8.1. Plot of compressional wave velocity versus time. The plots for the various compositions are generally in order and for clarity only the limiting alumina contents have been labelled. The legend, shown in this figure only, is applicable to all figures showing composition dependence.

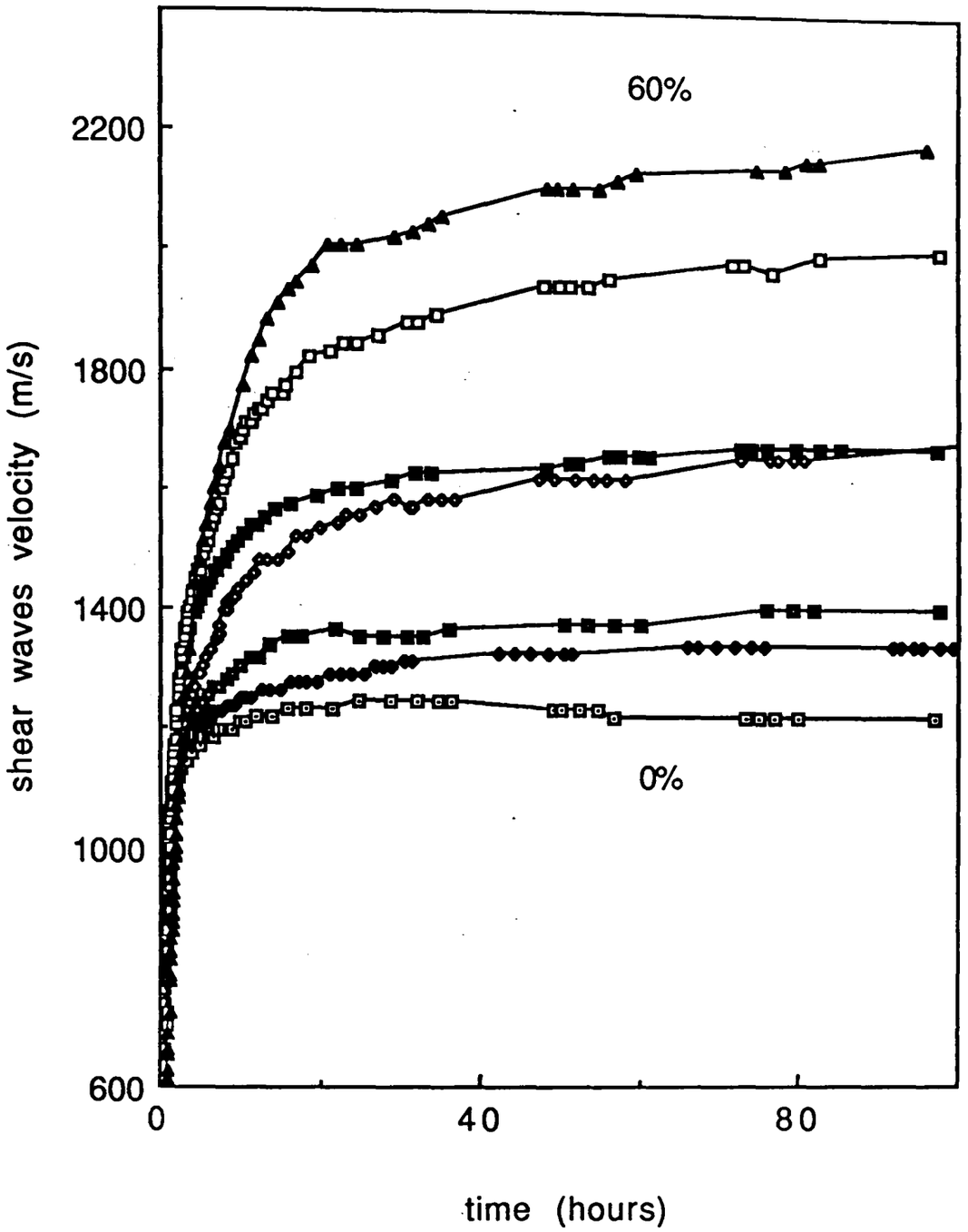

Figure 8.2. Plot of shear wave velocity versus time, legend for the compositions as in figure 8.1.

correction in all later transit time measurements on that sample. This work was based upon a feasibility study carried out in conjunction with Mr K.S. Tan, a masters student working under my guidance and supervision. This feasibility study was published and the paper, Tan (1989).

From the compressional and shear wave velocity graphs, it can be seen that the velocity increased with time, eventually reaching a constant value after 15 to 100 hours, depending upon alumina fraction. It is also clear that the sound velocity increases with increasing alumina content.

8.2. THE COMPOSITION DEPENDENCE OF THE ELASTIC PROPERTIES.

It was established earlier that there is little change in the density of the material between the initial and the final states. From the final density of the material, assuming constant density, and equations (11) to (15), section 3.3, the elastic moduli and Poisson's ratio were determined. The calculated elastic moduli; (Young's modulus, bulk modulus and shear modulus), and Poisson's ratio were plotted against the elapsed time as shown in figures 8.3 to 8.6.

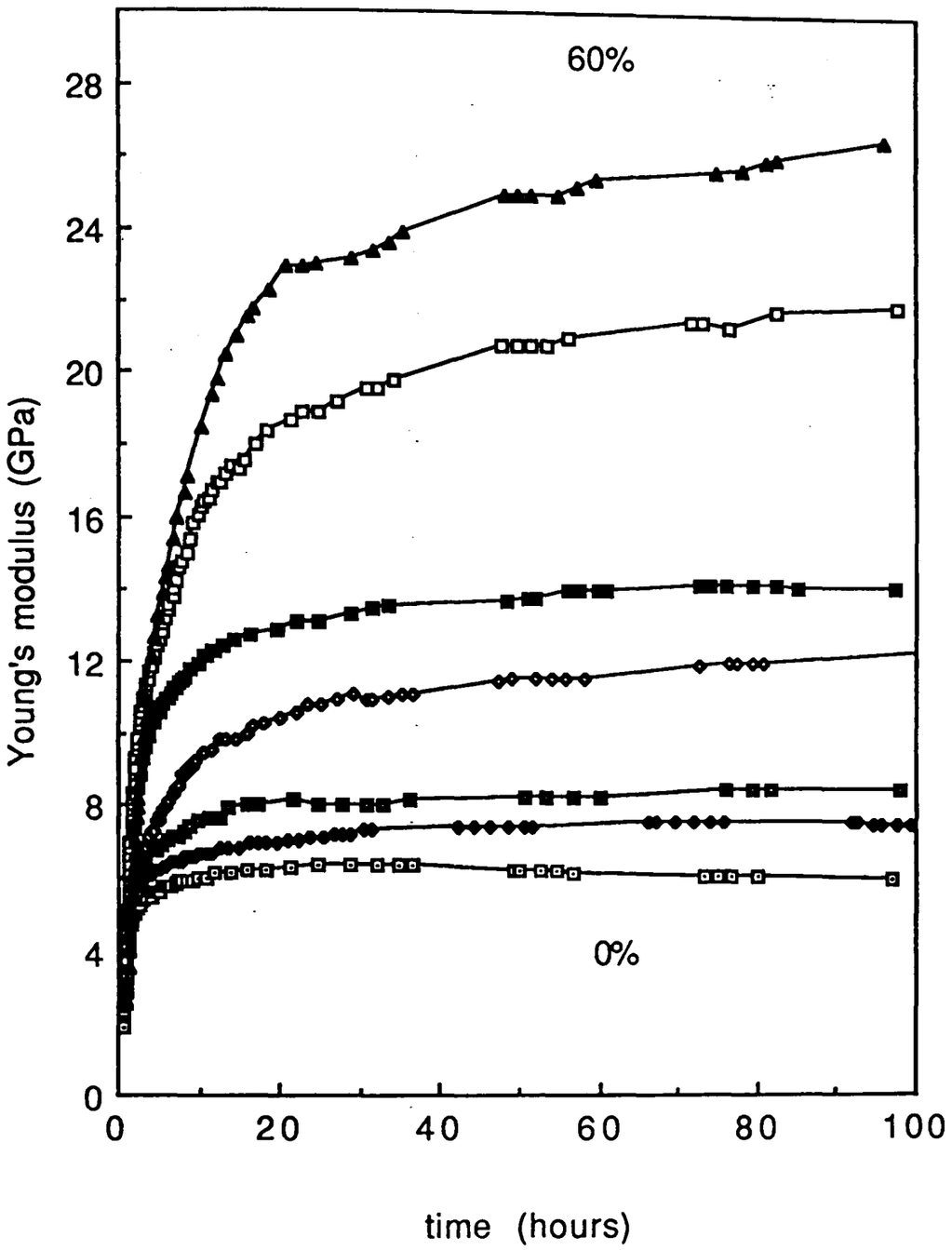

Figure 8.3. Plot of Young's modulus versus time , legend for the compositions as in figure 8.1.

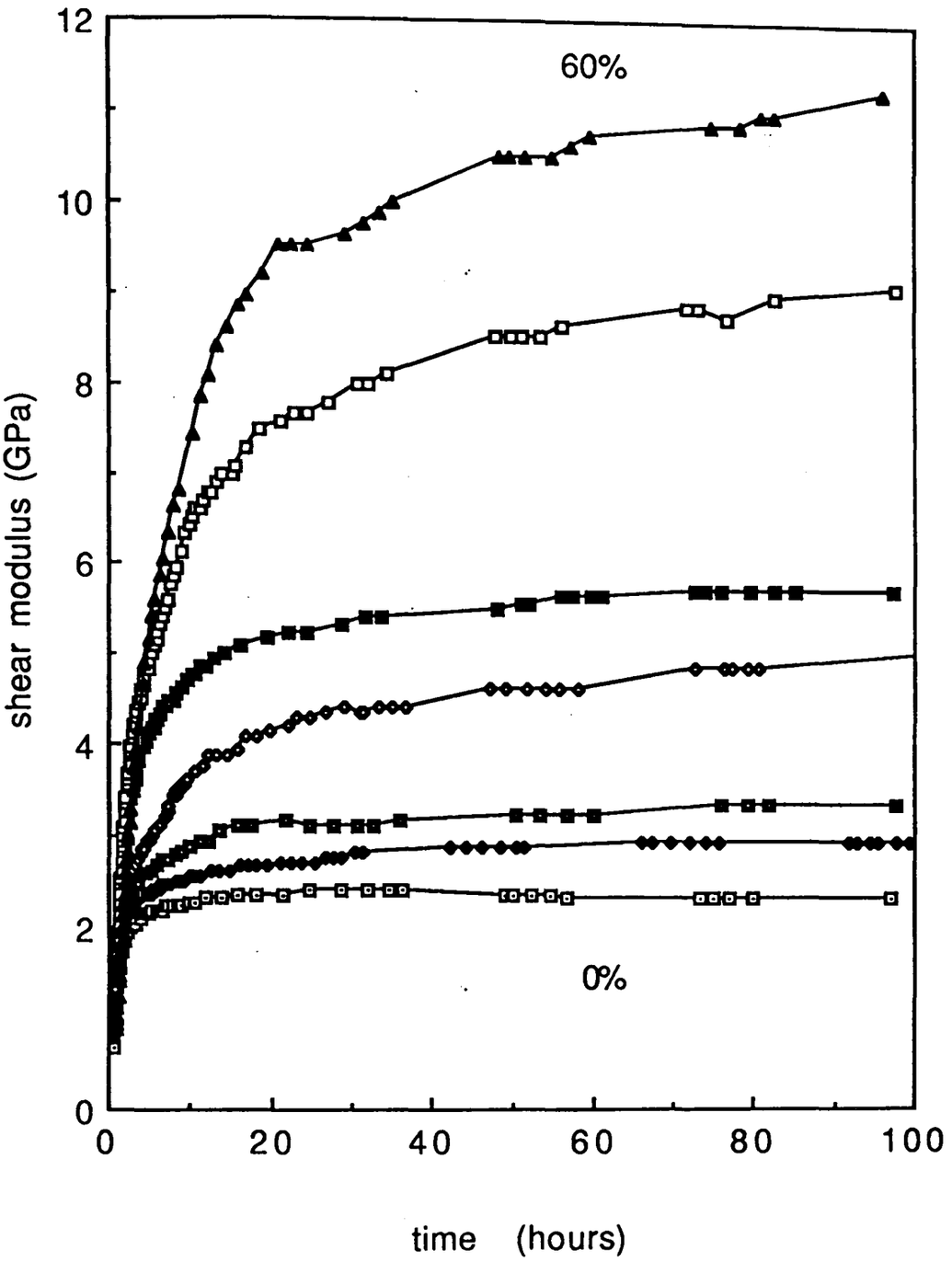

Figure 8.4. Plot of shear modulus versus time , legend for the compositions as in figure 8.1.

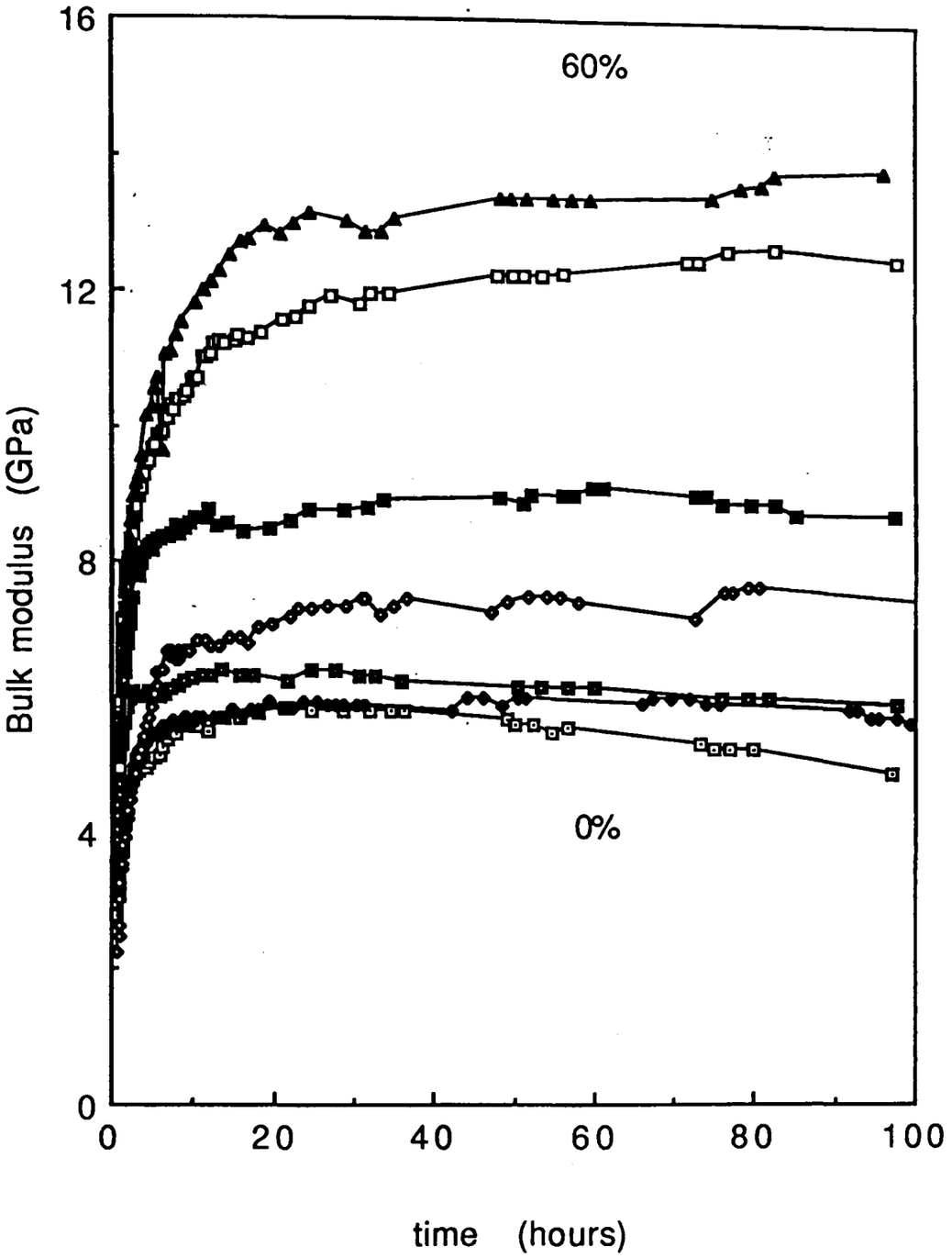

Figure 8.5. Plot of bulk modulus versus time , legend for the compositions as in figure 8.1.

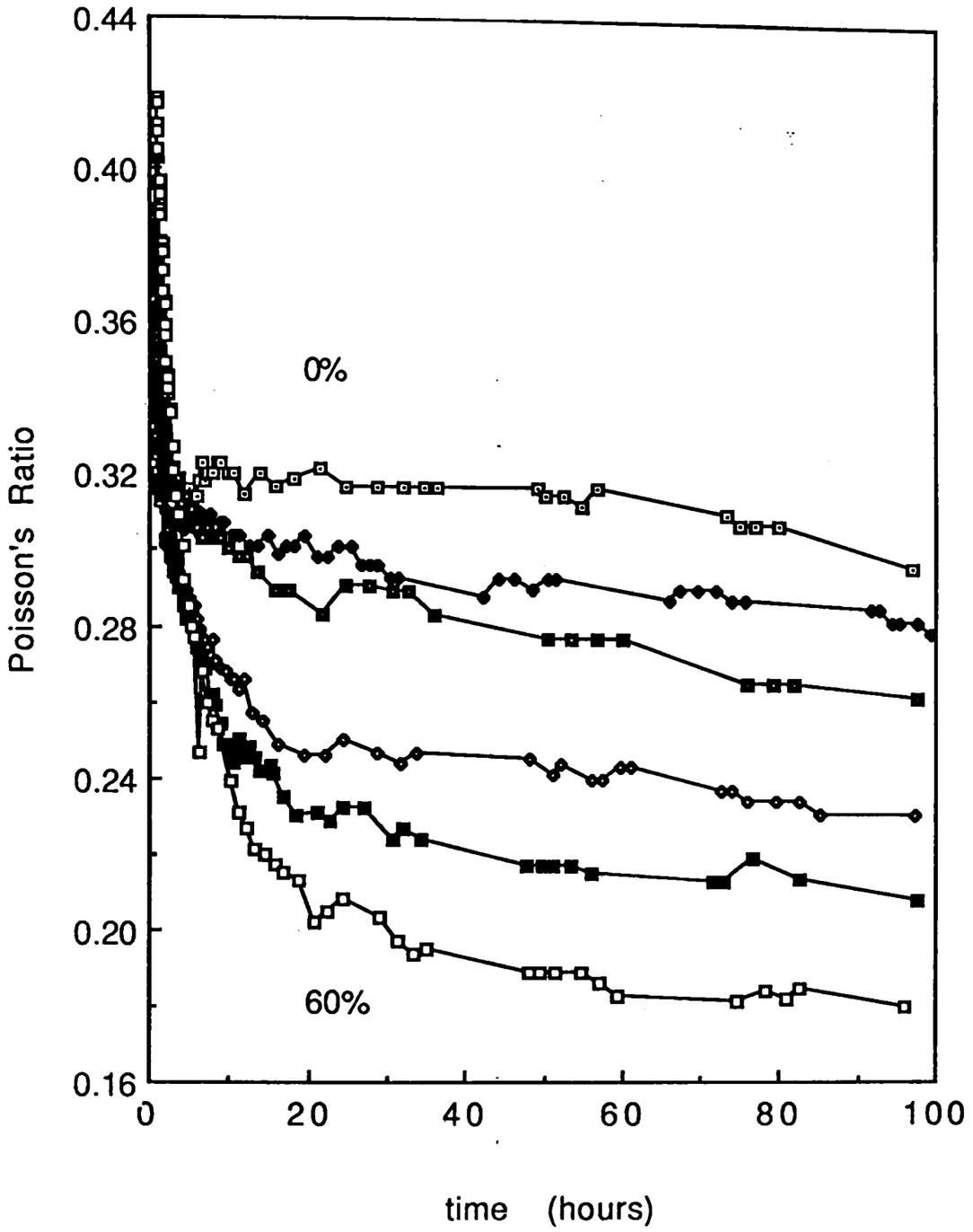

Figure 8.6. Plot of Poisson's ratio versus time , legend for the compositions as in figure 8.1.

From these graphs it can be seen that the elastic moduli increase with time due to the curing of the sample, eventually reaching a constant higher value, as would be expected, for the fully cured sample.

From the graph of Poisson's ratio, with the exception of the sample having 30% by weight alumina, the monitored Poisson's ratio began with a high value, then decreased with time to a constant lower value. Kingery states that for viscous flow and plastic flow, the volume remains constant so that the Poisson's ratio has a value of 0.5, hence the high initial value of Poisson's ratio observed during the early stages of the reaction, Kingery (1950, 1976).

By writing Poisson's ratio in the form (E/2G)-1 its subsequent behaviour is easily understood. Initially, whilst flow can be observed with the naked eye at low shear stress, G is clearly very low, and therefore E/2G is very high. As the sample cures, G increases more rapidly than does E (flow no longer being visible), hence the observed asymptotic decrease in Poisson's ratio with increasing time.

The graph of Poisson's ratio for the sample with 30% alumina content is shown in figure 8.7. This was initially a low value and increased to

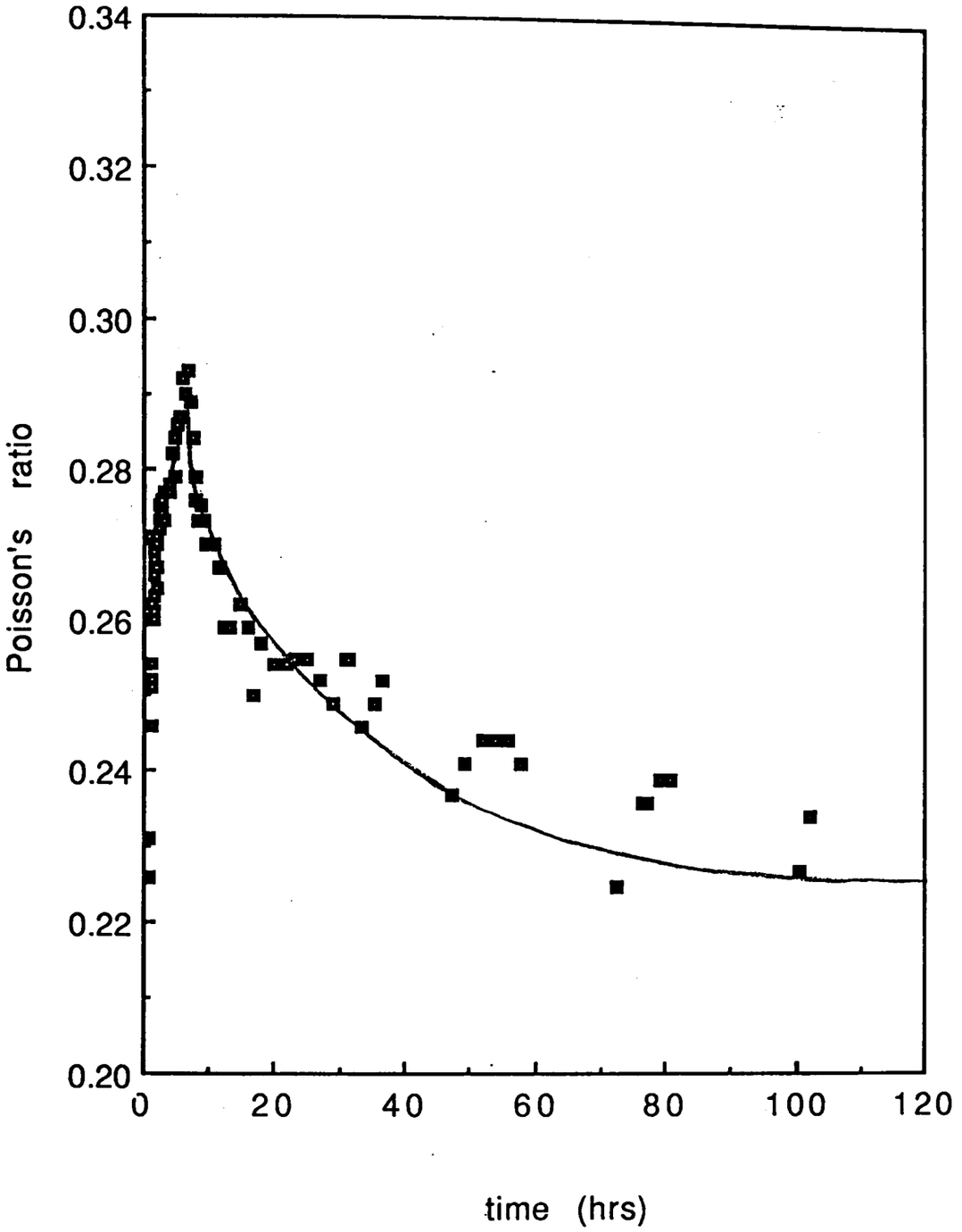

Figure 8.7. Plot of Poisson's ratio versus time for a sample 30 wt.% alumina.

a maximum, and then decreased asymptotically to a constant level. This behaviour had been observed previously and the low initial value attributed to a transitional phase, Tan (1989). It would appear from the inconsistent nature of this phenomenon that the amount of this phase and its duration is dependent upon certain factors which are not fully understood at present. The presence of impurities or variations in the mixing procedure could be involved but further work is required in order to establish this. The composition dependence of the elastic moduli of the samples, after completion of all chemical reactions, were compared with the theoretical bounds of Hashin and Shtrikman, see chapter 7.

Since the matrix is complex, values for material constants cannot be found in tables or calculated theoretically, therefore values determined from measurements of unfilled (ie; 0% alumina) samples were ascribed to the matrix, i.e. the alumina filler is assumed to be entirely inert and its indirect effect upon the reaction taking place in the matrix is neglected in the discussion of this section. These values for the bulk modulus and shear modulus respectively are:

$$K_1 = 5.2 \text{ GPa}$$

$$G_1 = 2.3 \text{ GPa}$$

and the elastic moduli of the filler (alumina) are, Anderson (1965) :

K_2 = 251.2 GPa

G_2 = 163.4 GPa

The measured elastic moduli for the final product, after 80 hours curing, are listed in Table 8.2.

The volume fractions were calculated from equation 20. Again the matrix density , ρ_1= 1561 kg/m^3, is taken to be that of the sample with 0% alumina content, ρ_2 is the density of the alumina filler, 3980 kg/m^3, and ρ is the measured density of the sample.

It can be seen from figures 8.3-8.5 that the elastic moduli are highly dependent on the alumina content. The variations of the elastic moduli with filler volume fraction for two-phase materials are related to the roles of matrix and filler. The elastic moduli would be expected to increase with increasing filler volume fraction, up to a limit where there is insufficient matrix for satisfactory filler-matrix bonding. Beyond this limit one would not expect the Hashin and Shtrikman bounds to hold. The mechanical properties of the ceramic would deteriorate and the elastic moduli would be expected to

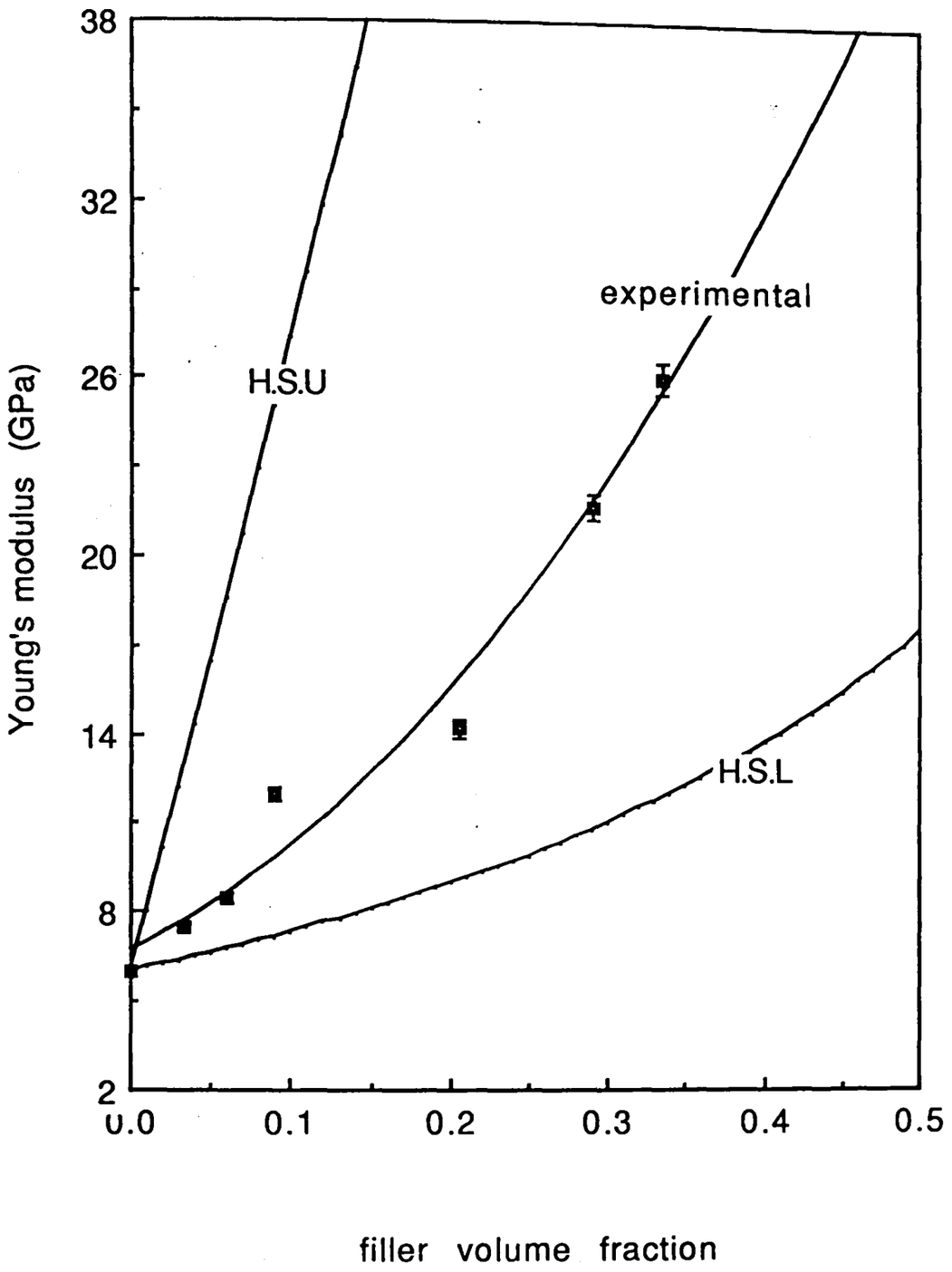

Figure 8.8. Composition dependence of Young's modulus, HSU and HSL denote the Hashin and Shtrikman upper and lower bounds respectively.

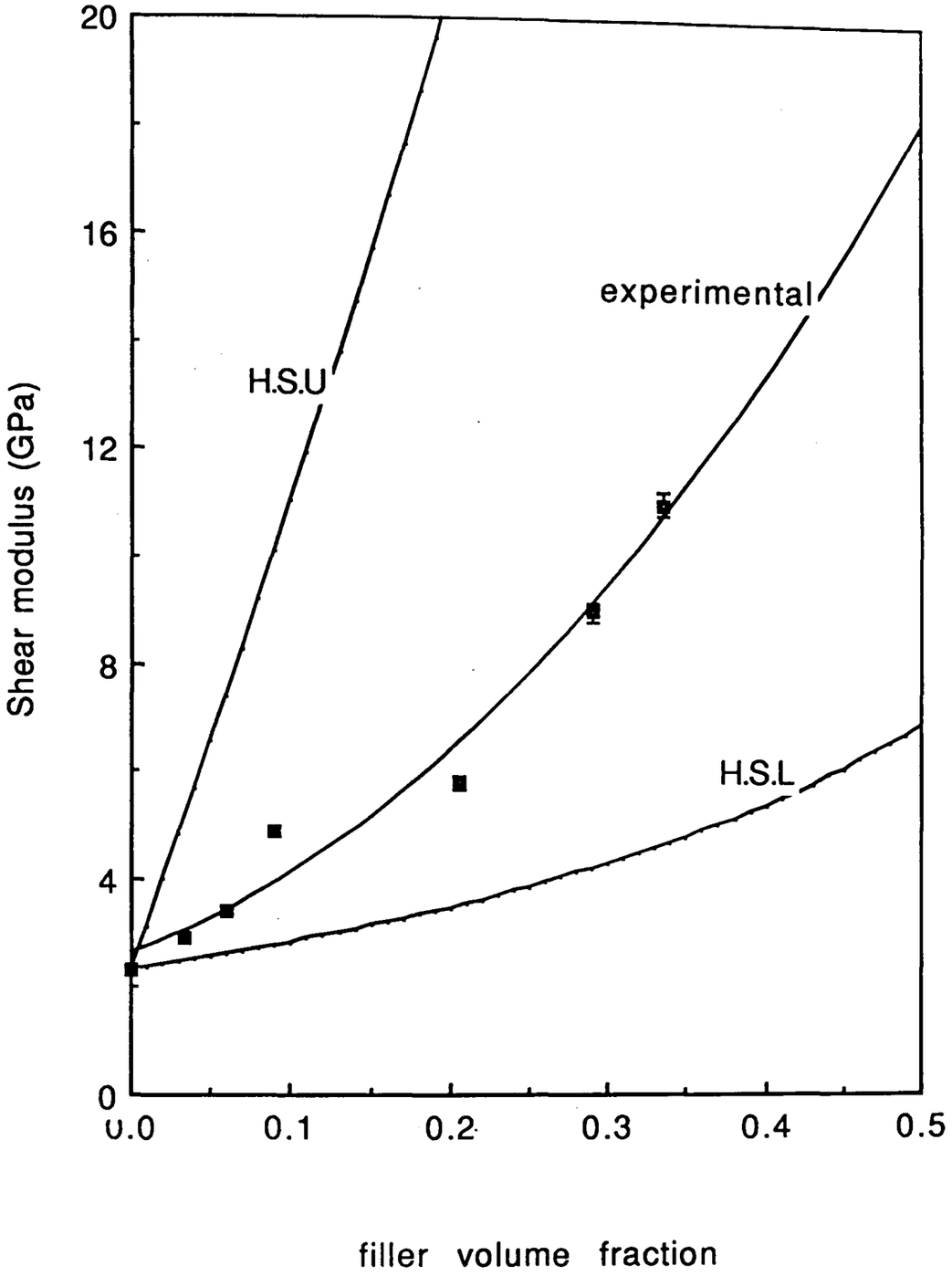

Figure 8.9. Composition dependence of shear modulus, HSU and HSL denote the Hashin and Shtrikman upper and lower bounds respectively.

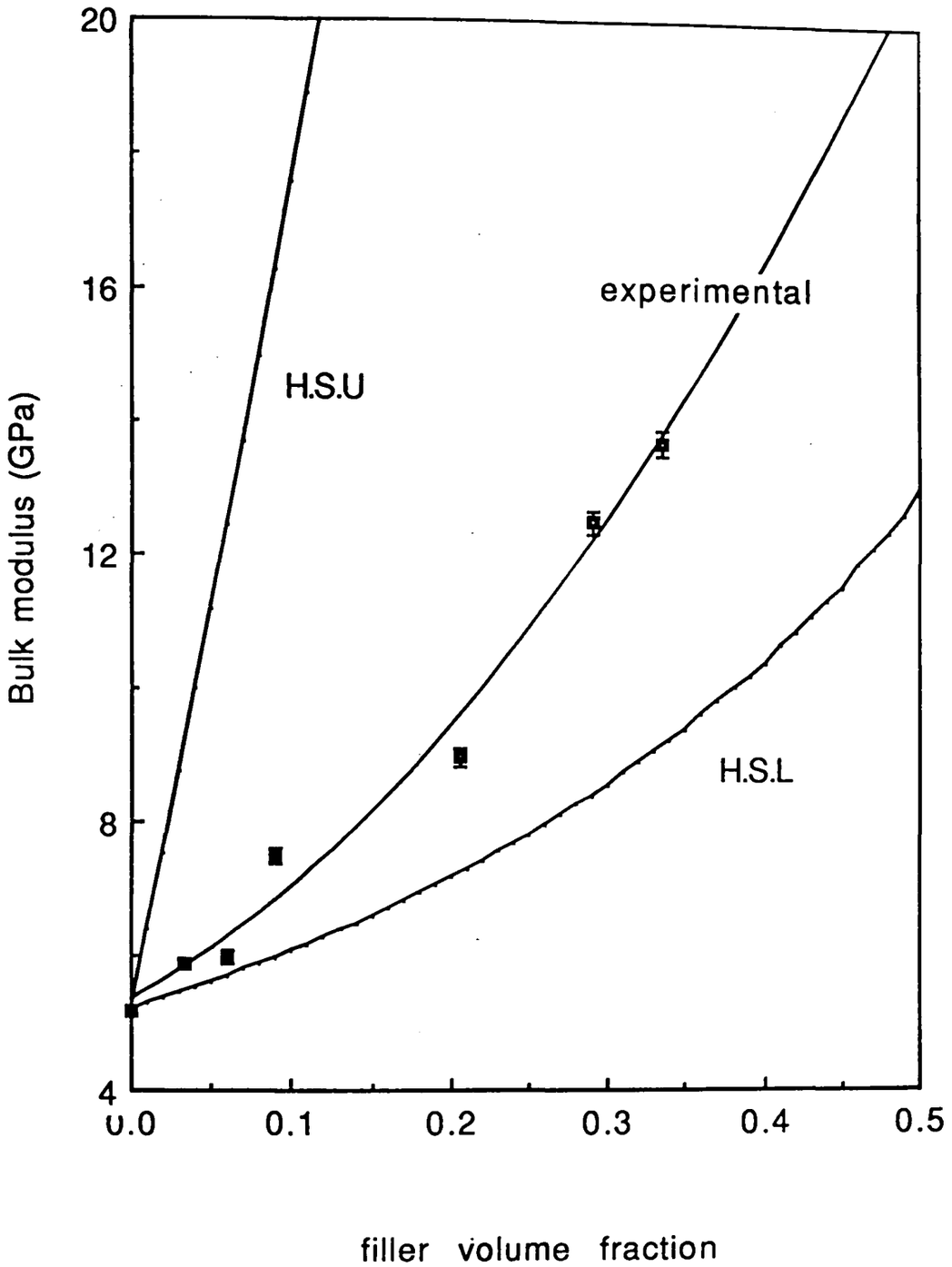

Figure 8.10. Composition dependence of bulk modulus, HSU and HSL denote the Hashin and Shtrikman upper and lower bounds respectively.

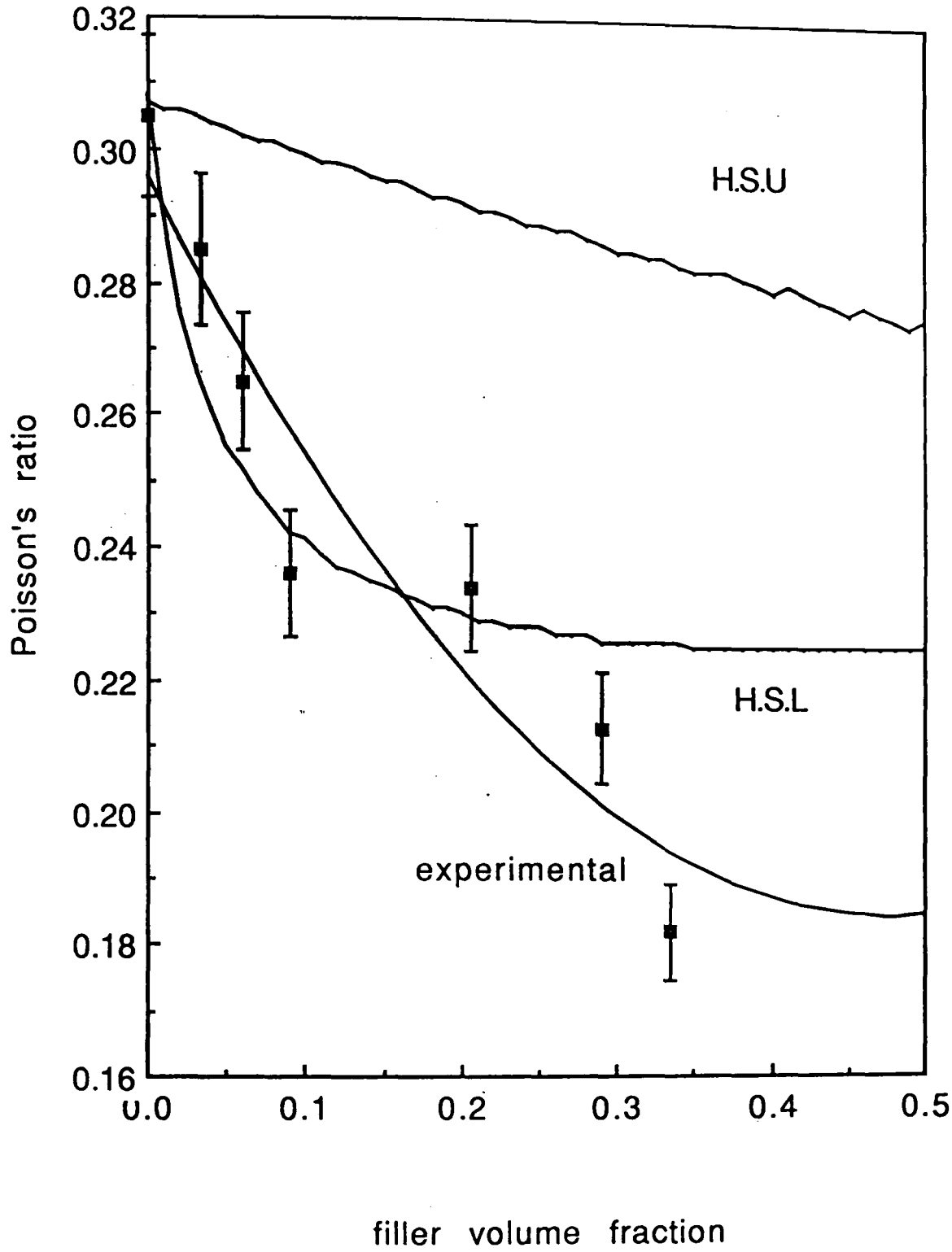

Figure 8.11. Composition dependence of Poisson's ratio, HSU and HSL denote the Hashin and Shtrikman upper and lower bounds respectively.

decrease.

The experimentally determined elastic moduli lie between the Hashin and Shtrikman bounds, figures 8.8-8.10. This suggests that the alumina filler particles were well dispersed and well bonded to the matrix, but since the data lie well above the lower bound the particles are not spherical, elongated grains probably being present. As already noted microscopy shows that plate-like grain growths predominate.

For filler volume fractions up to about 0.3, the experimental data for Poisson's ratio, shown in figure 8.11, lies, to a first approximation, on the lower bound. This implies that in the 60 wt% alumina sample the basic theoretical assumptions of Hashin and Shtrikman no longer hold, suggesting that the limiting filler volume fraction has been exceeded. As this result is at variance with the conclusion reached in the preceding paragraph we may conclude that the Poisson's ratio plot may be a more sensitive indicator of the filler-matrix bonding condition than are plots of the elastic moduli, or that the Hashin- Shtrikman model is a poor predictor of Poisson's ratio.

8.3 CHEMICAL REACTION RATES.

According to Stepisnik, Stepisnik (1981), the relationship between the shear moduli and elapsed time can be expressed empirically as :

$$G(t) = G_{\infty} \{ 1 - \exp.(-Bt^{n}) \} \qquad (34)$$

where G(t) is the elastic shear modulus at time t, B is a constant, t is the elapsed time, G_{∞} is the elastic shear modulus at infinite time and n is a value between 1 and 4 depending on the geometry of the growth.

From equation (34) :

$$\ln \ln [G_{\infty} / \{G_{\infty} - G(t)\}] = \ln B + n \ln t \qquad (35)$$

Equation (35) can be applied to the experimental data. Graphs of $\ln \ln [G_{\infty}/\{G_{\infty}-G(t)\}]$ versus $\ln t$, for samples with alumina contents in the range 0-60% by weight, are given in figure 8.12 a-g. These essentially show linear relationships in each case with a change in gradient occurring at times ranging from 0.9-2.2 hours.

The rate of the reactions involved in the curing process can be quantified by the values of the multiplier B and the exponent ,n, in

equations (34) and (35). This latter term could be considered to be the reaction rate index, and its values determined from the gradients in figure 8.12, a-g.

Considering data for a midrange sample with alumina content of 40% by weight, figure 8.12 e, the initial line is given by :

$$y = -1.20 + 1.66\,x \qquad R=0.99 \tag{36}$$

and the later line by :

$$y = -0.47 + 0.43\,x \qquad R=1.00 \tag{37}$$

where R is the correlation coefficient .

The reaction rate index can thus be determined from the gradients in figure 8.12 e, given by the final terms in equations (36) and (37). Thus the curing process under investigation has two stages, the first with a value for n of 1.66, and the second with a value for n of 0.43 .

Stepisnik observed that the changes in reaction rate were due to the changes in the grain geometry, such that when n = 3 to 4 the grains are polyhedral, and when n=1 to 2 they are plate like. The experimentally determined values of n, lower than Stepisnic's, would therefore tend to confirm the presence of plate-like grains as suggested earlier.

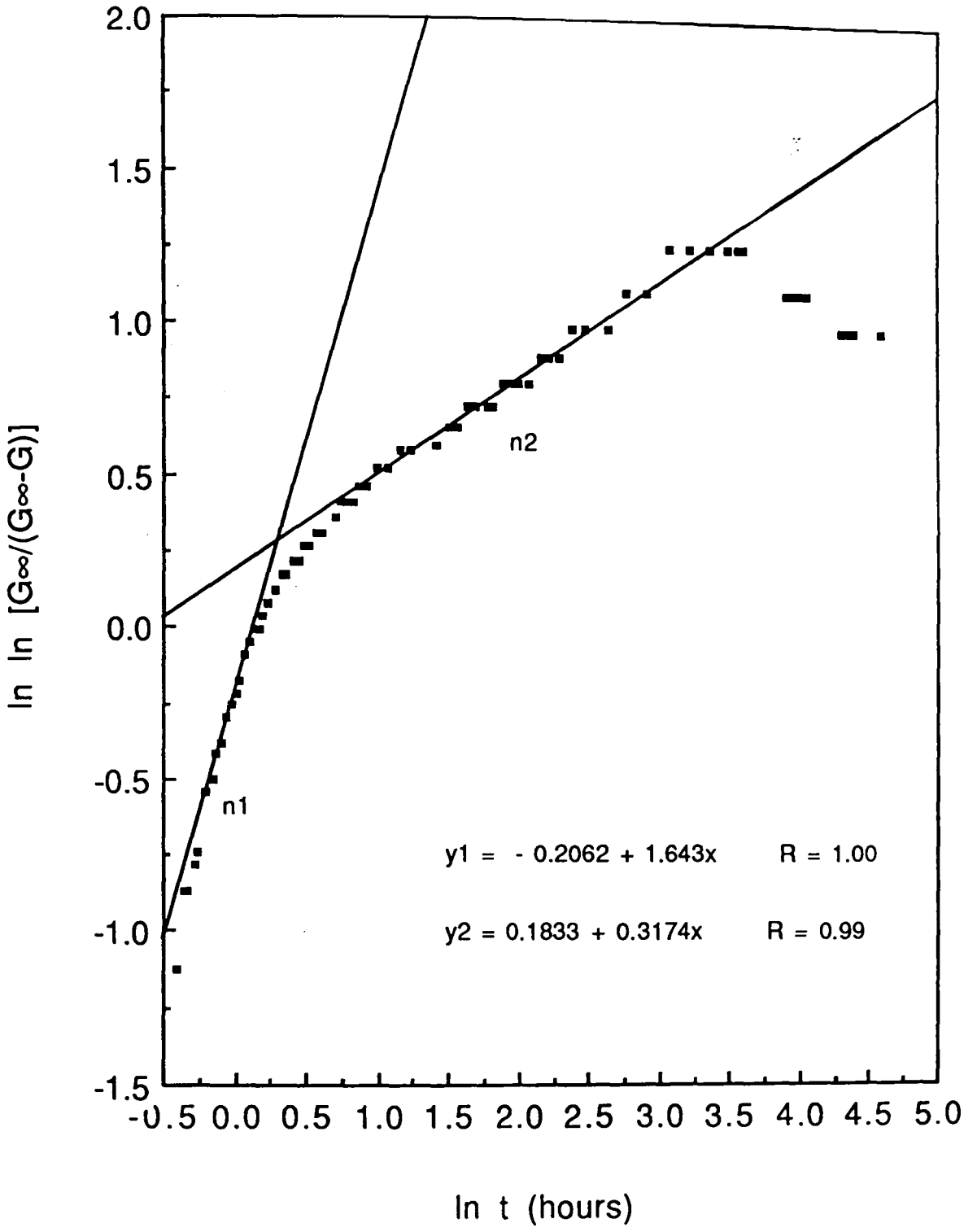

Figure 8.12.a Plot of calculated ln ln [G∞/(G∞-G)] versus ln t for sample containing 0% alumina.

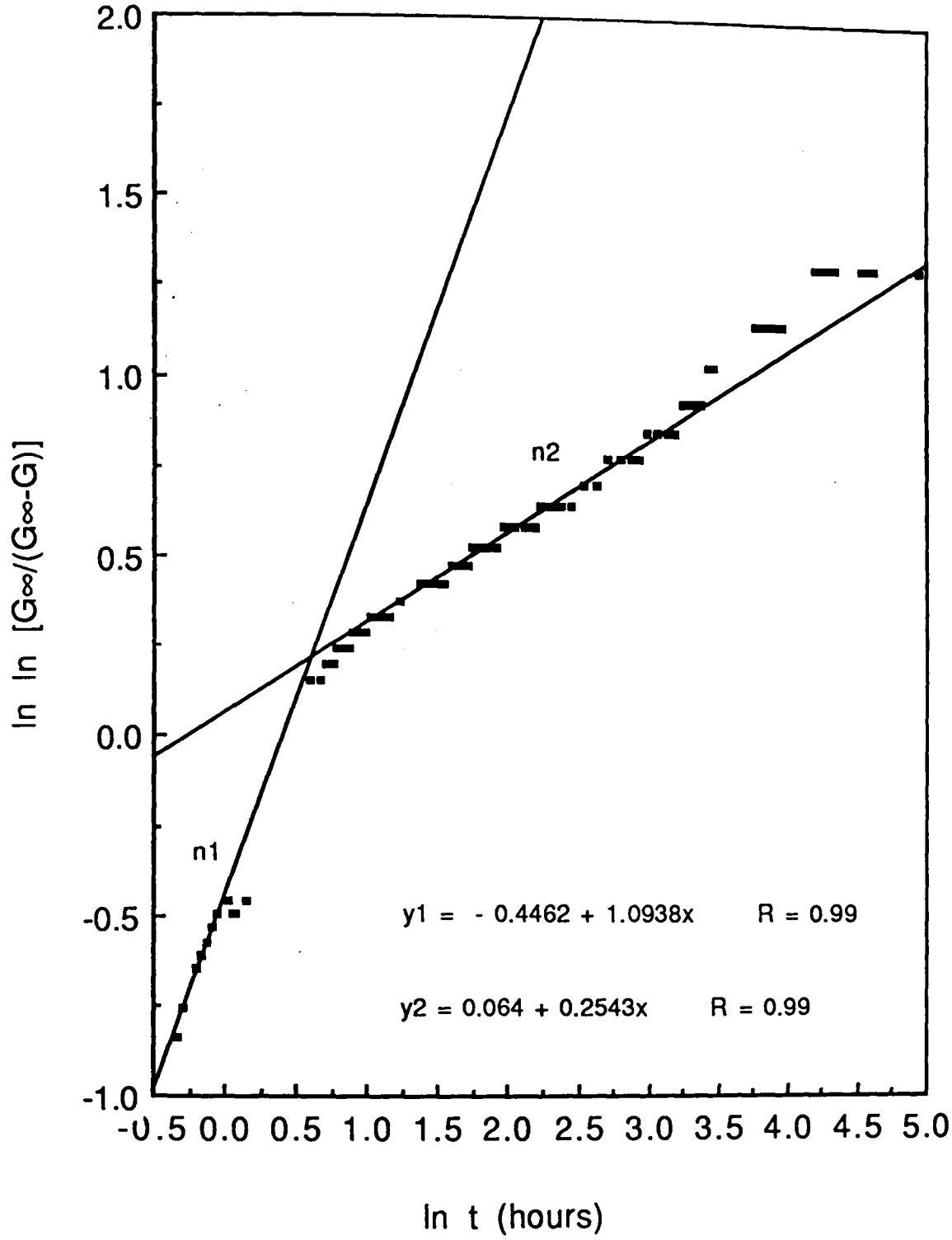

Figure 8.12.b Plot of calculated ln ln [G∞/(G∞-G)] versus ln t for sample containing 10% alumina.

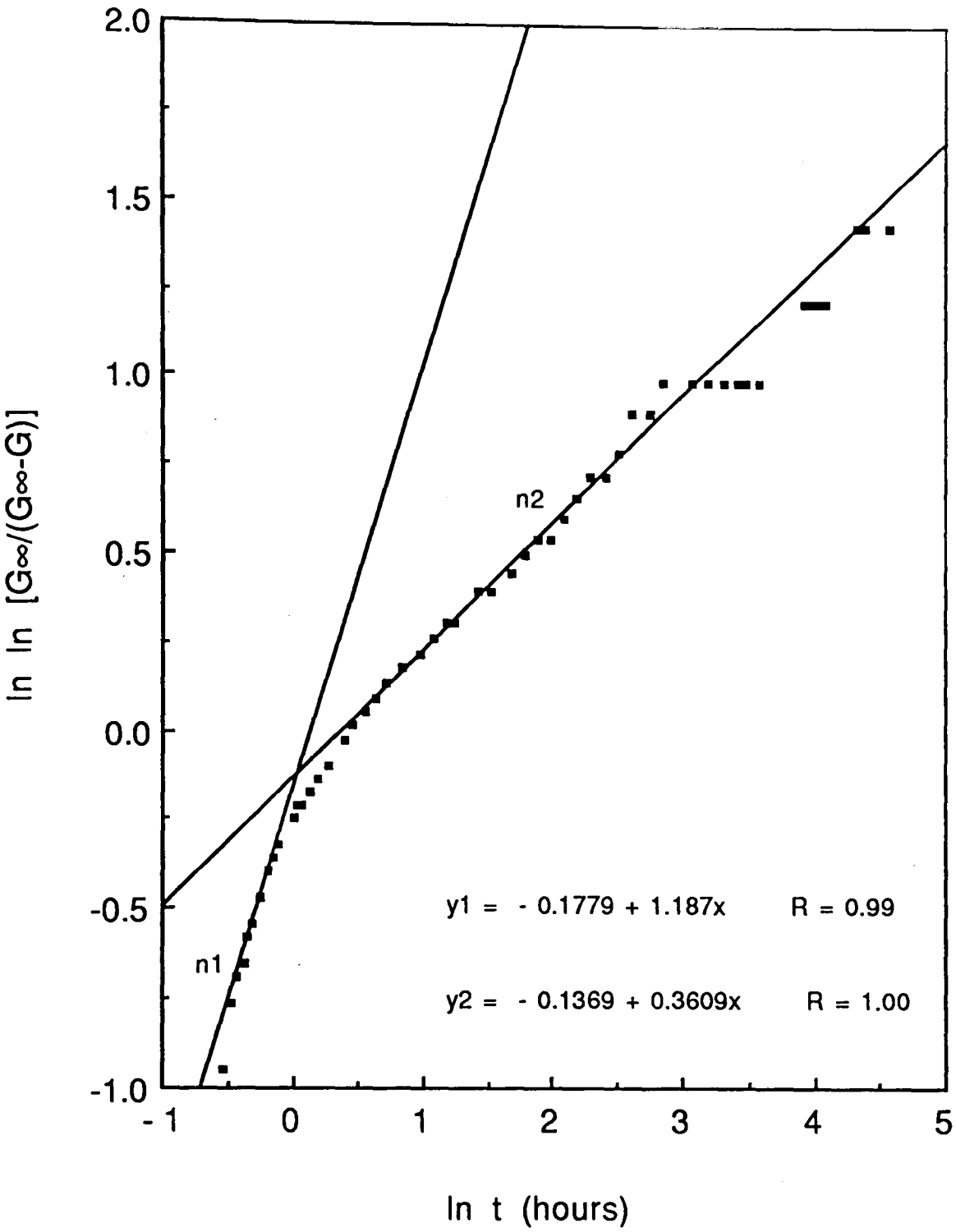

Figure 8.12.c Plot of calculated ln ln [G∞/(G∞-G)] versus ln t for sample containing 20% alumina.

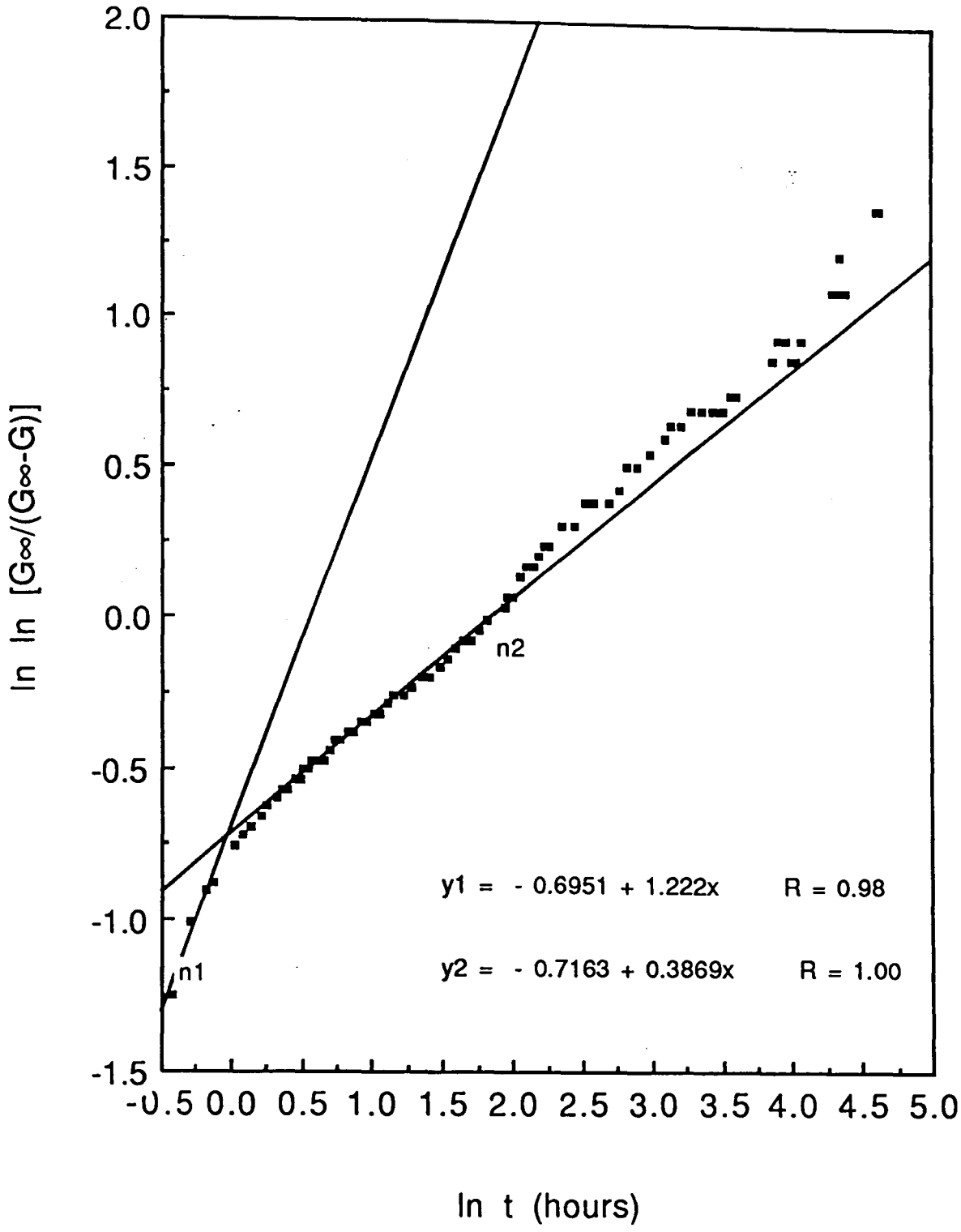

Figure 8.12.d Plot of calculated ln ln [G∞/(G∞-G)] versus ln t for sample containing 30% alumina.

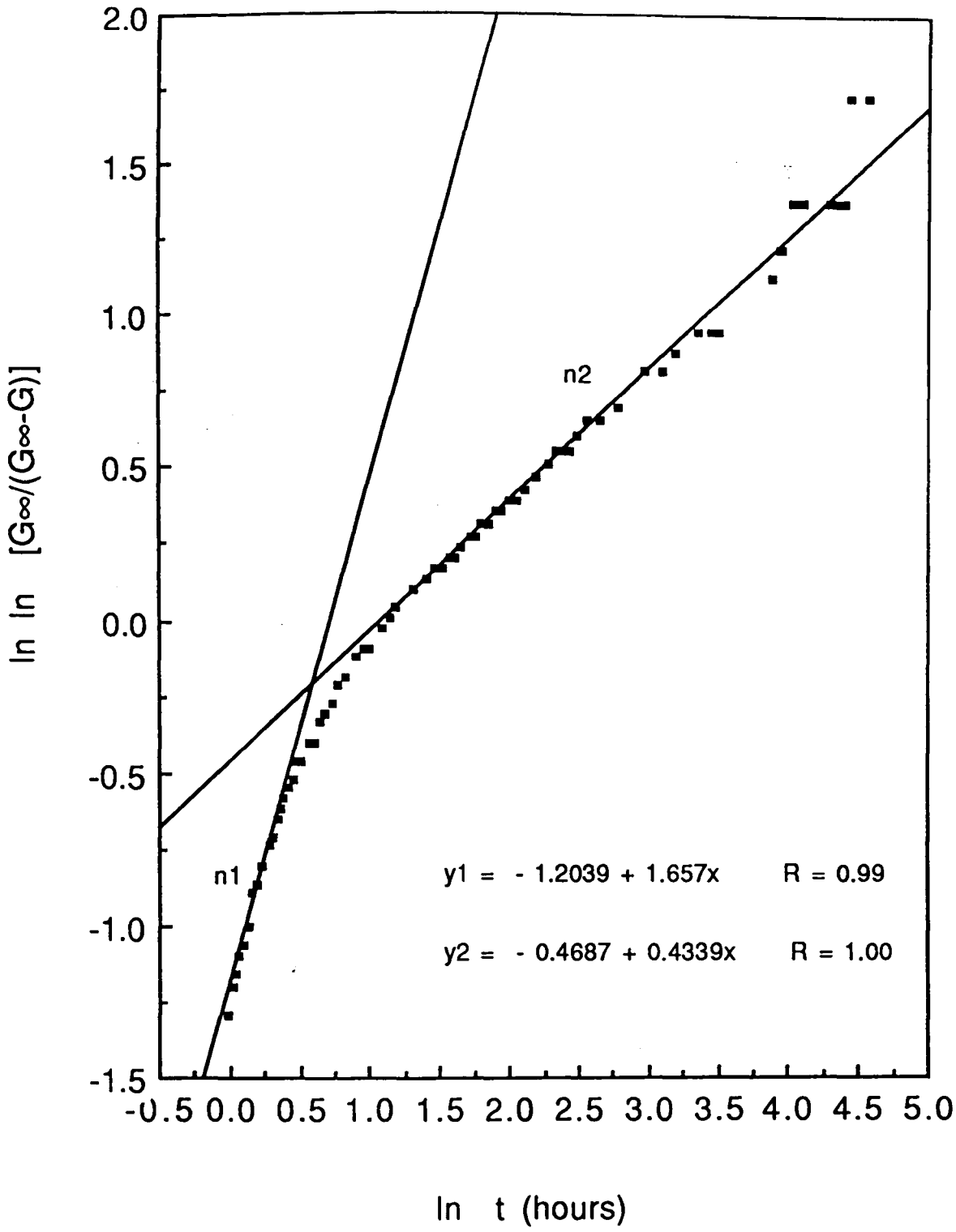

Figure 8.12.e Plot of calculated ln ln [G∞/(G∞-G)] versus ln t for sample containing 40% alumina.

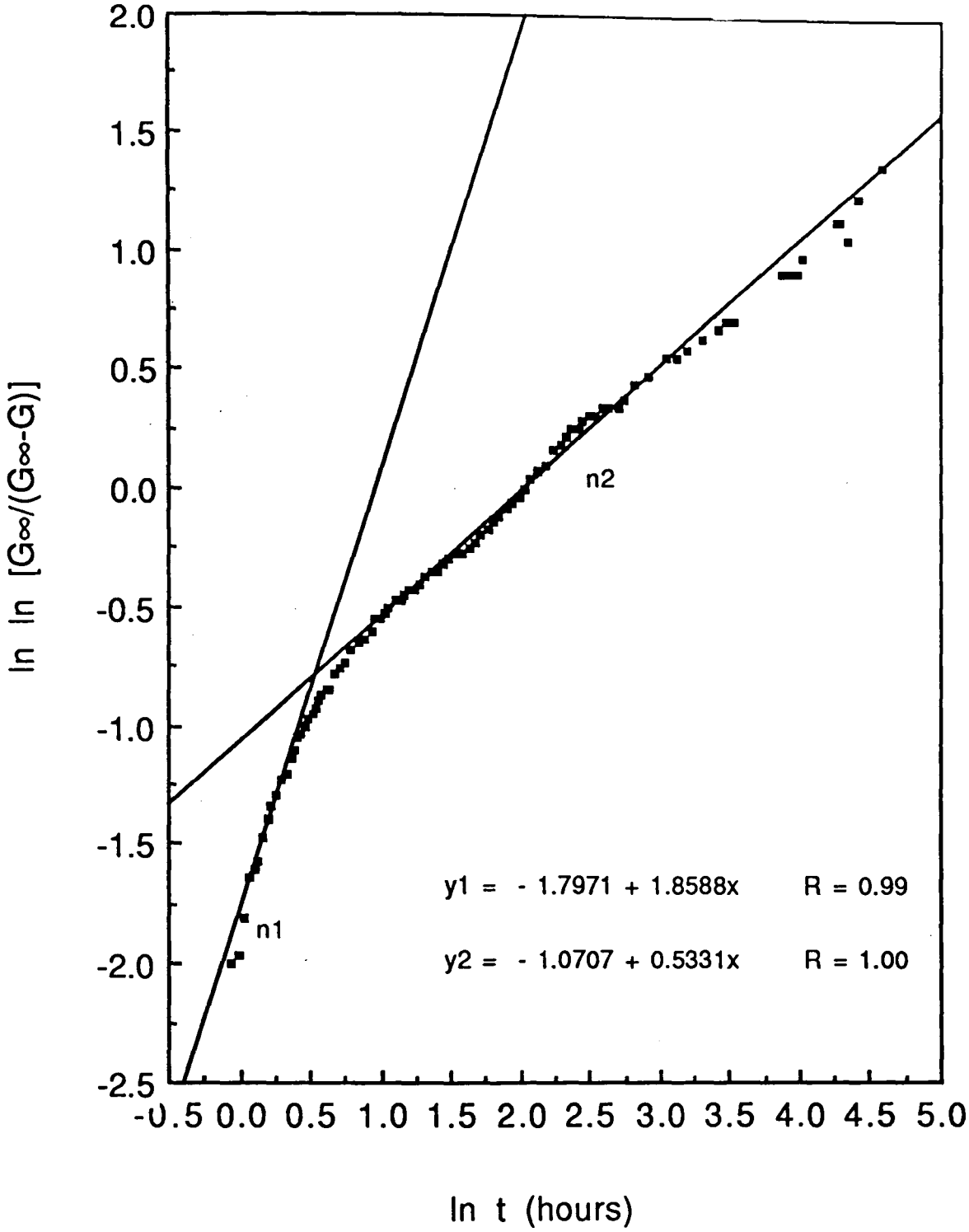

Figure 8.12.f Plot of calculated ln ln [G∞/(G∞-G)] versus ln t for sample containing 50% alumina.

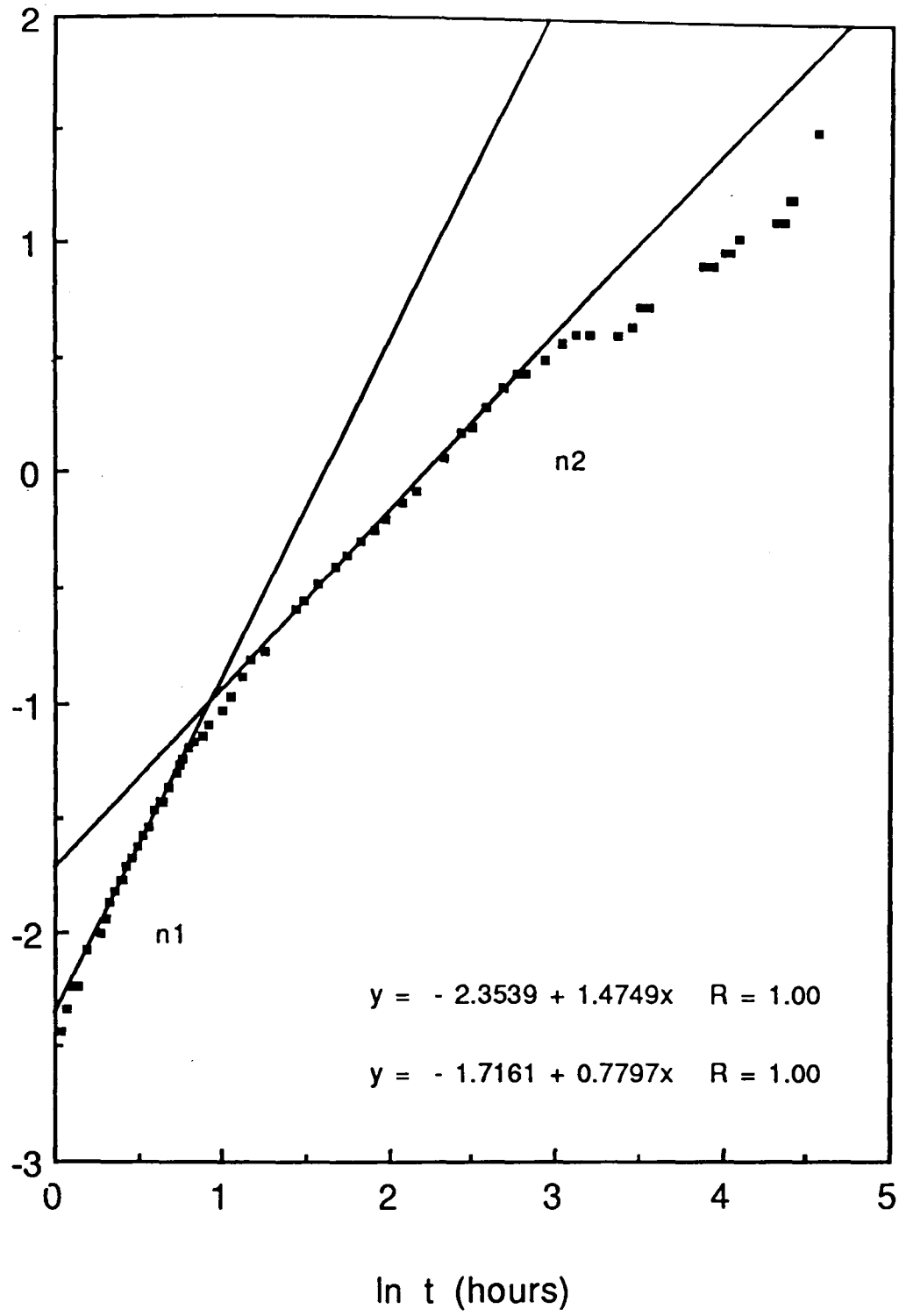

Figure 8.12.g Plot of calculated ln ln [G∞/(G∞-G)] versus ln t for sample containing 60% alumina.

From equations (36) and (37), $\ln B_1 = -1.20$ and $\ln B_2 = -0.47$, hence $B_1 = 0.3$ and $B_2 = 0.63$. (hours)^n for this particular sample.

B has units of (hours)^n so it is convenient to introduce a time constant, τ, such that

$$\tau = \sqrt[n]{B}$$

or $$B = \tau^n .$$

Thus $$\ln (\tau_1) = \ln (B_1)/n_1 = -0.726$$

$$\tau_1 = 0.483 \text{ hours}$$

and $$\ln (\tau_2) = \ln (B_2)/n_2 = -1.080$$

$$\tau_2 = 0.339 \text{ hours}$$

Data from seven samples with alumina contents in the range 0-60 wt% were similarly analysed and the values of n and τ listed in Table 8.2. The correlation between the reaction rate indices and the volume fraction of alumina is shown in figure 8.13. The reaction rate of the first and second stages generally increased with increasing filler volume fraction, though in the case of the initial reactions a maximum

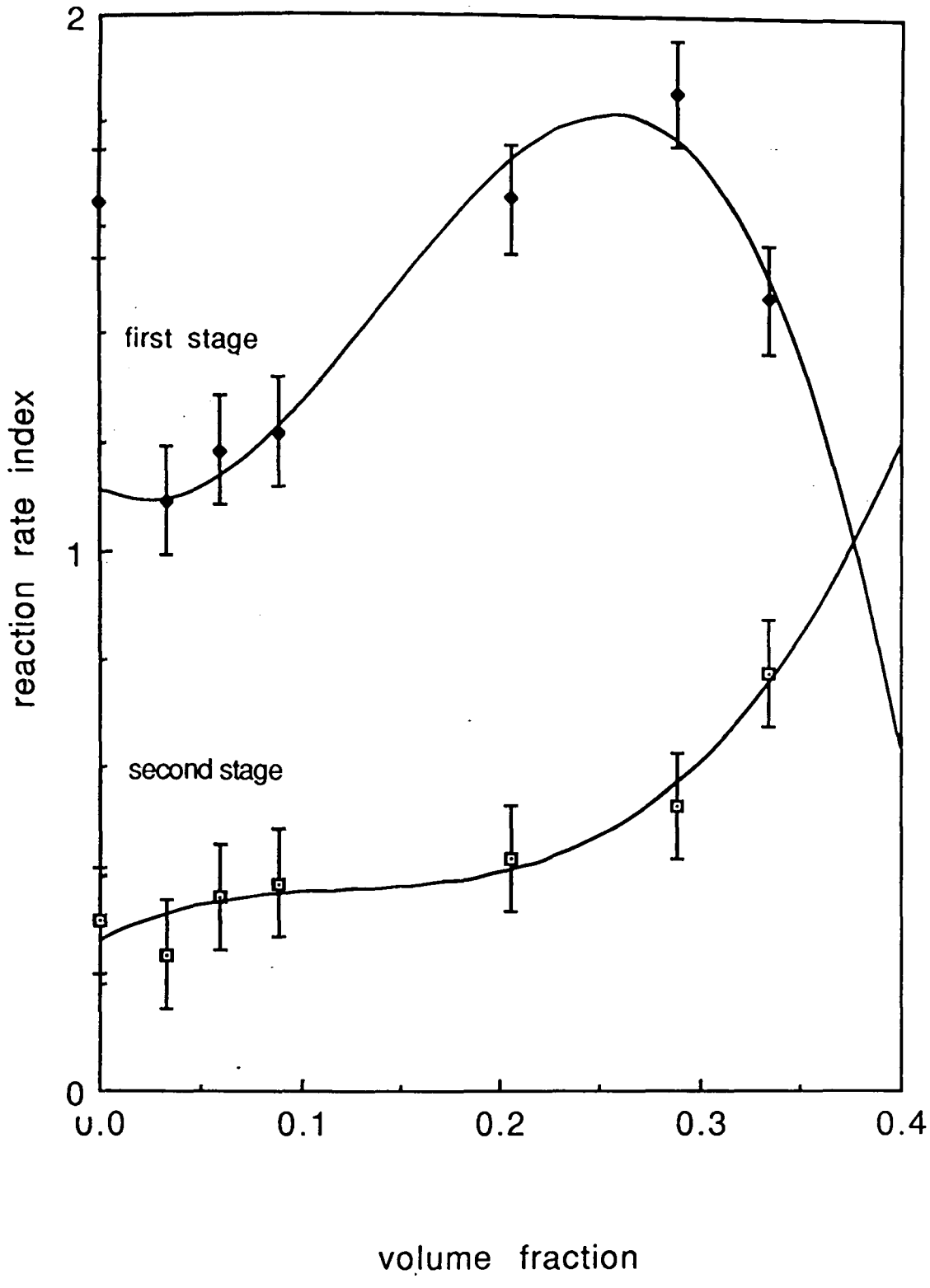

Figure 8.13. Plot of reaction rate index versus volume fraction of alumina for the first and the second stage.

is reached at a volume fraction of about 0.25 probably due to the reduced water content of the system. This again suggests the possibility that the optimum alumina content has been exceeded.

The correlation between time constant and the filler volume fraction as shown in figure 8.14 indicates that the time constant for both stages increases with increasing filler volume fraction, the time constant of the second stage being shorter than that of the first.

From inspection of equation (34) we note that the reaction rate dG/dt, at constant t, increases as both B and n increase. This suggests that there are two mechanisms affecting the reaction rate, one manifesting itself through n and the other through B.
B is probably less significant than n , and an increase in n will always be assumed to be associated with an increase in reaction rate.

Stepisnik et al take the view that the reaction rate index is a function of the geometry of the grains developing during the hydration reaction but there are other factors to be considered. Independent measurements with a thermometer buried in the centre of starting mixtures established that there was a considerable initial temperature rise peaking typically at 40-50°C after a few hours. This

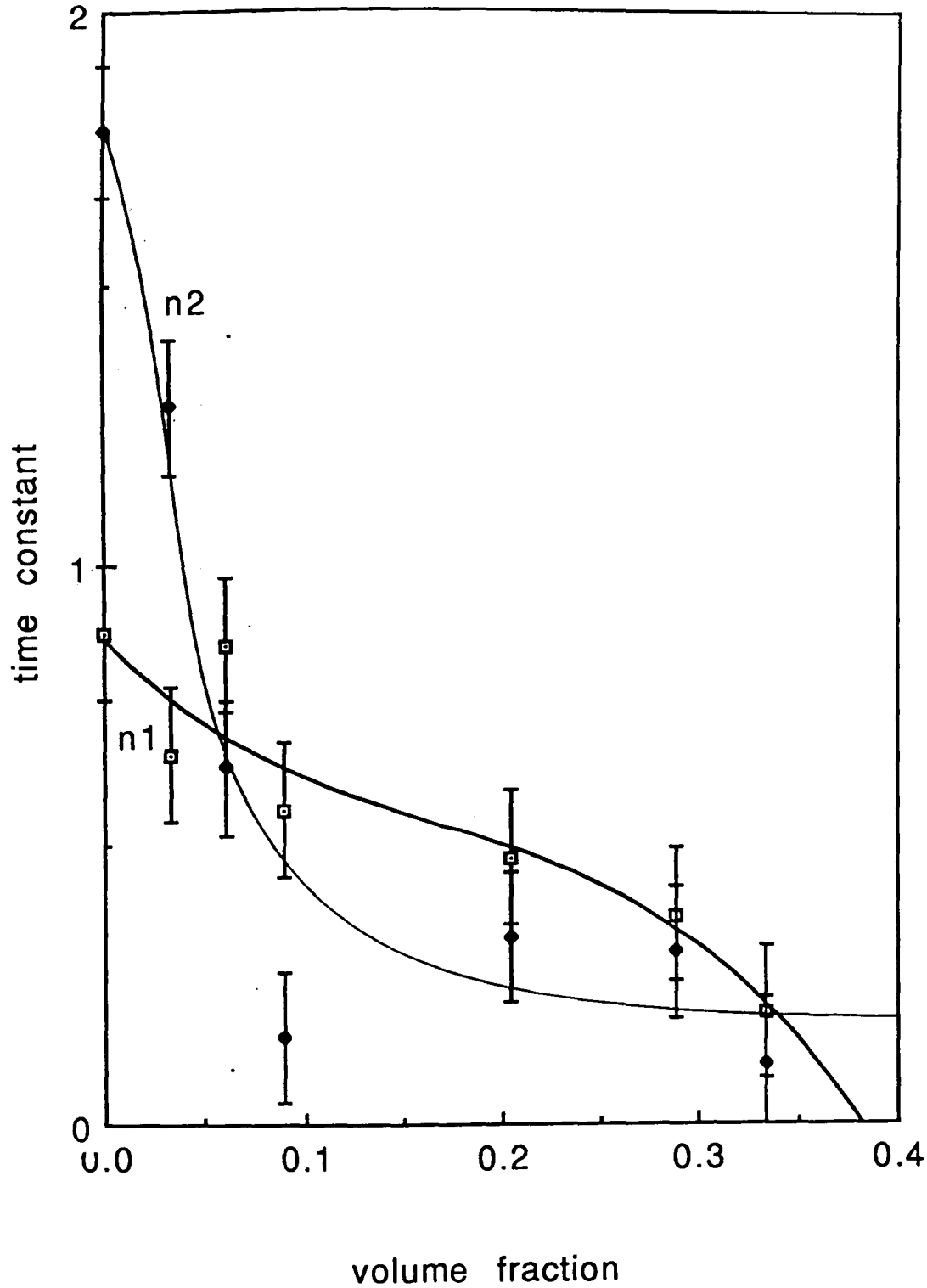

Figure 8.14. Plot of time constant versus volume fraction of alumina for the first and the second stage.

coincided with a peak in Poisson's ratio evident in figure 8.7.

The presence of a peak value for n_2 at an intermediate level of filler volume fraction suggests that the reaction rate is governed by two opposing factors. Increasing the filler content tends to decrease the amount of reactants per unit volume and hence to reduce the rate and magnitude of the temperature rise. Another contributory factor tending to cause n_1 to decrease with increasing filler content is the fact that the non-reactive filler inhibits the degree of physical contact between the reactants. However, an increase in the amount of filler, which has low thermal conductivity, will inhibit the heat loss by thermal conduction and therefore, in respect of this, will tend to increase the magnitude of the initial temperature rise.

The fact that n_2 increases monotonically with filler volume fraction shows that another mechanism affecting the reaction rate must also be present since the initial temperature-rise effect has ceased. It is tempting to conclude that the alumina must have some catalysing effect on the reaction.

However, whilst the bulk of the filler has been described as inert, some interfacial reactions between the matrix and filler particles

must take place for satisfactory filler-matrix bonding to occur. There may be chemical reactions or merely a physical bond as the matrix keys into the surface irregularities of the alumina particles. The chemical concentration of the mixture between filler particles, which governs the rate of reaction to form the the matrix, is little affected by the filler concentration at low levels of filler content content. As filler content is increased its effect upon the concentration of reacants and the physical properties of the curing material will become more significant.

In this thesis the rates of progression of the chemical reactions, and their effects upon the physical condition of the paste, are investigated by the changes in its physical interactions with ultrasonic waves. It would therefore seem logical that there should be at least two mechanisms involved. The first governing the rates of progression of the chemical reactions in the matrix, the other governing the interaction between this forming matrix and the filler particles dispersed within it. This latter mechanism could be expected to show a maximum curing rate or minimum curing time corresponding, to a first approximation, to a maximum strength composition with well filled interstices.

The ascribed reaction rate indices and time constants are subject to the above constraints, and therefore abstracted from the actual rates of reactions of the matrices of the various samples. This is not a major problem, since for practical purposes the rate of change in the physical condition, rather than that of the chemical conditon, is the important parameter, and that which corresponds most closely to the measured parameters

8.4 POROSITY - ELASTICITY RELATIONSHIPS.

Kupperman has reported on several investigations into porosity which show that Young's modulus increases exponentially as porosity decreases, Kupperman (1987). This can be expressed as :

$$E = E_0 (1-P)^e \tag{38}$$

or

$$\ln E = \ln E_0 + \ln(1-P) \tag{39}$$

where E_0 is Young's modulus for the nonporous material, P is the porosity of the material expressed as a volume fraction and e is the appropriate exponent. Plotting ln E versus lnP, as shown in figure 8.15, gives an approximately linear correlation between Young's modulus (ln E) and porosity. Similarly, bulk and shear moduli could be

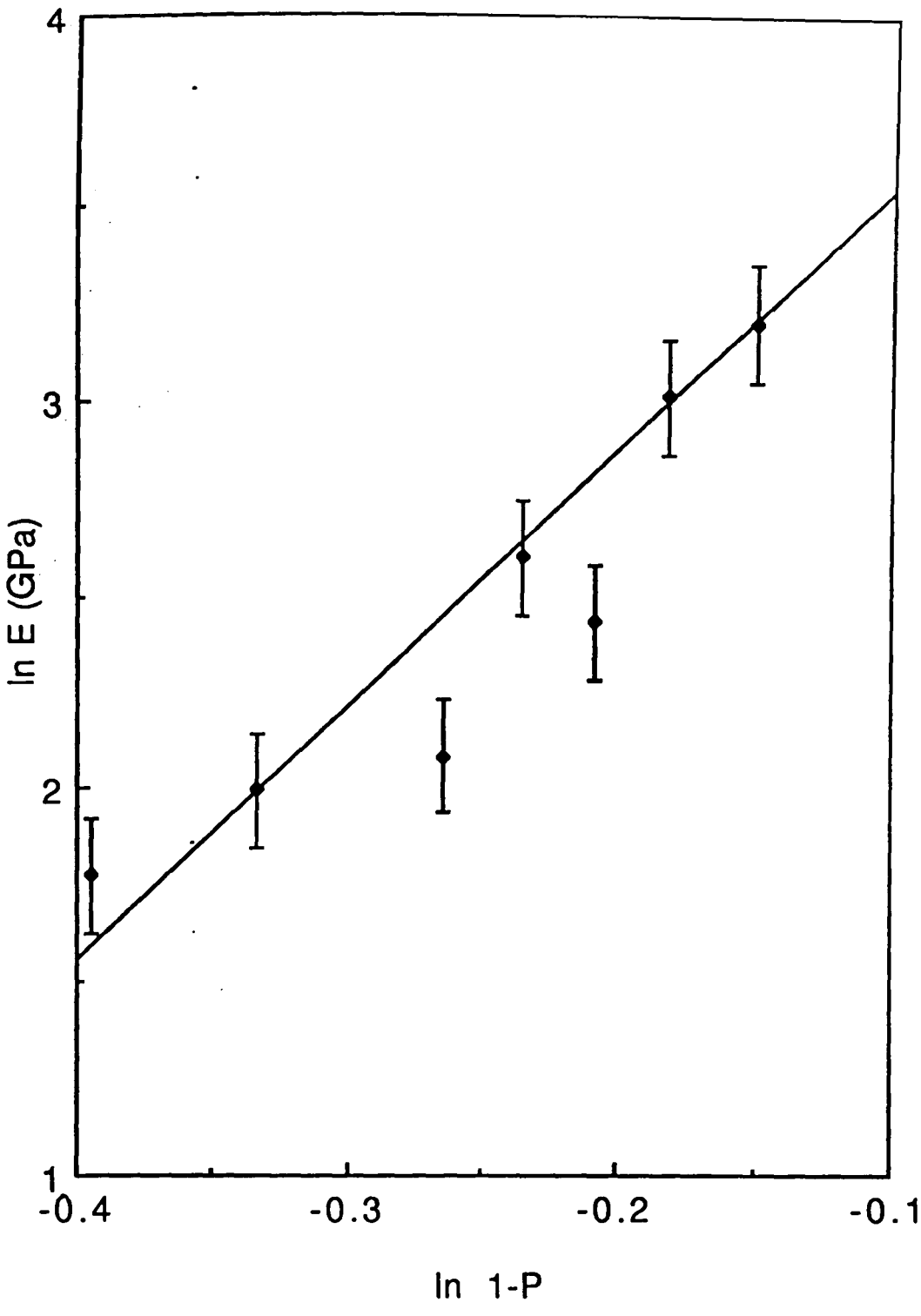

Figure 8.15. The relationship between Youngs modulus and porosity expressed in terms of ln E versus the volume fraction of solid material.

correlated with porosity.

Essentially Eo will vary with filler volume fraction and should lie between the Hashin and Shtrikman upper and lower bounds. Therefore, it is interesting that the seven data points for E and P (corresponding to seven different volume fractions) fit equation (39) quite well with a nominally constant Eo, as indicated by the straight line in the plot in figure 8.15. Thus, the inverse logarithm of the intercept on the E axis gives a value of 67GPa for Eo with a standard deviation of ±10. The value of the exponent e is 6.67 as determined from the gradient of the line. It is clear that Eo varies between relatively small bounds compared with the variation of E with volume fraction in real (i.e. porous) samples.

However, the measured value of Eo, i.e. the value of E, for the pore-free matrix is much higher than would have been expected in the light of the theoretical predicted bulk modulus of (10.4 GPa) in chapter 7.

With a knowledge of the correlation between the elastic moduli and porosity for a particular ceramic product, ultrasonic examination can be used as a method of porosity measurement. The conventional methods which involve knowledge of the theoretial and bulk density

determinations or mercury porosimetry are accurate and convenient for small artefacts or those of a regular shape whose volume can be calculated. Such methods are inaccurate and inconvenient for articles of complex shape, and inappropriate if not impossible in the case of large structures. Furthermore the inference of porosity from the difference between theoretical density and bulk density assumes that the material comprising the artefact is homogeneously distributed. If this is not a valid assumption, or if the theoretical density of the material is unknown an ultrasonic method of density determination could be useful. Such determinations would be of only secondary importance the elastic moduli being of greater significance and use.

This chapter was based upon research carried out in conjunction with Miss T Kathrina, a masters student working under my guidance and supervision, which has now been published, Katarina (1991).

9. CONCLUSIONS.

9.1 EVALUATION OF FULLY CURED MATERIAL.

1 At low frequencies, in the range 24 -500kHz, such that the wavelength is significant compared with the size of the samples, inconsistencies in the measured velocities were observed. An explanation in terms of the simultaneous propagation of the rod wave mode and the first one or two longitudinal wave modes, and an assumption that the pulse bandwidths are about ±10% has been offered, but not by any means proved. This would tend to limit the use of equipment operating at these frequencies to large articles or structures.

2 With considerable further work a theoretical explanation for the observed anomalies may be deduced. The variations may be highly sensitive to material property variations and therefore suitable for N.D.E. purposes. Unfortunately such data would be extremely difficult to determine practically and interpret theoretically. On line computers and probe development facilitate the application of these techniques.

3 In materials of reasonable density the high-frequency shear and compressional velocities, and hence the elastic moduli, could be determined easily. This technique is therefore useful for Q.A. and N.D.E. purposes. Alternatively, an indication of density could be obtained, assuming a standard value for the modulus of the specimen. Inability to propagate at or above a specified frequency,such as 2MHz, could be taken as an indication of substandard material.

4 It is possible to determine the attenuation-frequency relationship and from this to estimate the grainsize of the material assuming grain boundary scattering. This was carried out for the samples examined and confirmed microscopically. Since the grain size is dependent upon the production process and chemical reaction, and may even be indicative of the end point of the reaction, spectrum analyser plots and attenuation-frequency curves could prove invaluable in process monitoring and quality control of the material.

5 It is possible to differentiate between the three samples examined by observation of their attenuation spectra. The extent of the ability of this technique to characterise specimens has yet to be determined. It should be possible to identify poor material by changes in the spectrum,and it may be possible to differentiate between batches of similar material in a quality assurance situation, dependent upon the extent of the material property variation.

6 In all samples there are two main phases visible, one phase containing the majority of the porosity and a second phase, less porous and probably of greater density. Precise compositions and structures of these two phases are not yet available from x-ray diffraction studies, hence it is not at this point possible to determine Hashin and Shtrikman upper and lower bounds based on these phases. However, a theoretical calculation of bulk modulus based on the assumption that the matrix consisted of 80% newberyite and 20% aluminium orthophosphate by volume, was in excellent agreement with the measured matrix modulus after allowing for porosity. Such comparisons highlight the potential value of ultrasound velocity measurements for nondestructive evaluation and testing, and quality control of this ceramic material.

9.2 MONITORING OF SETTING AND COMPOSITION DEPENDENCE.

The setting (hydration) process in ceramics produced by the reaction of aluminium orthophosphoric acid with magnesia in the presence of an inert filler of alumina has been monitored by means of time-of-flight measurements on MHz frequency ultrasound pulses. The ultrasonic measurements allow the possibility of several important properties to be evaluated on-line and non-destructively, namely reaction rates, porosity levels, the optimum time for sample machining, the geometry of grain growth, and the time taken for samples to reach their maximum elastic moduli and strength values (not the infinite time implicit in reaction rate theory but the time beyond which no further increases can be observed outside the standard deviation of the measurements). The important physical parameters are the time constants. The summary of the main conclusions of the measurements are as follows.

1 The strength of the ceramic material increased asymptotically to a maximum value after about 100 hours. It was established that the velocity and elasticity values at any point in time increase with

increasing alumina content to an upper limit of about 60% by weight. Beyond this amount there is insufficient matrix material for proper mixing, which results in a weak friable material which defied evaluation.

2 It was thus established that the optimum alumina content for maximum strength is about 60% by weight. The observed variations in the elastic moduli would tend to indicate that the optimum alumina content lies within the range 50 to 60wt%. Further work within this range of compositions is required in order to establish this optimum alumina content more closely and thus maximise the potential applications of the material.

3 To a good approximation the chemical reaction can be divided into two stages, each having different reaction rates with the first stage being the fastest. The temperature rise transient during the initial stage obviously has a direct effect on reaction rate. However it also has an indirect effect through the fact that changes in the temperature-time profile will produce changes in grain growth. The reaction rate in both stages increases as the filler volume fraction increases due largely to an increase in temperature.

4 The composition dependences of the elastic properties were compared with the Hashin and Shtrikman bounds for two-phase materials. All experimental data lie in between upper and lower Hashin and Shtrikman bounds, suggesting that the filler particles were well dispersed, and well bonded to the matrix. However the data lie so far above the lower bound as to suggest that the particles were far from spherical which was as expected. This was confirmed by the low values of n ($n<2$) in the empirical reaction rate equation which indicate a plate structure.

5 It was also established that the elastic moduli increase exponentially with decreasing porosity within large errors.

10. REFERENCES.

ADUDA, O.B.C. and RAWLINGS, R.D. (1996). Br. Ceram. Trans., **95**,1, 10-14.

AKITT, J.W. (1992). N.M.R. and Chemistry, 3rd edition, Chapman and Hall.

ANDERSON, O.L, and NAFE, J.E. (1965). J. Geophys. Res. **70**, 16, 3951-63.

ANDERSON, D.L and ANDERSON, O.L. (1971). J. Geophys. Res. **75**, 3494-3500.

ANJORIN, M.O. (1988). M.Sc. Dissertation, Brunel University.

APPLETON, S., HUTCHINS, D.A. and LEWIS, M.H. (1991). J. European Ceram. Soc., **8**, 339-44.

ARNOLD, W.W.and REITER, H. (1991). Key Engineering Materials, **57**, 393-410.

ASHLEY, S. (1993). Mechanical Engineering, **115**, 70-71.

ASKELAND, D.R., The Science and Engineering of Materials, 3rd edition, Chapman and Hall, 1996.

BELL, D.A. (1989). Br. Ceram. Trans. J., **88**, 4, 133-37.

BERTHAUD, Y. (1991). Cement and Concrete Research, **21**,1, 73-82.

BHARWAJ, M.C. (1990). Metal and Ceramic Matrix Composites; Processing, Modeling and Mechanical Behaviour, Bhagat et al (eds), The Minerals, metals and Materials Society, 509-22.

BIRCHALL, J.D., HOWARD, A.J. and KENDALL, K. (1981). Nature (London), **289**, 388-89.

BIRCHALL, J.D., HOWARD, A.J. and KENDALL, K. (1982 a). Proc. Br. Ceram. Soc. **32**, 25-32, March.

BIRCHALL, J.D., HOWARD, A.J. and KENDALL, K. (1982 b). Chemistry in Britain, 860-63, December.

BIRCHALL, J.D., HOWARD, A.J. and KENDALL, K. (1983 a). The Metalurgist and Materials Technologist, 35-38, January.

BIRCHALL, J.D. (1983 b). Technology in the 1990's: Developments in Hydraulic Cements, Hirsch, P. (ed), Phil. Trans. Royal Society, London, A **310**, 31-42.

BITTENCE, J.C. (1989). Advanced Materials and Processing, **136**, 5, 25-40.

BOSSI, R.H. and GEORGESON, G.E. (1991). J. Minerals, Metals and Materials Society, **43**, 9, 8-15.

BOVING, K.G. (1989). N.D.E. Handbook, Butterworths.

BRAY, D.E. and STANLEY, R.K. (1989). Nondestructive Evaluation, McGraw-Hill.

BRIDGE, B., PATEL, N.D. and WATERS, D.N. (1983). Phys. Stat. Solidi (a), **77**, 655-68.

BRIDGE, B. and HIGAZY, A.A. (1986 a). Phys. Chem. Glasses, **27**, 1, 1-14.

BRIDGE, B. and PATEL, N.D. (1986 b). J. Mat. Sci. **21**, 3783-3800.

BRIDGE, B. and BAGHINI, N. (1987 a). Phys. Chem. Glasses **28,** 34-38.

BRIDGE, B., Br. J. NDT, **29**, (1987 b). 326-31.

BRIDGE, B. and CHENG, K.H. (1987 c). J. Mat. Sci. Lett. **23**, 3118-28.

BRIDGE, B. (1988 a). J. Mat. Sci., **23**, 988-94.

BRIDGE, B. and ROUND, R. (1988 b). J. Mat. Sci. Lett., **24**, 63-65.

BRODEUR, P.H. (1994). Tappi Journal, **77**, 3, 213-8.

BUTCHER, R. (1993). Ceramic Forum International, **70**, 10, 550-51.

BUNGEY, J.H. (1993). Proc. Inst. Civ. Engs. Structs. Buildings., **99**, 2, 64-67.

BYE, G.C. (1983). Portland cement, Pergamon, Oxford.

C.R.C. Press. (1989). Handbook of Chemistry and Physics, Table B69.

CALLISTER, W.D., Materials Science and Engineering, 3rd edition, Wiley, 1994.

CASSIDY, J.E. (1977). High Temperature Chemistry of Inorganic and Ceramic Materials, Glasser, F.P. (ed), Chemical society. 192-203.
CHANDRA, L. and CLYNE, T.W. (1993). J. Mat. Sci. Lett., **12**, 3, 191-95.

COTTON, F.A., and WILKINSON, G. (1972). Advanced Inorganic Chemistry, Interscience Publishers, 3rd edition, table 3-3.

CROSTACK,H.A., MORLO,H., and NIEHUS, R. (1987). Non Destructive Testing, Proceedings of the 4th European Conference, London, 2289-99, 13-17 September.

DAVIDGE, R. (1989). Br. Ceram. Trans. J., **88**, 4, 17-23.

DAS,A.C., NIYOGI, S.K. and MUKERGEE,S. (1991). J. Mat.Sci. Lett., **27**, 10, 173-75.

DEPERRIOS, J.M. (1988). Industrie Ceramique, 1988, **10**, 702-3.

DEWHURST, R.J., HUTCHINS, D.A., PALMER, S.B. and SCRUBY, C.B. (1982). J. Appl. Phys., **53**, 6, 4064-71.

DEWHURST, R.J., EDWARDS, C., McKIE, A.D.W. and PALMER, S.B. (1988). J. Appl. Phys., **65**, 8, 1225-27.

DOYLE, P.A. (1986). J.Phys. D, **19**, 9, 1613-23.

DRAPER, E.A., SCALNY, J, and ROSENTHAL, M.S. (1994). Cement technology, **40**, 187-94.

EDWARDS, G.R. (1989). Br. Ceram. Trans. J., **88**, 4, 117-23.

EKENHORST, D., GOEBBELS, J. and WOLFF, V. (1993). Ceramic Forum Int. **70**, 10, 557-60.

ELLINGSON, W.A., SINGH, J.P., HOLLOWAY, D.L., DIEKMAN, S.L., SINGH, D., SIVERS, E.A., SHEEN, S.H and WHEELER, M.J. (1992 a). Proceedings of the Sixth Annual Conference on Fossil Energy Materials. 229-39, July.

ELLINGSON, W.A., SINGH, J.P., SIVERS, E.A., HOLLOWAY, D.L., JACOBS, T.D., DIEKMAN, S.L. and SINGH, D. (1992 b). Proceedings of the Sixth Annual Conference on Fossil Energy Materials. 119-30, July.

ELLINGSON, W.A., AYAZ, D.M., BRADA, M.P. and O'CONNELL, W. (1993). NIST Special Publication 847, Proc. Int. Conf. on Advanced Mats., Gaithersburg, Maryland, 147-57, 20-22 July.

ENGLER, P. and FRIEDMAN, W.D. (1990). Materials Evaluation, **48**, 5, 623-29.

FAN, K., KHALID,A., SATTAR, T., CHENN,S., and BRIDGE,B. (1995). Non Destructive Testing and Evaluation, 12, 3, 181-196.

FINCH, T. and SHARP, J.H. (1989). J. Mat. Sci, **24**, 4379-86.

FRASER, J.D., AMIN, K.E. and KHURI-YAKUB, B.T. (1991). Nondestructive evaluation and Material Properties of Advanced Materials, Liaw et al (eds), The Minerals, metals and materials Society, 1-3.

GAI, H. and LOCKYEAR, C.F. (1993). Acoustic Sensing and Imaging, I.E.E. Conf. Proc., 120-125, 29-30 March.

GEORGESON, G.E. and BOSSI, R.H. (1991). Nondestructive Evaluation and Material Properties of Advanved Materials, Minerals, Metals and Materials Society, Liaw et al (eds), 99-108.

GENERAZIO, E.R., ROTH,D.J., STANG,D.B. (1989). J. Am. Ceram. Soc. **72**, 7, 1282-85.

GERHARDT, R. (1994). Ceramic Engineering and Science Proceedings, **15**, 5, 1174-81.

GIANARIS, N.J. and GREEN, R.E. (1991). Nondestructive Evaluation and Material Properties of Advanved Materials, Minerals, Metals and Materials Society, Liaw et al (eds). 29-35.

GLASSER. F.P. (1990). Br. Ceram. Trans. J., **89**, 6, 195-202.

GOOBERMAN, G.L. (1968). Ultrasonic Theory and application, English Universities Press. London.

GORDON,G., TITTMANN,B., CANUMALLA, S. and SEGALL,A.E. (1993). Ceramic Industry, 79-82, May.

GOUDA, G. and ROY, D.M. (1976). J. Am. Ceram. Soc., **59**, 412-14.

GREEN, A. (1987). Private communication.

GRUBER,J.J., SMITH,J.M., and BROCKLEMAN,R.H. (1988). Materials Evaluation, **46**,1, 90-96.

HALMSHAW, R. (1987). Non-destrucnve Testing, Edward Arnold, London.

HANSTEAD, P.D. (1987). Non Destructive Testing, Proceedings of the 4th European Conference, London. 13-17 September. 2279-88.

HASHIN, Z., J. (1962). Appl. Mech., **29**, 143-50.

HASHIN, Z., and SHTRIKMAN, S. (1963). J. Mech, Phys. Solids, **11**, 127-140.

HAYASHI, K. KATSUHIRO, K. KOSE, K. and INOUYE, (1988). T., J. Phys. D. **21**, 1037-39.

HEARLE, A.G. and HABER, R.A. (1995). J. Am. Ceram. Soc., **78**, 3, 819-23.

HEFETZ, M. and ROKHLIN, S. (1992). J. Am. Ceram. Soc., **75**, 7, 1839-45.

HIRSCH, P. (1983). (ed). Technology in the 1990's: Developments in Hydraulic Cements, Phil. Trans. Royal Society, London, A **310**.

HJORTH. L. (1983). Technology in the 1990's: Developments in Hydraulic Cements, Hirsch, P. (ed), Phil. Trans. Royal Society, London, A **310**, 167-73.

HUTCHINS,D.A. (1985). J. Phys. E, **18**, 1, 69-73.

HUTCHINS, D.A. and MAIR, H.D. (1989). J. Mat. Sci. Lett., **25**, 8, 1185-87.

JEN, K-C. and NERO, C. (1993). J. Am. Ceram. Soc., **76**, 3, 712-16.

JONES,M.P., BLESSING. G.V. and ROBBINS, C.R. (1986). Materials Evaluation, **44**, 6, 859-62.

KARUNANITHY, S. and MOOIBROEK, S. (1989 a). J. Mat. Sci., **24**, 3686-90.

KARUNANITHY, S. and FALK, M. (1989 b). Ceram. Eng. Sci. Proc., **10**, 998-1002.

KARUNANITHY, S. (1991). J. Mat. Sci., 26, 2169-72.

KATERINA, T., ROUND, R. and BRIDGE, B. (1991). J. Phys. D, **24**, 1673-86.

KAUTZ, H.E. (1989). Acousto-ultrasonics, Theory and Application, Duke, J.C. (ed), Plenum.

KAWASHIMA, K. and WRIGHT, O.B. (1992). J. Appl. Phys., **72**, 10, 4830-39.

KENDALL, K., HOWARD, A.J. and BIRCHALL, J.D. (1983). Technology in the 1990's: Developments in Hydraulic Cements. Hirsch, P. (ed), Phil. Trans. Royal Society, London, A **310**, 139-53.

KINGERY, W.D. (1950). J. Am. Ceram.Soc., **33**, 8, 239-50.

KINGERY, W.D., BOWEN,H.K. and UHLMANN,D.R. (1976). Introduction to Ceramics, 2nd edition, Wiley.

KNAB, L.I., BLESSING, G.V. and CLIFTON, J.R. (1983). Am. Concrete Inst. J. 17-27, Jan-Feb.

KOLSKY, H. (1963). Stress Waves in Solids, ch 3, Dover books.

KONSZTOWICZ, K.J. (1990). J. Am. Ceram. Soc., **73**, 10, 2809-14.

KREHER W, RANACHOWSKI, J. and RAYMUND F. (1977). Ultrasonics **15**, 70-74.

KUDRYATSEV, A.B. and PYATKOVA, A.V. (1989). Industrial Laboratory, **55**, 4, 426-32.

KULKARNI, N., MOUDGIL, B. and BHARDWAJ, M. (1994 a). Am. Ceram. Soc. Bull., **73**, 6, 146-53.

KULKARNI, N., MOUDGIL, B. and BHARDWAJ, M. (1994 b). Am. Ceram. Soc. Bull., **73**, 7, 83-85.

KUPPERMAN, D.S. and KARPLUS, H.B. (1984). Ceramic Bulletin, **63**, 12, 1505-09.

KUPPERMAN, D.S. (1987). Materials Analysis by Ultrasonics: Metal, Ceramics, Composites., Vary, A. (ed). Noyes Data Corporation, New Jersey, USA, 99-111.

KUNERTH, D.C., TELSCHOW, K.L. and WALTER, J.B. (1989). Materials Evaluation, **47**, 571-75, May 1989.

LAWRENCE, F.V. YOUNG, J.F. and BERGER, R.L. (1974). Proceedings of the 6th International congress on the chemistry of cement, Moscow, 134-44.

LEA, F.M. (1970). The Chemistry of Cement and Concrete, Edward Arnold.

LEE,R.J., DRAPER,E.A. and SKALNY, J. (1992). Mat. Res. Soc. Symp. Proc., **245** 349-57.

LEMMENS, J.W. (1991). Ceramic Bulletin, **70**, 2, 208.

MAJUMDAR, A.J. and LAWS, V. (1983). Technology in the 1990's: Developments in Hydraulic Cements. Hirsch, P. (ed), Phil. Trans. Royal Society, London, A **310**, 191-202.

MAKISHIMA, A. and MACKENZIE, (1973). J.D., J. Non. cryst. Solids, **12**, 35-45.

MAKISHIMA, A. and MACKENZIE, J.D. (1975). **17**, 147-57.

MATURANA, L.L. (1988). M.Sc. dissertation, Brunel University.

MAYNARD, J. (1996). Physics Today, **49**, 1, 26-31.

MIGLIORI, A. (1993). Materials Technology, **8**, 139-41.

MILNE, (1991). UK patent 2 237 113A.

NEVILLE, A.M. and BROOKS, J.J. (1987). Concrete Technology, Longman.

NONAKA,T., HAYAKAWA,Y., TAKEDA,S. and NISHIMORI,H. (1989). Materials Evaluation, **47**, 5, 542-46.

O'HARA, M.J., DUGGA, J.J., and SHEETS, H. D. (1972). Amer. Ceram. Soc. Bull., **51**, 590-95.

OZAKI, Y., SUMITANI,H., TOMODA,T., and TANAKA, M. (1987). Non Destructive Testing, Proceedings of the 4th European Conference, London. 13-17 September. 2489-98.

PAIN, H.J. (1983). The Physics of Vibrations and Waves. Wiley.

PANAKKAL, J.P. (1992). Br. J. NDT. **34**,11, 529-32.

PAPADAKIS, E.P. (1976). Physical Acoustics: Principles and Methods; Academic Press, New York, San Francisco, London. Vol xii, 277-374..

PAPADAKIS, E.P. (1984). J. Testing and Evaluation, **12**, 5, 273-79.

PARADIS, L., DE VADDER, D., and SAMAIN, E. (1987). Non Destructive Testing, Proceedings of the 4th European Conference, London 13-17 September. 2475-82.

PATEL, N.D., BRIDGE, B. and WATERS, D.N. (1983). Phys. Chem. Glasses, **24**, 5, 122-29.

PHILLIPS, D.H. and LANNUTTI, J.J. (1993). Am. Ceram. Soc. Bull.,**72**, 11, 69-75.

POPOVICS, S., ROSE,J.L. and POPOVICS,J.S. (1990). Cement and Concrete Research, **20**, 2, 259-70.

POTET, P., BATHIAS, C. and DEGRIGNY, B. (1988). Materials Evaluation, **46**, 7, 1050-54.

QUINN, G.D. and MORRELL, R. (1991). Design Data for Engineering Ceramics; A Review of the Flexure Test. J. Am. Ceram. Soc. **74**, 9, 2037-66.

RAPOPORT, Y.M., SLOUSHCH, V.J. (1994). Refractories, **35**,1-2, 26-31.

REYNOLDS, W.N. and SMITH, R.L. (1984 a). J. Phys.D, **17**, 109-16.

REYNOLDS, W.N. (1984 b). Br. J. N.D.T., **26**,1, 11-14.

REYNOLDS, W.N. (1985). and SMITH, R.L. Br. J. NDT., September, 291-94.

REYNOLDS, W.N. SCUDDER, L.P and PRESSMAN, H. (1986). Polymer testing, **6**, 325-36.

REYNOLDS, W.N. (1989). Br. Ceram. Trans. J., **88**, 4, 124-26.

ROBERTS, R.A. (1988). Materials Evaluation, **46**, 7, 758-66.

ROGOFSKY, A.J. (1991). Materials Evaluation, **49**, 12, 1491-97.

ROUND, R., and BRIDGE, B. (1987). J. Mat. Sci. Lett., **23**, 6, 1471-72.

ROUND, R., BRIDGE, B. and GREEN, A. (1988 a). J. Mat. Sci. Lett., **24**, 7, 604-6.

ROUND, R., BRIDGE, B. and GREEN, A. (1988 b). J. Mat. Sci. Lett., **24**, 7, 748-52.

ROTH, D.J., STANG, D.B., SWICKARD, M.S., DEGUIRE, M.R. and DOLHERT, L.E. (1991). Materials Evaluation, **49**, 883-88.

ROY, D.M. and GOUDA, G. (1973). J. Am. Ceram. Soc. **56**, 549-50.

ROY, D.M. (1980). report NMAB-361, National Materials Advisory Board, National research Council, Washington D.C.

ROY, D.M. (1987). Science, **235**, 652-8, February.

SAYERS, C.M and SMITH, R.L. (1985). A.E.R.E. Harwell report R 11589.

SCHINDEL, D.W. and HUTCHINS,D.A. (1995). J. Acoust. Soc. Am., **97**,3,1650-59.

SHEETS, H. D., BULLOFF, J.J., and DUCKWORTH, W.H. (1958). Brick and Clay Record, **133**, 55-57.

SHEPPARD, L.M. (1990). Advanced Materials and Processes, **132**, 5, 53-60.

SHEPPARD, L.M. (1991). Ceramic Bulletin, **70**, 8, 1265-79.

SMITH, R.L., REYNOLDS, W.N. and SCUDDER, L.P. (1984). Proceedings of the 5th Riso symposium on metallurgy and materials science, 519-23.

SMITH, R.L. (1985). A.E.R.E. Harwell report R 11885.

SMITH, R.L. (1987). NDT Int. **20**, 1, 43-48.

SMITH, S.D. (1990). Optical Engineering, **29**, 5, 524-34.

SMITH, M.E. and STRANGE, J.H. (1996). Meas. Sci. Technol., **7**, 449-75.

SOGA, N. and ANDERSON, D.L. (1966). Proceedings of the 7th Int. Congress on Glass.

SPLITT, G. (1987). Nondestructive Testing, Proceedings of the 4th European Conference, London 13-17th September. 2300-04.

STANLEY, C.C. (1979). Highlights in the History of Concrete. Cement and Concrete Association.

STEPISNIK,J. LUKAS,M. and KOCUVAN, I. (1981). Ceram. Bull, **60**,4, 481-83.

STINSON, M.P., HOLLOWAY, D.A. and ELLINGSON, W. (1993). Ceramic Engineering and Science Proceedings, **14**, 7-8, 485-91, 1993.

SUTOR, D. J. (1967). Acta Cryst., 1967. **23**, 418-22.

SZILARD,J. (ed). (1982). Ultrasonic Testing, non conventional techniques. Wiley-Interscience.

TALREJA, R. (1989). Acousto-ultrasonics, Theory and Application, Duke, J.C. (ed), Plenum. 177-190.

TAN,K.S., ROUND,R. and BRIDGE,B. (1989). Br. Ceram. Trans. J., **88**, 4, 138-43.

TAYLOR, H.F.W. (1966). Chemistry of Cements, R.I.C. Lecture series.

TAYLOR, H.F.W. (1981). Chemistry of Cements, J. Inst. Ceram., December, 6-12.

TELSCHOW, K.L. and CONANT,R.J. (1990 a). J. Acoust. Soc. Am. **88**, 3, 1494-1502
Correction: 1991. **89**, 5, 2463.

TELSCHOW,K.L., WALTER, J.B., and GARCIA, G.V. (1990 b). J. App. Phys., **68**, 12, 6077-6082.

TIWARI, A., REIFSNIDER, K.L. and HENNEKE, E.G. (1995). J. Composite Mats., **29**, 13, 1680-94.

THOMPSON, I. and RAWLINGS, R.D. (1991). J. Mat. Sci., **26**, 12, 4534-4540.

VAIDYA, U.K. and RAJU, P.K. (1994). Materials Evaluation, **52**, 6, 682-88.

VAINBERG,I.A., DOLGOMIROV, B.A., GRABOVSKII, S.B., ABRAMOV, V.A. and FEDOROV, A.B. (1993). Glass Ceramics, **50**,1-2, 23-6.

VARY, A. (1989). Acousto-ultrasonics, Theory and Application, Duke, J.C. (ed), Plenum, 1989. 1-21.

VARY, A. (1991). J. Acoust. Soc. Am., **49**, 4, 581-91.

VOGEL, J.A. and BRUINSMA, A.J.A. (1987). Nondestructive testing, Proceedings of the 4th European Conference, 13-17 September. 2267-78.

WANG, P.S., MINOR, D.B. and MALGHAN, S.G. (1993). J. Mat. Sci., **28**, 4940-43.

WINTERFELD, J., TEITZ, H.D. and DEITZ, M. (1993). Ceramic Forum International, **70**, 10, 554-57.

WOLFENDEN, A., HARMOUCHE, M.R., BLESSING, G.V., CHEN, Y.T., TERRANOVA, P., DAYAL, V., KINRA, V.K., LEMMENS, J.W., PHILLIPS, R.R., SMITH, J., MAHMOODI, P. and WANN, R. (1989). J. Test. Eval. **17**, 1, 2-5.

WRIGHT, W.D.M., HUTCHINS,D.A. and HAYWARD,G. (1993). Acoustic Sensing and Imaging, **29**, March, 245-250.

WRIGHT, W.D.M., HUTCHINS,D.A. and LEWIS, M.H. (1995). J. Mat. Sci. Lett.,**14**, 336-39.

WYCKOFF, R.W.G. (1965). Crystal Structures, vol 3, Interscience Publishers, 2nd edition.

YAMANAKA,K., JEN, C.K., NERON,C. and BUSSIERE, J.F. (1989). Materials Evaluation, **47**, July, 828-34.

YAMICAWA, (1993). US Patent no 5,217,503, 8th June.